Stony Brook University

Erythrocyte Aggregation due to Surface Nanobubble Interactions During the Onset of Thermal Burn Injury

A Dissertation Presented

by

Harrison S. Seidner

The Graduate School

in Partial Fulfillment of the

Requirements

for the Degree of

Doctor of Philosophy

in

Biomedical Engineering

Stony Brook University

May 2016

Stony Brook University

The Graduate School

Harrison S. Seidner

We, the dissertation committee for the above candidate for the

Doctor of Philosophy degree, hereby recommend

acceptance of this dissertation.

Mary D. Frame – Dissertation Advisor
Associate Professor
Biomedical Engineering, Physiology, and Biophysics

Wei Yin – Chairperson of Defense
Assistant Professor
Biomedical Engineering

David A. Rubenstein
Associate Professor
Biomedical Engineering

Roland N. Pittman – External Member
Professor of Physiology and Biophysics, Biomedical Engineering, and Emergency Medicine
Medical College of Virginia Campus
Virginia Commonwealth University, Richmond, Virginia

This dissertation is accepted by the Graduate School

Charles Taber
Dean of the Graduate School

Abstract of the Dissertation

Erythrocyte Aggregation due to Surface Nanobubble Interactions

During the onset of Thermal Burn Injury

by

Harrison S. Seidner

Doctor of Philosophy

in

Biomedical Engineering

Stony Brook University

2016

Red Blood Cell (RBC) aggregation is an important hemorheological phenomenon especially in microcirculation. In healthy individuals, RBCs are known to aggregate and gravitate toward the faster flow in the center of vessels to increase their throughput for more efficient oxygen delivery. Their aggregation is known to occur during a variety of environmental, pathological, and physiological conditions and is reversible when aggregates are subject to the relatively high shear forces in the circulation. The likelihood that aggregates will monodisperse in flow is dependent on the conditions during which they form. In situations where such aggregates are not sheared to monodispersion their presence can impact the perfusion of microvascular networks. More specifically, aggregates subject to the low shear rates in the zone of stasis near regions of thermal burn injury are capable of occluding vessels in the microcirculation and inhibiting the delivery of oxygen and nutrients to tissue downstream. The basic mechanism leading to erythrocyte aggregation at the onset of thermal injury is unknown.

This dissertation investigates parameters involved in erythrocyte aggregation, methods of measuring and testing erythrocyte aggregation, and incorporates modeling based on first principles ultimately to propose a mechanism of this phenomenon.

Table of Contents

List of Figures

List of Tables

List of Abbreviations

RBC – Red Blood Cell

PBS – Phosphate Buffered Saline

DIDS – 4, 4'-diisothiocyanostilbene-2, 2'-disulfonic acid

H_T – Tube Hematocrit

H_D – Discharge Hematocrit (Systemic Hematocrit)

HCT – Hematocrit

D – Vessel Diameter

EDTA - Ethylenediaminetetraacetic acid

WBC – White Blood Cell

TSS – Threshold Shear Stress

CSS – Critical Shear Stress

LORCA – Laser-assisted Optical Rotational Cell Analyzer

GYPC- Glycophorin C

IMP – Inter-Membrane Particle

AI – Aggregation Index

CFA – Cell-Free Area

Ig – Immunoglobulin

Ig G – Immunoglobulin G

Ig A – Immunoglobulin A

Ig M – Immunoglobulin M

DO – Dissolved Oxygen

SO_2 – Hemoglobin Oxygen Saturation %

PO_2 – Partial Pressure of Oxygen

PCO_2 – Partial Pressure of Carbon Dioxide

PN_2 – Partial Pressure of Nitrogen

P_{50} – Partial Pressure of 50% SO_2

2, 3 DPG – 2, 3 diphosphoglycerate

T – Temperature

Hb – Hemoglobin

C_{Hb} – Oxygen Binding Capacity of Hemoglobin

Hb_{RBC} – Hemoglobin concentration of a single erythrocyte

A – Arterial

V – Venous

$K_{H,\,pc}$ – Henry's Constant

R_b – Base radius of bubble

R_c – Radius of curvature of bubble

γ – Surface tension

l – Liquid

v – Vapor

s – Solid

γ_{lv} – Surface tension at the liquid-vapor interface

θ – Contact angle of bubble

H_o – Maximum coexistence separation

ΔP – Excess pressure within a supported bubble

ΔP_{free} – Excess pressure within a free bubble

P_o – Atmospheric Pressure

IACUC – Institutional Animal Care and Use Committee

PPP – Platelet Poor Plasma

A – Cross sectional Area

Re – Reynolds Number

Sigma – Standard Deviation of image pixel intensities

Glut – Glutaraldehyde

Specific Aims

Aggregation of erythrocytes and formation of rouleaux in microcirculation is a dynamic process involving many collective variables. Near regions of thermal injury, erythrocytes are known to a form into characteristic structures known as rouleaux. Rouleau are face-to-face, linear aggregates of RBCs. When multiple rouleau assemble into side-to-side, or side-to-face orientations they form three dimensional, branching structures, termed rouleaux. Rouleaux are capable of occluding blood vessels and blocking the flow of oxygen and nutrients to peripheral tissue which can lead to progression of the zone stasis to necrosis. This phenomenon can to occur during a variety of physiological, pathological and environmental conditions and is reversible. Known factors involved with erythrocyte aggregation include, but are not limited to, temperature, pH, percent hematocrit, hemoglobin oxygenation, membrane proteins, plasma proteins, cytoskeletal proteins, viscosity, and shear force/rate. There are many methods of measuring and influencing aggregation kinetics, however, there is a gap in knowledge concerning the fundamental mechanism or mechanisms underlying their aggregation during physiological and pathological conditions. The principle objective of this dissertation is to assemble the basic knowledge that is essential for a complete understanding of the mechanism or mechanisms involved with erythrocyte aggregation because it largely influences tissue perfusion and blood flow behavior in the microcirculation. Specifically, this study is to determine the contribution of various pathological plasma macromolecules to the pH and solubility of dissolved oxygen in blood with respect to temperature. Oxyhemoglobin dissociation was calculated in these environments and the relationship between gas solubility and dissociated oxygen from hemoglobin allowed for the testing of the hypothesis that excess gas present in the solution that is capable of forming bubbles. This provided a framework for a hypothesis aimed at

investigating the contribution of surface nanobubble interactions to thermally induced erythrocyte aggregation.

Hypothesis 1: Interactions between surface nanobubbles on erythrocytes contribute to erythrocyte aggregation during the onset of thermal injury.

Rationale 1: ***The development of a model of nanobubble formation and interactions will provide insight into nanobubble dynamics that will help identify the key parameters that likely influence bubble behavior on the erythrocyte membrane.***

*Specific Aim 1**:** To develop a theoretical model of thermally induced erythrocyte aggregation by surface nanobubble interactions.*

By integrating concepts and equations describing oxyhemoglobin dissociation, and nanobubble formation from existing literature with empirically derived data from the experiments below, an accurate theoretical model of surface nanobubble formation and interactions can be developed.

Hypothesis 2: **Blood plasma proteins and temperature contribute to dissolved oxygen solubility and pH.**

Rationale 2: It is known that gas solubility and bubble formation is influenced by temperature, and solution composition. While these factors have already been well characterized, blood contains too many proteins to allow for the hypothesis driven testing of individual proteins.

Specific Aim 2: To measure the contribution of plasma proteins and temperature to gas solubility and pH.

SA 2.1: Dissolved O_2 concentrations and pH of PBS and autologous plasma absence of RBCs will be measured at temperatures ranging from 37-49°C.

SA 2.2: Dissolved O_2 concentrations and pH of PBS in the absence of RBCs will be measured with the addition of varied concentrations of plasma proteins including fibrinogen, and albumin, corresponding to pathological and physiological conditions. Dissolved O_2 and pH measurements will be performed at temperatures from 37-49°C.

Hypothesis 3: Human Erythrocyte aggregation in PBS solution containing one of each candidate plasma protein will be greatly reduced (or increased) in response to heating and hemoglobin oxygenation state.

***Rationale 3**: The second specific aim will render information about the solubility of O_2 and pH with regard to temperature and plasma proteins. Before ascribing gas dissolution as a causality, erythrocyte aggregation in PBS with the addition of these proteins, and in plasma must be evaluated in the presence (oxyhemoglobin) and absence (deoxyhemoglobin) of dissolved oxygen.*

*Specific Aim 3**:** To measure the contribution of plasma proteins, hemoglobin oxygenation state and temperature to erythrocyte aggregation.*

Aggregation of erythrocytes at various hemoglobin oxygenation states in PBS solutions containing one of the candidate plasma proteins, and in plasma will be tested and quantified at each of the temperatures in the range of 37°C to 49°C. The results of the above experiments will also be compared in the presence of DIDS-treated erythrocytes.

Background and Significance

Burn injuries are a common cause of injury and death in the United States and worldwide. Approximately one million individuals seek medical attention for burns, one third of which seek emergency care. While the vast majority of burn injuries do not require hospitalization, severe burns can warrant surgical intervention, lead to potential morbidity, and often require an elongated recovery process [15]. In addition to accidental burn injuries, many surgical procedures require cauterization to stop bleeding and can result in an increased risk of infection[16]. Another clinical treatment that causes thermal injury is cardiac ablation, over 50,000 procedures are performed each year in American and the rate of cardiac ablation procedures to treat cardiac arrhythmias has increased by 15% each year since 1990 [17]. Thermal burns, both accidental and interventional, have similar temperature gradients emanating from the burn center including regions in the temperature range of 42°C to 45°C, and both undergo spatiotemporal progression. Thermal burns in this temperature range is the clinical focus of this dissertation.

Thermal Burn Injury Progression

The extent of immediate tissue destruction from thermal trauma and the wound's spatiotemporal progression is directly related to temperature, burn area, and duration of exposure. There exist three zones at the site of thermal injury that were first described in 1953 by Jackson [14]. Immediately following a thermal insult most tissue is lost as a result of heat coagulation, this is the zone of irreversibly damage and is called the zone of coagulation. Surrounding the zone of coagulation is a region of decreased perfusion, termed zone of stasis; followed by a zone of hyperaemia. The latter two zones are considered to be at risk of becoming necrotic, this is where thermally induced erythrocyte aggregation is likely to occur and increase

the risk of tissue necrosis. Erythrocyte aggregation in the zone of stasis impedes flow and causes reduced perfusion of the zone of stasis resulting in subsequent tissue loss [14] (Figure 1).

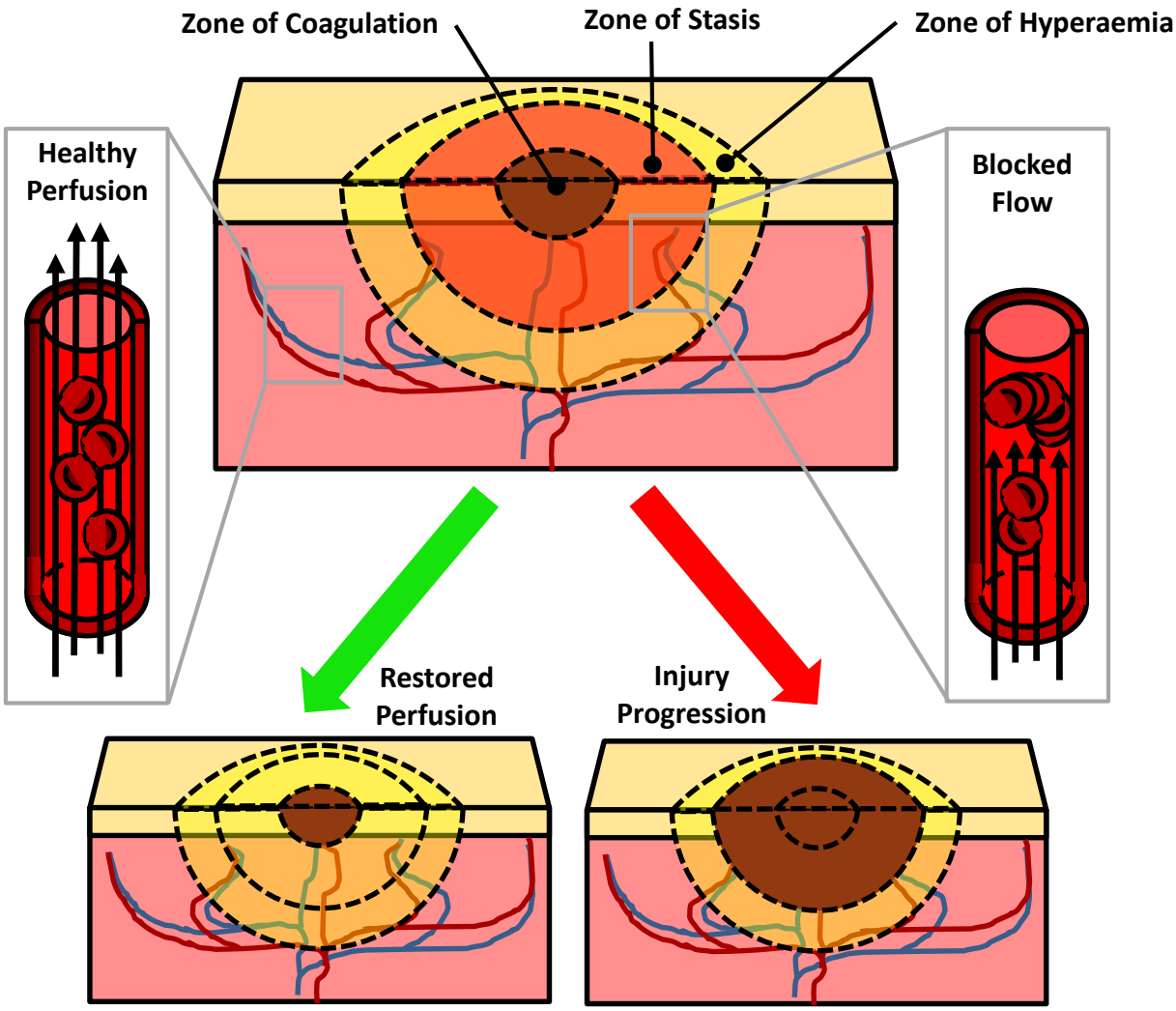

Figure 1: *Three zones of thermal injury. Schematic representation of the three zones present at the site of thermal injury (top-center). Blocked flow (top-right) can result in an increased zone of coagulation and injury progression (bottom right). Restored perfusion (top-left) can resuscitate the zone of stasis and prevent injury progression (bottom-left). Figure adapted from Gunter[3] and Jackson [14].*

In a series of experiments by Moritz and Henriques, burn injury was studied with a goal of characterizing the relative importance of time, and surface temperature dependent thresholds in the causation of cutaneous burns of porcine skin. It was observed that second- and third-degree burns resulted from prolonged exposure to temperatures greater than 44 ˚C, and momentary exposure to temperatures greater than 60 ˚C [18]. In their studies erythrocyte

aggregation was observed in tissues subject to first-degree burns and in tissue where the temperature ranged from 42 to 45 ˚C, the peak temperature range of the zone of stasis [18].

Erythrocyte aggregation in the zone of stasis is reversible for the first four hours post-burn. In a study by Clark et al., a porcine model was used to study coagulation in periburn tissue [19]. It was observed that coagulation occurred between 1 and 4 hours postburn [19]. Such coagulation is known to result in tissue death in the subsequent 24 to 72 hours, thus it is postulated that intervention within the first 4 hours postburn is necessary to limit the effects of burn injury progression [14; 19; 20]. A future clinical treatment that would reduce aggregation immediately after the onset of thermal injury would reduce coagulation in the zone of stasis, prevent necrosis, and thereby prevent expansion of the inflammatory region.

Erythrocyte Rheology

Blood is a suspension comprised of plasma with proteins, blood cells, and platelets. Red blood cells are the most abundant cell type in blood with a hematocrit ranging from 30-55% (systemic hematocrit) of whole blood and are involved in the transport of respiratory gasses between peripheral tissue and lungs. There are approximately 20x more RBCs than platelets and 1000x more RBCs than white blood cells in our blood. Blood cells and platelets cause the fluid to be non-Newtonian, exhibiting viscosity changes with applied shear stress [1].

In microcirculation, erythrocytes, erythrocyte aggregates, and larger cell types gravitate toward the center of the vessel where they travel faster than the plasma near the vessel wall [21]. This phenomena is thought to enhance RBC throughput in circulation in order to improve oxygen delivery. Interestingly, athletic mammalian species have been shown to exhibit a larger degree of erythrocyte aggregation (that is, in the absence of fibrin) which is likely an

evolutionary advantage [8; 22]. Such two-phase flow is described by the Fahraeus effect (Equation 1) [21].

$$\text{Equation 1:} \quad \frac{H_T}{H_D} = H_D + (1 - H_D) * (1 + 1.7e^{-0.415D} - 0.6e^{-0.011D})$$

where H_T represents tube hematocrit, H_D represents discharge hematocrit (i.e. systemic hematocrit), and D represents vessel diameter. The Fahraeus effect explains the heterogeneity and low hematocrit found in microcirculation. The Fahraeus-Lindquist effect explains the variation in apparent viscosity with respect to H_D and D (Equation 2) with (Equation 3) [21].

$$\text{Equation 2:} \quad \eta_{relative} = 1 + \frac{e^{-H_D * \alpha} - 1}{e^{-0.45 * \alpha} - 1} * (110e^{-1.42D} + 3 - 3.45e^{-0.035D})$$

$$\text{Equation 3:} \quad \alpha = 4/[1 + e^{-0.593 * (D - 6.74)}]$$

From Equation 2 and Equation 3, it is clear that the relative viscosity increases exponentially with hematocrit for large diameter vessels (D>15um) but for smaller diameter vessels (D<5um) viscosity increases mostly linearly with respect to hematocrit. While investigating erythrocyte aggregation in the microcirculation, it is important to consider the center-seeking behavior of aggregates and the physiological tube hematocrit that would exist in the vessel of a given diameter. This phenomenon is advantageous for oxygen delivery when considering larger vessels but can lead to a blockage of flow when the aggregates reach the microcirculation.

Viscosity and Fluid Shear

Blood viscosity is largely dependent on RBC aggregation, and temperature. Aggregation occurs mostly in post-capillary venules where shear stress is low [23; 24]. The extent of aggregation is a limited by the negative surface charge of erythrocytes and flow-induced shear stresses. The viscosity, measured with a pressure-scanning capillary viscometer, of whole blood and plasma

largely depends on shear rate and temperature. For instance, at a shear rate of 10 s^{-1}, the plasma viscosity decreased from 2.3mPa*s to 1.65mPa*s (a reduction of 28.3%) when the temperature increased from 4°C to 37 °C (Figure 2) [11].

The viscosity of blood and its constituents have been shown to change as a function of temperature. The apparent viscosity of human plasma decreased from 3.2mPa*s to 1.7mPa*s with a temperature change from 4°C to 37°C (Figure 2), a reduction of 48% [11], while the apparent viscosity of whole human blood 45% hematocrit with EDTA and without WBCs also decreased with increased temperature [11]. It is important to consider that $\eta_{relative} = \eta_{apparent}/\eta_{plasma}$ where η_{plasma} = 1.3cP at 37°C. An observed decrease of the η_{plasma} caused by increased temperature would show a decreased $\eta_{apparent}$, however, this apparent decrease in viscosity may be a result of the annular cell free layer (plasma), whereas the central portion of flow comprised of the RBC aggregates may actually have a higher viscosity that will have been unnoticed. A decrease in plasma viscosity would likely increase the probability of

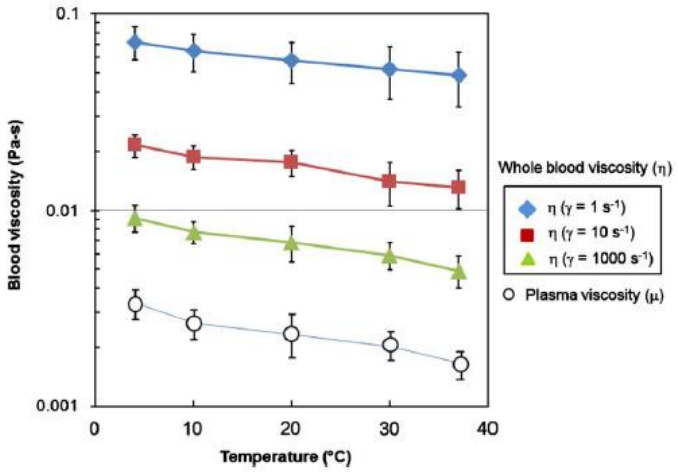

Figure 2: *Blood viscosity versus temperature and shear rate. Blood component (whole blood versus plasma) viscosity changes as a function of temperature. Viscosity plotted for various shear rates. Figure from [11].*

RBCs colliding through Brownian motion thus increasing their likelihood of aggregating. Of course, the ability of the aggregates to remain intact is dependent on the fluid shear stress.

Threshold Shear Stress (TSS), the product of threshold shear rate and the corresponding whole blood viscosity is measured with LORCA and is a measure of aggregative strength. Critical Shear Stress (CSS) is the threshold shear stress required to keep red cell aggregates dispersed in a channel flow system and is determined through a simple microfluidic aggregometer with simultaneous measurements of the pressure and the optical density. TSS and CSS decrease with increased temperature from 4°C to 30°C. At temperatures higher than 30°C, both CSS and TSS begin to increase. In Figure 3 the TSS obtained from a previous study is plotted as well for comparison [11]. The adhesive force between RBCs in buffered solution at room temperature is 28.8±8.9 pN [4]. Based on the results in Figure 3, at this temperature a shear stress of 1.1 Pa would be required to separate them.

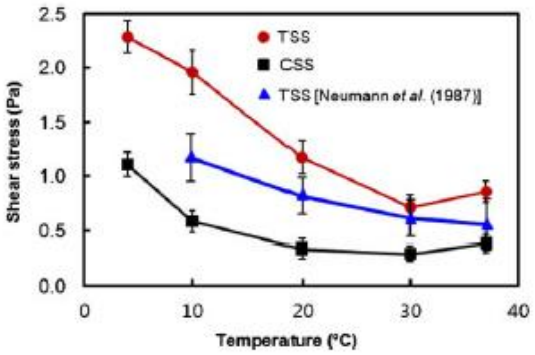

Figure 3: *Threshold Shear Stress and Critical Shear Stress versus temperature. A comparison of the Threshold Shear Stress (TSS) determined through LORCA and Critical Shear Stress (CSS) measured directly through a microfluidic aggregometer as a function of temperature. Figure from [11].*

Erythrocyte Structure and Composition

The RBC is shaped like a biconcave disk shape which makes it such that they have large surface area for the exchange of Carbon Dioxide and Oxygen. In humans their average dimensions (Figure 4) are as follows: Diameter = 7.8um, Maximum thickness = 2.6um, Minimum thickness = 0.8um, with a volume of ~90 fL and ~136 μm^2 surface area. [1] The protein hemoglobin is responsible for transporting most of the oxygen found in blood. The concentration of hemoglobin inside human erythrocytes is 330 g/L and it has been empirically determined that hemoglobin has the capacity to bind 1.34 mL O_2 per gram of hemoglobin [13].

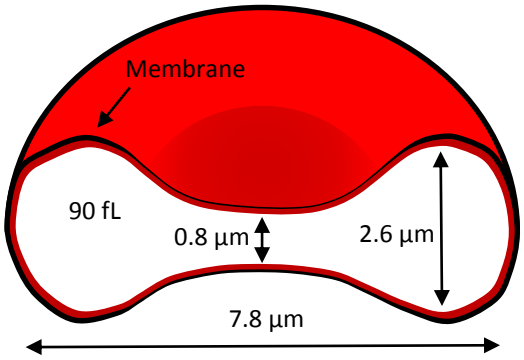

Figure 4: *Average dimensions of human erythrocyte. Diameter=7.8um, Maximum thickness=2.6um, Minimum thickness=0.8um, with a volume of ~90 fL and ~136 μm^2 surface area Figure adapted from [1].*

The erythroid membrane is comprised of a lipid bilayer (40%) with globular proteins (52%) embedded within that can move about the plane of the membrane giving the lipid bilayer similar characteristics to a viscous fluid [1; 25]. On the extracellular side of the membrane, carbohydrate residues (8% of the membrane) on glycoproteins and glycolipids form a ~0.5 µm thick glycocalyx that mediates interactions between the cell and its environment [25; 26]. The membrane also shows elastic properties because the spectrin cytoskeleton is fixed to proteins on the intracellular side of the membrane by ankyrin [1] (Figure 5). The viscoelastic nature of the erythrocyte membrane resulting from spectrin-membrane interactions allows for the flexibility

and deformability required for these cells to withstand high shear forces as they pass through vessels that are sometimes smaller than themselves [27].

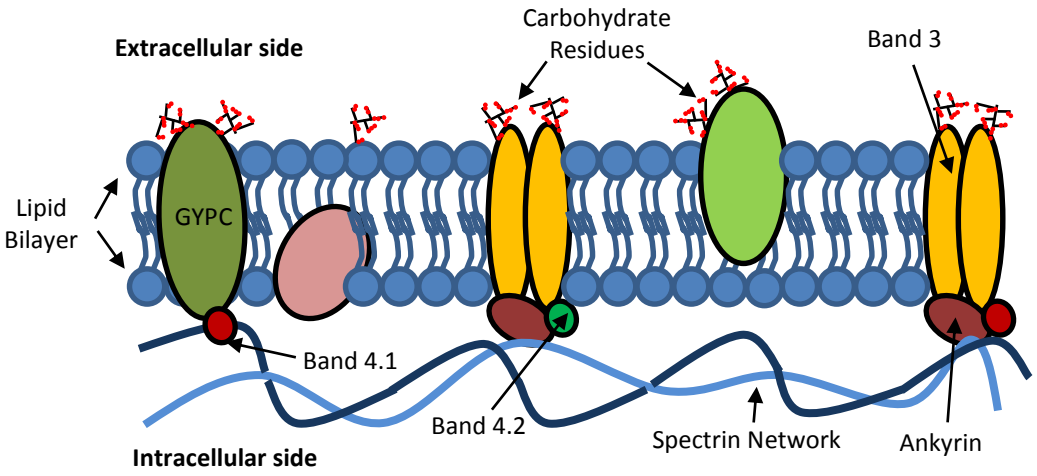

Figure 5: *Schematic representation of the erythrocyte membrane. Spectrin, on the intracellular side, acts as a cytoskeleton. Proteins within the lipid bilayer interact with spectrin on the intracellular side. Carbohydrate residues on the extracellular side form the glycocalyx. Figure adapted from [10]*

The interactions between spectrin and integral membrane proteins, namely Band 3 and glycophorin C (GYPC), are mediated by intracellular peripheral membrane proteins known as ankyrin, Band 4.2 (palladin) and Band 4.1[10; 28]. These interactions regulate the erythrocyte shape.

GYPC is a 36.5 kDa transmembrane protein. It comprises less than 1% of the total erythrocyte membrane proteins having 0.5 to 1 x10^5 copies per cell [29]. Together with the three other varieties of glycophorins in the RBC membrane glycophorins still comprise less than 2% of the total erythrocyte membrane proteins. Despite the low concentration of glycophorins on the erythroid membrane, 60% of the RBC's negative charge can be attributed to the high sialic acid content on their extracellular domains. For this reason, glycophorins are thought to play a major role in modulating RBC-RBC interactions [30].

Band 3 is a 90-100 kDa transmembrane protein. It comprises approximately 30% of the total erythrocyte membrane proteins, having about a million copies per cell [31]. Band 3 functions

as a structural protein as well as an anion exchanger of bicarbonate for chloride, 1:1, across the erythrocyte membrane. The erythroid structural component of band 3 relies on band 3's lateral and rotational mobility on the membrane, and ability to oligomerize, both of which are known to be temperature dependent [12]. Hyperthermic conditions have been shown to cause heterogeneous distributions of band 3 throughout the erythrocyte membrane, thus changing the erythrocyte structure through the interactions of band 3's cytoplasmic domains with spectrin.

Membrane Deformation

While investigating the aggregation of erythrocytes during hyperthermia, it is important to consider the morphological transformations that occur as a function of temperature. It has been shown that structural changes of RBC membranes occur as a result of heat treatment. Spectrin undergoes a series of conformational changes in the range of 21-72°C, with the largest temperature dependence occurring in the range 35-49°C before denaturing at 49.5°C after which these changes become irreversible [32; 33]. This happens in addition to oligimerization of Band 3 in the temp range 46-49°C which increases Band 3's lateral and rotatory mobility [12]. These phenomena lead to alterations in the cell membrane which has shown to increase micro-viscosity of the membrane and may induce vesiculation [12]. IMP (Inter-Membrane Particles) can aggregate and redistribute within the lipid membrane leaving large, protein-free, lipid areas (Figure 6 *left*) [12], or they can aggregate to form a continuous networks having a similar morphology to that of the membrane skeletal network (Figure 6 *right*) [12]. Membrane

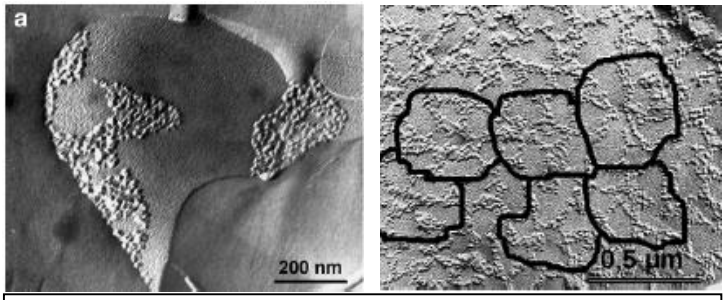

Figure 6: *Arrangements of inter-membrane particles on erythrocyte membrane. Aggregation if IMPs on RBC membrane form of: left) large protein-free, lipid areas that are typical of a spectrin-free vesicle, and right) continuous network resembling the spectrin network. Figure from [12].*

proteins' rotatory and lateral mobility on membrane are limited by the spectrin-actin membrane-skeleton. Changes in the behavior of Band 3 are likely a result of changes in spectrin-Band 3, and spectrin-GYPC interactions. Hyperthermia induced IMP aggregation in the form of a continuous geometry that looks similar to that of a mesh-like cytoskeletal spectrin network indicates that there is a strengthening of membrane protein affinity with spectrin molecules.

A study by Stefanovic et al. showed the involvement of hemoglobin oxygenation with the affinity of ankyrin to Band 3 [34]. Deoxygenation of hemoglobin resulted in displacement of ankyrin from Band 3, and subsequent release of spectrin from the erythrocyte membrane.

In a study by Van Dort et al., it was observed that following the removal of ankyrin, Band 3 oligomers slowly converted to dimers and ultimately monomers. In the reverse procedure, the addition of excess ankyrin to membranes enriched with dissociated Band 3 resulted in the preferred tetrameric form of Band 3. With the addition of a well characterized Band 3 inhibitor, known as 4, 4'-Diisothiocyano-2, 2'-stilbenedisulfonic acid (DIDS), their study showed a shift of most Band 3 to a dimeric state and an elimination of the majority of ankyrin-binding sites on the membrane [28]. DIDS inhibits chloride channels by interacting with band 3 on the extracellular surface of the erythrocyte membrane [35]. The loss of ankyrin binding sites resulting from DIDS treatment likely changes the extracellular side of the erythrocyte membrane thus providing a strong basis for the investigation of DIDS as a mediator of erythrocyte membrane deformation and aggregation.

There are notable differences in the membrane shape of human umbilical RBCs, at 46°C (Figure 7 *left*) and 20% hematocrit with Heparin in PBS and 2.5% Glutaraldehyde (1:1), compared to that of rat RBCs under the same conditions (Figure 7 *right*)[12]. It is proposed that the differences in membrane surface morphology between species are causes by differences in protein composition, and spectrin-membrane protein interaction.

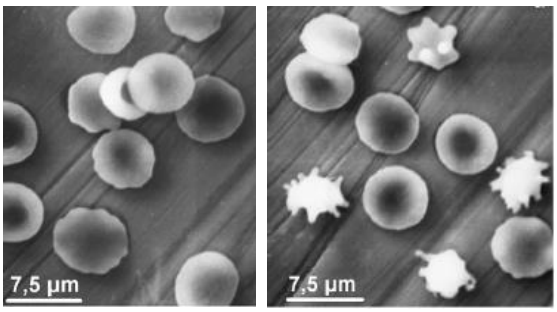

Figure 7: *Membrane deformation of human and rat erythrocytes. Differences in deformation between:* ***left)*** *Human umbilical cord RBCs at 46°C* ***Right)*** *Rat RBCs at 46°C. Figure from [12].*

Thermally induced erythrocyte membrane deformation are caused by conformational changes of spectrin and its interactions with transmembrane proteins Band 3 and GYPC. For example, ankyrin, Band 4.2 (palladin) and Band 4.1 are primarily responsible for mediating the interaction of spectrin and Band 3. In the absence of palladin, as for horses, it is postulated that spectrin could be linked directly to Band 3. In this case, a conformational change of spectrin would directly translate to a deformation of the membrane. This phenomena is likely responsible for differences in temperature dependent RBC morphology between species.

Erythrocyte membrane proteins comparison between species

Concentrations of erythrocyte membrane proteins of various mammalian species were determined using polyacrylamide (12% acrylamide) gel electrophoresis then compared to human concentrations [36]. Significant differences in concentration of membrane proteins were observed between species. Bands 1 and 2 (spectrins): lower in non-human species, and was significantly lower in horses. Bands 2.1-2.3: significantly lower in rabbit and rat, slightly lower in mouse, significantly higher in sheep. Band 3 (the anion exchanger): higher molecular weight (100kDa)

Table 1: Erythrocyte Membrane Protein Composition of Various Species Compared to Human
*Represents significant difference ($p<.05$), symbols indicate difference from human. Adapted from [36 37]

Membrane Protein	Horse	Cow	Sheep	Rabbit	Rat	Guinea Pig	Mouse
Bands 1,2 (Spectrins)	↓*	↓	↓	↓	↓	↓	↓
Bands 2.1 – 2.3	↑	≈	↑*	↓*	↓*	≈	↓
Band 3 (Anion Exchanger)	↑*	↓	↓*	↑*	↓	↓	↓
Band 4.1	↑	≈	≈	≈	↑*	↑	≈
Band 4.2 (Palladin)	X	≈	≈	≈	↓*	≈	≈

in cow, guinea pig and mouse: lower molecular weight (90kDa) in sheep, significantly lower concentration in sheep, significantly higher concentration in horse, and rabbit. Band 4.1: significantly higher in rat, slightly higher in horse, and guinea pig [36]. Band 4.2 (palladin): higher concentration in human than rat, missing in horse [37]. Band 4.5: significantly higher in horse and rat. Band 4.9 (dematin): significantly higher in horse, rabbit and guinea pig. Band 6 (glyceraldehyde 3-phosphate dehydrogenase): undetectable in horse, rat and mouse, significantly lower in sheep, rabbit, and guinea pig. Band 7: significantly higher in mouse. Band 8: undetectable in horse, cow and guinea pig, significantly higher concentration in rat [36]. These differences between species in concentrations of membrane, proteins, specifically Bands 1

through 4.2 (Table 1), may contribute to the differences observed in membrane morphology between species and is important to consider while choosing an animal model of human erythrocyte aggregation.

RBC membrane deformation is important in rouleaux formation to provide parallel alignment between adjacent RBCs. Deformability is a function of surface area/volume ratio, membrane viscoelasticity, internal viscosity of the cell, shear rate, and hematocrit. Cells with low surface area to volume ratios are more rigid and less likely to aggregate [38]. An increased surface area to volume ratio is thought to increase the available area for cell-cell interactions to occur, thus increasing aggregation. The interaction between Band 3 and spectrin greatly influences the morphology of the erythrocyte membrane and presents a strong basis for investigating the contributions to aggregation of the mediators of Band 3-spectrin bridging.

Erythrocyte Aggregation

Erythrocyte aggregation the process of erythrocytes forming three dimensional clusters of linear erythrocyte aggregates, known as rouleaux. The process is reversible and has various indices capable of being measured by several instruments and techniques. Aggregation indices and kinetics are characteristic of the erythrocyte suspension under investigation, specifically the properties and composition of the cells and medium in which they are suspended.

A commonly used tool in measuring hemorheological parameters including aggregation behavior and deformability of red blood cells is Laser –assisted Optical Rotational Cell Analyzer (LORCA). LORCA relies on syllectometry (backscattering of a laser versus time) in order to measure both static and kinetic parameters in the aggregation process. The LORCA system consists of a Couette-system of two concentric cylinders with a gap of .3mm in which 1mL of

blood is placed. The outer cylinder rotates at varying speeds while the laser for syllectometry, a photodiode sensor, and a temperature control unit are located in the fixed inner cylinder. This tool is capable of measuring the extent of RBC aggregation, rates of aggregation, aggregation index, threshold shear rate, aggregation tendency, and aggregate stability [39]. RBC aggregation index (AI) is a conventional parameter that is used to quantify aggregation of RBCs and is based on the increase of light transmission through an RBC suspension that occurs when individual cells aggregate; when there are gaps between the aggregates, more light can pass through the suspension and a greater AI is measured. Furthermore, the aggregation index is extenuated in flow by cell-free area caused by the Fahraeus effect.

The magnitude of these aggregation indices vary with conditions involving, but not limited to, temperature, shear stress, shear rate, plasma proteins, membrane proteins, skeletal proteins, hematocrit percentage, and species from which the RBCs were harvested.

Species Dependence

Aggregation kinetics differ between species which indicates that the mechanisms involved with erythrocyte aggregation likely involve the proteins that erythrocytes are comprised of or plasma proteins. This means that it is important to consider which species to use as a model for human erythrocyte aggregation. There are significant differences in aggregation between horse, human and rat. Horse RBCs with 40% hematocrit in autologous plasma aggregates 18x more than rat, and ~10x more than human RBCs in autologous plasma at 25 °C [37]. Another study showed a significant difference in RBC adhesive forces and aggregation indexes between horse, sheep and calf with 40% hematocrit in autologous plasma with EDTA and at 37°C [38]. They showed that horse RBC aggregation was 16% more than human, sheep RBC aggregation was

60% less than human, calf RBC aggregation was 63% less than human, and pig RBC aggregation showed no significant difference in aggregation when compared to human. They also showed that the adhesive forces between pig RBCs were not significantly different than that of human, the adhesive forces between horse RBCs were too strong to be measured with their instrument but were at least 600% stronger than that of human, the adhesive forces between sheep RBCs are 75% weaker than that of human, and that the adhesive forces between calf RBCs are 77% stronger than that of human [38]. To eliminate the effects of species dependence on aggregation, this research will focus on human erythrocytes.

Temperature Dependence

Studies have shown that erythrocyte aggregation to be enhanced by elevated temperature making this parameter of particular interest in studies of RBC aggregation in thermal injury. It has been shown that in whole human blood without WBCs with a 45% hematocrit with **E**thylene**d**iamine**t**etraacetic **a**cid anticoagulant (EDTA) in autologous plasma [11], when the temperature was changed from 4°C to 37 °C, the aggregation index increases 32% [11]. In a similar study, human RBCs in whole blood with EDTA and 45% hematocrit, human RBCs showed a 16% increase in their aggregation index with an increase in temperature from 20°C to 40°C (Table 2) [39]. In addition to an increase in the aggregation index, when the temperature was changed from 4°C to 37°C there was also an observed change in aggregation rate ($T_{1/2}$), a three-fold increase in aggregation rate was observed in human RBCS (45% hematocrit) in autologous plasma without WBCs [11]. There is an apparent

Table 2: Aggregation index of human erythrocytes. Aggregation Index of erythrocytes (45% hematocrit) with EDTA in PBS at various temperatures (table adapted from [39])

Temperature (°C)	Aggregation Index (%)
20	56
25	58
30	61
37	61±1.9
40	65

correlation between temperature and erythrocyte aggregation in some suspensions more than others, however, the causation remains unclear.

Plasma Proteins

Pathological stresses and conditions including, but not limited to, thermal injury, diabetes, sepsis, thrombosis, myocardial infarction, renal failure, and microcirculatory diseases have a tendency to increase the concentration of various plasma proteins [40].

A key study by Levin et al. sought to investigate the role of plasma and erythrocyte factors in change of aggregation in burn disease. Through a series of experiments in which erythrocyte aggregation was measured when blood plasma from burn patients was added to erythrocytes from healthy donors and vice versa [41]. It was observed that erythrocytes, when suspended in burn patient plasma, showed a sharp increase in aggregation compared to reduced aggregation of those suspended in plasma from a healthy donor. The differences in aggregation found between the plasma from healthy and burn patient donors were the same whether or not the plasma was autologous [41]. This indicates that the cause of aggregation in burn disease is related primarily to changes in the constituents and properties of the plasma. During inflammation the concentration of fibrinogen is known to increase from its normal value of 1.8-4.0 mg/mL [8]. Fibrinogen concentration is elevated 20% by obesity [42], and even more so during pathological

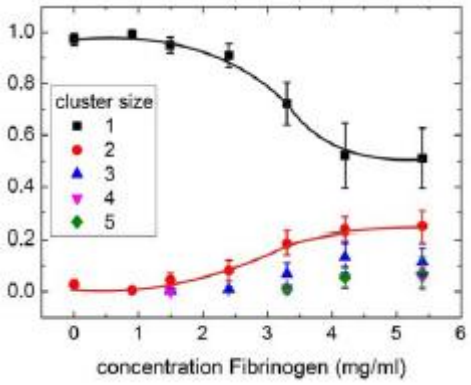

Figure 8: *Aggregate size versus fibrinogen concentration. Statistical distribution of RBC aggregates of different sizes at various concentrations of fibrinogen. Figure from [8].*

conditions including cardiac disease and sepsis [8]. Following severe thermal injury, fibrinogen concentration has been shown to increase up to 5.54 mg/mL from a healthy concentration of 2.93 mg/mL [41]. Fibrinogen is a large, soluble glycoprotein synthesized in the liver by hepatocytes that is involved with the formation of clots after it is converted by thrombin to fibrin which is insoluble. It has been shown that an increased concentration of fibrinogen increases aggregation between washed RBCs with EDTA in PBS at 45% hematocrit (Figure 8) [8]. Increased concentration of fibrinogen is also known to increase the interaction energy between washed RBCs with EDTA in PBS at 45% hematocrit and was measured using single cell force spectroscopy (interaction energy = area under the curve) (Table 3) [8].

Table 3: Concentration of fibrinogen versus interaction energy between RBCs (table adapted from [8])

Fibrinogen (mg/mL)	Interaction Energy (μJ/m^2)
0.0	0.6
0.9	1.9
1.5	2.1
2.4	2.9
3.3	3.25
4.2	3.6
5.4	4.6
6.5	4.9
8.0	6.6

Immunoglobulins (Igs) are also known to affect the aggregation of RBCs. It is thought that positively charged immunoglobulins in high concentration are capable of forming electrostatic bonds with RBCs and cause increased aggregation. Immunoglobulins are antibodies used by the immune system to identify antigens and constitute 30% (by concentration) of the total plasma proteins with the exception of fibrinogen. Of the immunoglobulins in plasma, 99% of it is Ig G, Ig A, and Ig M. Their concentration, similarly to fibrinogen, is increased during pathological stresses. A normal concentration of Immunoglobulin A is 1.4–4.2 g/L. A normal concentration of Immunoglobulin G is 8.0-17.0 g/L. A normal concentration of Immunoglobulin

M is 0.5-1.8 g/L. When any of these Ig concentrations are raised above their normal values, RBCs are more likely to aggregate (Figure 9) [7].

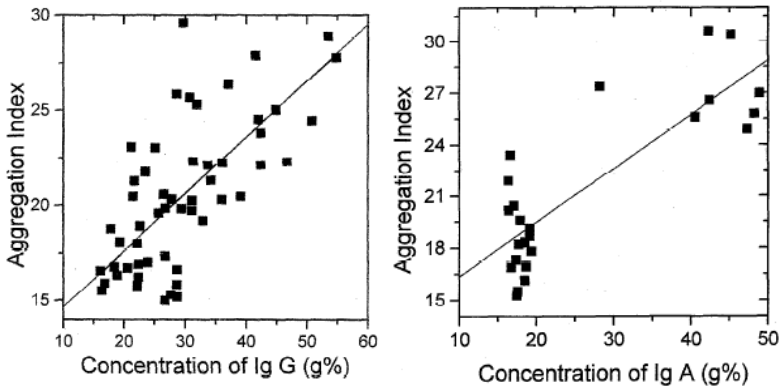

Figure 9: *Aggregation index of erythrocytes treated with immunoglobulins. Aggregation index plotted versus percent concentration of Immunoglobulin G (Left) and Immunoglobulin A (Right). Figure from [7].*

Albumin is a plasma protein that helps transport small molecules in the blood and maintains oncotic pressure. A normal albumin concentration is 34.0 -54.0 g/L. Thermal injury has been shown to decrease the albumin concentration in blood to as low as 20.0 g/L, this is likely a cause of edema [43]. Unlike most other plasma proteins, increased albumin concentration has resulted in contradicting results. Some studies have shown it to result in a decreases of erythrocyte aggregation [40], while others have shown its contribution to hyperaggregation. The opposing results of albumin's contribution to aggregation indicate that there is coexisting factor in plasma that interacts plasma proteins to yield such results. One of the principle functions of blood is to deliver oxygen via oxy-hemoglobin dissociation in the microcirculation. Thus, the oxygenation state of hemoglobin becomes of particular interest in the study of aggregation.

Hemoglobin: Oxygenation and Concentration

It has been shown that the hemoglobin oxygenation level of an erythrocyte solution has a significant effect on aggregation parameters with respect to the extent of aggregation and its rate, however, the mechanism is unknown [44; 45]. Erythrocyte aggregation in oxygenated blood samples aggregate faster, but to a lesser extent than deoxygenated blood [45]. Interestingly, the oxygenation status of the blood samples only contributed to aggregation measurements made using a specific

instrument (LORCA, Mechatronics, The Netherlands [39]) but not with others. This is likely due to the technical differences between LORCA and other systems, LORCA is based on backscattered light (670nm) while most other systems are based on light transmission. The LORCA system, however, showed only small differences in aggregation, compared to other systems, as a function of temperature possibly because it requires that the sample be heated to the test temperature before aggregation measurements can be taken. This method could potentially be missing the aggregation that may result from the changes in oxygen solubility in plasma, and affinity to hemoglobin with respect to temperature change (See "Proposed Model: Surface Nanobubble Coalescence" section).

The in-vivo age of erythrocytes has been shown to have an effect on aggregation[46]. Erythrocytes typically live for about 120 days before they are removed from the circulation[47]. During their aging process they are known to display an increase in density and cytoplasmic hemoglobin concentration. Using high speed centrifugation the cells can be age-separated based on their densities[48]. The aggregation indices of the lowest density cells (top 10% of packed RBCs) was lower than that of the highest density cells (bottom 10% of packed RBCs) when suspended in 3% dextran 70 kDa [46]. These findings are consistent with earlier findings that indicated ~100% difference in aggregation between old and young cells suspended in autologous plasma [46; 49]. The increased aggregability of old cells can likely be attributed to their greater capacity to carry oxygen. These studies provide a strong basis for investigating dissolved oxygen solubility and hemoglobin oxygenation states as potential mediators of aggregation.

Models of Erythrocyte Aggregation

The mechanism of erythrocyte aggregation has yet to be fully characterized and has become a popular research subject. The multitude of factors and conditions that have been shown

to influence aggregation have given rise to two fundamentally different, and mutually exclusive models to explain the phenomenon; the bridging model, and the depletion layer model.

Bridging Model

The Bridging model suggests that plasma proteins and macromolecules are non-specifically absorbed into and onto the RBC membrane and form a "bridge" between two adjacent cells (Figure 10). Aggregation will occur when bridging forces between cells exceed the forces that inhibit aggregation such as shear, electrostatic repulsion, and membrane strain [4; 37]. Most studies of erythrocyte aggregation test the contribution of protein bridging, hence, this is likely the most widely accepted model [4; 8; 46].

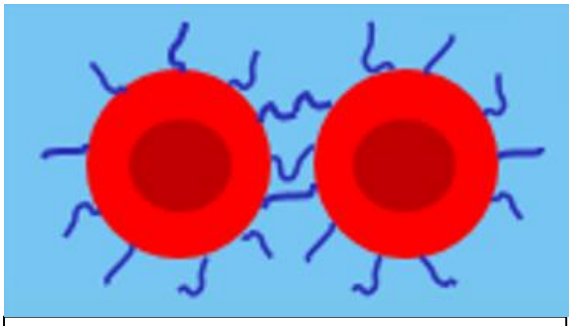

Figure 10: *Bridging model of erythrocyte aggregation: schematic representation of macromolecular bridging leading to intracellular adhesion. [4].*

Depletion Model

The Depletion model suggests that aggregation occurs when the concentration of a polymer or protein near the RBC surface is less than the concentration of the bulk fluid; this is thought to cause an osmotic gradient that draws fluid away from the region between cells thus causing aggregation. In this system, a "depletion layer" surrounds the RBC and the thickness of this layer equals the radius of the protein in solution. When two depletion layers overlap, an additional free volume force is present for the proteins which

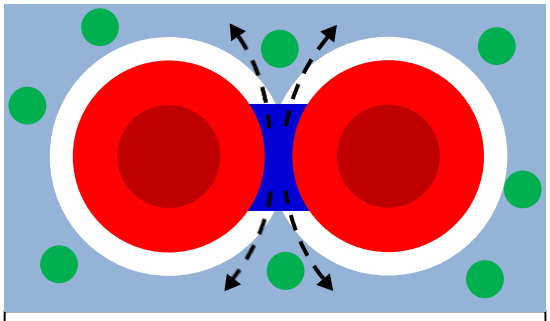

Figure 11: *Depletion model of erythrocyte aggregation: Schematic representation of depletion layer in a RBC and plasma protein system. Depletion layer surrounding cells (white). When two adjacent depletion layers overlap, a volume (dark blue) is expelled to become available for plasma proteins with diameter d_2 (green). [4].*

leads to an effective osmotic pressure that results in an attractive force between two adjacent cells (Figure 11) [4].

Proposed Model: Surface Nanobubble Coalescence

The specific aims of this dissertation are aimed at investigating our proposed model that challenges the fundamental mechanisms of the two widely accepted mechanisms of erythrocyte aggregation, the "bridging model" and the "depletion model". In this model, we suggest that an increase in temperature and reduction of pH causes oxygen to dissociate from hemoglobin (Figure 12 left) while simultaneously causing a reduction in solubility of dissolved gas in plasma (Figure 12 right). The pH of a given solution and the solubility of dissolved gas for a given temperature is a function of plasma protein composition and concentration. When the amount of dissociated oxygen surpasses the solubility of the solution, there becomes an excess volume of oxygen gas. The excess volume of gas resulting from the sum of the dissociated oxygen from hemoglobin, and dissoluted gas species from the change in solubility

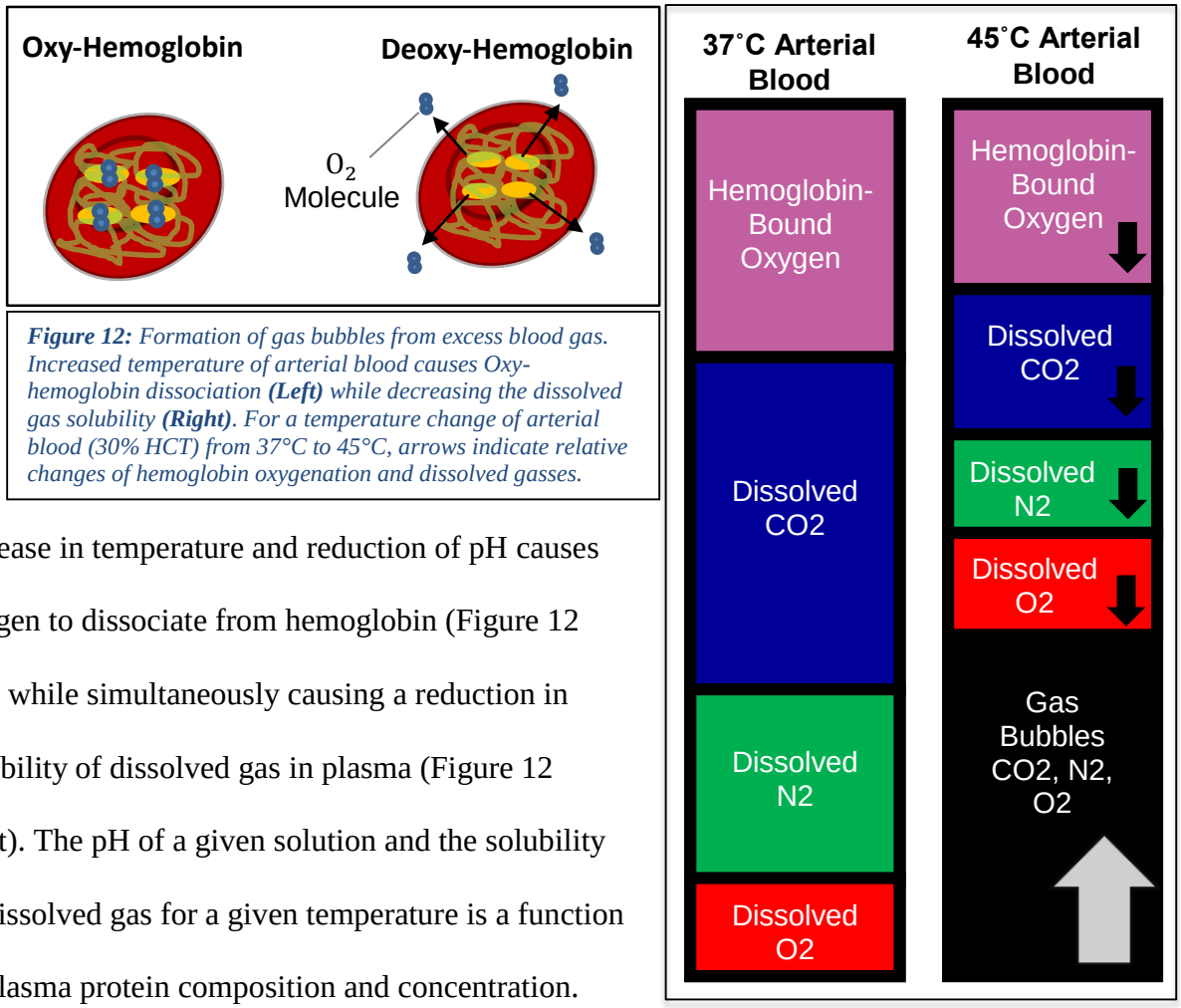

Figure 12: *Formation of gas bubbles from excess blood gas. Increased temperature of arterial blood causes Oxy-hemoglobin dissociation* ***(Left)*** *while decreasing the dissolved gas solubility* ***(Right)****. For a temperature change of arterial blood (30% HCT) from 37°C to 45°C, arrows indicate relative changes of hemoglobin oxygenation and dissolved gasses.*

subsequently form nanobubbles on the thermally deformed erythrocyte membranes, treating the troughs of the membrane as bubble nucleation sites. Nanobubbles on the membranes of adjacent erythrocytes are attracted to each other and coalesce drawing the erythrocytes together (Figure 13).

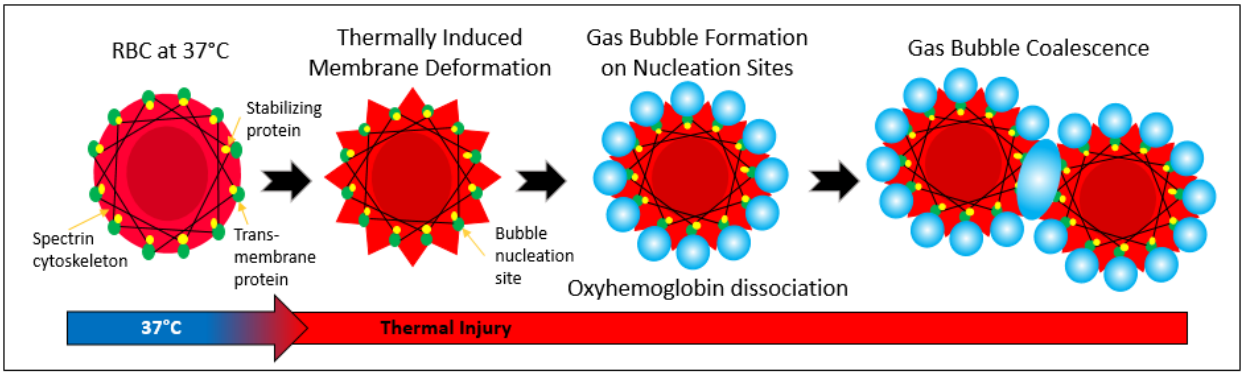

Figure 13: *Thermally induced nanobubble formation and coalescence.* ***Left to Right.*** *Schematic of erythrocyte membrane. Thermally induced membrane deformation forms potential bubble nucleation sites on membrane surface (second image shows exaggerated membrane deformation not to be confused with crenation). Temperature induced dissociation of oxygen from hemoglobin, and reduction of gas solubility. Gas nanobubble formation on membrane surface. Surface nanobubble coalescence and aggregation of erythrocytes. Gas bubble coalescence stabilizing an aggregate of erythrocytes. The schematic representation shown here is not drawn to scale.*

Oxyhemoglobin Dissociation

Hemoglobin oxygen saturation percent (SO_2) is a function of the partial pressure of oxygen (PO_2) (Table 4), this curve is called the oxygen saturation curve or the oxygen dissociation curve and is expressed by Hill's equation (Equation 4):

Table 4: Partial Pressures of gasses in blood phases (mmHg) [13]

Gas Species	Arterial Blood	Mixed Venous Blood
PO_2	100	40
PCO_2	40	46
PN_2	573	573

Equation 4: $$SO_2 = \frac{(PO_2/P_{50})^n}{[1+(PO_2/P_{50})^n]}$$

Where P_{50} represents the partial pressure of oxygen (in mmHg) such that 50% of hemoglobin is bound to oxygen, and n is the hills coefficient (n = 2.7 for humans) [13]. The oxygen dissociation

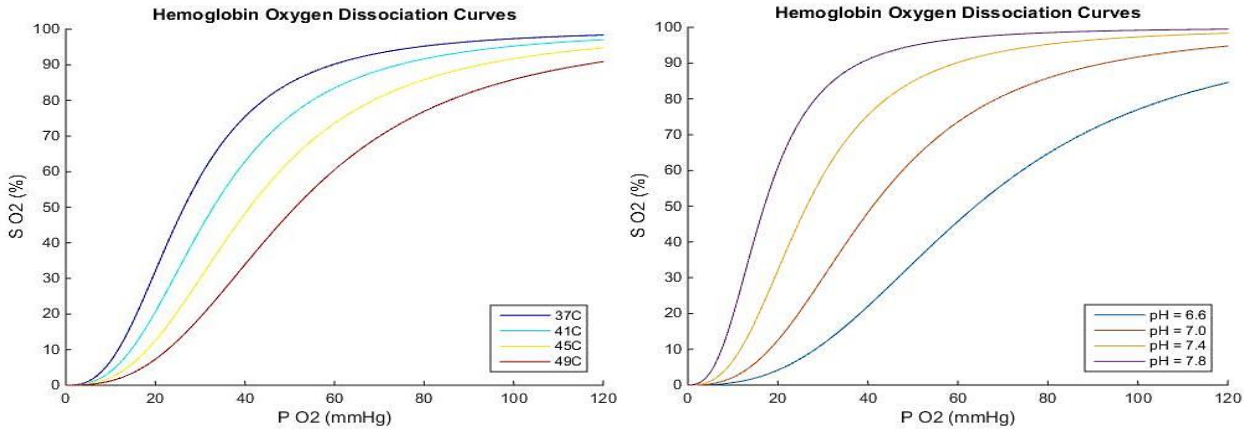

Figure 14: *Shifts in the oxygen dissociation curves due to changes in temperature and pH. Oxygen dissociation curve plotted versus PO_2 compared between changes of temperature (left) and pH (right). Based on equations from* [5 13].

curve is known to shift to the right with increases in temperature, $[H^+]$ (decreased pH), PCO_2, and 2,3 diphosphoglycerate (2,3 DPG) concentration (Figure 14). 2, 3 DPG is produced within the RBC as a glycolytic intermediate that influences the affinity of hemoglobin for oxygen. In venous blood, increased bicarbonate and carbonic acid corresponds to increased CO_2 and $[H^+]$. The decrease in pH causes a decrease in [2, 3 DPG] thus making oxyhemoglobin dissociation more likely to occur in venous blood (pH 7.35) than arterial (pH 7.4). In the case of thermal injury, pathological concentrations of plasma proteins may influence the blood pH by acting as either sources or absorbers of hydrogen ions; this would in turn affect oxyhemoglobin affinity. Dissociation curves for various temperatures (T), and pH for man can be computed from the normal SO_2 curve by multiplying the P_{50} value by a factor for temperature (f_T) (Equation 5) and pH (f_{pH}) (Equation 6): [5; 50]

Equation 5: $$f_T = 10^{0.024 * (T - 37)}$$

Equation 6: $$f_{pH} = 10^{-0.48 * (pH - 7.4)}$$

The total volume of oxygen (mL/L) bound to hemoglobin (Hb) in blood can be calculated from the hematocrit (HCT), oxygen binding capacity (C_{Hb}) of hemoglobin (C_{Hb} = 1.34 mL

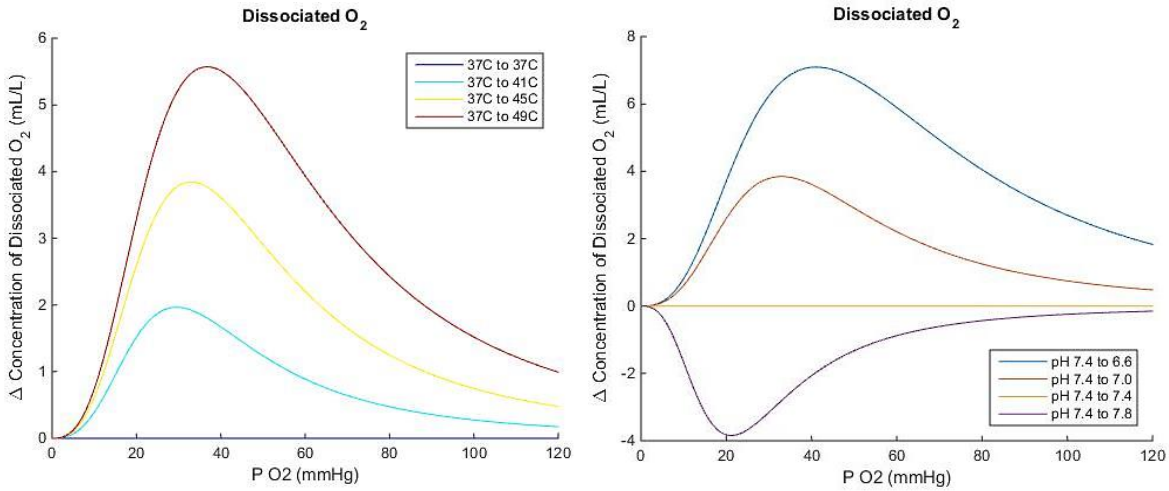

Figure 15: *Dissociated oxygen curves for changes of temperature and pH. Calculated volume of O_2 dissociated from human hemoglobin (30%HCT) due to change in temperature from 37°C to a target temperature(left) and change in pH from 7.4 to a target pH (right).*

O_2/gram Hb for humans), and hemoglobin concentration of a single erythrocyte ($[Hb]_{RBC}$) ($[Hb]_{RBC}$ = 33 g/L for humans)[13] (Equation 7).

Equation 7: $$[O_2]_{Bound} = SO_2 * HCT * [Hb]_{RBC} * C_{Hb}$$

When the temperature of a blood solution is increased, the oxygen dissociation curve is shifted rightward resulting in the dissociation of bound oxygen from hemoglobin. By subtracting the S_{O2} at various temperatures from the SO_2 at 37˚C, one can calculate the volume of bound O_2 that was released from hemoglobin as the temperature increased from 37˚C (Figure 15 left). By subtracting the SO_2 at various pH from the SO_2 at pH 7.4, one can calculate the volume of bound O_2 that was released from hemoglobin as the pH changed from pH 7.4 (Figure 15 right). The combined effects of temperature change, and pH changed from 37 ˚C and pH 7.4, respectively, on oxyhemoglobin dissociation in venous and arterial blood are shown in Figure 16.

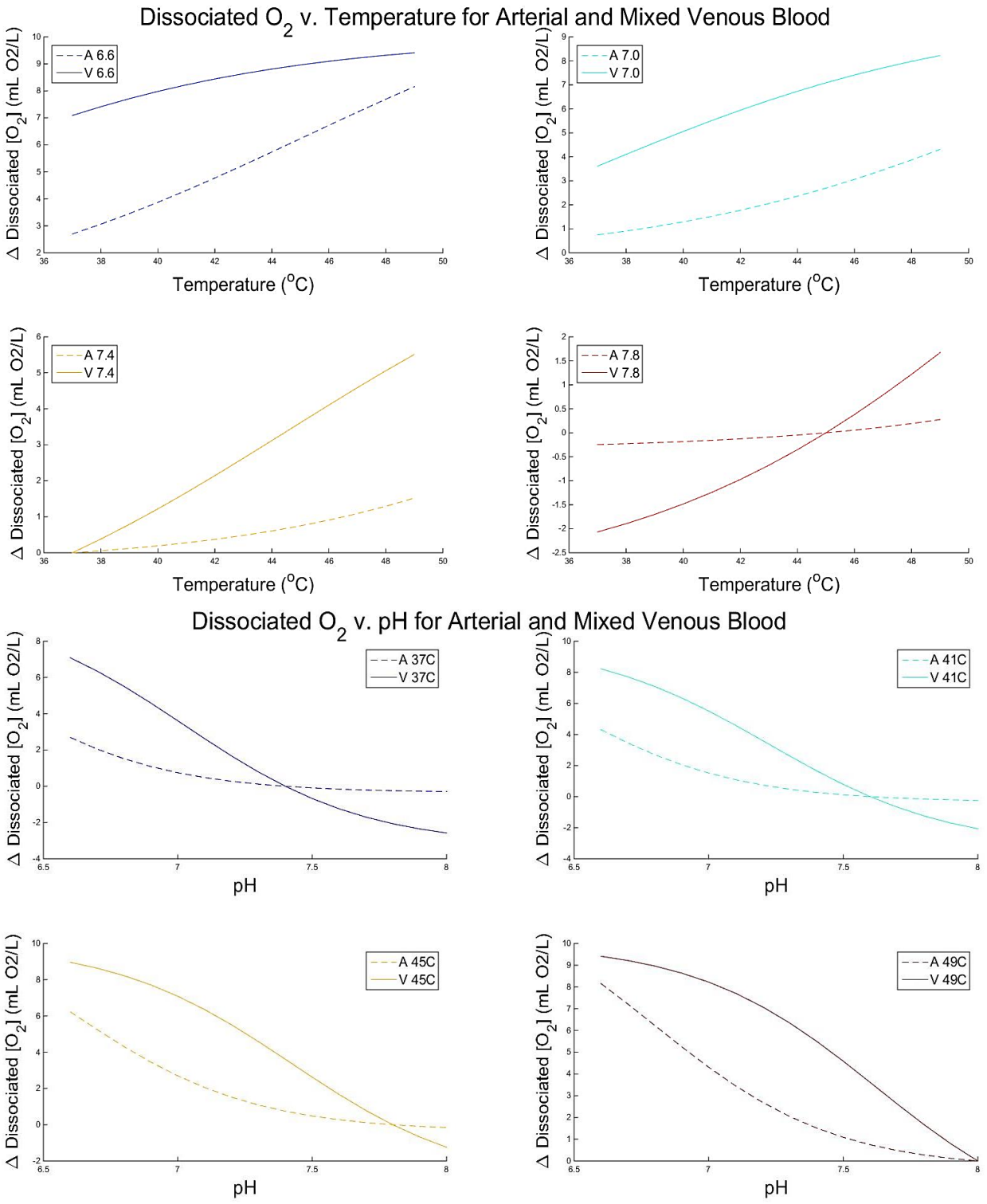

Figure 16: *Dissociated oxygen verses Temperature and pH for arterial and mixed venous blood. Calculated volume of O_2 dissociated from human hemoglobin (30%HCT) as a function of temperature and pH for arterial (A) (PO_2=100 mmHg) and mixed venous blood (V) (PO_2=40 mmHg).*

The results of the model indicates that the largest volume of oxygen is dissociated from

hemoglobin when the PO_2 is 32 mmHg for the temperature increase from 37˚C to 45˚C, and when the PO_2 is 38 mmHg for the temperature increase from 37˚C to 53˚C. The PO_2 in human arterial blood is 100 mmHg, and 40 mmHg in mixed venous blood. Interestingly, this suggests that more oxygen is dissociated from hemoglobin in mixed venous blood than in arterial blood. If, at these temperatures, the volume of oxygen dissociated from hemoglobin surpasses the solubility of oxygen in the plasma, bubbles will form. This may be an explanation for why erythrocyte aggregation would be more likely to occur in veins than arteries. The solubility of gas in solution is known to be temperature dependent, however, plasma proteins likely influence it as well.

Temperature Dependence of Henry's Law

The solubility of a given gas is a function of temperature as described by Henry's Law (Equation 8) [51].

Equation 8*:* $$k_{H,pc}(T) = k_{H,pc}(T^{\theta})e^{(-C\left(\frac{1}{T}-\frac{1}{T^{\theta}}\right))}$$

Where $k_{H,pc}(T)$is Henry's constant at some Temperature, $k_{H,pc}(T^{\theta})$ is Henry's constant at body temperature (310.15K), and C is the heat capacity of a given gas in water ($C_{O2} = 1700$, $C_{CO2} = 2400$, $C_{N2} = 1300$). The heat capacity of a given gas in blood has yet to be determined, this gap in knowledge will be addressed in Specific Aim 2. For the purpose of the model, the heat capacity of blood was assumed to be the same as that of water. The Henry's constant of each gas were calculated for temperatures ranging from 37°C to 53°C. For arterial and mixed venous blood phases, the concentration of each gas (mL/L) was then calculated at all temperatures by dividing their partial pressure by Henry's constant[13]. With an increase in temperature the amount of dissolved gas for all gas species decreased, in other words, gas is dissoluted as temperature is

increased. The dissoluted volume of gas is calculated by subtracting the dissolved gas volume at 37°C (Table 4) from that at a given temperature. This instantaneous dissolution of gas occurs with a simultaneous oxyhemoglobin dissociation and can cause more than 10 mL/L of total gas to be forced from solution (Figure 17). This gas cannot easily escape into the atmosphere so it

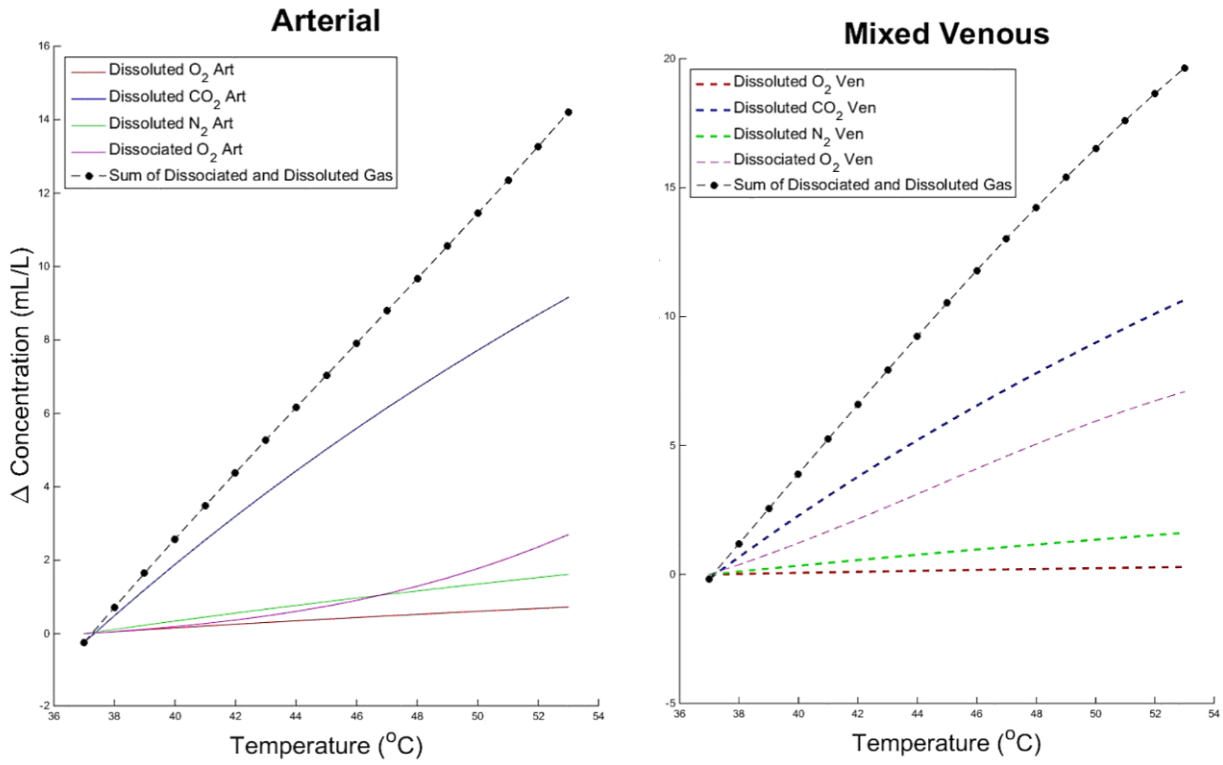

Figure 17: *Dissociated and dissoluted gas versus temperature in arterial and venous blood. Volume of O_2, CO_2, and N_2 gas dissoluted and O_2 dissociated from hemoglobin as a function of temperature for arterial and mixed venous blood.*

must form bubbles on blood components. Being that hemoglobin is contained within the RBC, when oxyhemoglobin dissociation occurs the released oxygen is already located near or around the RBC and is unable to diffuse into the plasma because of the decreased solubility caused by elevated temperature.

Dissolved CO_2 accounts for a small fraction of blood CO_2 transport [52]. Carbonic anhydrase is only within the RBC, and does not catalyze the reaction of CO_2 to bicarbonate in the plasma. CO_2 must diffuse into the RBC to be converted to bicarbonate before it is exchanged

with chloride by band 3 back into the plasma, on a one-for-one basis, by a process known as the chloride shift [52; 53]. Most CO_2 is carried in the blood as bicarbonate and, in normal blood, is converted from CO_2 to bicarbonate at a rate of 200 mL/minute [52]. The fast conversion of CO_2 to bicarbonate by carbonic anhydrase makes it such that CO_2 likely contributes less to the sum of dissoluted gas in Figure 17 than does O_2. These combined effects make it likely that oxygen is the main component of nanobubbles on the surface of the RBC membrane.

Nanobubble Model

In the case of erythrocytes, the nucleation sites in which the nanobubbles form are dependent on the shape of the membrane (see membrane deformation section). The sizes and behavior of such nanobubbles are dependent upon the volume of oxygen dissociated from hemoglobin, and the ability of the solution to dissolve this oxygen along with other gasses. Membrane deformation, gas solubility, bubble contact angle, and oxyhemoglobin dissociation all provide possible explanations for our observed differences in erythrocyte aggregation between species.

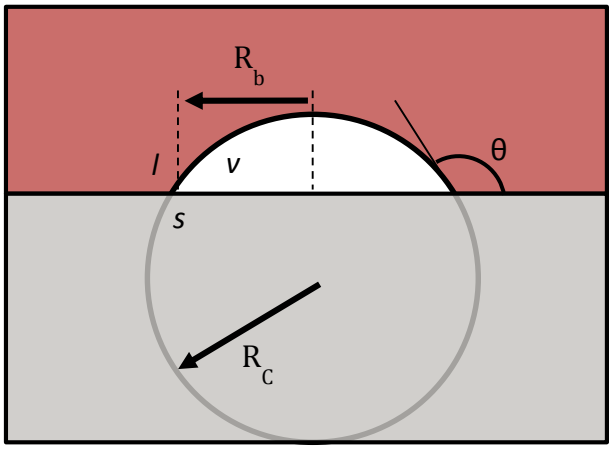

Figure 18: *Schematic representation of vapor nanobubble. Vapor (v, white) in liquid (l, red) supported by solid material (s, grey) R_b, R_c, and θ represent base radius, radius of curvature, and contact angle, respectively. Figure adapted from [2]*

Surface nanobubbles are known to nucleate and persist on imperfections of a surface. Nanobubbles have geometries described by their base radius (R_b), radius of curvature (R_c), and contact angle (θ) (Figure 18). As described in the 'Membrane Deformation' section, intermembrane proteins, namely Band 3, tend to aggregate on the surface of erythrocytes in a formation resembling the spectrin skeletal network[12]. This aggregation is a function of temperature for some species. The divots that form

between aggregates of Band 3 on the extracellular membrane surface have a radius of ~100nm. Assuming a bubble base radius to be similar to that of the divots described above, and with knowledge of the surface area of a whole erythrocyte, simple geometry allows for an estimation of the number of bubble nucleation sites per cell, and subsequently in an erythrocyte solution with respect to the hematocrit and bubble radius .With an erythrocyte surface area of 136 um^2 and assumed a bubble base radius' of 25nm, 50nm, 100nm, and 150nm each erythrocyte would have 6.9264_{x10^6}, 1.7316_{x10^6}, 4.3290_{x10^5}, 1.9240_{x10^5} potential bubble nucleation sites, respectively. The total number of nucleation sites on cells in one liter of erythrocyte solution can then be calculated as a function of hematocrit for a given base radius for erythrocytes each having a volume of 90 fL (Figure 20).

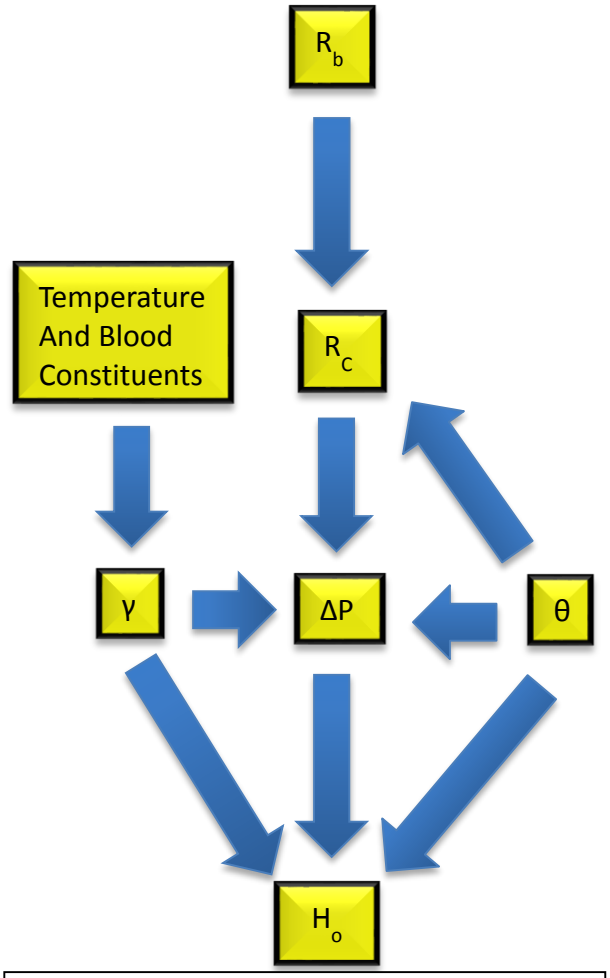

Figure 19: *Flow-diagram representation of variables that impact nanobubble dynamics and behavior. R_b is base radius, R_c is radius of curvature, γ is surface tension, ΔP is the pressure difference between the bubble and atmosphere, θ is contact angle, and H_0 is the maximum coexistence separation between two bubbles.*

The dynamics and behavior of surface nanobubbles depends on the interplay between various variables that are characteristic of the unique properties of the liquid in which the cells are suspended, and the surface of the erythrocyte. Figure 19 shows a flow chart of the relationship between these

variables some of which are displayed schematically in Figure 18. Using trigonometry the bubbles radius of curvature (R_c) can be calculated as (Equation 9):

Equation 9: $$R_c = \frac{R_b}{\sin\theta}$$

where R_b is base radius, and θ is contact angle [2].

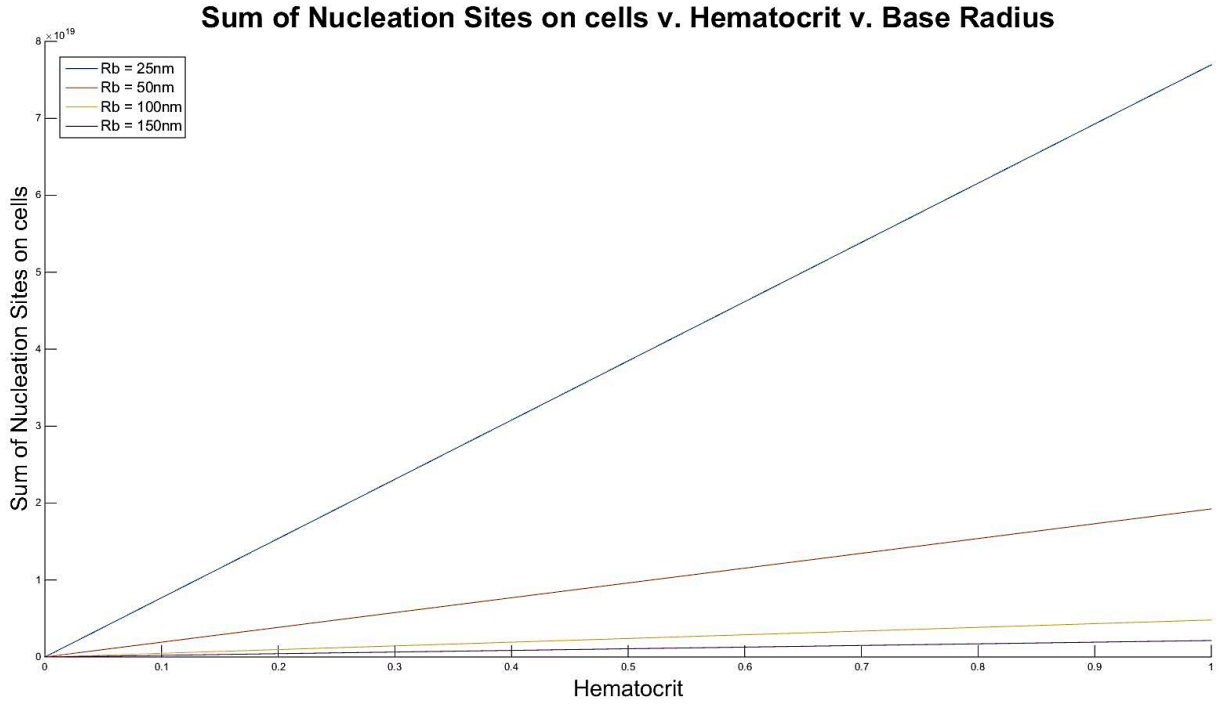

Figure 20: *Sum of potential bubble nucleation sites on erythrocytes versus hematocrit and bubble base radius. Number of nucleation sites in one liter of erythrocyte solution as a function of hematocrit (0% -100%) for bubbles of base radius' of 25 nm, 50 nm, 100 nm, and 150 nm.*

According to the Young-Laplace equation, the excess pressure inside a free (non-supported) gas bubble (ΔP) with respect to the pressure of the liquid surrounding it is calculated as (Equation 10);

Equation 10: $$\Delta P = \frac{2\gamma}{R_c}$$

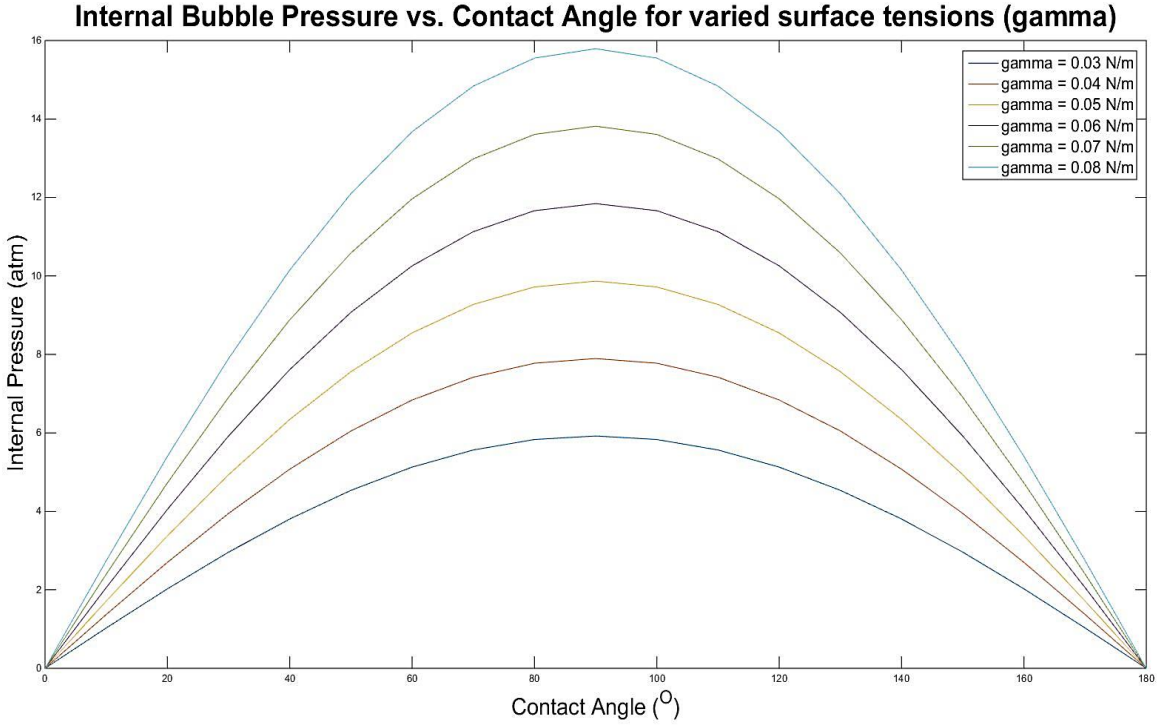

Figure 21: *Internal bubble pressure as a function of contact angle. Plotted for surface tensions ranging from 0.03 to 0.08 N/m.*

where γ (gamma) is surface tension at the liquid-vapor interface [54] (Figure 21).

Surface tension at the liquid-vapor interface, for most fluids, is known to decrease with increased temperature. For blood serum from healthy human donors this relationship has been empirically described as (Equation 11):

Equation 11: $\gamma_{blood\ Serum} = -0.3676T + 66.072$

where T is temperature [9] (Figure 22).

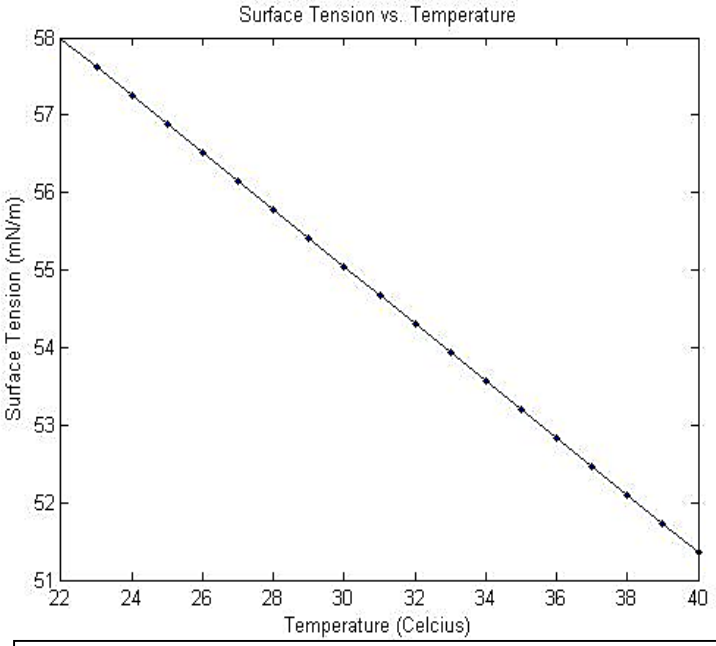

Figure 22: *Temperature dependence of liquid-vapor surface tension of blood serum. Calculated from Equation 11.* [9]

It is also noted that plasma proteins including fibrinogen and albumin have been shown to act as surfactants in the blood and in doing so, influence the surface tension as a function of temperature and pH [55; 56].

When a nanobubble becomes attached to a solid surface, there is a reduction of pressure within the bubble. This makes their attachment to a surface energetically favorable. Compared to the excess pressure (ΔP_{free}) within a free bubble, the excess pressure (ΔP) within a supported bubble is smaller and the ratio is given by the relation below [2] (Equation 12)(Figure 24);

Equation 12: $$\frac{\Delta P}{\Delta P_{free}} = [\, f(\theta)]^{1/3}$$

with (Equation 13) (Figure 23);

Equation 13: $$f(\theta) = \frac{1}{2}(1 + \cos\theta) + \frac{1}{4}(\cos\theta \sin(\theta)^2)$$

From the calculations of excess pressure within a bubble it is found that the total pressure within a bubble (P_i) is described by Equation 14;

Equation 14: $P_i = P_o + \Delta P$

where P_o is atmospheric pressure, and ΔP is the pressure difference between the supported bubble and atmosphere [54]. It is important to notice that in the case of non-wetting ($\theta = 180^{\circ}$), the bubble becomes a thin film on a surface and does not have excess

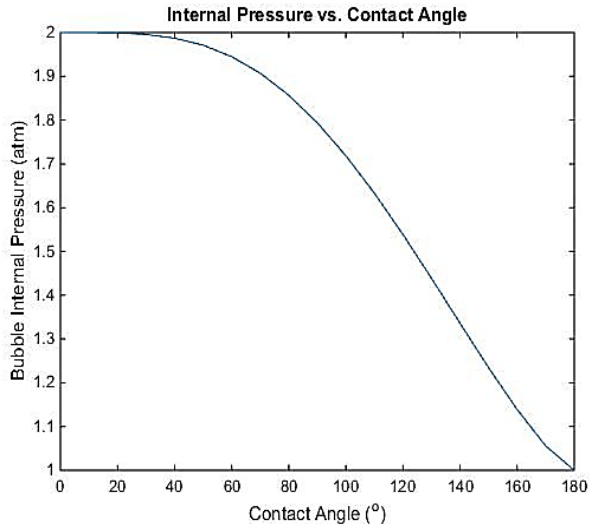

Figure 23: *Internal bubble pressure versus contact angle. Sigmoidal relationship between the ratio between internal bubble pressure of a supported bubble and a free bubble as a function of contact angle. Calculated from Equation 13.* [2]

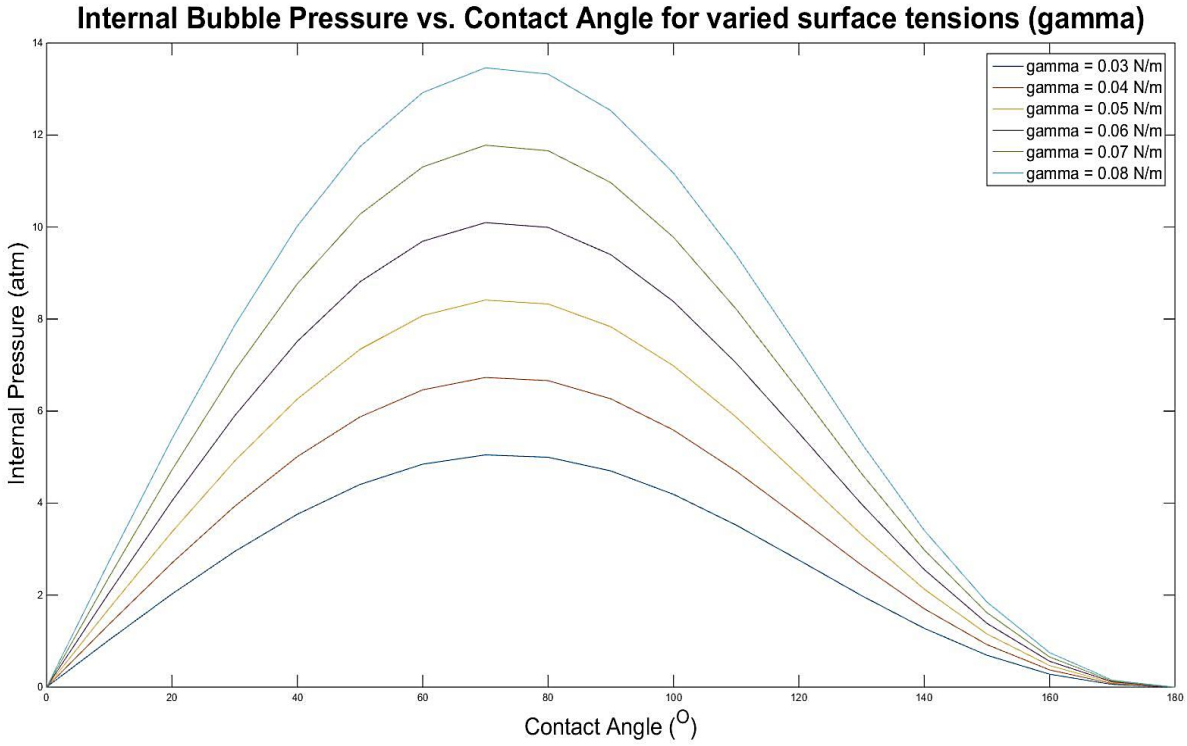

Figure 24: *Internal bubble pressure as a function of contact angle and surface tension. Plotted for surface tensions ranging from 0.03 to 0.08 N/m including compensation with Equation 13.*

pressure. In the opposite extreme of total-wetting ($\theta = 0^{\circ}$), the bubble is has the same excess pressure as its free counterpart [2].

Bubbles coalescence occurs as a result of a long-range attractive forces that exist between bubbles. To this end, empirical and computational models of bubble-bubble interactions have become the subject of many research groups. In a study by Parker et al., surface forces between glass surfaces were measured as a function of temperature. As temperature is increased from 22 to 41°C, the range of the attraction force between the surfaces in water increased (Figure 25) [6]. After the system was allowed to cool back to room temperature (middle curve), the strength of the attractive interaction did not immediately return back to its value at room temperature before heating. The failure of the attractive force to return to its value before heating suggests that if the measured forces are a result of coalesced bubbles as it was hypothesised, that these bubbles are persistant. To test the effects of surface tension on the attraction and adhesion forces between the surfaces the experimental procedure was repeated for NaCl solutions with the addition of varied concentrations of ethanol. NaCl, increased the liquid-vapor surface tension and increased the range, strength, and adhesion forces between the surfaces. The addition of ethanol, reduced the liquid-vapor surface tension and decreased such parameters [6]. These results corroborate that the increase in attractive force with increased temperature may be a result of surface bubble interactions as gas de-dissolves from the solution, and is a function of surface tension [6].

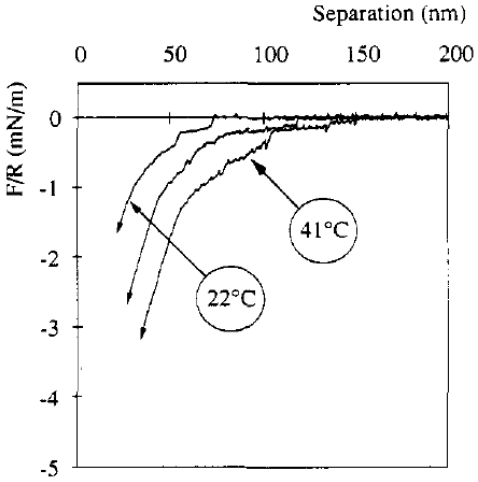

Figure 25: *Long-range attractive forces between nanobubbles versus temperature and distance. Forces measured between surfaces in water for two temperatures (indicated by arrows) as a function of separation distance (indicated by arrows). Middle curve represents the measured force after apparatus was allowed to cool to room temperature from 41 °C. Figure from [6].*

Small nanobubbles have higher inner pressures than larger nanobubbles. It has been shown that when two nanobubbles coalesce, the inner pressure of the coalesced bubble is significantly less than the inner pressures of the bubbles from which it formed (Table 5). This is in addition to the significant increase in volume of the coalesced bubble after coalescence indicating that bubble coalescence is energetically favorable [54].

Table 5: Bubble properties before and after coalescence. Bubble dimensions, inner pressure and volume. Measurements before and after bubbles 1 and 2 coalesced to form a third bubble. Table adapted from [54].

Bubble	Height (nm)	Base Radius (nm)	Pressure (atm)	Volume ($x10^6$ nm^3)
1	72.4	574	1.58	37.7
2	28.6	279	2.02	3.5
Coalesced	96.4	821	1.40	102.8

There is an abundance of oxygen in blood and a notable temperature-, and PO_2-dependence of its dissociation from hemoglobin, and dissolution out of blood plasma. Furthered by the increased tendency of oxygen to dissociate from hemoglobin in blood with PO_2 and pH typical of venous blood, there is a strong basis for the investigation of oxygen solubility and partial pressure as mediators of erythrocyte aggregation. The results of this model indicate that venous blood provides a more favorable environment for erythrocyte aggregation than arterial blood.

Experimental Materials and Methods

Blood Acquisition, Preservation, and Storage

All experiments were performed under the oversight of, and in compliance with the guidelines established by Stony Brook University's Institutional Animal Care and Use Committee (IACUC) through a tissue sharing program. Whole blood from healthy mammalian species (pigs, sheep, mice, and rats) was drawn via cardiac puncture or venipuncture and collected into vacutainers containing EDTA as an anticoagulant. Whole blood collected via venipuncture, with the addition of disodium-EDTA, from healthy human volunteers was purchased commercially (Bioreclamation IVT, Westbury NY). Erythrocytes were separated from other blood constituents via centrifugation. Platelet poor plasma (PPP) was aspirated following the first centrifugation and stored separately for use in experiments that required erythrocytes suspended in autologous plasma. Erythrocytes were then washed three times by resuspension in PBS (Sigma), centrifugation (The Drucker Co.) at 3369 rpm for five minutes, and aspiration of the supernatant.

All specimens were washed three times daily and maintained at 4˚C for one week, at most, or until signs of cell lysing were noticed. Following each centrifugation, the color of the supernatant was recorded as one of the following; clear, slightly cranberry, or cranberry. The color of the supernatant served as an indication of cell viability. A clear supernatant after the third washing cycle indicated the absence of lysed cells, while a cranberry color indicated free hemoglobin in the supernatant from lysed cells. If the supernatant was cranberry colored after the third centrifugation, the cells were discarded.

Erythrocyte Suspensions and Treatments

Erythrocyte suspensions of known hematocrits were made prior to each experiment by adding prescribed volumes of packed erythrocytes to a known volume of prepared solution. Solutions containing dextrans of molecular weight 500 kDa (Fluka BioChemika), and 110 kDa (Sigma), bovine serum albumin (BSA) (Sigma Aldrich), human serum albumin(Millipore), human plasma fibrinogen (MilliPore), were prepared in PBS. It has been reported that erythrocyte aggregate sizes are similar in dextran 500 kDa to that of normal, autologous plasma and the intensity of such aggregation is dependent upon the polymer molecular size and concentration [57; 58]. Suspensions were also made in autologous platelet poor plasma (PPP), and PBS (Sigma). All specimens were used within one hour of preparation.

Erythrocytes were incubated with purchased rabbit polyclonal antibodies (Abcam) to Band 3 and Glycophorin C (GYPC) with human reactivity. For non-specific binding, anti-$\alpha_v\beta_3$ (Chemicon International) was purchased. To prevent repeated freeze-thaw cycles between trials, anti-Band 3 and anti-GYPC were aliquoted and stored at -20 ˚C. Anti-$\alpha_v\beta_3$ was stored at 4 ˚C as suggested by the manufacturer. Anti-Band 3, and anti-$\alpha_v\beta_3$ were stored at a concentration of 1 mg/mL in PBS, and anti-GYPC was stored at 1 mg/mL in PBS buffer with 50% glycerol. Erythrocytes were treated with DIDS (Sigma), stored at 4 ˚C. Erythrocytes were also fixed with glutaraldehyde, stored at -20 ˚C.

Erythrocyte treatments, to allow for specific or non-specific binding to occur, were performed by incubating and stirring 50% hematocrit solutions in PBS for 15 minutes at 37 ˚C with the concentrations of antibodies recommended by their manufacturer, and previous literature [59]. For treatments with anti-Band 3, anti-GYPC, and anti-$\alpha_v\beta_3$ erythrocytes were incubated in concentrations of 5.0 µg/mL, 6.25 µg/mL, and 10.0 µg/mL, respectively. Anti-band

3 binding was validated by flow cytometry at room temperature and 37 ˚C. Erythrocytes were treated with DIDS, in a concentration of 0.1 mg/mL, using the same procedure as for antibody treatments. Erythrocytes were fixed by incubating, and stirring 10% hematocrit solutions in 0.05% glutaraldehyde in PBS for 10 minutes at 37 ˚C.

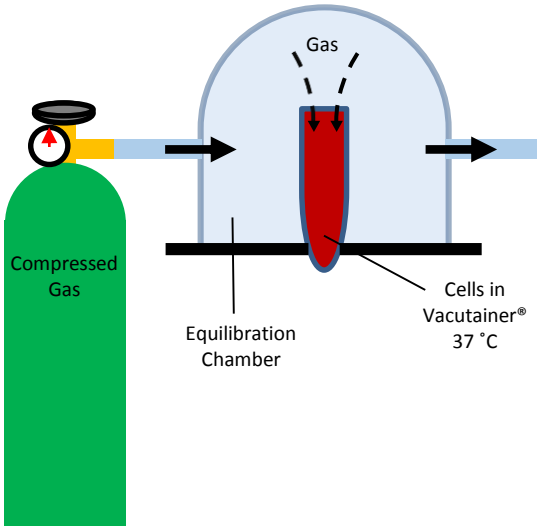

Figure 26: *Equilibration of erythrocyte solutions. Schematic representation of erythrocyte solution in a temperature-controlled equilibration chamber.*

Equilibration of erythrocyte solutions (20% HCT) was performed in a sealed, and temperature-controlled equilibration chamber schematically represented in Figure 26. The equilibration chamber allowed for testing of particular hemoglobin oxygenation states (Figure 27) and was constructed from an enclosed water jacket heated to 37 ˚C by warm water pumped within its walls. Compressed gas was mixed to a prescribed partial pressure of oxygen in residual nitrogen (Extra Dry, Airgas, LLC) and connected to the chamber where a continuous gas stream was passed through the interior of the chamber. Erythrocyte suspensions were allowed to equilibrate with the controlled atmosphere inside the equilibration chamber for 15 minutes before each experiment. Continuous stirring (Fisher Scientific Thermix 120S) of the erythrocyte solution at 200 rpm with a magnetic stir bar expedited the equilibration process.

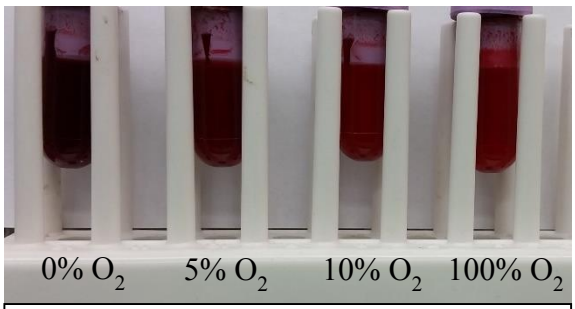

Figure 27: *Image of erythrocyte suspensions equilibrated with 0, 5, 10, and 100% oxygen (left to right). Image of 20% HCT in fibrinogen 2 mg/mL with DIDS inhibitor.*

Dissolved Oxygen and pH Measurement

Measurements of pH and dissolved oxygen were performed for 2mL test solution samples in glass test tubes. Test solutions were made by serial dilutions with PBS then heated for 15 minutes using a dry bath incubator (Fisher Scientific) to a prescribed temperature of 37°C, 41°C, 45°C, or 49°C. For each test solution, while being heated, a pH measurement was made with a pH electrode (VWR Scientific) followed by a dissolved oxygen measurement performed using a modified Winkler's method for small sample volumes [60; 61]. All purchased reagent solutions (Hach, Inc.) were prepared as per standard methods (Method No. 4500-O-C) [61] and used within one day of preparation.

The dissolved oxygen measurement procedure was performed as follows: 1mL mineral oil (Walgreen, Co.) was added to the top of the incubating 2 mL test sample to avoid contact between air and the sample limiting atmospheric oxygen diffusion into the sample during the dissolved measurement [62]. Next, 20 µL $MnSO_4$ was introduced into the sample below the mineral oil layer, followed by a similar addition of 20 µL alkali-iodide-azide. In the presence of oxygen, a manganese hydroxide precipitate (orange/brown) formed immediately after the additions and was complete within 3 minutes [60]. Afterwards, 0.2 mL of concentrated sulfamic acid was added to the manganese hydroxide precipitate below the mineral oil layer, dissolving it within 3 minutes and forming yellow iodine solution, in proportion to the oxygen concentration below the mineral oil layer. Exactly 1 mL of the yellow iodine solution was extracted from below the mineral oil layer and transferred into a beaker. The 1 mL of iodine solution in the beaker was diluted to 10 mL by adding de-ionized water to improve the resolution and ease of the titration measurement. By adding de-ionized water to the iodine solution, the iodine was only diluted, the concentration of iodine in the solution remained unchanged. 1 mL of 0.025 M

sodium thiosulfate solution was also diluted to 10 mL with the addition of de-ionized water, also to improve the resolution and ease of the titration measurement. Next, 1-2 drops of starch indicator solution was added to the iodine solution and a blue color appeared. Finally the iodine-starch solution was titrated with the diluted sodium thiosulfate solution until the color changed from a dark blue to a colorless end point. 0.1 mL of this titrant corresponds to 2 mg/L of DO in the original sample.

In-Vitro Aggregation Models

Temperature-Controlled Heated Stage

A series of aggregation experiments was conducted in the absence of flow to evaluate the effects of temperature on aggregation, the contribution of macromolecules to erythrocyte aggregation and the intrinsic species dependence. These experiments were enabled by the

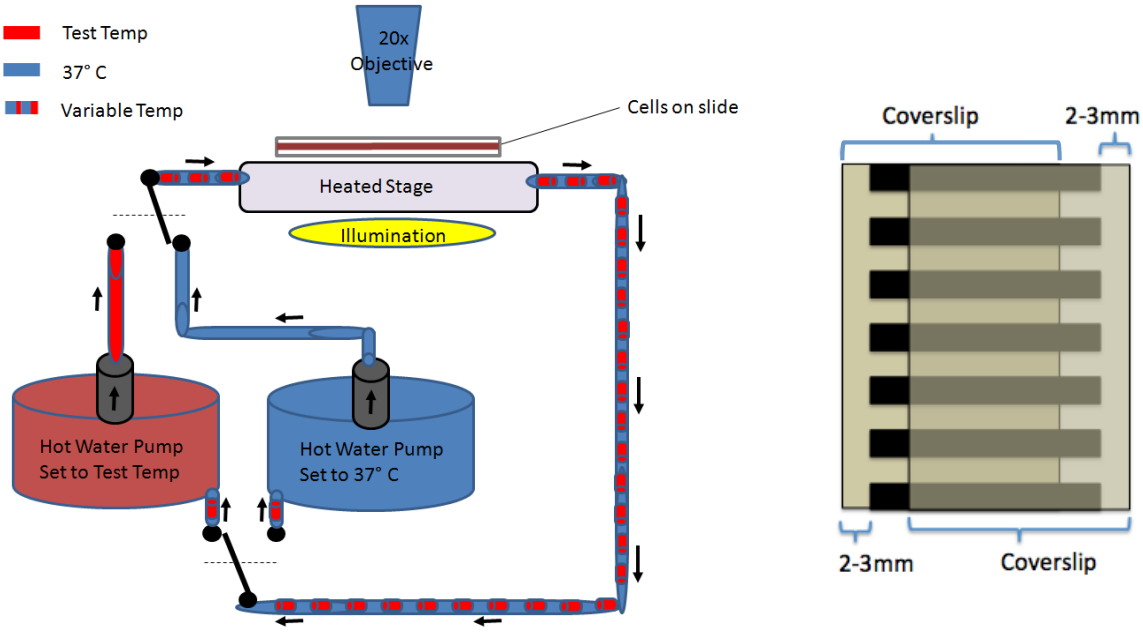

Figure 28: *Schematic representation of heating stage and temperature control system. Constructed to allow for a quick change of temperature in the heating stage by switching flow from a 37°C pump to a test temperature pump (Left). Slide with channels (depth = 160 μm) (Right).*

construction of an apparatus such that simultaneous heating and imaging of erythrocytes could be performed as described below (Figure 28).

Channels of fixed depth (160 μm) were created between two cover slips by affixing double-sided carbon tape strips (Electron Microscopy Sciences) between the pair of cover slips (Corning, Inc.)(Borosilicate glass, 0.17 mm thick). The tape precisely spaced the coverslips 160 μm apart (Figure 28 right). Each slide contained six channels with dimensions 3-5 mm wide and 20-25mm long, each capable of accommodating 9.6-20 μL blood samples. Before constructing the channels these coverslips were washed, for a minimum of 12 hours, with 1 M sodium hydroxide to minimize cell-slide interactions [63]. Blood samples were introduced to each channel at one end and were allowed to wick into them until full.

The absence of flow in this model allowed for the sedimentation of RBCs to the bottom of the channels, this sedimentation allowed a given hematocrit to appear much higher after settling than before. To account for this apparent increase of hematocrit caused by settling a 2-dimensional approximation of hematocrit, termed "monolayer hematocrit", was introduced that displayed hematocrit as % cells by area instead of % cells by volume (Figure 29).

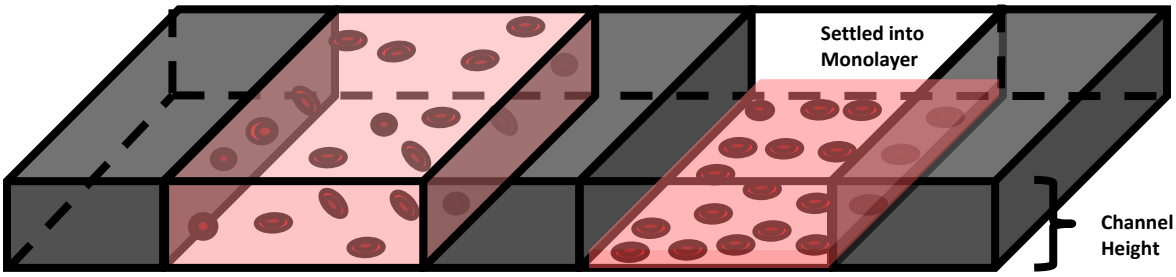

Figure 29: *Sedimentation of erythrocyte into monolayer. Erythrocyte suspension in channel before (left) and after (right) settling into a monolayer.*

The actual hematocrit of a sample that is required for a desired monolayer hematocrit was approximated using Equation 15 ;

Equation 15: $$Actual\ HCT = Monolayer\ HCT\ * \frac{RBC\ height}{Channel\ Height}$$

where the channel height is 160 µm and the RBC height is 2 µm. Thus, to achieve 5, 10, 20, and 30% monolayer HCT, solutions having actual hematocrits of 0.0625, 0.125, 0.25, and 0.375%, respectively, were used.

These channels were heated using a hot water circulation system (Figure 28) which we have constructed to emulate the rapid change of temperature that blood is subject to during thermal injury while allowing for the observation of a given sample before (37 °C), during, and after heating. This heating system allows us to quickly (< 3 seconds) and precisely (±0.3°C) change the temperature of the system. In short, two hot water pumps (VWR Scientific) each heat a 5 gallon water reservoir from which water is pumped and circulated through a glass walled heating stage on which the channels containing the samples are placed. One of the pumps is set to 37 °C and the other is changed to the required test temperature for each trial.

The glass walled heating stage used in these experiments was constructed from 1.0 mm thick borosilicate glass microscope slides (Fisher Scientific) spaced 0.5 cm apart with glass tubing, and similar glass tubing serving as the inflow and outflow (Figure 28). The heating stage was sealed with two-part epoxy. The optically transparent glass from which it was constructed allowed for trans-illumination and also quickly conducted heat from the water within to the cells in the channels. Throughout the experiments, the temperature of the water inside the heating stage was monitored with an electronic thermometer (Fisher Scientific) inserted in the heating stage and was confirmed outside (next to the channels) with thermochromic film (Edmund Optics) (Figure 30). The heat profile and heating time shown experimentally by the thermochromic film on the heating stage confirmed

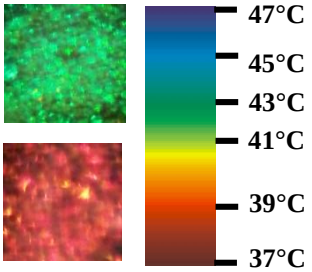

Figure 30: *Thermochromic film.* ***Left-Top)*** *Magnified image (200x) of thermochromic film heated to 41°C.* ***Left-Bottom)*** *Magnified image (200x) of thermochromic film heated to 38°C.* ***Right)*** *Thermochromic film calibration scale.*

that the high flow rate and conduction of heat through the glass layers was sufficient to and uniformly heat our samples.

While thermochromic film proved to be a good measure of the temperature at the top surface of the heating stage, the plastic film and liquid crystals from which it is composed are likely to have different heat conduction properties than that of blood surrounded by glass. In order to ensure that the temperature measured with thermochromic film is the same as temperature of the cells of interest, a calculation of the time required for heat transfer was necessary. This was estimated using the one-dimensional form of Fourier's Law of Conduction (Equation 16);

Equation 16: $q_x = -k\frac{dT}{dx}$

where q_x represents the local heat flux density ($W \cdot m^{-2}$), k is the material conductivity ($W \cdot m^{-1} \cdot K^{-1}$), x is the position within a material (m), and T is temperature (K). When the above equation is integrated from the bottom surface to the top surface of a homogeneous material at a constant temperature, the heat flow rate is calculated as (Equation 17);

Equation 17: $\frac{\Delta Q}{\Delta t} = -k\,A\,\frac{\Delta T}{\Delta x}$

where A is the cross sectional surface area (m^2), $\Delta Q = qA$ is the amount of heat transferred (W), ΔT is the temperature difference between the top and bottom surface (m), Δx is the thickness of the material (m), and Δt is the total time required for heat transfer from bottom to top.

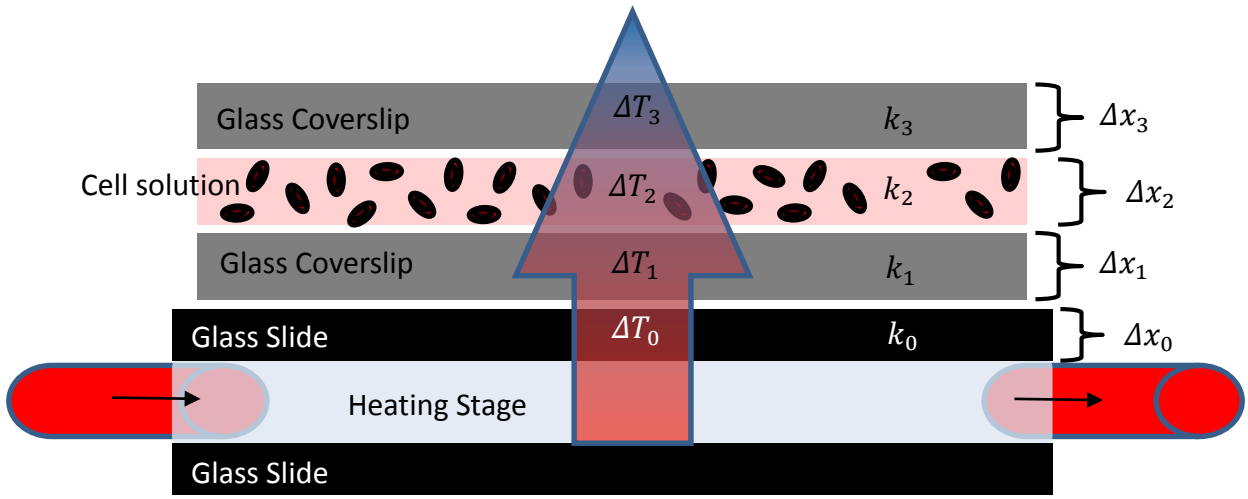

Figure 31: *Heat transfer schematic. Heat transfer through each layer from the heating stage to the erythrocytes in solution. Δx represents the thickness of each layer (m), k represents the material conductivity ($W \cdot m^{-1} \cdot K^{-1}$), and ΔT represents the difference in temperature between the top and bottom of each layer (Kelvin). The fixed values represented in the figure are as follows; $\Delta x_1 = \Delta x_3 = 1.0_{x10^{-3}}$, $\Delta x_2 = 1.7_{x10^{-4}}$ m, $k_0 = k_1 = k_3 = k_{borosilicate\ glass} = 1.2\ W \cdot m^{-1} \cdot K^{-1}$. Values for ΔT depend on the prescribed test temperature.*

In the case of heat transfer from our heating chamber to the cells of which it is heating, each layer that the heat will pass through must be calculated separately. A schematic representation of heat transfer through the system is shown in Figure 31. The time required to heat the cells is equal to the sum of the heating times required for the top of the heating chamber (Δt_0, borosilicate glass slide, $k_0, \Delta x_0$), the bottom of channel (Δt_1, borosilicate glass coverslip, $k_1, \Delta x_1$), and the cell solution (Δt_2, PBS, $k_2, \Delta x_2$). Based on these equations, the time required to heat cells from 37˚C to 45˚C is 2.57 seconds.

Aggregation of Stationary Erythrocytes: Dynamic Heating

In the stationary, dynamic heating experimental group we incubated erythrocytes suspended in PBS at 37 ˚C before adding them to a slide, also at 37 ˚C, where they were allowed to settle before rapidly increasing their temperature to a test temperature (stationary dynamic heating) with our temperature control system (see Figure 28) while images were acquired. Erythrocytes from species including pig, rat, sheep, and mouse were suspended in PBS with hematocrits ranging from 5.0% to 20.0% tested at temperatures in the range of 35-49 ˚C after equilibration with room gas. As a control experiment, the test temperature was set to 37 ˚C. An image was taken at a rate of 1Hz for a period of 150 seconds. The stationary nature of this system enabled us to test the hypothesis that, upon a rapid temperature change, there exists a long-ranged attractive force between neighboring erythrocyte membranes that differs between species.

Aggregation of Settling Erythrocytes: Static Hyperthermia

In the settling, static hyperthermia experimental model, erythrocytes from pigs, mice, and rats were suspended in PBS with added macromolecules of various concentrations. The solutions contained PBS with either bovine serum albumin or dextran 110kDa which were heated to a test temperature of 37 ˚C, 45 ˚C and 53 ˚C in a sample cup (Evergreen Scientific), and equilibrated with room gas before being added to a slide of the same temperature (static hyperthermia) where they were allowed to settle before image acquisition. The solutions tested contained bovine serum albumin (BSA) and dextran at concentrations of 1.5, 3.0, 4.5, and 6.0 g/dL. RBCs suspended in PBS were used as a control group. This series of experiments differs from the settled dynamic heating experiments in that the temperature of the cells was not changed, rather they are maintained at the test temperature for the duration of the experiment.

Vertical Flow System

Erythrocyte aggregation is known to increase the sedimentation rate within a solution, however, it can be prevented by high shear forces. At high flow rates, the radial distribution of erythrocytes in a channel is uniform in both horizontal and vertical flow systems. At low flow rates, erythrocytes aggregate and sediment. This presents a problem with studying aggregation in horizontal flow systems because the radial distribution of erythrocytes in the channel becomes asymmetric when cells settle to the bottom and a cell-free layer forms above[64]. Eventually, low flow in a horizontal channel can obscure observed aggregation behavior by increasing flow

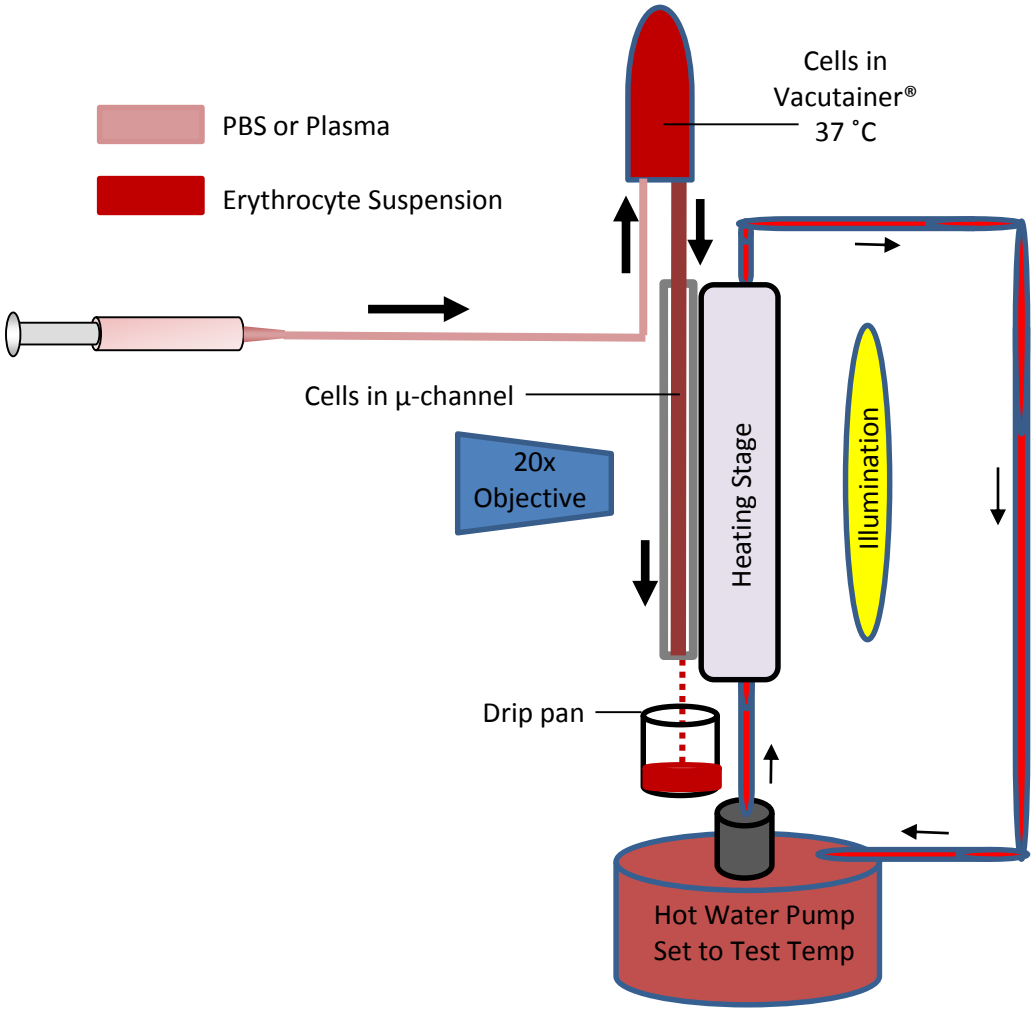

Figure 32: *Schematic representation of the vertically oriented microfluidic system. A horizontally oriented microscope imaged erythrocytes in a vertical channel. Temperature was controlled with heating stage.*

resistance and apparent viscosity [24; 64; 65; 66]. The asymmetry that occurs in horizontally oriented channels does not occur in vertically oriented channels, however, changes in the annular cell-free region become influenced by aggregation as described by the Fahraeus effect [24].

A vertically oriented microfluidic channel was designed as a model of erythrocyte aggregation in the zone of stasis immediately after thermal injury (Figure 32). In this model the limitations of the settling and stationary aggregation models were addressed by allowing normal interactions between erythrocytes to occur in flow. This enabled the observation of dynamic aggregation behavior and subsequent rheological effects.

Erythrocyte suspensions were prepared as described above, and added to a vacutainer and oriented up-side-down directly above the microchannel. The vacutainers were filled with the erythrocyte suspension by overfilling and sealing from the atmosphere, caution was taken not to allow air into the vacutainer. By isolating erythrocytes from the atmosphere we ensured maintenance of their oxygenation state. The vacutainer served as a feed reservoir and was attached to a syringe/syringe pump with polyethylene tubing (Becton Dickinson, inner diameter = 0.86mm, outer diameter = 1.27mm). The syringe pump (KD Scientific) was set to infuse in order to pressurize the vacutainer and drive flow of the solution toward the microchannel. The vertically oriented microchannel (Drummond Scientific, inner diameter = 0.487mm) was connected to the vacutainer with an inert, silicone-based elastomer tubing (A-M Systems Inc., inner diameter r = 0.635mm, outer diameter = 1.193mm), and was attached to the heating stage which was mounted on an x,y,z-micropositioner (WPI Inc.). The flow of the erythrocyte solution from the vacutainer until the discharge of the microchannel was always vertical, this was confirmed with a level attached to the heating stage. A horizontally oriented microscope was positioned to observe the sample flowing through the microchannel (Figure 32).

The design of the vertical flow system likely introduced some intrinsic difficulties involving gravity effects, maintaining the sample hematocrit constant over time, and cross-contamination of samples. It is likely that, over time, the erythrocytes in the vacutainer were settling and increasing the observed hematocrit within the microchannel. To help control for this consequence, the vacutainer was inverted between each study (every 3.5 minutes). During the 3 minute duration of image acquisition, however, the vacutainer could not be inverted as that would disrupt the flow profile being imaged. To control for the possible increase in sample hematocrit during the duration of the experiment, the hematocrit of samples of discharge from the microchannel were measured using a microhematocrit system (STI, Inc.). There were no significant differences between hematocrit measurements at the beginning and end of the 3 minute experiment. As a result of gravity, even without pressure-driven flow, erythrocytes settle. The velocity profile of erythrocytes (HCT = 0.0005%) in the micro channel was measured using a particle tracking software in MATLAB. After high flow was abruptly stopped, the erythrocytes reached a steady-state settling rate of 50 pixels/second in less than 5 seconds. To prevent cross-contamination of subsequent samples, the entire portion of the system that came into contact with the samples was cleaned before and after each experiment. The system was cleaned with a series of perfusions of deionized water, followed by 30% hydrochloric acid, and lastly PBS (before subsequent experiments) or 100% ethanol (to prevent residue accumulation overnight).

Aggregation of Erythrocytes in Model of Stasis Onset

Using the vertical flow system, measurement of the dynamic aggregation behavior and subsequent rheological effects in a model of stasis were measured as a function of temperature in the presence of plasma macromolecules. The physiological hematocrit that would be expected in

a vessel of this size is approximately 35% [67], however, in this system erythrocyte samples of slightly lower hematocrit (20% hematocrit) were used to maximize optical clarity.

Erythrocytes were suspended in PBS (negative control), autologous platelet poor plasma (positive control), or in various test solutions and treatments as described in 'Erythrocyte Suspensions and Treatments' section. All samples were maintained at 37˚C in a vacutainer into which their corresponding solvent was pumped to drive high Reynolds flow into the vertically oriented channel. One minute of high Reynolds flow was qualitatively determined to monodisperse any aggregates in the channel and served to set a controlled starting point for aggregation comparisons between groups.

The high Reynolds flow required to achieve total monodispersion of aggregates was achieved with a volumetric flow rate (Q) of 27.5 µL/min, corresponding to a Reynolds number of 0.254.

Equation 18: $Re = \frac{\rho v D}{\mu}$

$$Re \approx \frac{\left(1060\ \frac{kg}{m^3}\right)(0.00246\ \frac{m}{s})(0.000487\ m)}{0.005\ Pa * s}$$

$$Re \approx 0.254$$

where ρ represents the density of blood, v represents the mean fluid velocity ($v = \frac{Q}{A}$), A represents the cross-sectional area of the vessel, D represents the vessel diameter, and μ represents the estimated dynamic viscosity of 20% hematocrit blood at 37˚C and a shear rate of $100s^{-1}$ described in literature [68]. The Re used here for monodispersion exceeds that found in the microcirculation ($0.001 < Re < 0.01$)[69], and is typical of veins, and small arteries[70].

After monodispersion was confirmed qualitatively, flow was abruptly stopped and aggregates were allowed to form in a low shear environment where their subsequent center-seeking behavior was observed. The sudden cessation of flow emulated the environment encountered by erythrocytes in the zone of stasis immediately after the occlusion of microvessels in the zone of coagulation during the onset of thermal injury. To study the effects of hyperthermia on aggregation of erythrocytes in stasis the experimental procedure was performed for samples heated to 37 ˚C, 41 ˚C, 45 ˚C, and 49 ˚C.

Image Processing Software

Digital image processing tools were employed for quantification of erythrocyte aggregation in images of settled erythrocytes on horizontal slides, and rheological effects of aggregation in images of flowing erythrocytes in vertical channels.

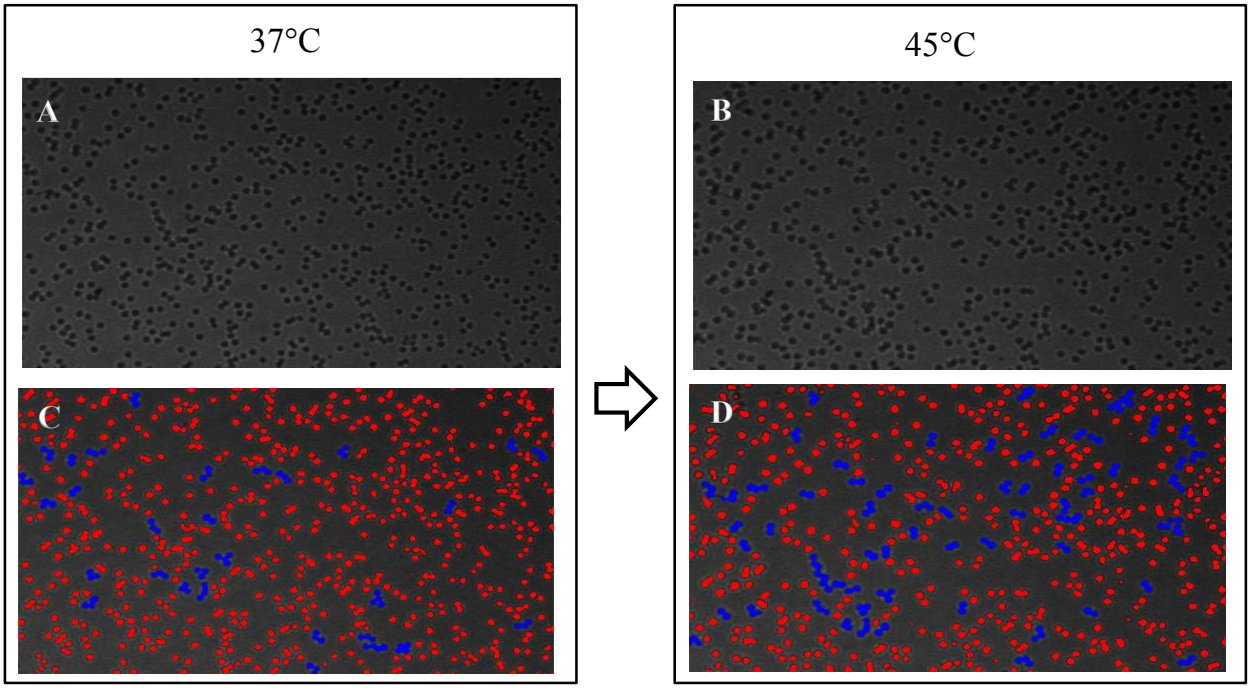

Figure 33: *Image processing for identification of cells and aggregates. RBCs heated from 37°C to 45°C (porcine). A,B) Grayscale image of RBCs at 37°C and 45°C, respectively (10% HCT) C,D) Detected RBCs and aggregates at 37°C and 45°C, respectively (10% HCT)*

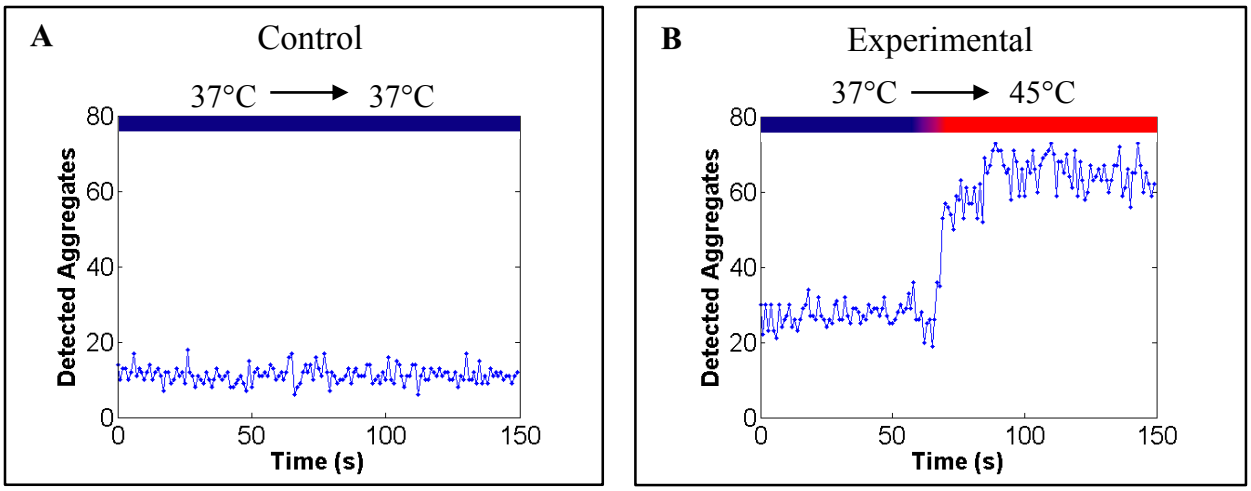

Figure 34: *Image processing for counting erythrocyte aggregates. Shown are raw data tracings of detected aggregates during dynamic heating in the stationary model (porcine). A) Number of detected aggregates for control trial (37°C to 37°C, 10% HCT); B) Number of detected aggregates for experimental trial (37°C to 45°C, 10% HCT)*

Using a MATLAB-based image analysis script (Mathworks®), written with Geoffrey Gunter (50% contribution) [3], we were capable of identifying (Figure 33) and counting settled cells and aggregates (Figure 34) based on set parameters including pixel intensity and object area. Aggregates are defined as three or more coincident cells. This program uses a variety of image processing techniques for image pre-processing to compensate for non-uniform illumination. A top-hat transform algorithm, followed by a median filter, and gamma correction reduced the illumination heterogeneities in the image. A graphical user interface allowed an operator to manually apply an intensity-based threshold to the image to distinguish between cells and background in a binary image. Once the images was converted to binary, the operator applied a size-based threshold, based on the number of connected pixels in an object, to distinguish between aggregated and non-aggregated erythrocytes. From the binary image solution hematocrit was verified computationally, and the percent of which was aggregated was measured based on percent-by-area of cells.

A Python-based image processing script, writtten with Geoffrey Gunter (50% contribution) [3], enabled quantification of rheological effects of aggregation in a vertical channel

based on pixel intensity. For three minutes, images were acquired every 2.5 seconds. The cell-free region of each image was quantified using an intensity-based threshold, where a pixel of high intenisty corresponds to a cell-free point. The Cell-Free Area (CFA) of each image was calculated as a percent of the total image area. A large CFA corresponded to a high level of large aggregates. Although the same intensity threshold was used for all images in these analyses, the use of a threshold led to omition of information about small aggregate formation. For this reason

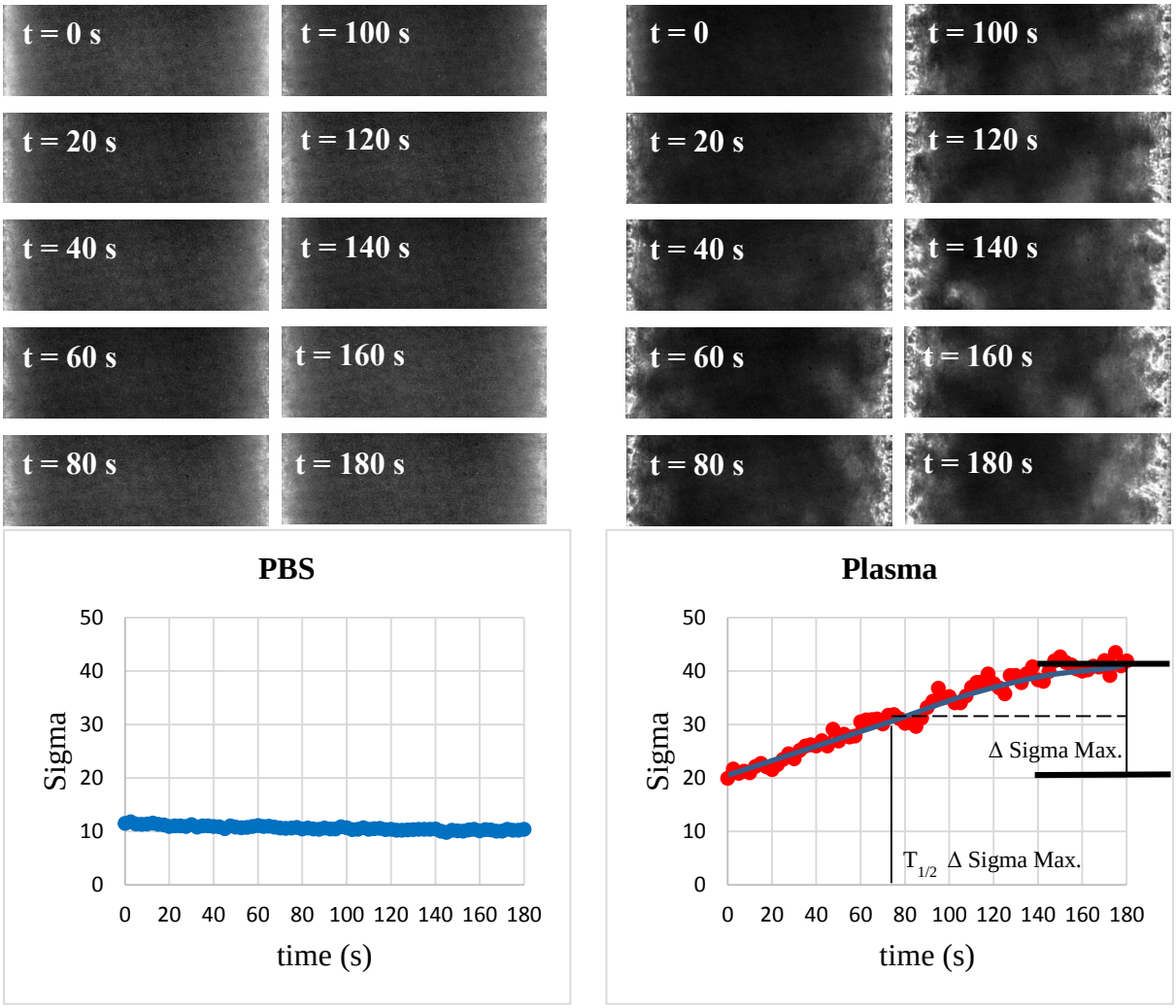

Figure 35: *Image sequence of erythrocyte aggregation in onset of stasis model.* ***Left-Top)*** *Shown are time series (180 seconds,) images of human erythrocytes in PBS in the absence of antibodies. Images were acquired every 2.5 seconds starting immediately after secession of flow.* ***Left-Bottom)*** *corresponding raw data tracings, from 6-30-2015, of the standard deviation of the pixel intensities as a function of time.* ***Right-Top)*** *Shown are time series (180 seconds,) images of human erythrocytes in autologous Plasma in the absence of antibodies. Images were acquired every 2.5 seconds starting immediately after secession of flow.* ***Right-Bottom)*** *corresponding raw data tracings, from 9-24-2015, of the standard deviation of the pixel intensities as a function of time with Δ Sigma Max., and $T_{1/2}$ Δ Sigma Max..*

another metric of aggregation was needed. The standard deviation of the image pixel intensities, sigma, was used to quantify aggregation. Sigma is analagous to the aggregation index used in literature as it is a direct measure of light transmission through the erythrocyte solution [39]. In the absence of aggregation, the pixel intensities of an image would be relatively uniform and would have a small standard deviation (Figure 35 Left), the opposite is true in the presence of aggregation (Figure 35 Right). The standard deviation, sigma, was determined and fit to a second-order polynomial best fit. Data was normalized for each trial by subtracting the minimum sigma value of the fitted line from each subsequent image before statistical analysis. The normalized sigma values are termend Δ Sigma. For each trial Δ Sigma Max. was calculated and the time required to reach half of Δ Sigma Max., $T_{1/2}$ Δ Sigma Max., was determined (Figure 35).

Research Design

The focus of this study is to develop and test a theoretical model of thermally induced erythrocyte aggregation by surface nanobubble interactions. The experimental design is described below, and was performed using the materials and methods outlined above.

Specific Aim 1: **To develop a theoretical model of thermally induced erythrocyte aggregation by surface nanobubble interactions**

In the "Proposed Model: Surface Nanobubble Coalescence" section, hemoglobin SO_2 is described with respect to temperature, pH, and PO_2 based on governing equations. By changing temperature and pH in the model, subsequent changes in hemoglobin SO_2 occurred. Simultaneously, the temperature dependence of gas solubility was calculated and excess gas in solution was estimated as the sum of the concentrations of oxygen dissociated from hemoglobin and dissoluted gas.

The results of the model indicate that at 37°C and pH 7.4, and 0 mmHg O_2 hemoglobin is deoxygenated ($SO_2 \approx 0\%$), thus oxy-hemoglobin dissociation cannot occur. At 38 mmHg O_2 ($SO_2 \approx 65\%$), and at 76 mmHg O_2 ($SO_2 \approx 90\%$) hemoglobin is oxygenated and experiences a high degree of oxy-hemoglobin dissociation when temperature is increased. At 760 mmHg O_2 ($SO_2 \approx 100\%$) hemoglobin is fully oxygenated and the abundance of dissolved oxygen in solution makes oxy-hemoglobin dissociation highly unfavorable at any of the temperatures tested in the model.

The results of the model indicate that, at all temperatures, low magnitudes of erythrocyte aggregation will be observed in solutions equilibrated with at 0 mmHg O_2, and 100 mmHg O_2, and high magnitudes of aggregation will be observed in solutions equilibrated with 38 mmHg

O_2, and 76 mmHg O_2. Temperature-dependence of aggregation is expected only for solutions equilibrated with 38 mmHg O_2, and 76 mmHg O_2. Low magnitudes of aggregation are expected in solutions with minimal temperature-dependent oxygen solubility, and high magnitudes of aggregation are expected in solvents with highly temperature-dependent oxygen solubility. Temperature-dependent aggregation is expected to be proportional to the temperature dependence of solution pH, and oxygen solubility.

Specific Aim 2: To measure the contribution of plasma proteins and temperature to gas solubility and pH

It is known that gas solubility and bubble formation is influenced by temperature, and solution composition. While these factors have already been well characterized, blood contains too many proteins to allow for the hypothesis driven testing of individual proteins. The aim of Specific Aim 2 was to determine the contribution of plasma proteins to pH, and dissolved oxygen content in PBS-protein solutions at specific temperatures. To test the hypothesis that blood plasma proteins and temperature contribute to dissolved oxygen solubility and pH, plasma proteins were added to PBS solutions in concentrations as follows: fibrinogen (2.0 and 8 mg/mL), and albumin (20, and 50 mg/mL), corresponding to physiological (low) and pathological (high) concentrations , respectively [8; 41; 46]. The protein solutions, and concentrations, were chosen for use in this experiments because of their known contributions to erythrocyte aggregation [46]. The contribution of each concentration of protein to oxygen solubility were compared to a control PBS solution without added protein. These samples were heated to one of the prescribed test temperatures (37°C, 41°C, 45°C, or 49°C) in an incubator while a pH, and subsequent dissolved oxygen measurement was performed using a modified Winkler titration method (‘Experimental Materials and Methods’ Section). The outcome variables of this

study were pH and dissolved oxygen concentration. The hypothesis would be supported if differences in the outcome variables are detected between test solutions or if the outcome variables, for a given test solution, change as a function of temperature.

Specific Aim 3: To measure the contribution of plasma proteins, hemoglobin oxygenation, and temperature to erythrocyte aggregation

The second specific aim rendered information about the solubility of O_2 and pH with regard to temperature and plasma proteins of varied concentrations. Before ascribing gas dissolution as a causality of aggregation, erythrocyte aggregation in PBS with the addition of these proteins, and in plasma was evaluated in the presence varied hemoglobin oxygenation states. To test the hypothesis that erythrocyte aggregation is influenced by solution composition, pH, dissolved oxygen, and ultimately oxy-hemoglobin dissociation, erythrocyte suspensions were equilibrated with specific oxygen gas mixtures of 0, 5, 10, and 100% O_2 (in residual nitrogen) with theoretical partial pressures of oxygen 0 mmHg, 38 mmHg, 76 mmHg, and 760 mmHg, respectively, to control the hemoglobin oxygenation state (as described in "Materials and Methods" section). The oxygen partial pressures were chosen based on the results shown in Figure 14 and Figure 15.

Following equilibration with the prescribed partial pressures of oxygen (or room gas), aggregation of non-treated erythrocytes and erythrocytes treated with DIDS inhibitor and suspended in autologous plasma, fibrinogen (2.0 and 8 mg/mL), and albumin (20, and 50 mg/mL) was evaluated at 37°C, 41°C, 45°C, and 49°C using the onset of stasis model (described in "Materials and Methods"). The outcome variables of this experiment were Delta Sigma Maximum, and half-time to Delta Sigma Maximum. The hypothesis would be supported if erythrocyte aggregation is minimal in samples equilibrated with 0% O_2 and 100% O_2, and

elevated for samples equilibrated with 5% O_2 and 10% O_2. The hypothesis would also be supported if the outcome variables were temperature-dependent in solutions having temperature-dependent pH and/or temperature-dependent dissolved oxygen, or if in the presence of DIDS erythrocytes exhibit reduced aggregation.

Statistical Analysis

The statistical methods performed in the comparison between groups in the stationary, settling models, and onset of stasis models were used for the analysis of dissolved oxygen and pH. Changes in the outcome variables between the control solutions of PBS or plasma, and solutions of PBS containing the candidate proteins of varied concentration were compared at the prescribed temperatures and/or oxygen equilibration levels stated above with Welch's t-tests. Assuming all normally distributed data, statistical analyses were performed on the means of each data set using only software packages that employ the standard equations, mainly using the R language for statistical computing. To evaluate trends, residuals of linear regressions were reviewed before using non-linear models if necessary. Multiple comparisons were made between groups with ANOVA with repeated measures and a Tukey HSD post-hoc test with temperature or oxygen level as a covariate. With sample size of $n = 4$ per group and an assumed probability of a Type I error $\alpha<0.05$, the maximal probability of committing a Type II error was less than $\beta = 0.20$. Our statistical power $(1- \beta)$ is greater than 80%.

Results

Here the results of each experimental model are presented in the order they were performed. The erythrocyte aggregation studies using the stationary, settling, and onset of stasis models used samples equilibrated with room gas and were performed in collaboration with Geoffrey Gunter (50% contribution) and are presented in his Master's thesis [3]. The computational model was used to select the specific oxygenation levels that were used in the assay using the onset of stasis model where samples were equilibrated with controlled gas conditions.

Stationary Model: Aggregation of Mouse, Ovine, Porcine and Rat Erythrocytes

A study of aggregation was performed for erythrocytes, subject to dynamic heating, from four species in a stationary model of erythrocyte aggregation. The percent of sedimented erythrocytes that were aggregated was measured. For each of the species tested, aggregation was

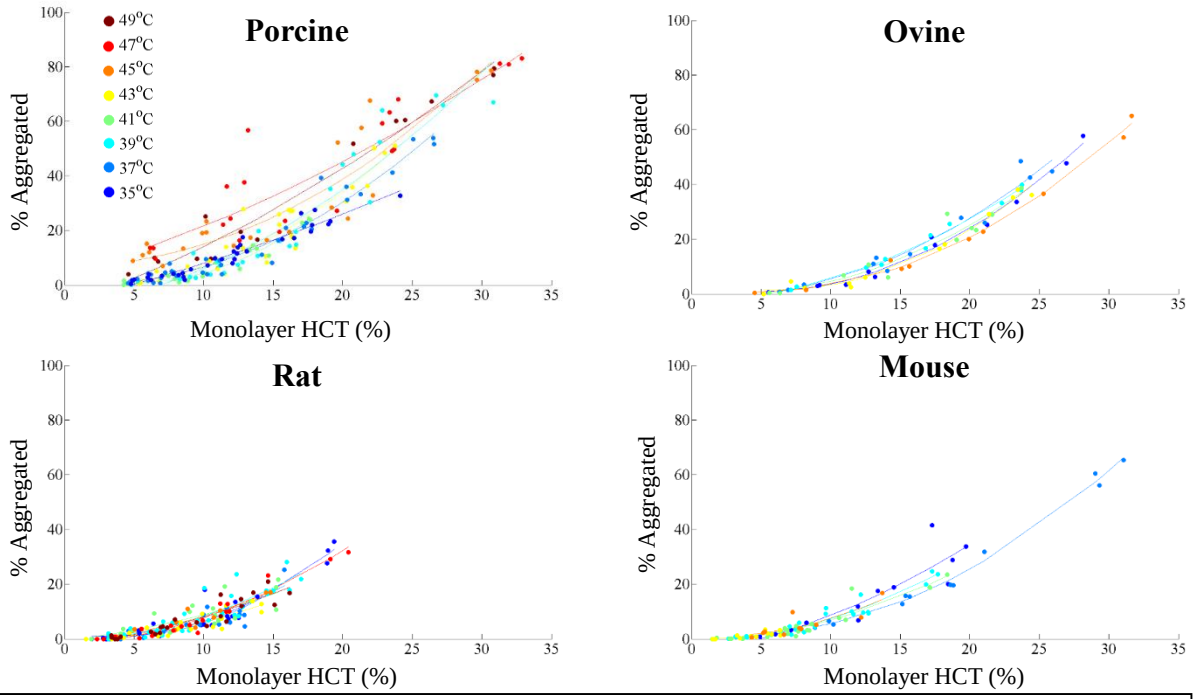

Figure 36: *Percent of aggregated erythrocytes versus species after dynamic heating in stationary model. Aggregation represented as a function of monolayer HCT (%) and compared between porcine (n=4), ovine (n=1), rat (n=3), and mouse (n=2) erythrocytes. Trend lines are second-order polynomial best fit (least squares) for each temperature.*

measured at a range of hematocrits and temperatures (Figure 36). No significant differences in aggregation were detected between species at 37 ˚C. Significant changes in aggregation with respect to temperature were only observed for porcine erythrocytes. At temperatures of 47˚C, and 49˚C, porcine erythrocytes showed significantly ($p < 0.001$) more aggregation than at 37˚C. Aggregation of ovine, rat, and mouse erythrocytes did not show significant temperature dependence. For all species and temperatures, a nonlinear increase of aggregation was observed with increased hematocrit.

Settling Model: Aggregation of Mouse, Porcine, and Rat Erythrocytes

A study of aggregation was performed for erythrocytes, subject to static hyperthermia, from three species in a settling model of erythrocyte aggregation. The percent of sedimented erythrocytes that were aggregated was measured. For each species, aggregation was measured in

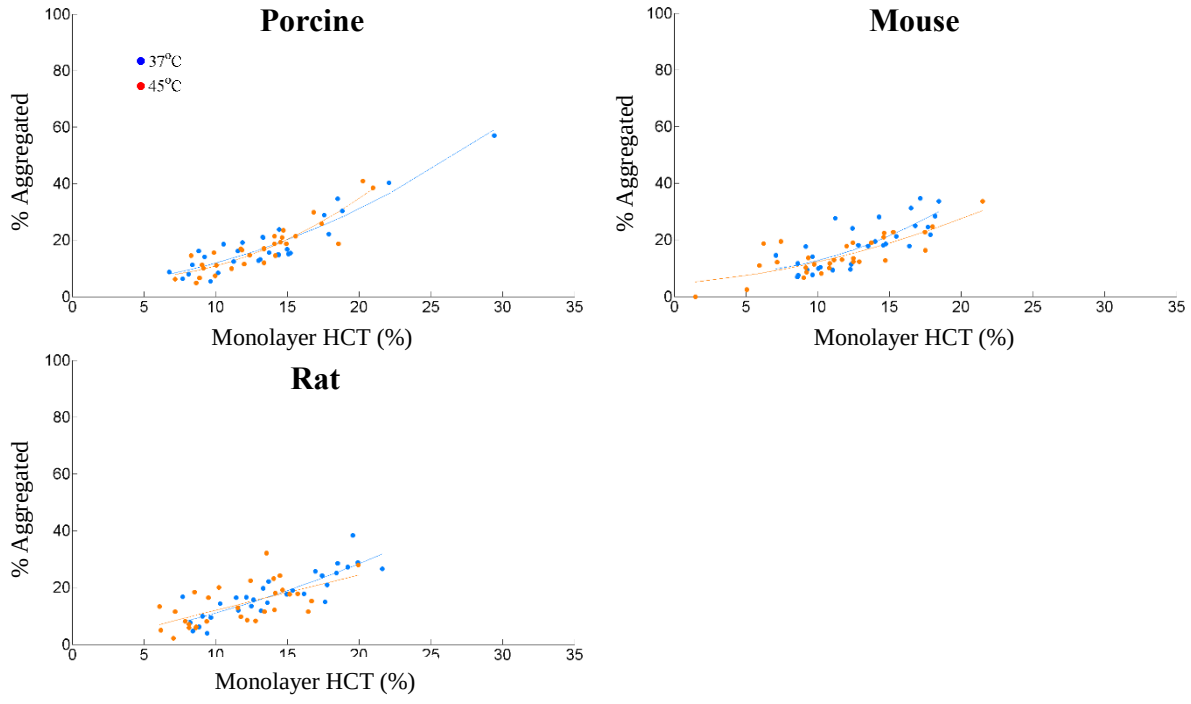

Figure 37: *Percent of aggregated erythrocytes versus species after static hyperthermia in settling model. Aggregation of erythrocytes suspended in PBS, PBS+6g/dL BSA, PBS+6g/dL dextran 110 kDa after static hyperthermia and settling at 37°C and 45°C. Aggregation represented as a function of monolayer HCT (%) and compared between ovine (n=2), rat (n=2), and mouse (n=2) erythrocytes. Trend lines are second-order polynomial best fit (least squares) for each temperature.*

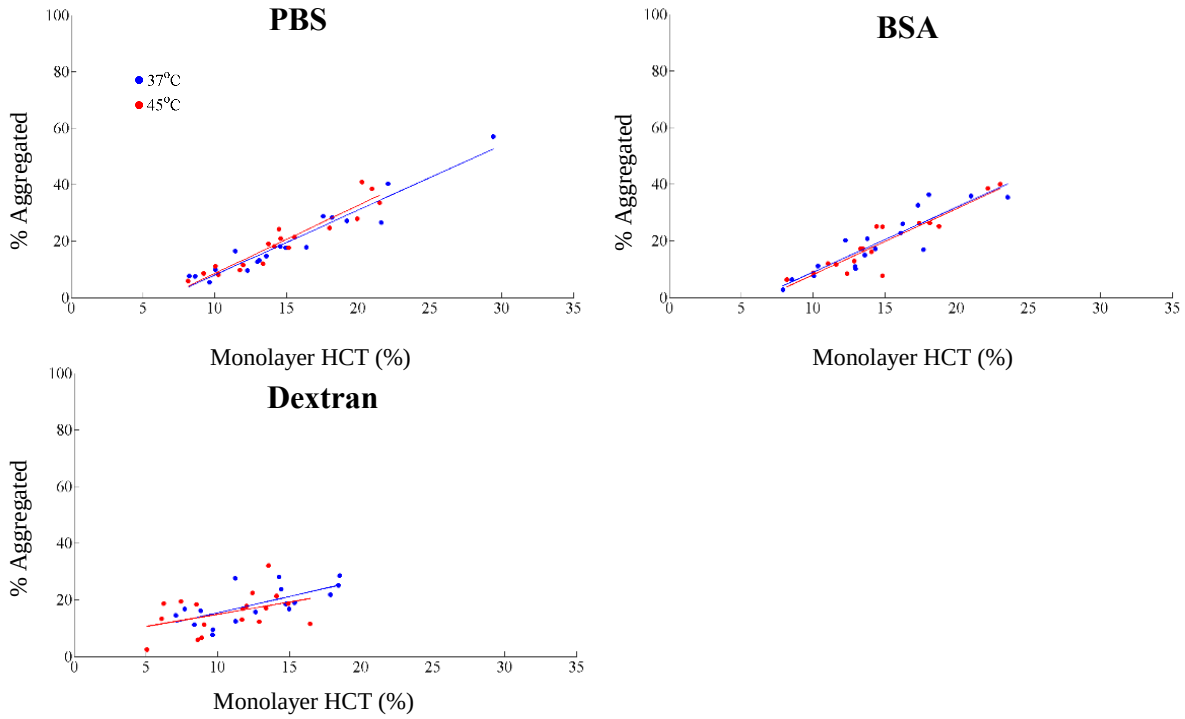

Figure 38: *Percent of aggregated erythrocytes versus solution after static hyperthermia in settling model. Aggregation of erythrocytes (porcine, rat, and mouse) at 37°C and 45°C suspended in PBS (n=2), PBS+6g/dL BSA (n=2), PBS+6g/dL dextran 110 kDa (n=2). Aggregation represented as a function of monolayer HCT (%) and compared between solvents. Trend lines are linear regressions (least squares).*

PBS at temperatures of 37˚C and 45 ˚C in the presence of 6g/dL dextran 110 kDa, and BSA for a range of hematocrits. Aggregation of rat, mouse, and porcine erythrocytes did not show significant temperature dependence (Figure 37). Neither dextran 110 kDa nor BSA resulted in significant changes in aggregation between temperatures of 37˚C and 45˚C for any of the species tested (Figure 38). For all species, temperatures, and solutions tested aggregation increased with hematocrit.

Onset of Stasis Model (Room Gas): Aggregation of Human Erythrocytes

A study of aggregation was performed for human erythrocytes, equilibrated with room gas, immediately following an abrupt reduction of shear in a vertical channel. For each image in all series of images (180 second duration after flow-stop) corresponding to each trial, the pixel intensity standard deviation, Sigma, was measured and fit to a second-order polynomial best fit

trend line. Sigma was then normalized, Delta Sigma, by subtracting Sigma at t = 0 from the fitted Sigma value of each subsequent image. For every trial the maximum Delta Sigma was determined from a second-order polynomial best fit trend line and from that the time required to reach half of Delta Sigma maximum, $T_{1/2}$, was calculated. The maximum Delta Sigma, and Delta Sigma $T_{1/2}$ for erythrocytes suspended in PBS, autologous plasma, and 0.5 g/dL dextran 500kDa was compared at various temperatures, and after treatment with various compounds.

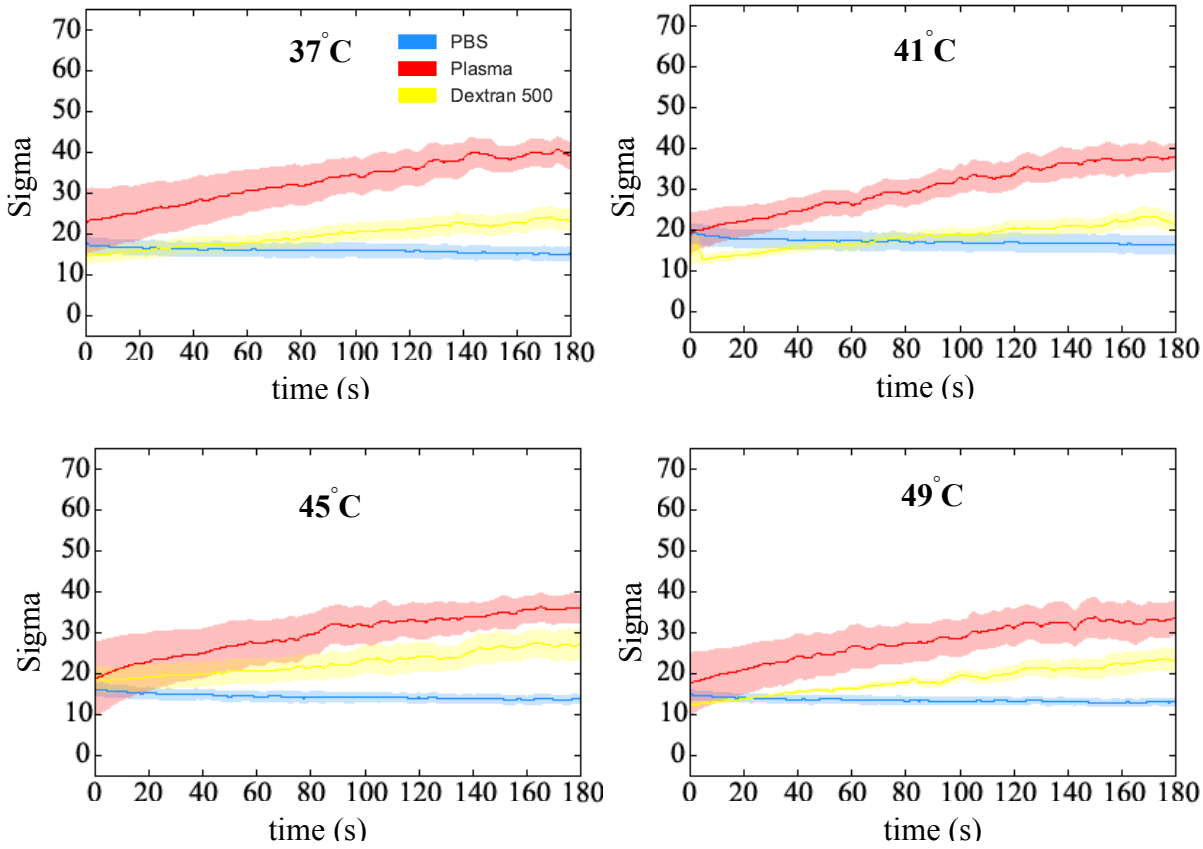

Figure 39: *Time series of aggregation versus solution in onset of stasis model. Standard Deviation, Sigma, of image pixel intensities over time for 20% HCT erythrocyte suspensions in PBS (n = 4), autologous Plasma (n = 7), and 0.5 g/dL dextran 500 kDa (n = 4). Samples were equilibrated with room gas, and in the absence of antibodies. Lines + transparent filled areas represent mean ± standard error.* ***Top Left)*** *37°C.* ***Top Right)*** *41°C.* ***Bottom Left)*** *45°C.* ***Bottom Right)*** *49°C.*

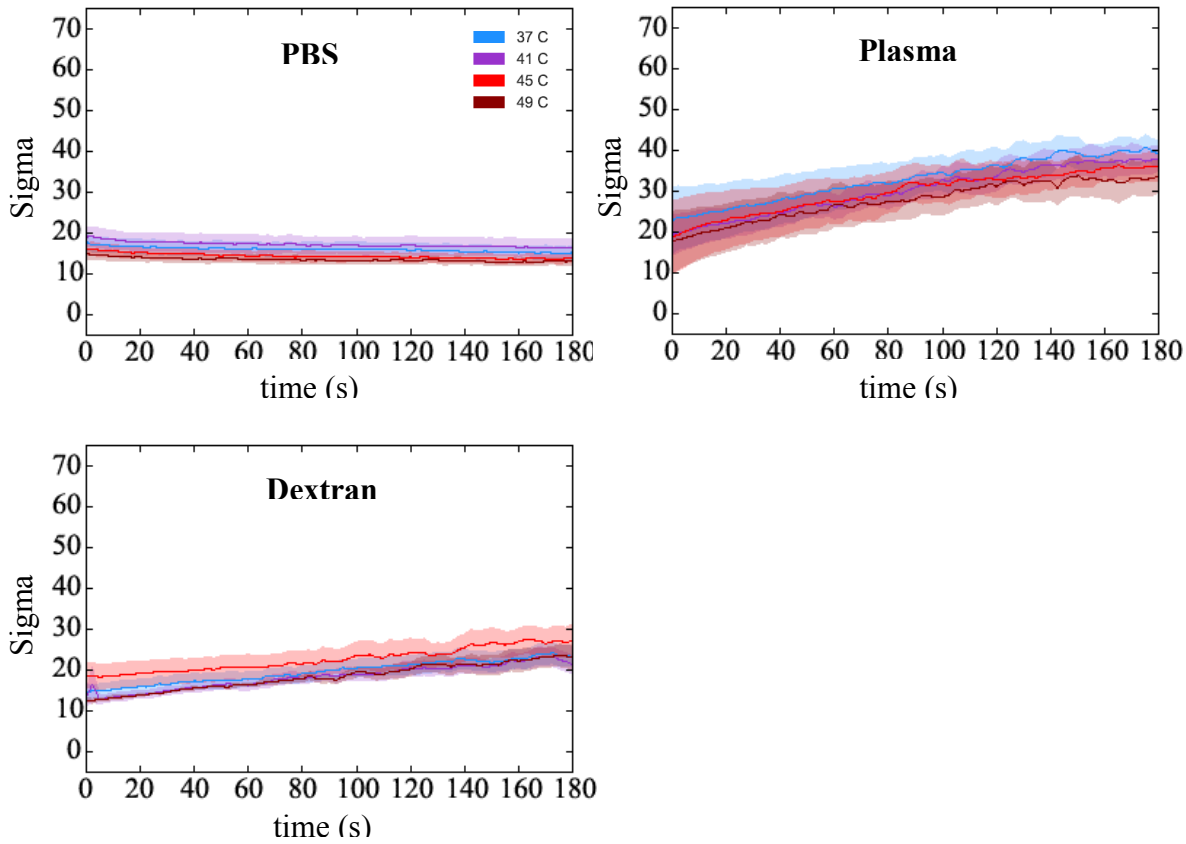

Figure 40: *Time series of aggregation versus temperature in onset of stasis model. Standard Deviation, Sigma, of image pixel intensities over time for 20% HCT erythrocyte suspensions at 37°C, 41°C, 45°C, and 49°C. Samples were equilibrated with room gas, and in the absence of antibodies. Lines + transparent filled areas represent mean ± standard error.* ***Top Left)*** *PBS (n = 4).* ***Top Right)*** *autologous plasma (n = 7).* ***Bottom Left)*** *0.5 g/dL dextran 500 kDa (n = 4).*

Immediately after the secession flow, the Sigma for erythrocytes suspended in PBS, and 0.5 g/dL dextran 500 kDa, were similar, with an average of 10 to 20 at all temperatures and autologous plasma was slightly higher. The variance between measurements of Sigma was larger for erythrocytes suspended in autologous plasma than for PBS and 0.5 g/dL dextran 500 kDa. The variance between measurements of Sigma decreased over time for erythrocyte solutions in autologous plasma at 37°C and 45°C, and increased over time for 0.5 g/dL dextran 500 kDa solutions at 41°C and 49°C. Throughout the 180 second period of observation an apparent linear increase in Sigma was observed for erythrocyte solutions in 0.5 g/dL dextran 500 kDa, and a slight linear decrease for erythrocyte solutions in PBS. A nonlinear increase in Sigma was

observed for erythrocyte solutions in autologous plasma at all temperatures tested, Sigma increased at a decreasing rate over time (Figure 39) (Figure 40).

In the absence of antibodies the magnitude of the maximum Delta Sigma over three

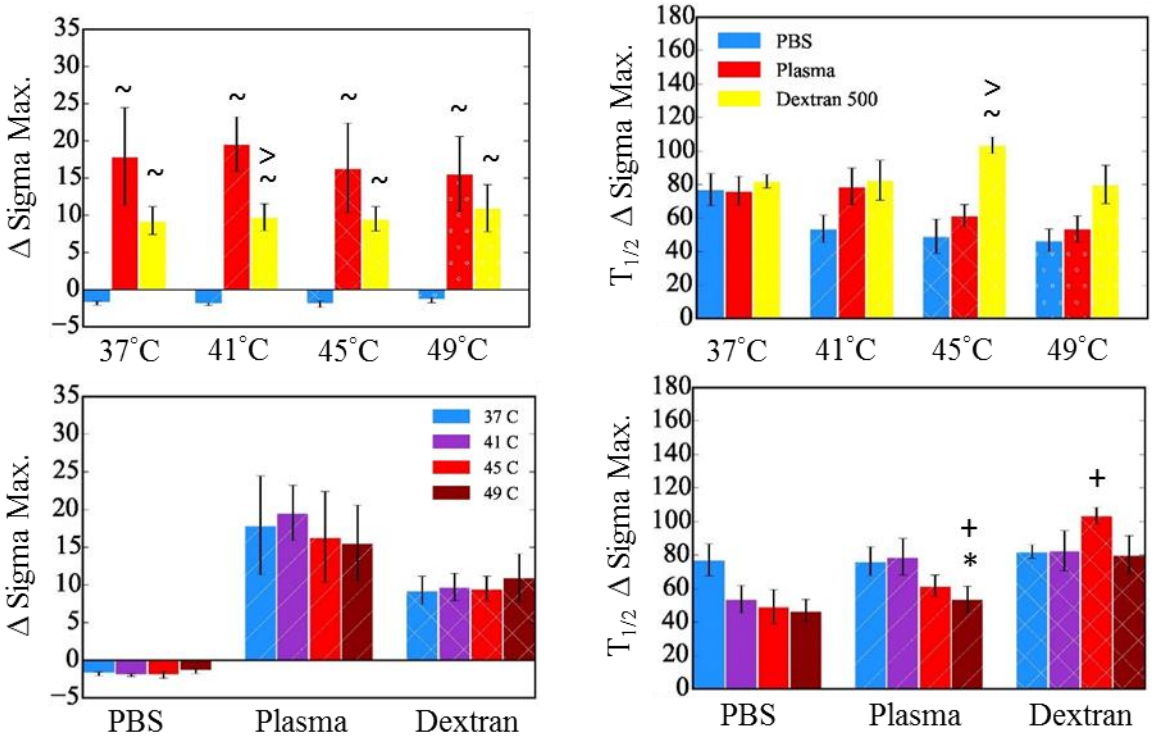

Figure 41: Aggregation magnitude and rate vs temperature and solution in onset of stasis model (Room Gas). Comparison of 20% HCT erythrocyte suspensions equilibrated with Room Gas in PBS (n = 4), autologous plasma (n = 7) and 0.5g/dL dextran 500 kDa (n = 4) at 37°C, 41°C, 45°C, and 49°C in absence of antibodies. Error bars represent mean ± standard error. **Left**) Maximum change in sigma from that at t = 0. **Right)** Time to reach half maximum change in sigma. [~ differs from PBS, $p < 0.05$], [> differs from plasma, $p < 0.05$], [+ differs vs 37°C, $p < 0.05$], [* differs from 41°C, $p < 0.05$].

minutes was significantly different (by Welch's t-test) between erythrocytes suspended in PBS and plasma (greater) at 37°C, 41°C, 45°C, and 49°C, between PBS and 0.5 g/dL dextran 500 kDa (greater) at 37°C, 41°C, 45°C, and 49°C, and between plasma (greater) and 0.5 g/dL dextran 500 kDa only at 41°C (Figure 41). Significant differences in Delta Sigma $T_{1/2}$ were observed between erythrocytes suspended in PBS and 0.5 g/dL dextran 500 kDa (slower) at 45°C, and between plasma and 0.5 g/dL dextran 500 kDa (slower) only at 45°C.

A one-way ANOVA was conducted to compare the effect of temperature on aggregation magnitude and rate in PBS, autologous plasma, and 0.5 g/dL dextran 500 kDa. In the absence of antibodies, there was a significant effect of temperature on aggregation rate (increase) in PBS at the $p < 0.05$ level [$F(1,14)=4.666$, $p=0.0486$]. Also, in the absence of antibodies, there was a significant effect of temperature on aggregation rate (increase) in autologous plasma at the $p < 0.05$ level [$F(1,26)=7.713$, $p=0.01$]. Aggregation rate in plasma was significantly faster in plasma at 49°C than at 37°C or 41°C and significantly slower in 0.5 g/dL dextran 500 kDa at 45°C than at 37°C (Figure 41 Right).

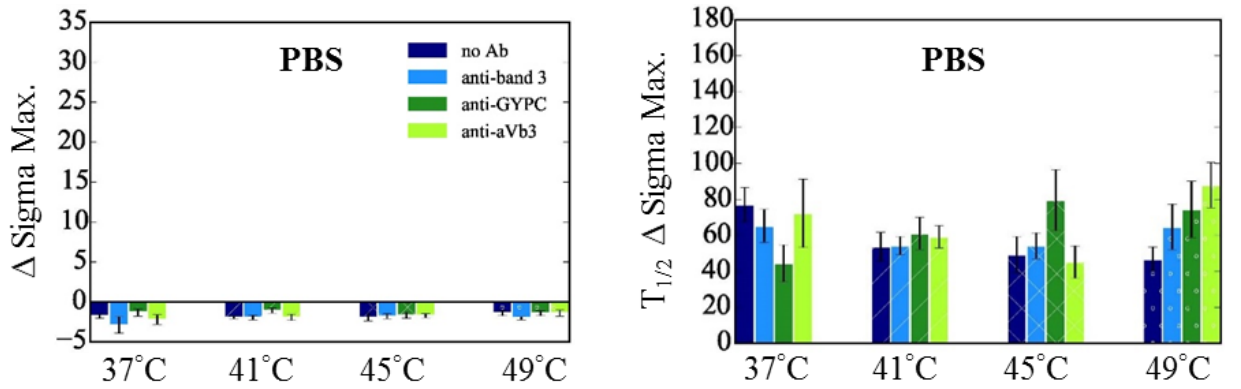

Figure 42: *Aggregation magnitude and rate in PBS vs temperature and treatment in onset of stasis model (Room Gas). Comparison of 20% HCT erythrocyte suspensions in PBS at 37°C, 41°C, 45°C, and 49°C. Samples were equilibrated with Room Gas, and in the presence of anti-band 3 (n = 4), anti-GYPC (n = 4), anti-$\alpha_v\beta_3$ (n = 3), and control (no Ab) (n = 4). Error bars represent mean ± standard error.* ***Left)*** *Maximum change in sigma from that at t = 0.* ***Right)*** *Time to reach half maximum change in sigma. [@ differs from no Ab, $p < 0.05$], [† differs from Band 3, $p < 0.05$], [~ differs from GYPC, $p < 0.05$], [$ differs from $\alpha v\beta 3$, $p < 0.05$].*

No significant differences in erythrocyte aggregation were observed between non-treated erythrocytes suspended in PBS and erythrocytes treated with anti-band 3, anti-GYPC, or anti-$\alpha_v\beta_3$ suspended in PBS at any of the temperatures tested (Figure 42). In autologous plasma at 37°C, 45°C, and 49°C no significant differences in aggregation magnitude were detected between non-treated and treated erythrocytes. At 41°C aggregation magnitude in autologous plasma was significantly reduced in the presence of anti-band 3. An apparent trend of increased aggregation magnitude with increased temperature was observed for erythrocytes treated with

DIDS band-3 inhibitor and suspended in autologous plasma. Significant differences in aggregation rate, but not aggregation magnitude, were only observed in plasma only at 49°C

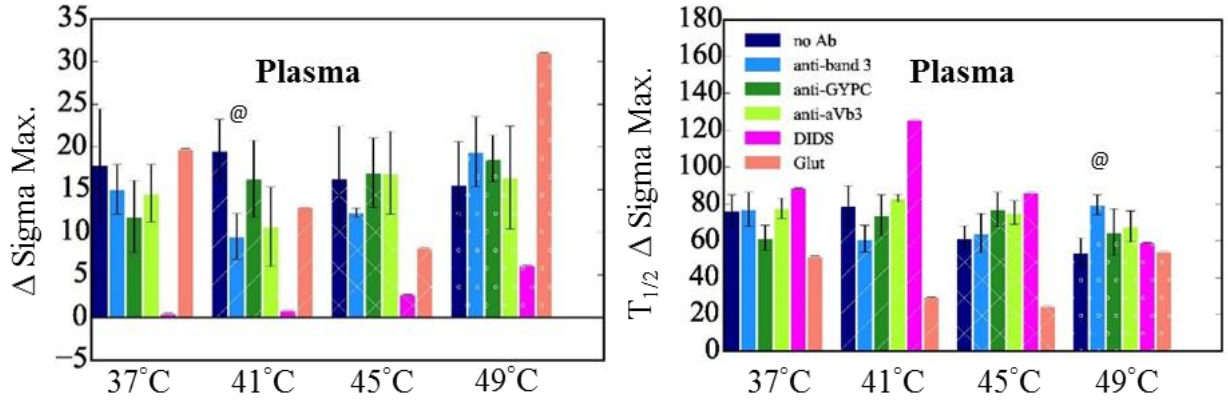

Figure 43: *Aggregation magnitude and rate in plasma vs temperature and treatment in onset of stasis model (Room Gas). Comparison of 20% HCT erythrocyte suspensions in autologous plasma at 37°C, 41°C, 45°C, and 49°C. Samples were equilibrated with Room Gas, and in the presence of anti-band 3 (n = 4), anti-GYPC (n = 4), anti-$\alpha_v\beta_3$ (n = 3), DIDS (n = 1), Glutaraldehyde (n = 1), and control (no Ab) (n = 7). Error bars represent mean ± standard error.* ***Left)*** *Maximum change in sigma from that at t = 0.* ***Right)*** *Time to reach half maximum change in sigma. [@ differs from no Ab, p < 0.05], [† differs from Band 3, p < 0.05], [~ differs from GYPC, p < 0.05], [$ differs from αvβ3, p < 0.05].*

between non-treated erythrocytes and erythrocytes treated with anti-band 3 (slower) (Figure 43).

Dissolved Oxygen and pH of Plasma Protein Solutions

A study of dissolved oxygen and pH was performed for heated plasma protein solutions of fibrinogen (2 and 8 mg/mL), and albumin (20 and 50 mg/mL) in PBS to determine the effects of temperature and solution on these outcome variables. At each temperature (37, 41, 45, and 49°C), pH was measured with a glass pH electrode and a subsequent dissolved oxygen (DO) measurement of the same solution was performed using a modified Winkler's protocol (see 'Dissolved Oxygen and pH Measurement' section). For all protein solutions, with the exception of albumin (20 and 50 mg/mL) and plasma, the DO protocol was performed successfully. Fibrinogen solutions exhibited a cloudy appearance following exposure to 49°C for 15 minutes, this was more noticeable in fibrinogen 8 mg/mL than in fibrinogen 2 mg/mL and was likely

caused by thermally induced fibrinogen aggregation, no changes in the appearance of PBS was observed.

A one-way ANOVA was conducted to compare the effect of temperature on dissolved oxygen and pH in the protein solutions. With increased temperature, a significant decrease of DO was observed at the $p < 0.05$ level in fibrinogen 2 mg/mL [$F(1,12)=15.21$, $p=0.00211$] where DO at 49°C was significantly less than that at 37°C. Similarly, a significant decrease of DO was observed with increased temperature of PBS [$F(1,12)=21.86$, $p=0.000537$] where the DO measured at 45°C was significantly less than at 37°C, and the DO measured at 49°C was significantly less than at 37°C and 41°C. The reverse effect was observed with increased temperature fibrinogen 8 mg/mL, a significant increase of DO [$F(1,12)=12.68$, $p=0.00392$] was observed with no change in DO in the temperature range of 37°C to 45°C, followed by a significant increase in DO at 49°C (Figure 44). The only solution that exhibited a significant

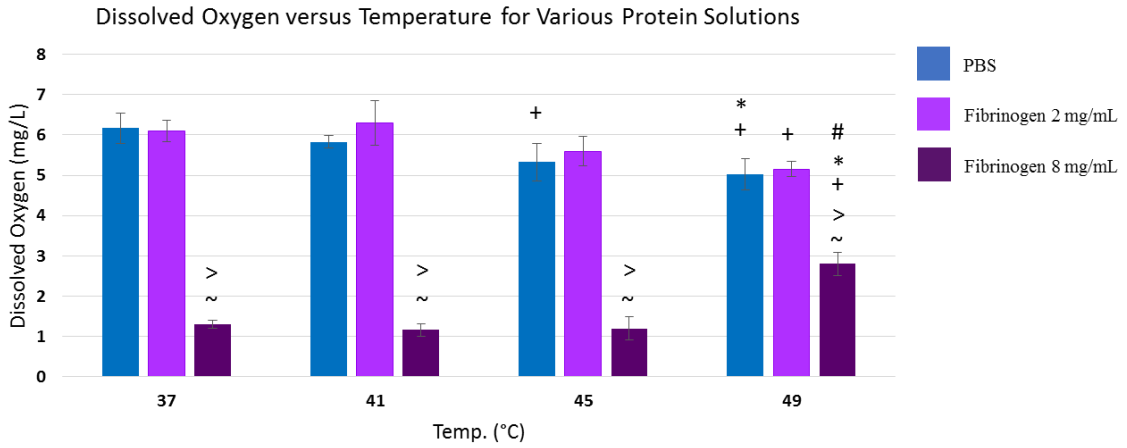

Figure 44: *Dissolved Oxygen concentration as a function of temperature (37, 41, 45, and 49°C) for Phosphate Buffered Saline (PBS), fibrinogen 2 mg/mL, and fibrinogen 8 mg/mL. Error bars represent mean ± standard deviation. [+ differs from 37°C, $p < 0.05$], [* differs from 41°C, $p < 0.05$], [# differs from 45°C, $p < 0.05$], [~ differs from PBS, $p < 0.05$], [> differs from fibrinogen 2 mg/mL, $p < 0.05$].*

temperature-dependent change in pH was fibrinogen 2 mg/mL where pH was significantly lower at 45°C than at 41°C (Figure 45) (see 'Appendix C' for all statistical comparisons).

A one-way ANOVA was conducted to compare the effect of protein concentration on

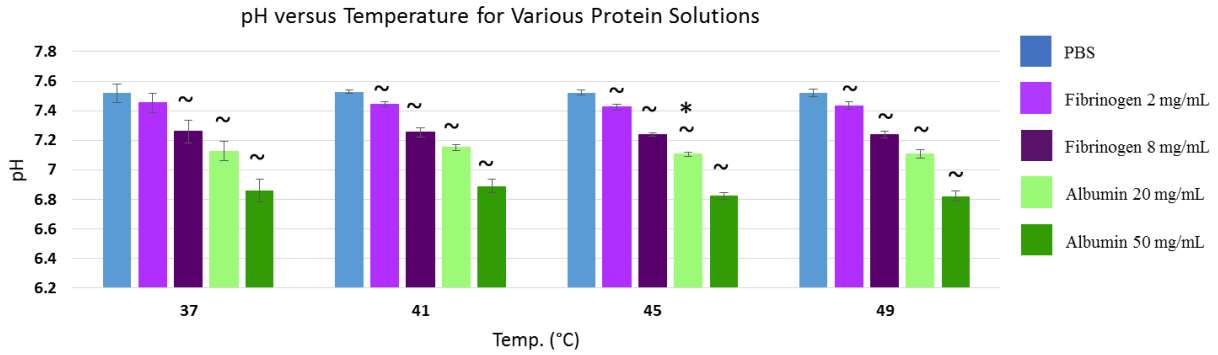

Figure 45: *pH values as a function of temperature (37, 41, 45, and 49°C) for Phosphate Buffered Saline (PBS), fibrinogen 2 mg/mL, fibrinogen 8 mg/mL, Albumin 20 mg/mL, and Albumin 50 mg/mL. Error bars represent mean ± standard deviation. [~ differs from PBS, p < 0.05], [* differs from 41°C, p < 0.05].*

dissolved oxygen and pH in the protein solutions. With increased plasma protein concentration, a significant decrease of DO was observed at the $p < 0.05$ level in samples heated to 37°C, 41°C, 45°C, and 49°C ([F(2,6)=313.9, p=8.49e-07], [F(2,6)=203.3, p=3.07e-06], [F(2,9)=172.6, p=6.65e-08], [F(2,9)=76.98, p=2.19e-06], respectively). For all of the temperatures tested, no significant differences were observed between PBS and fibrinogen 2 mg/mL, and significantly less DO was measured in fibrinogen 8 mg/mL than in PBS and fibrinogen 2 mg/mL (Figure 44). The pH of the protein solutions became increasingly acidic with increased protein concentration at 37°C, 41°C, 45°C, and 49°C ([F(4,10)=43.32, p=2.77e-06], [F(4,10)=250.2, p=5.64e-10], [F(4,15)=1083, p<2e-16], [F(4,15)=412.1, p=3.88e-15], respectively) (Figure 45). At any given temperature, the pH of all solutions tested were significantly different with the exception of PBS and fibrinogen 2 mg/mL at 37°C, and fibrinogen 8 mg/mL and albumin 20 mg/mL at 37°C. A direct relationship of increasing acidity was observed with respect to protein concentration, regardless of protein type (see 'Appendix C' for all statistical comparisons).

Onset of Stasis Model (Controlled Gas): Aggregation of Human Erythrocytes

A study of aggregation was performed for human erythrocytes, equilibrated with prescribed oxygen levels, immediately following an abrupt reduction of shear in a vertical channel. For each image in all series of images (180 second duration after flow-stop) corresponding to each trial, the pixel intensity standard deviation, Sigma, was measured and fit to a second-order polynomial best fit trend line. Sigma was then normalized, Delta Sigma, by subtracting Sigma at t = 0 from the fitted Sigma value of each subsequent image. For every trial the maximum Delta Sigma was determined from a second-order polynomial best fit trend line and from that the time required to reach half of Delta Sigma maximum, $T_{1/2}$, was calculated. The maximum Delta Sigma, and Delta Sigma $T_{1/2}$ for erythrocytes suspended in autologous plasma, fibrinogen (2 mg/mL and 8 mg/mL), albumin (20 mg/mL and 50 mg/mL) was compared at various temperatures, and after treatment with DIDS inhibitor.

A one-way ANOVA was conducted to compare the effect of temperature on aggregation magnitude and rate in autologous plasma in the presence and absence of DIDS inhibitor. In the absence of DIDS and after equilibration with 0% oxygen, there was a significant effect of temperature on aggregation rate (increase) at the $p < 0.05$ level in autologous plasma [$F(1,13)=2.874$, $p=0.0182$]. In the presence of DIDS and after equilibration with 0% oxygen, there was a significant effect of temperature on aggregation magnitude (increase) and rate (increase) in autologous plasma at the $p < 0.05$ level [$F(1,13)=4.884$, $p=0.0457$], and [$F(1,13)=6.568$, $p=0.0236$], respectively. Similarly, in the presence of DIDS and after equilibration with 5% oxygen, there was a significant effect of temperature on aggregation magnitude (increase) and rate (increase) in autologous plasma at the $p < 0.05$ level [$F(1,14)=8.985$, $p=0.0096$], and [$F(1,14)=5.556$, $p=0.0335$], respectively. Significant differences

in aggregation magnitude were observed in autologous plasma, and fibrinogen 8 mg/mL in the presence of DIDS (reduced) compared to control (Figure 46). Minimal aggregation was observed in fibrinogen 2 mg/mL, and albumin 20 mg/mL and 50 mg/mL, thus significant differences were observed between autologous plasma and these protein solutions. Erythrocytes suspended in fibrinogen 8 mg/mL exhibited a higher level of aggregation in the absence of DIDS than fibrinogen 2 mg/mL and albumin 20 mg/mL and 50 mg/mL, however, the aggregation magnitude observed in fibrinogen 8 mg/mL was significantly less than that of autologous plasma (see 'Appendix E' for all statistical comparisons) (Figure 46 - Figure 52).

A one-way ANOVA was conducted to compare the effect of oxygen equilibration on aggregation magnitude and rate in autologous plasma in the presence and absence of DIDS inhibitor. In the absence of DIDS and at 49°C, there was a significant effect of oxygen on aggregation magnitude (decrease) at the $p < 0.05$ level in plasma [$F(1,14)=3.053$, $p=0.0432$] (Figure 51). A trend of increasing aggregation magnitude and increasing aggregation rate with temperature, although not all statistically significant, was observed for all oxygen equilibration states of autologous plasma in the presence of DIDS (Figure 46).

In the absence of DIDS in autologous plasma the temperature-dependence of aggregation magnitude and rate differed with respect to the oxygen level in which it was equilibrated. No significant changes in aggregation magnitude were observed with rising increasing temperature after equilibration with 0% oxygen. At the 5% oxygen level, a trend of aggregation magnitude increase was observed with temperature in the range of 37°C to 45°C but not at 49°C. At the 10% oxygen level, a trend of aggregation magnitude increase was observed with temperature in the range of 37°C to 45°C before decreasing at 49°C. At the 100% oxygen level, no significant

changes in aggregation magnitude were observed with a rising temperature from 37°C to 45°C, however a significant reduction of aggregation magnitude was observed at 49°C (Figure 46).

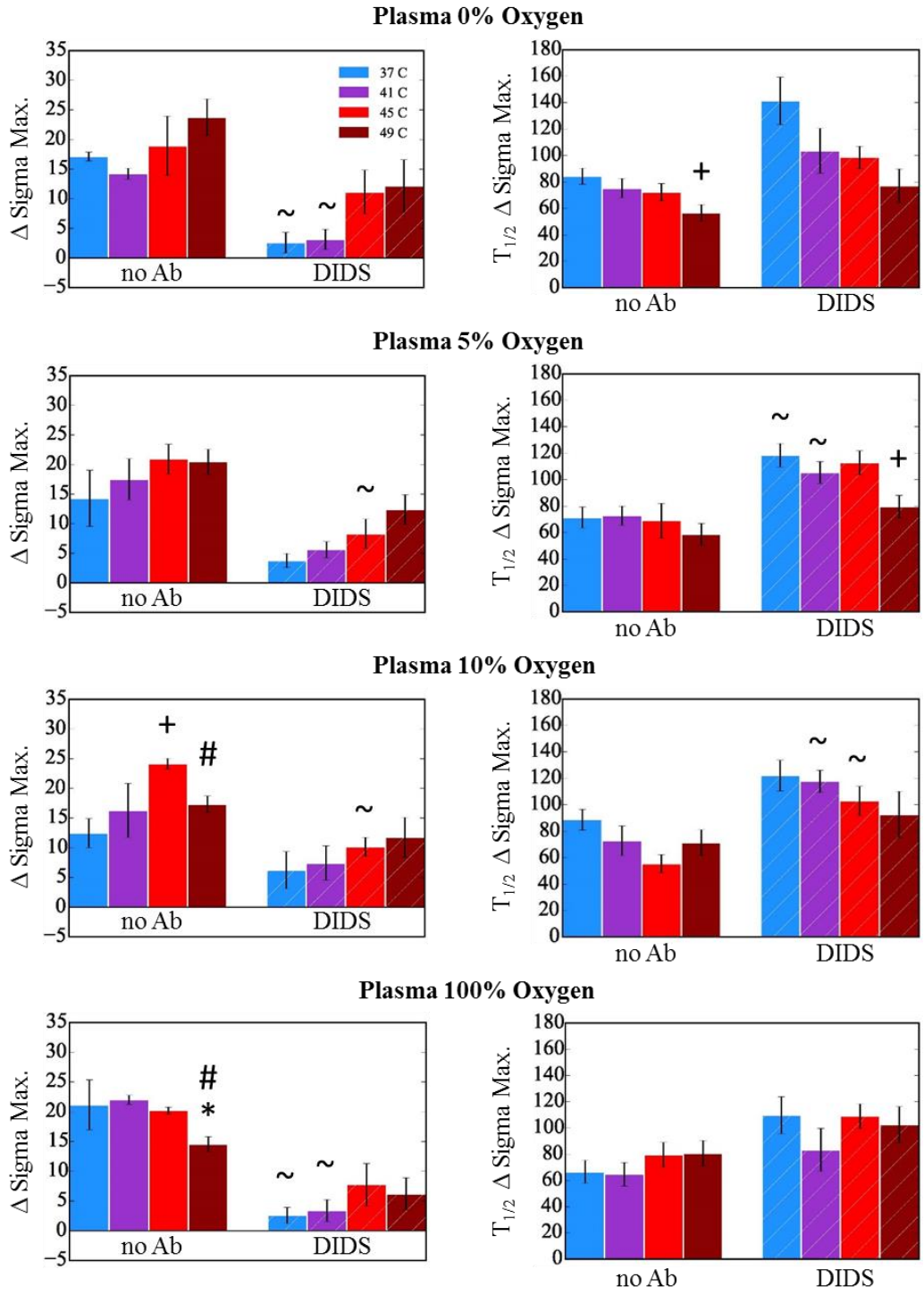

Figure 46: *Aggregation magnitude and rate vs temperature in autologous plasma in onset of stasis model (Controlled Gas). Comparison of 20% HCT erythrocyte suspensions equilibrated with 0%, 5%, 10%, an 100% oxygen at 37°C, 41°C, 45°C, and 49°C in absence (no Ab) and presence of DIDS (n = 4 each). Error bars represent mean ± standard error.* ***Left)*** *Maximum change in sigma from that at t = 0.* ***Right)*** *Time to reach half maximum change in sigma. [+ Differs from 37°C, p <0.05], [* Differs from 41°C, p <0.05], [# Differs from 45°C, p <0.05], [~ Differs from no Ab, p <0.05].*

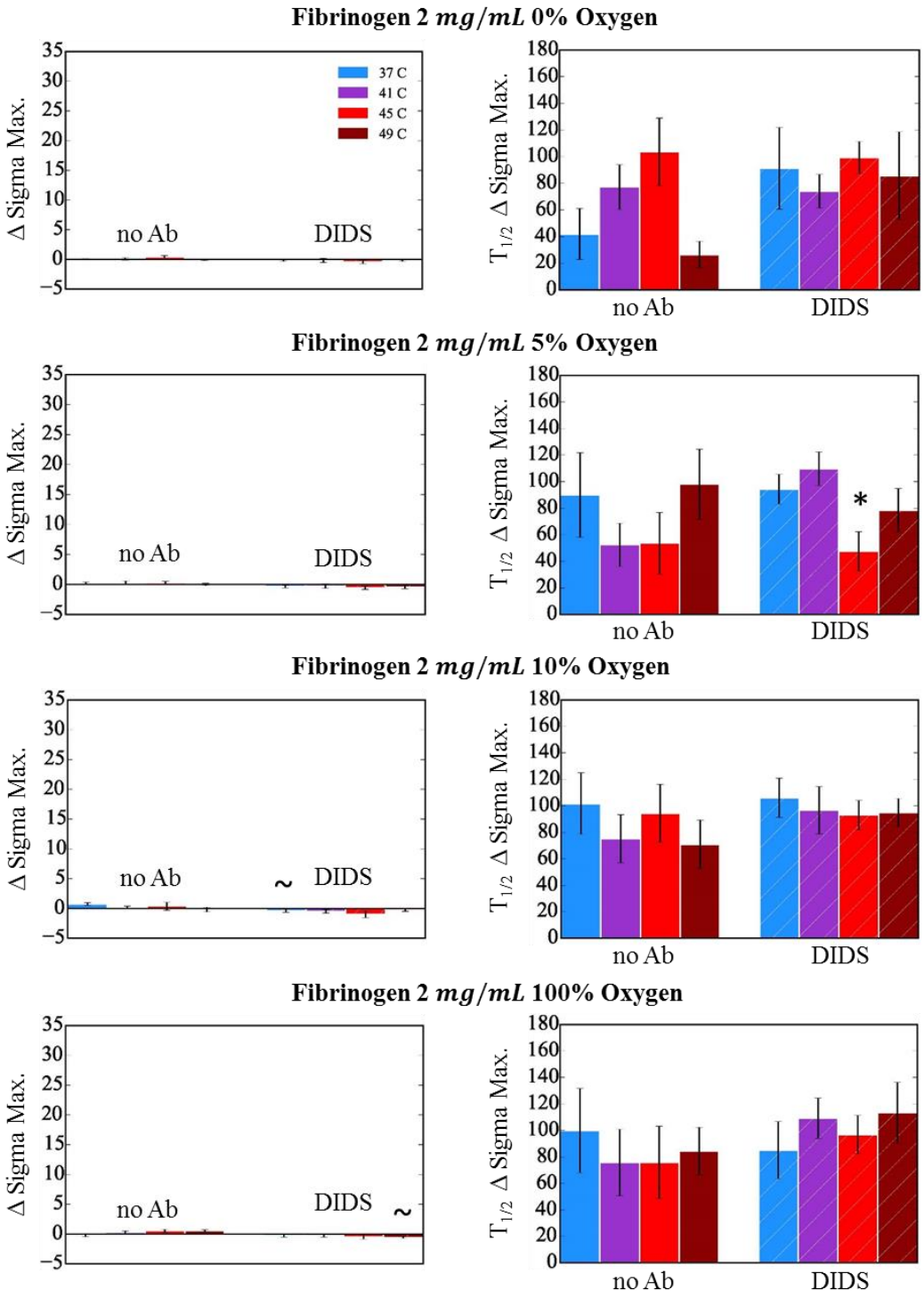

Figure 47: *Aggregation magnitude and rate vs temperature in fibrinogen 2 mg/mL in onset of stasis model (Controlled Gas). Comparison of 20% HCT erythrocyte suspensions equilibrated with 0%, 5%, 10%, an 100% oxygen at 37°C, 41°C, 45°C, and 49°C in absence (no Ab) and presence of DIDS (n = 4 each). Error bars represent mean ± standard error.* ***Left)*** *Maximum change in sigma from that at t = 0.* ***Right)*** *Time to reach half maximum change in sigma. [+ Differs from 37°C, p <0.05], [* Differs from 41°C, p <0.05], [# Differs from 45°C, p <0.05], [~ Differs from no Ab, p <0.05].*

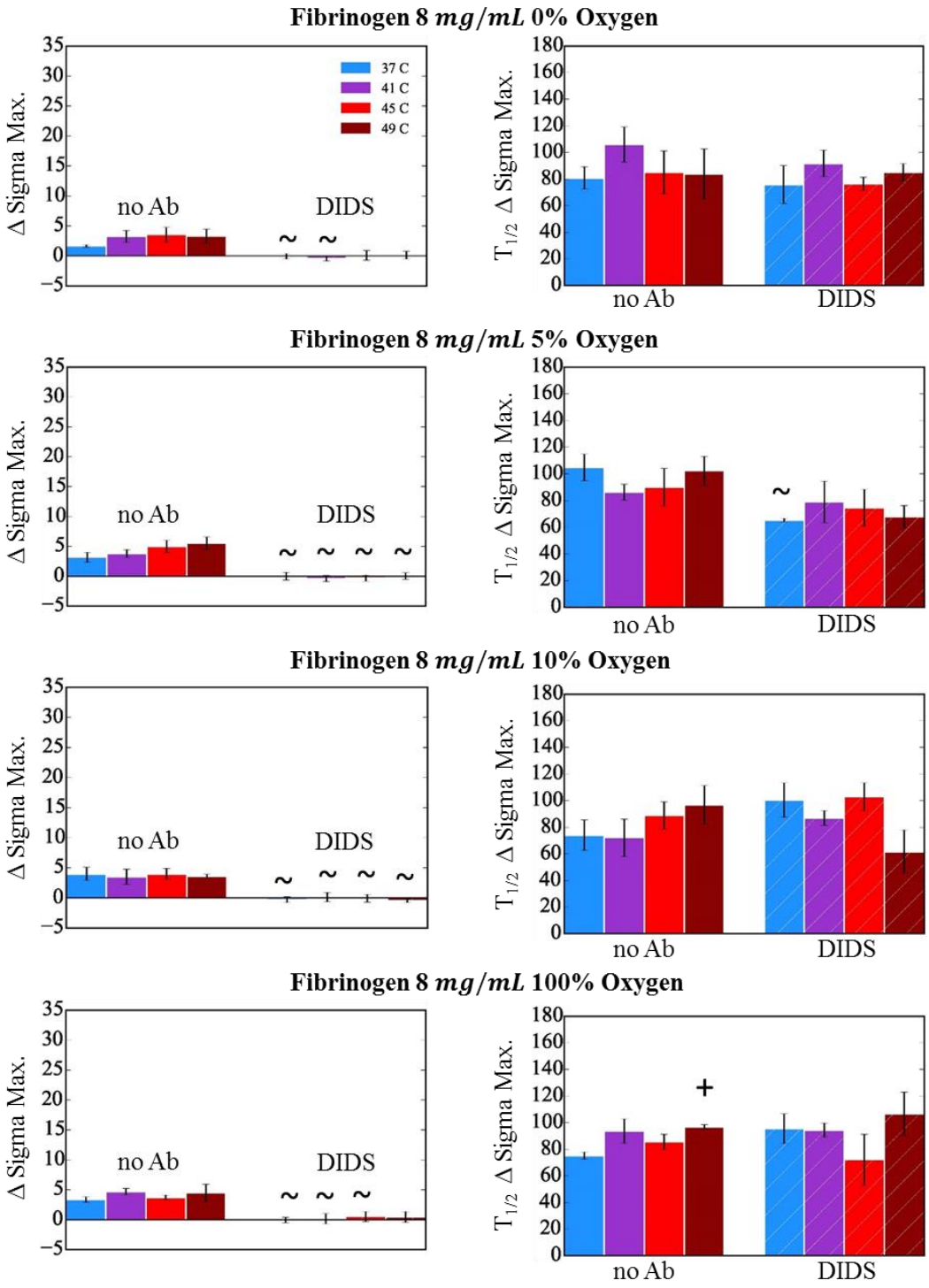

Figure 48: *Aggregation magnitude and rate vs temperature in fibrinogen 8 mg/mL in onset of stasis model (Controlled Gas). Comparison of 20% HCT erythrocyte suspensions equilibrated with 0%, 5%, 10%, an 100% oxygen at 37°C, 41°C, 45°C, and 49°C in absence (no Ab) and presence of DIDS (n = 4 each). Error bars represent mean ± standard error.* ***Left)*** *Maximum change in sigma from that at t = 0.* ***Right)*** *Time to reach half maximum change in sigma[+ Differs from 37°C, p <0.05], [* Differs from 41°C, p <0.05], [# Differs from 45°C, p <0.05], [~ Differs from no Ab, p <0.05].*

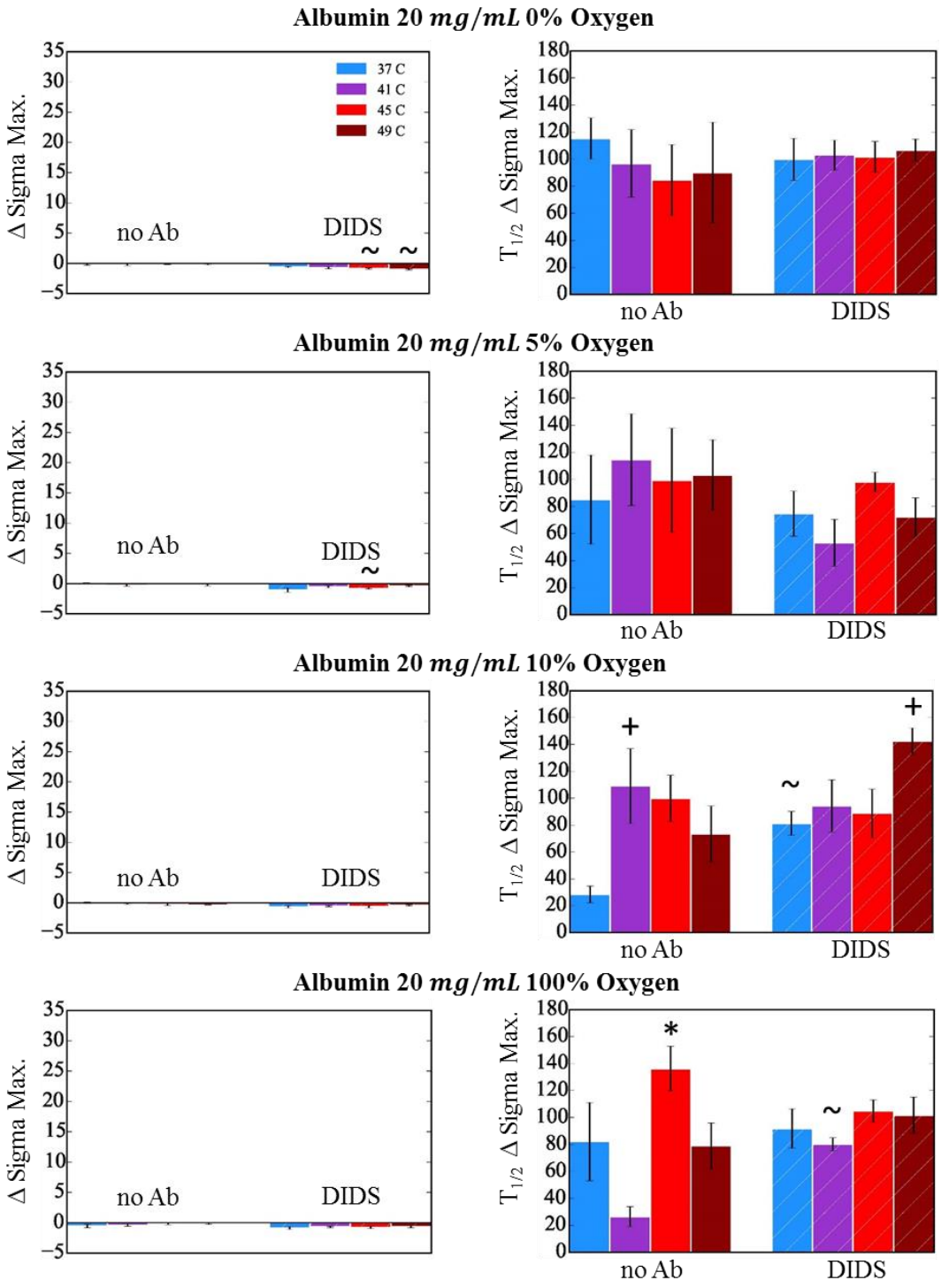

Figure 49: *Aggregation magnitude and rate vs temperature in albumin 20 mg/mL in onset of stasis model (Controlled Gas). Comparison of 20% HCT erythrocyte suspensions equilibrated with 0%, 5%, 10%, an 100% oxygen at 37°C, 41°C, 45°C, and 49°C in absence (no Ab) and presence of DIDS (n = 4 each). Error bars represent mean ± standard error.* ***Left)*** *Maximum change in sigma from that at t = 0.* ***Right)*** *Time to reach half maximum change in sigma. [+ Differs from 37°C, p <0.05], [* Differs from 41°C, p <0.05], [# Differs from 45°C, p <0.05], [~ Differs from no Ab, p <0.05].*

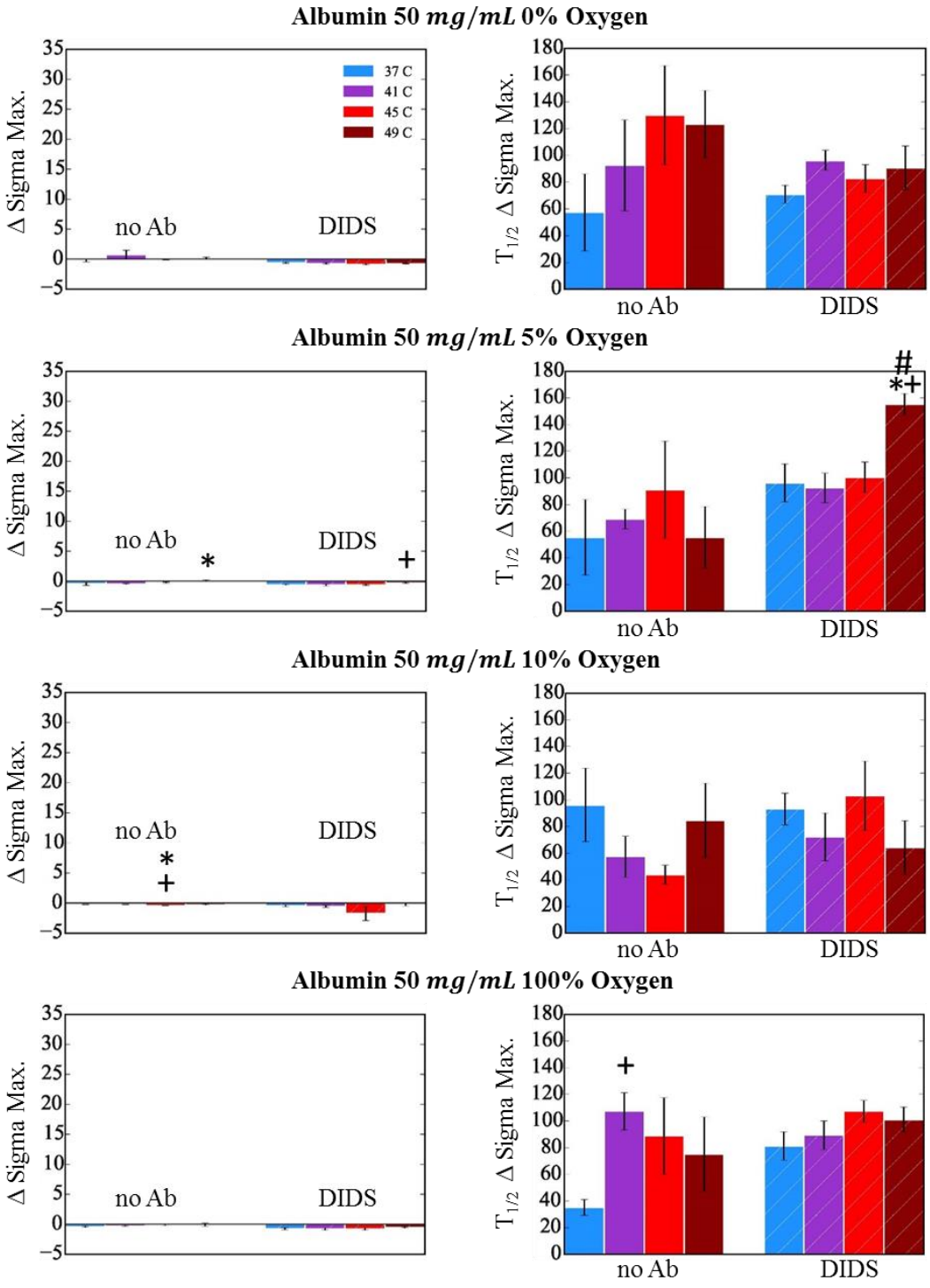

Figure 50: *Aggregation magnitude and rate vs temperature in albumin 50 mg/mL in onset of stasis model (Controlled Gas). Comparison of 20% HCT erythrocyte suspensions equilibrated with 0%, 5%, 10%, an 100% oxygen at 37°C, 41°C, 45°C, and 49°C in absence (no Ab) and presence of DIDS (n = 4 each). Error bars represent mean ± standard error.* ***Left)*** *Maximum change in sigma from that at t = 0.* ***Right)*** *Time to reach half maximum change in sigma. [+ Differs from 37°C, p <0.05], [* Differs from 41°C, p <0.05], [# Differs from 45°C, p <0.05], [~ Differs from no Ab, p <0.05].*

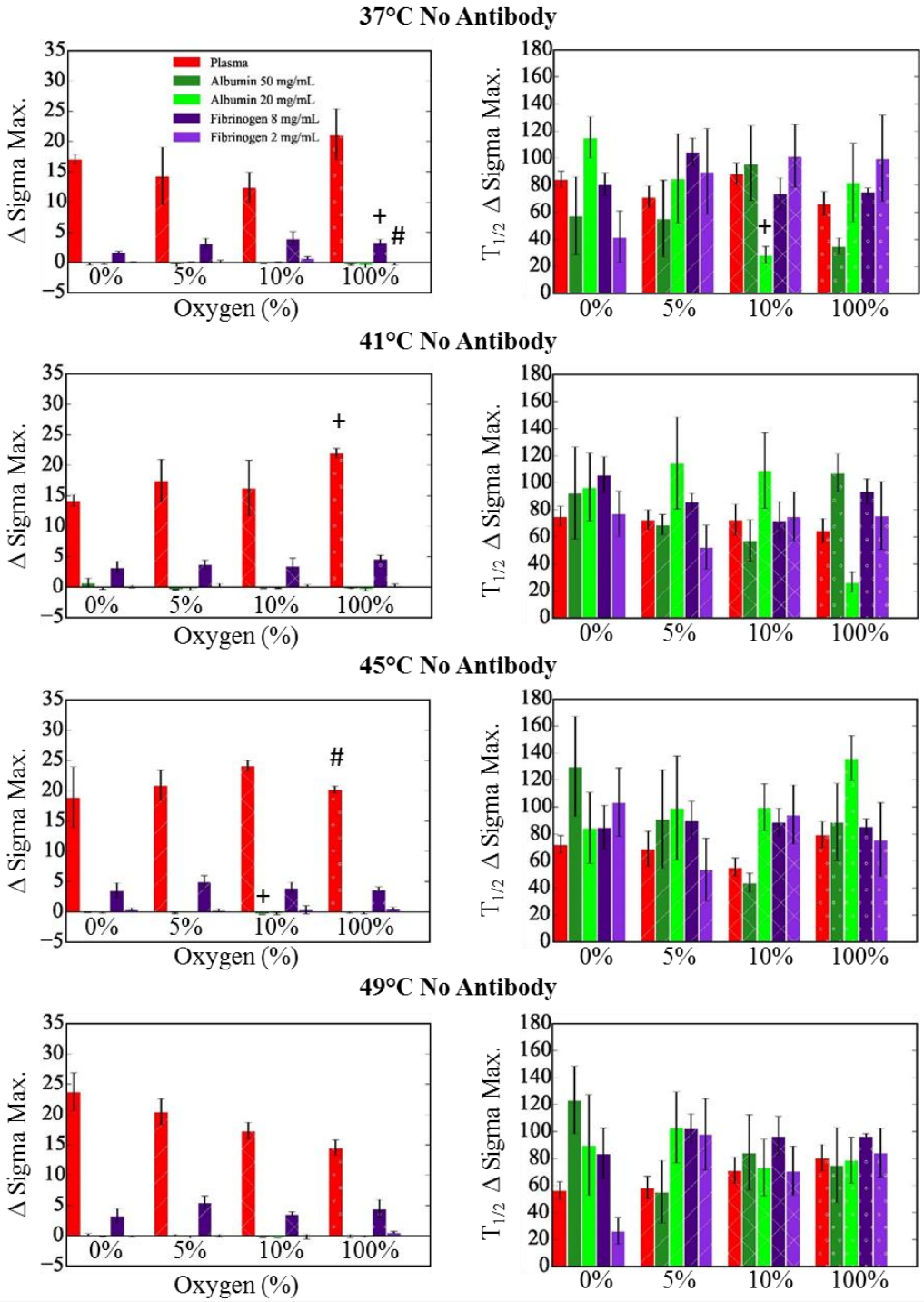

Figure 51: *Aggregation magnitude and rate vs oxygen concentrations in various protein solutions in onset of stasis model (Controlled Gas). Comparison of 20% HCT erythrocyte suspensions equilibrated with 0%, 5%, 10%, an 100% oxygen at 37°C, 41°C, 45°C, and 49°C in autologous plasma, albumin 50 mg/mL, albumin 20mg/mL, fibrinogen 8 mg/mL, and fibrinogen 2 mg/mL (n = 4 each). Error bars represent mean ± standard error.* ***Left)*** *Maximum change in sigma from that at t = 0.* ***Right)*** *Time to reach half maximum change in sigma. [+ Differs from 0%, p <0.05], [* Differs from 5%, p <0.05], [# Differs from 10%, p <0.05].*

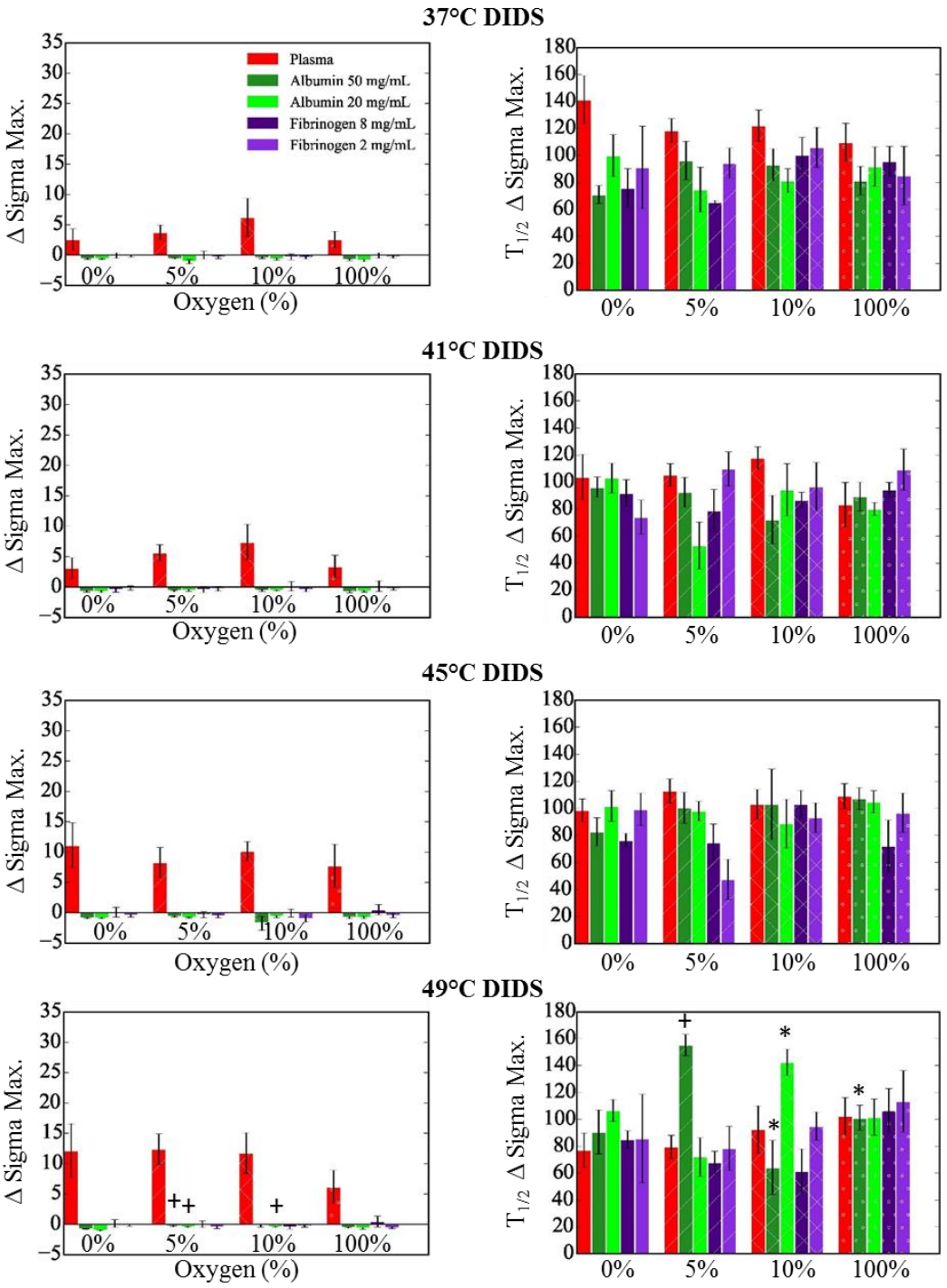

Figure 52: *Aggregation magnitude and rate vs oxygen concentrations in the presence of DIDS in various protein solutions in onset of stasis model (Controlled Gas). Comparison of 20% HCT erythrocyte suspensions equilibrated with 0%, 5%, 10%, an 100% oxygen at 37°C, 41°C, 45°C, and 49°C in autologous plasma, albumin 50 mg/mL, albumin 20mg/mL, fibrinogen 8 mg/mL, and fibrinogen 2 mg/mL (n = 4 each). Error bars represent mean ± standard error.* ***Left)*** *Maximum change in sigma from that at t = 0.* ***Right)*** *Time to reach half maximum change in sigma. [+ Differs from 0%, p <0.05], [* Differs from 5%, p <0.05], [# Differs from 10%, p <0.05].*

Challenges and Limitations of the Specific Aims

From the observations of erythrocyte aggregation in the stationary (dynamic heating) and settling (static hyperthermia) models, we gained information about the importance of the solvent, temperature, hematocrit, and species from which the cells are harvested. Direct measurements of spatial and temporal parameters of erythrocyte aggregation were enabled by the stationary and settling models with the use of our novel transparent heating stage. The stop-flow model of the onset of stasis also helped improve our knowledge of the contributions of solution-dependent aggregation, while highlighting the involvement of band 3 which indicated a role for spectrin in the creation of potential bubble nucleation sites. In the stop-flow model several controls were established to ensure the measurements reflect erythrocyte aggregation. Temperature changes were confirmed with an electronic thermometer, thermochromic film, and rhodamine-B. After flow (of several flow rates) was stopped, no differences in the time required for the velocity profiles to reach a steady settling rate were observed for PBS nor plasma. The flow rate required to achieve monodispersion of erythrocytes in our system was measured by comparing aggregation at varied flow rates and increasing the flow rate until aggregation was unchanged by further increases. A flow rate of 27.5 μL/min was proven sufficient for monodispersion of erythrocytes in all suspensions tested. Even so, the potential for problems exist: variations of atmospheric pressure with weather systems may have influenced oxygen solubility in the solutions tested, vibration of the flow system or operator related mistakes may have obscured aggregation measurements. In Specific Aim 2, for albumin solutions and plasma, upon addition of the starch indicator solution to the iodine solution the blue color did not appear, thus an endpoint of the Winkler titration was not able to be determined for these solutions. While we took great precautions to prevent the equilibration of atmospheric gas into our samples during the

experiments in Specific Aims 2 and 3, there was the possibility that during handling and evaluation of the test solutions they may have equilibrated with atmospheric gas, this would have obscured the results. If this was the case, the experimental groups of which dissolved oxygen was manipulated (either by temperature change or by equilibration with prescribed oxygen partial pressures) would have been most susceptible to obscured results.

Discussion

In the studies described in this dissertation, several in-vitro experimental models were designed for the study of the mechanism of erythrocyte aggregation. In the stationary model (dynamic heating), erythrocyte aggregation was studied in PBS in a monolayer after erythrocytes from several mammalian species settled then were heated. In the settling model (static hyperthermia), erythrocytes from several mammalian species were subject to hyperthermia in PBS during settling in the presence of dextran 110 kDa, and albumin of varied concentrations. In these models, differences in aggregation metrics were detected between species. When comparing results from the static hyperthermia and dynamic heating models it was observed that the temperature-dependent aggregation was dependent on temperature change rather than temperature itself. These results, combined with knowledge of temperature-dependent oxyhemoglobin saturation, temperature-dependent oxygen solubility, and temperature-dependent protein arrangement gave rise to the proposed model of erythrocyte aggregation by surface nanobubble interactions. Several parameters were incorporated into a computational model of erythrocyte aggregation by surface nanobubble interactions to help predict conditions that are more, or less conducive to aggregation. Finally, several conditions described by the computational model were tested in the stasis onset model (with use of dynamic heating), human erythrocytes in PBS, autologous plasma, 0.5 g/dL dextran 500 kDa, fibrinogen (2 and 8 mg/mL), and albumin (20 and 50 mg/mL) were allowed to aggregate following equilibration with prescribed oxygen levels or room gas and after monodispersion by high shear. The aggregation rate and magnitude was measured in the stasis onset model for human erythrocytes subject to various treatments. Dissolved oxygen and pH of each solution was measured, and erythrocyte aggregation observations were analyzed using novel image processing software. Aggregation

metrics were compared between temperatures, oxygenation levels, pH, species, solvents, treatments, and experimental models. Many of the experimental results corroborate the outcomes predicted by the model and support the global hypothesis that surface nanobubble interactions contribute to thermally induced erythrocyte aggregation.

Experimental Models of Erythrocyte Aggregation

Each of the outcomes of the experimental models highlighted possible improvements to be made to subsequent experimental models. In both the stationary and settling models, the experiments were limited by the extremely low hematocrits (<1%) required to distinguish between adjacent erythrocytes in a monolayer after sedimentation had occurred. The low hematocrits used in the stationary and settling models likely reduced the likelyhood of cell interactions simply by increasing the distance between cells. Furthermore, while some Brownian motion was detected in the stationary model, interactions were limited by the lack of mobility of the sedimented cells. While the settling model attempted to address the problem of immobility (seen in the stationary model) by allowing pre-heated cells to settle, the requirement of such low hematocrit samples still limited cell-cell interactions. Switching to the settling model from the stationary model highlighted the importance of dynamic heating to erythrocyte aggregation, cells subject to static hyperthermia in the settling model did not aggregate while cells subject to dynamic heating in the stationary model did.

To alleviate the problems caused by low hematocrit samples and immobility of sedimented cells, a vertical flow model was designed that incorporated dynamic heating and allowed for use of higher hematocrit samples for increased cell-cell interaction. Instead of performing studies of aggregation in continuous (downward) vertical flow, we created an experimental model that directly mimics the in-vivo onset of stasis in a thermal burn injury. To

best model the onset of stasis, a protocol was designed using the vertical flow model that required the abrupt stop of a high flow rate. After stopping flow, aggregation was allowed to occur in a reduced shear environment with simultaneous dynamic heating. This model of the onset of stasis was used to address the specific aims of this dissertation.

Species Dependence of Erythrocyte Aggregation

In this study, aggregation differences between species were observed only in the dynamic heating model. Porcine erythrocytes, suspended in PBS, aggregated more than those harvested from mouse, rat, and sheep. The results of this study are consistent with previous comparisons of aggregation properties between species showing intense aggregation of pig erythrocytes, and moderate to low levels of aggregation for rat, sheep, and mouse erythrocytes [38]. Human erythrocytes were not tested in the settling or stationary models, however, based on similar aggregation studies it is expected that aggregation of human erythrocytes would resemble that of porcine erythrocytes in these experimental models [38; 71]. It is postulated that the observed differences in aggregation between species are a result of differences in erythrocyte membrane composition. For example, band 3 concentration varies greatly between species and is in higher concentration on the membranes of more athletic species like horses which exhibit more intense aggregation than species with low band 3 concentration as for rodents which exhibit minimal aggregation [36; 37; 38]. In studies of erythrocyte aggregation using animal models, it is important to ensure that the aggregation exhibited by the animal model of choice is substantially similar to that of humans.

Solvent Dependence of Erythrocyte Aggregation

In the settling model, no differences in erythrocyte aggregation were detected between PBS, and any of the concentrations of dextran 110 kDa or BSA tested. This is likely a result of

reduced cell-cell interactions because of the low hematocrit used in this model and needs to be tested in a more robust experimental model of aggregation.

In the onset of stasis model (Room Gas), at all temperatures tested, aggregation magnitude was notably less in 0.5 g/dL dextran 500 kDa than in autologous plasma although the only significant differences detected between erythrocytes these groups was at 41°C. Our inability to detect significant differences between these groups was likely due to the large variability of aggregation magnitude observed in plasma (coefficient of variation in plasma and dextran heated to 37, 41, 45, 49°C, respectively: plasma = 0.79, 0.41, 0.79, 0.70, dextran 500 kDa = 0.47, 0.42, 0.40, 0.67). The results of this study contest the results of previous studies that claim aggregation of erythrocytes in 0.5 g/dL dextran 500 kDa is a substantial model of aggregation in autologous plasma [57; 58]. The differences between aggregation detected in this study and aggregation detected in previous studies are likely a result of the use of different aggregation detection apparatuses (see "Hemoglobin: Oxygenation and Concentration" section).

In the onset of stasis model (Controlled Gas), at all temperature and oxygenation levels tested (with or without DIDS inhibition of band 3), the aggregation magnitude in autologous plasma was considerably higher than the other protein solutions tested. Aggregation magnitude observed in fibrinogen 2 mg/mL, albumin 20 mg/mL, and albumin 50 mg/mL was less than 10% of the magnitude measured in autologous plasma. Aggregation magnitude observed in fibrinogen 8 mg/mL was approximately 25% of the magnitude measured in autologous plasma. The protein concentration dependence of aggregation magnitude observed in fibrinogen corroborates previous studies, however, the lack of aggregation observed in albumin solutions (having two to four times the highest tested concentration of fibrinogen tested) indicated that aggregation is more influenced by protein type than by concentration, this contests the depletion layer model of

aggregation. Although significant differences in aggregation were observed between solutions of plasma proteins from human serum, none of the protein solutions tested exhibited the same aggregation properties as that of plasma and no aggregation was observed in PBS (corroborating the depletion layer model). The results indicate that aggregation in autologous plasma may be the result of interplay between various protein types in a solution rather than one particular protein and that the depletion layer model of erythrocyte aggregation may be exhibited in some protein solution mixtures not others. Systematic testing of aggregation in PBS solutions with varied protein mixtures in varied concentrations will lead to a better understanding of the mechanism or mechanisms of aggregation and would provide insight into the possibility that several mechanisms of aggregation may occur simultaneously.

Protein Solution Dissolved Oxygen and pH

The dissolved oxygen (DO) in all of the solutions tested decreased as a function of protein concentration. The predictions of the computational model indicate that aggregation is more favorable in solutions having low dissolved oxygen levels, this was supported by the decreased dissolved oxygen and corresponding increased aggregation magnitude observed in fibrinogen 8 mg/mL compared to fibrinogen 2 mg/mL. As expected, increased temperature caused a decrease of DO in PBS and fibrinogen 2 mg/mL, however the opposite effect was observed in fibrinogen 8 mg/mL. At 49°C, the DO in fibrinogen 8 mg/mL was much higher than at lower temperatures, this increased DO was accompanied by a change in the appearance of the solution. After heating to 49°C for 15 minutes, a precipitate formed in the fibrinogen 8 mg/mL solution as it became noticeably cloudy in approximately 25% of the total volume, while the remaining solution remained transparent. The inhomogeneous distribution of fibrinogen in the fibrinogen 8 mg/mL solution may have reduced the protein concentration of the transparent

regions of the sample, thus increasing the DO to a value closer to that of PBS. A similar change in appearance was observed to a lesser extent in fibrinogen 2 mg/mL, however, it did not cause an increase of DO. The different levels of precipitate formation in these protein solutions of different concentration is likely due to the increased likelihood of protein-protein interactions in the higher concentration sample. The protein-protein interactions that caused the fibrinogen precipitate to form are supportive of the bridging model of erythrocyte aggregation at 49°C, however, it does not explain thermally induced aggregation in the temperature range of 37°C to 45°C. Interestingly, in Onset of Stasis Model, a reduction of aggregation (relative to 45°C) was observed at 49°C in autologous plasma for samples equilibrated with high oxygen levels, this is likely due to the increase of DO caused by the plasma fibrinogen precipitation at this elevated temperature and is supportive of computational model's prediction that increasing the capacity of a solution to dissolve oxygen would decrease aggregation because surface nanobubbles would be more easily dissolved.

At all of the temperatures tested, the pH of the protein solutions decreased as a function of protein concentration. The predictions of the computational model indicate that aggregation is more favorable in solutions having low pH, this was supported by the decreased pH and corresponding increased aggregation magnitude observed in fibrinogen 8 mg/mL compared to fibrinogen 2 mg/mL. At all temperatures tested, albumin exhibited significantly lower pH values than fibrinogen (2 mg/mL and 8 mg/mL), however, this did not correspond to increased aggregation as predicted by the model. The discrepancy between the model's predictions for aggregation parameters in fibrinogen and albumin with respect to pH indicate that pH is not the principle contributor to aggregation in albumin solutions. A possible explanation is that the low pH of albumin solutions caused oxygen to dissociate from hemoglobin before the experiments

were performed (during the sample preparation). According to the model, for venous blood (PO_2 ≈ 40mmHg) a change of pH from physiological (as for PBS at 37°C) to pH 6.8 (as for albumin 50 mg/mL at 37°C) would cause the oxygen saturation of hemoglobin to reduce from 76% SO_2 to 33% SO_2 the moment the erythrocytes were suspended in albumin 50 mg/mL, that is before the start of the experiment. Being that the SO_2 in solutions with pH less than 7.4 at 37°C was reduced prior to the experiment, the contributions of pH-induced oxyhemoglobin dissociation to erythrocyte aggregation in these experiments may have been masked.

Temperature Dependence of Erythrocyte Aggregation

Dynamic heating of erythrocytes showed an increase in aggregation with increased temperature while the cells subject to static hyperthermia did not. In the onset of stasis model, aggregation rate increased in plasma with increased temperature. The results of these studies (shown as Figure 53 for ease of comparison) indicate that it is the increase in temperature that causes erythrocyte aggregation, not temperature itself. A potential explanation for the aggregation observed in the dynamic heating model (Figure 53 left), but not in the static

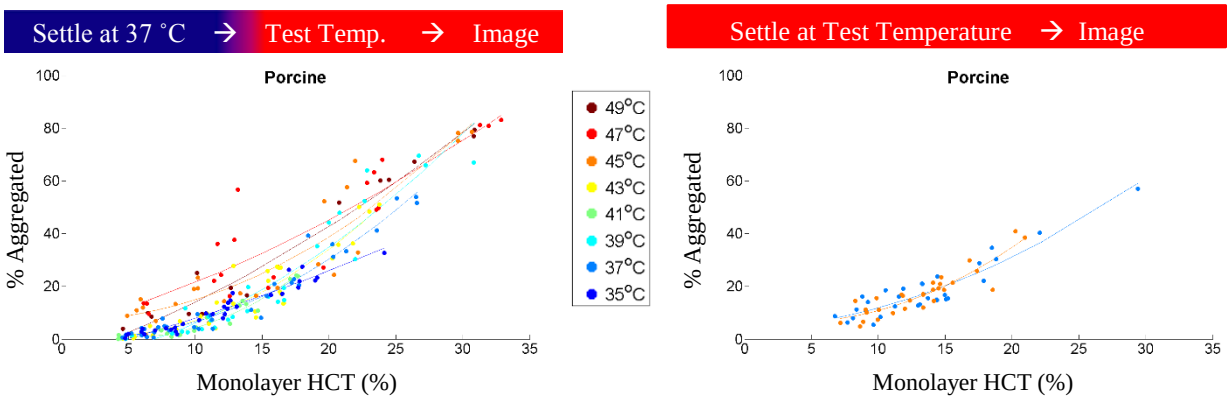

Figure 53: *Aggregation in dynamic heating model versus static hyperthermia model.* ***Left)*** *Figure 36: Washed erythrocytes in PBS were allowed to settle in a channel while subject to dynamic heating; or* ***Right)*** *Figure 37: static hyperthermia. Trend lines are second-order polynomial best fit (least squares) for each temperature.*

hyperthermia model (Figure 53 right) is that the hemoglobin oxygen saturation states were

different in the two models. In the dynamic heating model, erythrocytes likely experienced a temperature-induced reduction of oxygenated hemoglobin. In the case of the static hyperthermia model, the reduction of hemoglobin oxygenation from elevated temperature would not have occurred during image acquisition because the cells had been brought to the test temperature prior to imaging, this is supported by the computational model. To study the effects of temperature on erythrocyte aggregation, only experimental models using dynamic heating methods should be used.

In the Onset of Stasis model, no significant temperature-dependence of erythrocyte aggregation magnitude was observed for samples equilibrated with room gas, however, their aggregation rate was significantly increased with temperature for samples in autologous plasma. Interestingly, the temperature-dependence of aggregation metrics varied as a function of oxygen level in the Onset of Stasis model (controlled gas), this is discussed below.

Blood Oxygenation Dependence of Erythrocyte Aggregation

Samples equilibrated with prescribed oxygen levels in the Onset of Stasis model exhibited temperature-dependent aggregation magnitudes that were consistent with the predictions of the computational model. Samples suspended in autologous plasma, in the presence of DIDS inhibitor, showed a trend of increased in aggregation magnitude and rate with increased temperature from 37°C to 45°C for all oxygen levels tested except for 100% oxygen. Control samples suspended in autologous plasma that were equilibrated with oxygen levels similar to that of venous blood (5% and 10% oxygen) exhibited increased aggregation magnitude and rate with increasing temperature consistent with the results of the computational model that indicated oxyhemoglobin dissociation was likely to contribute to surface nanobubbles under these conditions. It was unexpected that samples suspended in autologous plasma equilibrated

with 0% oxygen also showed a trend of increasing aggregation magnitude and rate with temperature elevation, it was predicted that temperature would not have an effect on this group because, theoretically, there would not be any oxygen bound to hemoglobin, thus no oxyhemoglobin dissociation. A possible cause of the temperature dependence of aggregation in this sample could be contamination by atmospheric oxygen or that there exists an additional mechanism of aggregation that was not predicted by the model.

Interestingly, the aggregation magnitude of samples suspended in autologous plasma and heated to 49°C differed between groups with respect to oxygenation level. After a temperature-dependent increase in aggregation magnitude, with temperature rise from 37°C to 45°C in the samples equilibrated with 5% and 10% oxygen, no further changes were observed at 49°C in the 5% oxygen sample whereas a significant reduction of aggregation magnitude was observed at 49°C in the 10% oxygen sample. A similar reduction of aggregation magnitude was observed at 49°C in the 100% oxygen samples, after not having changed with temperature increase from 37°C to 45°C. The sharp reduction of aggregation magnitude at 49°C in samples equilibrated with higher oxygen levels is likely related to the increase of dissolved oxygen solubility caused by the inhomogeneity of protein in solution following the heat-induced coagulation of fibrinogen observed in specific aim 2.

Membrane Protein Treatment Effects on Erythrocyte Aggregation

In the onset of stasis model (Room Gas), minimal differences in the magnitude of aggregation were detected between non-treated erythrocytes and those treated with anti-band 3, anti-$\alpha_v\beta_3$, or anti-GYPC in PBS nor in autologous plasma. Anti-band 3, and anti-GYPC tested specific binding of extracellular regions of erythrocyte membrane proteins while anti-$\alpha_v\beta_3$ tested

non- specific binding of extracellular regions of erythrocyte membrane proteins. Anti-band 3, anti-$\alpha_v\beta_3$, and anti-GYPC all bind to the extracellular side of membrane proteins, thus the results of this study indicate that the mechanism erythrocyte aggregation is not sufficiently explained by the bridging model, however, the results do not refute the involvement of plasma proteins in erythrocyte aggregation. The lack of differences in aggregation in the presence of anti-band 3, and anti-GYPC indicate that the extracellular domains of these proteins are not mediators of aggregation but more studies need to be performed to investigate the intracellular domains of GYPC and band 3 as mediators of aggregation. The interaction of DIDS with band 3 is thought affect the intracellular domain of band 3 and cause reduction in the affinity of band 3 to spectrin which subsequently reduces temperature-dependent erythrocyte membrane deformation and subsequent reduction of aggregation. Although, due to small sample size (n=1) performed for DIDS inhibition of band 3 (n=1) in the Onset of Stasis (Room Gas) assay, the reduction of aggregation in the presence of DIDS was not significant, however, a clear reduction of aggregation and temperature-dependent trend was evident. This provided a strong basis for further investigation of DIDS as a mediator of aggregation in the Onset of Stasis model (Controlled Gas).

In the Onset of Stasis model (Controlled Gas), aggregation of erythrocytes suspended in autologous plasma and fibrinogen 8 mg/mL was significantly less (compared to control) for erythrocytes with band 3 inhibition by DIDS. In autologous plasma, aggregation magnitude was approximately halved in the presence of DIDS, and essentially eliminated for erythrocytes suspended in fibrinogen 8 mg/mL. It was expected that a similar reduction of aggregation magnitude were to be exhibited by erythrocytes suspended in the other protein solutions tested, however, the minimal aggregation observed in the control experiments provided minimal room

for reduction of aggregation by DIDS inhibition of band 3, thus no differences were detected. The results of these experiments support the hypothesis that the intracellular domain of band 3 is largely involved with erythrocyte aggregation.

Conclusion

This study presents new findings that will contribute to the discovery of new mechanisms of particle interactions. We proposed, computationally modelled, and experimentally tested a theoretical model of erythrocyte aggregation where excess gas from oxy-hemoglobin dissociation and gas dissolution forms nanobubbles on the extracellular surface of erythrocyte membranes and mediates interactions between neighboring cells. Many of the experimental results presented here served to validate those predicted by the theoretical model. While this study investigated the contribution of oxygen nanobubbles to erythrocyte aggregation during the onset of thermal burn injury, the general mechanism of nanobubble-mediated aggregation that was corroborated by our experiments may have relevance in other pathologies that are characterized by blood constituent changes including, but not limited to, diabetes, sickle cell anemia, and sepsis. Nanobubbles can also form by cavitation near mechanical heart valves and influence cell interactions in such scenarios.

The mechanism of particle interaction by surface nanobubble interactions may also be relevant to entirely different fields and could become the subject of future studies. For example, the mechanism of brewer's yeast flocculation during fermentation is still not fully understood. It is likely that carbon dioxide, a byproduct of fermentation, forms bubbles on yeast, when the solution in which they are suspended becomes super-saturated, leading to a similar scenario of aggregation by surface nanobubble interactions. The mechanism may also have applications in fields related to water treatment, and environmental engineering. Most previously proposed mechanisms of particle aggregation require particles or cells to come into contact by random Brownian motion before an interaction can occur, an interesting attribute of the mechanism proposed here is the non-random and relatively long-ranged attractive force between

nanobubbles resulting from surface tension. Future advances in super-resolution microscopy for in-situ imaging, where the sample environment is not perturbed by the imaging system, will enable visualization of nanobubbles and allow a better understanding of the contribution of surface nanobubbles to particle interactions.

References

1. Dobbe, I. (2002). Engineering Developments in hemorheology. PhD Thesis, UvA-DARE.
2. H. Elnaiem, D. C., P. Misra, S.M. Gatica. (2009). Nanobubbles at water-solid interfaces: Calculation of the contact angle based on a simple model. *Computers, Materials and Continua* **14**, 23-34.
3. Gunter, G. (2015). Band 3 and Glycophorin C as Potential Mediators of Erythrocyte Aggregation in Thermal Injury, Stony Brook University.
4. Wagner, C., Steffen, P. & Svetina, S. (2013). Aggregation of red blood cells: From rouleaux to clot formation. *Comptes Rendus Physique* **14**, 459-469.
5. Severinghaus, J. W. (1958). Oxyhemoglobin dissociation curve correction for temperature and pH variation in human blood. *J Appl Physiol* **12**, 485-6.
6. Parker, J. L., Claesson, P. M. & Attard, P. (1994). Bubbles, cavities, and the long-ranged attraction between hydrophobic surfaces. *The Journal of Physical Chemistry* **98**, 8468-8480.
7. Ramakrishnan, S., Degenhardt, R., Vietzke, K., Grebe, R., Singh, M. & Schmid-Schönbein, H. (2001). Influence of immunoglobulin G and immunoglobulin A on erythrocyte aggregation: a comparative study. *ITBM-RBM* **22**, 241-246.
8. Brust, M., Aouane, O., Thiébaud, M., Flormann, D., Verdier, C., Kaestner, L., Laschke, M. W., Selmi, H., Benyoussef, A., Podgorski, T., Coupier, G., Misbah, C. & Wagner, C. (2014). The plasma protein fibrinogen stabilizes clusters of red blood cells in microcapillary flows. *Sci. Rep.* **4**.
9. Rosina, J., Kvasnak, E., Suta, D., Kolarova, H., Malek, J. & Krajci, L. (2007). Temperature dependence of blood surface tension. *Physiol Res* **56 Suppl 1**, S93-8.
10. Luna, E. J. & Hitt, A. L. (1992). Cytoskeleton--plasma membrane interactions. *Science* **258**, 955-64.
11. Lim, H. J., Lee, Y. J., Nam, J. H., Chung, S. & Shin, S. (2010). Temperature-dependent threshold shear stress of red blood cell aggregation. *J Biomech* **43**, 546-50.
12. Repin, N. V., Bobrova, E. N. & Repina, S. V. (2008). Thermally induced transformation of mammalian red blood cells during hyperthermia. *Bioelectrochemistry* **73**, 101-5.
13. Pittman, R. N. (2011). Regulation of Tissue Oygenation. *Morgan & Claypool Life Sciences* **3**, 1-100.
14. Jackson, D. M. (1953). [The diagnosis of the depth of burning]. *Br J Surg* **40**, 588-96.
15. Edlich, R. F., Larkham, N., O'Hanlan, J. T., Berry, R., Hiebert, J., Rodeheaver, G. T. & Edgerton, M. T. (1978). Modification of the american burn association injury severity grading system. *Journal of the American College of Emergency Physicians* **7**, 226-228.
16. Soballe Md, P. W., Nimbkar Md, N. V., Hayward Dvm, I., Nielsen PhD, T. B. & Drucker Md, W. R. (1998). Electric Cautery Lowers the Contamination Threshold for Infection of Laparotomies 12. *The American Journal of Surgery* **175**, 263-266.
17. Kneeland, P. P. & Fang, M. C. (2009). Trends in Catheter Ablation for Atrial Fibrillation in the United States. *Journal of hospital medicine : an official publication of the Society of Hospital Medicine* **4**, E1-E5.
18. Moritz, A. R. & Henriques, F. C. (1947). Studies of Thermal Injury: II. The Relative Importance of Time and Surface Temperature in the Causation of Cutaneous Burns. *The American Journal of Pathology* **23**, 695-720.
19. Lanier, S. T., McClain, S. A., Lin, F., Singer, A. J. & Clark, R. A. (2011). Spatiotemporal progression of cell death in the zone of ischemia surrounding burns. *Wound Repair Regen* **19**, 622-32.
20. Kao, C. C. & Garner, W. L. (2000). Acute Burns. *Plast Reconstr Surg* **101**, 2482-2493.

21. Pries, A. R., Secomb, T. W., Gaehtgens, P. & Gross, J. F. (1990). Blood flow in microvascular networks. Experiments and simulation. *Circ Res* **67**, 826-34.
22. Gunter, G., Seidner, H. & Frame, M. (2015). Thermally Induced Erythrocyte Aggregation in Mammals. *The FASEB Journal* **29**.
23. Barshtein, G., Wajnblum, D. & Yedgar, S. (2000). Kinetics of linear rouleaux formation studied by visual monitoring of red cell dynamic organization. *Biophys J* **78**, 2470-4.
24. Alonso, C., Pries, A. R. & Gaehtgens, P. (1993). Time-dependent rheological behavior of blood at low shear in narrow vertical tubes. *Am J Physiol* **265**, H553-61.
25. Steck, T. L. (1974). THE ORGANIZATION OF PROTEINS IN THE HUMAN RED BLOOD CELL MEMBRANE : A Review. *The Journal of Cell Biology* **62**, 1-19.
26. Rasia, M. & Bollini, A. (1998). Red blood cell shape as a function of medium's ionic strength and pH. *Biochimica et Biophysica Acta (BBA) - Biomembranes* **1372**, 198-204.
27. Mohandas, N., Clark, M. R., Jacobs, M. S. & Shohet, S. B. (1980). Analysis of factors regulating erythrocyte deformability. *Journal of Clinical Investigation* **66**, 563-573.
28. Van Dort, H. M., Moriyama, R. & Low, P. S. (1998). Effect of band 3 subunit equilibrium on the kinetics and affinity of ankyrin binding to erythrocyte membrane vesicles. *J Biol Chem* **273**, 14819-26.
29. Mayer, D. C. G., Jiang, L., Achur, R. N., Kakizaki, I., Gowda, D. C. & Miller, L. H. (2006). The glycophorin C N-linked glycan is a critical component of the ligand for the Plasmodium falciparum erythrocyte receptor BAEBL. *Proceedings of the National Academy of Sciences of the United States of America* **103**, 2358-2362.
30. Chasis, J. A. & Mohandas, N. (1992). Red blood cell glycophorins. *Blood* **80**, 1869-79.
31. Poole, J. (2000). Red cell antigens on band 3 and glycophorin A. *Blood Rev* **14**, 31-43.
32. Ivanov, I. T., Paarvanova, B. & Slavov, T. (2012). Dipole relaxation in erythrocyte membrane: involvement of spectrin skeleton. *Bioelectrochemistry* **88**, 148-55.
33. An, X., Guo, X., Zhang, X., Baines, A. J., Debnath, G., Moyo, D., Salomao, M., Bhasin, N., Johnson, C., Discher, D., Gratzer, W. B. & Mohandas, N. (2006). Conformational stabilities of the structural repeats of erythroid spectrin and their functional implications. *J Biol Chem* **281**, 10527-32.
34. Stefanovic, M., Puchulu-Campanella, E., Kodippili, G. & Low, P. S. (2013). Oxygen regulates the band 3–ankyrin bridge in the human erythrocyte membrane. *The Biochemical journal* **449**, 143-150.
35. Lepke, S., Fasold, H., Pring, M. & Passow, H. (1976). A study of the relationship between inhibition of anion exchange and binding to the red blood cell membrane of 4,4'-diisothiocyano stilbene-2,2'-disulfonic acid (DIDS) and its dihydro derivative (H2DIDS). *J Membr Biol* **29**, 147-77.
36. Matei, H., Frentescu, L. & Benga, G. (2000). Comparative studies of the protein composition of red blood cell membranes from eight mammalian species. *J Cell Mol Med* **4**, 270-276.
37. Baskurt, O. K., Farley, R. A. & Meiselman, H. J. (1997). Erythrocyte aggregation tendency and cellular properties in horse, human, and rat: a comparative study. *Am J Physiol* **273**, H2604-12.
38. Weng, X., Cloutier, G., Pibarot, P. & Durand, L. G. (1996). Comparison and simulation of different levels of erythrocyte aggregation with pig, horse, sheep, calf, and normal human blood. *Biorheology* **33**, 365-77.
39. Hardeman, M. R., Dobbe, J. G. & Ince, C. (2001). The Laser-assisted Optical Rotational Cell Analyzer (LORCA) as red blood cell aggregometer. *Clin Hemorheol Microcirc* **25**, 1-11.
40. Singh, M. & Shin, S. (2009). Changes in erythrocyte aggregation and deformability in diabetes mellitus: a brief review. *Indian J Exp Biol* **47**, 7-15.
41. Levin, G. Y. & Egorihina, M. N. (2011). Aggregation of erythrocytes in burn disease. *International Journal of Burns and Trauma* **1**, 34-41.

42. Samocha-Bonet, D., Ben-Ami, R., Shapira, I., Shenkerman, G., Abu-Abeid, S., Stern, N., Mardi, T., Tulchinski, T., Deutsch, V., Yedgar, S., Barshtein, G. & Berliner, S. (2004). Flow-resistant red blood cell aggregation in morbid obesity. *Int J Obes Relat Metab Disord* **28**, 1528-34.
43. Alejandra Aguayo-Becerra, O., Torres-Garibay, C., Dassaejv Macías-Amezcua, M., Fuentes-Orozco, C., de Guadalupe Chávez-Tostado, M., Andalón-Dueñas, E., Espinosa Partida, A., Álvarez-Villaseñor, A. D. S., Cortés-Flores, A. O. & Alejandro, G.-O. (2013). Serum albumin level as a risk factor for mortality in burn patients. *Clinics* **68**, 940-945.
44. Uyuklu, M., Canpolat, M., Meiselman, H. J. & Baskurt, O. K. (2011). Wavelength selection in measuring red blood cell aggregation based on light transmittance. *Journal of Biomedical Optics* **16**, 117006.
45. Uyuklu, M., Meiselman, H. J. & Baskurt, O. K. (2009). Effect of hemoglobin oxygenation level on red blood cell deformability and aggregation parameters. *Clin Hemorheol Microcirc* **41**, 179-88.
46. Baskurt, O. K. (2011). Alterations in Red Blood Cell Aggregation. In *Red Blood Cell Aggregation*, pp. 223-268. 0 vols. CRC Press.
47. Berlin, N. I. (1964). DEtermination of red blood cell life span. *JAMA* **188**, 375-378.
48. Murphy, J. R. (1973). Influence of temperature and method of centrifugation on the separation of erythrocytes. *J Lab Clin Med* **82**, 334-41.
49. Nordt, F. J. (1983). Hemorheology in cerebrovascular diseases: approaches to drug development. *Ann N Y Acad Sci* **416**, 651-61.
50. Severinghaus, J. W. (1966). Blood gas calculator. *J Appl Physiol* **21**, 1108-16.
51. Sander, R. (2015). Compilation of Henry's law constants (version 4.0) for water as solvent. *Atmos. Chem. Phys.* **15**, 4399-4981.
52. Feher, J. (2012). 6.4 - Oxygen and Carbon Dioxide Transport. In *Quantitative Human Physiology* (Feher, J., ed.), pp. 586-594. Academic Press, Boston.
53. Geers, C. & Gros, G. (2000). Carbon dioxide transport and carbonic anhydrase in blood and muscle. *Physiol Rev* **80**, 681-715.
54. Li, D., Jing, D., Pan, Y., Wang, W. & Zhao, X. (2014). Coalescence and stability analysis of surface nanobubbles on the polystyrene/water interface. *Langmuir* **30**, 6079-88.
55. Rachana & Banerjee, R. (2004). Interactions between hematological derivatives and dipalmitoyl phosphatidyl choline: implications for adult respiratory distress syndrome. *Colloids and Surfaces B: Biointerfaces* **34**, 95-104.
56. Katona, E., Neumann, A. W. & Moscarello, M. A. (1978). The temperature dependence of the surface tension of aqueous solutions of plasma proteins. *Biochim Biophys Acta* **534**, 275-84.
57. Ami, R. B., Barshtein, G., Zeltser, D., Goldberg, Y., Shapira, I., Roth, A., Keren, G., Miller, H., Prochorov, V., Eldor, A., Berliner, S. & Yedgar, S. (2001). Parameters of red blood cell aggregation as correlates of the inflammatory state. *Am J Physiol Heart Circ Physiol* **280**, H1982-8.
58. Baskurt, O. K., Bor-Kucukatay, M., Yalcin, O., Meiselman, H. J. & Armstrong, J. K. (2000). Standard aggregating media to test the "aggregability" of rat red blood cells. *Clin Hemorheol Microcirc* **22**, 161-6.
59. Fox, R. J. & Frame, M. D. (2002). Arteriolar flow recruitment with vitronectin receptor stimulation linked to remote wall shear stress. *Microvasc Res* **64**, 414-24.
60. Shriwastav, A., Sudarsan, G., Bose, P. & Tare, V. (2010). Modification of Winkler's method for determination of dissolved oxygen concentration in small sample volumes. *Analytical Methods* **2**, 1618-1622.
61. Eaton, A. D., Clesceri, L. S., Greenberg, A. E., Franson, M. A. H., American Public Health, A., American Water Works, A. & Water Environment, F. (1998). *Standard methods for the examination of water and wastewater*, American Public Health Association, Washington, DC.
62. Will, Y., Hynes, J., Ogurtsov, V. I. & Papkovsky, D. B. (2007). Analysis of mitochondrial function using phosphorescent oxygen-sensitive probes. *Nat. Protocols* **1**, 2563-2572.

63. Hoek, I., Tho, F. & Arnold, W. M. (2010). Sodium hydroxide treatment of PDMS based microfluidic devices. *Lab Chip* **10**, 2283-5.
64. Alonso, C., Pries, A. R. & Gaehtgens, P. (1989). Time-dependent rheological behaviour of blood flow at low shear in narrow horizontal tubes. *Biorheology* **26**, 229-46.
65. Alonso, C., Pries, A. R., Kiesslich, O., Lerche, D. & Gaehtgens, P. (1995). Transient rheological behavior of blood in low-shear tube flow: velocity profiles and effective viscosity. *Am J Physiol* **268**, H25-32.
66. Cokelet, G. R. & Goldsmith, H. L. (1991). Decreased hydrodynamic resistance in the two-phase flow of blood through small vertical tubes at low flow rates. *Circ Res* **68**, 1-17.
67. Pries, A. R., Secomb, T. W. & Gaehtgens, P. (1995). Structure and hemodynamics of microvascular networks: heterogeneity and correlations. *American Journal of Physiology - Heart and Circulatory Physiology* **269**, H1713-H1722.
68. Chien, S., Usami, S., Taylor, H. M., Lundberg, J. L. & Gregersen, M. I. (1966). Effects of hematocrit and plasma proteins on human blood rheology at low shear rates. *J Appl Physiol* **21**, 81-7.
69. Rubenstein, D. A., Yin, W. & Frame, M. D. (2012). Chapter 6 - Microvascular Beds. In *Biofluid Mechanics* (Rubenstein, D. A., Yin, W. & Frame, M. D., eds.), pp. 181-215. Academic Press, Boston.
70. Popel, A. S. & Johnson, P. C. (2005). Microcirculation and Hemorheology. *Annual review of fluid mechanics* **37**, 43-69.
71. Namdee, K., Carrasco-Teja, M., Fish, M. B., Charoenphol, P. & Eniola-Adefeso, O. (2015). Effect of Variation in hemorheology between human and animal blood on the binding efficacy of vascular-targeted carriers. *Scientific Reports* **5**, 11631.

Appendix A: MATLAB-based Image Analysis Script (for Stationary and Settling Models)

```
%Analysis of Erythrocyte Aggregation in Stationary Model (Dynamic Heating)
%and Settling Model (Static Hyperthermia)

%2015 Harrison Seidner and Geoffrey Gunter

function varargout = catmintGUI4(varargin)
% CATMINTGUI4 MATLAB code for catmintGUI4.fig
%      CATMINTGUI4, by itself, creates a new CATMINTGUI4 or raises the
existing
%      singleton*.
%
%      H = CATMINTGUI4 returns the handle to a new CATMINTGUI4 or the handle
to
%      the existing singleton*.
%
%      CATMINTGUI4('CALLBACK',hObject,eventData,handles,...) calls the local
%      function named CALLBACK in CATMINTGUI4.M with the given input
arguments.
%
%      CATMINTGUI4('Property','Value',...) creates a new CATMINTGUI4 or
raises the
%      existing singleton*.  Starting from the left, property value pairs are
%      applied to the GUI before catmintGUI4_OpeningFcn gets called.  An
%      unrecognized property name or invalid value makes property application
%      stop.  All inputs are passed to catmintGUI4_OpeningFcn via varargin.
%
%      *See GUI Options on GUIDE's Tools menu.  Choose "GUI allows only one
%      instance to run (singleton)".
%
% See also: GUIDE, GUIDATA, GUIHANDLES

% Edit the above text to modify the response to help catmintGUI4

% Last Modified by GUIDE v2.5 27-Feb-2015 09:45:10

% Begin initialization code - DO NOT EDIT
gui_Singleton = 1;
gui_State = struct('gui_Name',       mfilename, ...
                   'gui_Singleton',  gui_Singleton, ...
                   'gui_OpeningFcn', @catmintGUI4_OpeningFcn, ...
                   'gui_OutputFcn',  @catmintGUI4_OutputFcn, ...
                   'gui_LayoutFcn',  [] , ...
                   'gui_Callback',   []);
if nargin && ischar(varargin{1})
    gui_State.gui_Callback = str2func(varargin{1});
end

if nargout
    [varargout{1:nargout}] = gui_mainfcn(gui_State, varargin{:});
else
    gui_mainfcn(gui_State, varargin{:});
end
% End initialization code - DO NOT EDIT

% --- Executes just before catmintGUI4 is made visible.
```

```
function catmintGUI4_OpeningFcn(hObject, eventdata, handles, varargin)

% Choose default command line output for catmintGUI4
handles.output = hObject;

% Update handles structure
guidata(hObject, handles);

% Initialize handles/sliders/axes, make message log uneditable
try
    if isfield(handles,'data')
        handles=rmfield(handles,'data');
    end

    handles.int_thresh = get(handles.slider1,'Value');
    set(handles.text3,'String',num2str(handles.int_thresh))
    handles.clump_thresh = get(handles.slider2,'Value');
    set(handles.text4,'String',num2str(handles.clump_thresh))

    handles.expt_date='';
    handles.date_cells_collected='';
    handles.mHTC='';
    handles.temp='';
    handles.expt_group='';
    handles.ID='';
    handles.species='';
    handles.gender='';
    handles.age='';
    handles.weight='';
    handles.treatment='';
    handles.date_review='';
    handles.inits='';
    handles.tophat=0;

    pos=[185,426,486,7];%get(handles.axes4,'Position');%
    handles.progbar=axes('Units','pixels','Position',pos,'XLim',[0
1],'YLim',[0 1],'XTick',[],'YTick',[]);
    uiprogbar(handles.progbar,0);

    % msglog_java=findjobj(handles.edit12);
    % set(msglog_java,'Editable',0);

    guidata(hObject, handles);
catch errorObj
    errordlg(getReport(errorObj,'extended','hyperlinks','off'),'Error');
end

% --- Outputs from this function are returned to the command line.
function varargout = catmintGUI4_OutputFcn(hObject, eventdata, handles)

% Get default command line output from handles structure
varargout{1} = handles.output;

% --- Executes on button press in pushbutton1.
function pushbutton1_Callback(hObject, eventdata, handles)
```

```
% "Open Folder" Pushbutton
try
    handles.data=uigetdir('.','Select Directory');
    msg=sprintf('Open Directory \t%s\n',handles.data);
    msglog=get(handles.edit12,'String');
    msglog{end+1}=msg;
    set(handles.edit12,'String',msglog)
    guidata(hObject, handles);
catch errorObj
    errordlg(getReport(errorObj,'extended','hyperlinks','off'),'Error');
end

% --- Executes on button press in pushbutton2.
function pushbutton2_Callback(hObject, eventdata, handles)
% "Open File" Pushbutton
try
    [filename,filepath]=uigetfile('./*.tif','Select File');
    handles.data=strcat(filepath,filename);
    msg=sprintf('Open File \t%s\n',handles.data);
    msglog=get(handles.edit12,'String');
    msglog{end+1}=msg;
    set(handles.edit12,'String',msglog)
    guidata(hObject, handles);
catch errorObj
    errordlg(getReport(errorObj,'extended','hyperlinks','off'),'Error');
end

% --- Executes on slider movement.
function slider2_Callback(hObject, eventdata, handles)
% "Clump Threshold" Slider
try
    handles.clump_thresh = round(get(handles.slider2,'Value'));
    set(handles.text4,'String',num2str(round(handles.clump_thresh)))
    guidata(hObject, handles);
catch errorObj
    errordlg(getReport(errorObj,'extended','hyperlinks','off'),'Error');
end

% --- Executes during object creation, after setting all properties.
function slider2_CreateFcn(hObject, eventdata, handles)
if isequal(get(hObject,'BackgroundColor'),
get(0,'defaultUicontrolBackgroundColor'))
    set(hObject,'BackgroundColor',[.9 .9 .9]);
end

% --- Executes on button press in pushbutton3.
function pushbutton3_Callback(hObject, eventdata, handles)
% "RUN CATMINT" Pushbutton
try
    data=handles.data;
    int_thresh=handles.int_thresh;
    clump_thresh=handles.clump_thresh;
    msg=sprintf('Run Catmint \tInt Threshold - %f, Clump Threshold -
%f\n',int_thresh,clump_thresh);
    msglog=get(handles.edit12,'String');
    msglog{end+1}=msg;
```

```
    set(handles.edit12,'String',msglog)
    [Objects,Clumps,Singlets,HTC_comp] =
catmint(data,int_thresh,clump_thresh,handles.tophat,handles.progbar);
    handles.Objects=Objects;
    handles.Clumps=Clumps;
    handles.Singlets=Singlets;
    handles.HTC_comp=HTC_comp;
    assignin('base','Objects',Objects)
    assignin('base','Clumps',Clumps)
    assignin('base','Singlets',Singlets)
    assignin('base','HTC_comp',HTC_comp)
    guidata(hObject,handles)
catch errorObj
    errordlg(getReport(errorObj,'extended','hyperlinks','off'),'Error');
end

% --- Executes on button press in pushbutton4.
function pushbutton4_Callback(hObject, eventdata, handles)
% "Export to Excel" Pushbutton
try
    uiprogbar(handles.progbar,0);
    [filename,pathname]=uiputfile('./*.xlsx','Select Excel File');
    handles.excel_out=strcat(pathname,filename);
    pause(0.5)

    msg=sprintf('Export to \t%s\n',handles.excel_out);
    msglog=get(handles.edit12,'String');
    msglog{end+1}=msg;
    set(handles.edit12,'String',msglog)

    fields=fieldnames(handles.Objects);
    [dates{1:length(fields),1}]=deal(handles.expt_date);
    [species{1:length(fields),1}]=deal(handles.species);
    [ID{1:length(fields),1}]=deal(handles.ID);
    [temps{1:length(fields),1}]=deal(handles.temp);
    [mHTCs{1:length(fields),1}]=deal(handles.mHTC);
    [groups{1:length(fields),1}]=deal(handles.group);
    [gender{1:length(fields),1}]=deal(handles.gender);
    [age{1:length(fields),1}]=deal(handles.age);
    [weight{1:length(fields),1}]=deal(handles.weight);
    [treatment{1:length(fields),1}]=deal(handles.treatment);
    [date_cells{1:length(fields),1}]=deal(handles.date_cells_collected);
    [review_date{1:length(fields),1}]=deal(handles.date_review);
    [inits{1:length(fields),1}]=deal(handles.inits);

    uiprogbar(handles.progbar,0.1);

    objects=zeros(length(fields),1);
    object_areas=zeros(length(fields),1);
    clumps=zeros(length(fields),1);
    clump_areas=zeros(length(fields),1);
    singlets=zeros(length(fields),1);
    singlet_areas=zeros(length(fields),1);
    HTC_comp=zeros(length(fields),1);
    for i=1:length(fields)
        objects(i)=length(handles.Objects.(fields{i}));
```

```
        object_areas(i)=mean(handles.Objects.(fields{i}));
        clumps(i)=length(handles.Clumps.(fields{i}));
        clump_areas(i)=mean(handles.Clumps.(fields{i}));
        singlets(i)=length(handles.Singlets.(fields{i}));
        singlet_areas(i)=mean(handles.Singlets.(fields{i}));
        HTC_comp(i)=handles.HTC_comp.(fields{i});
    end
    uiprogbar(handles.progbar,0.2);

    age_cells=datenum(dates)-datenum(date_cells);

ratio_cells_clumped=(clump_areas.*clumps)./(singlet_areas.*singlets+clump_are
as.*clumps);
    uiprogbar(handles.progbar,0.3);

    if exist(handles.excel_out,'file')
        [~,m,~]=xlsread(handles.excel_out,2);
        n=length(m(:,1))+1;
    else
        n=2;
    end


sheet=cat(2,dates,species,ID,temps,mHTCs,groups,gender,age,weight,treatment,.
..

date_cells,num2cell(age_cells),num2cell(HTC_comp),num2cell(objects),...

num2cell(object_areas),num2cell(clumps),num2cell(clump_areas),num2cell(single
ts),...

num2cell(singlet_areas),num2cell(ratio_cells_clumped),review_date,inits);
    uiprogbar(handles.progbar,0.4);

    xlswrite(handles.excel_out,sheet,2,strcat('A',num2str(n)))
    uiprogbar(handles.progbar,0.9);
    pause(0.5)
    uiprogbar(handles.progbar,1);
catch errorObj
    errordlg(getReport(errorObj,'extended','hyperlinks','off'),'Error');
end

function edit11_Callback(hObject, eventdata, handles)
% "Weight" text
try
    handles.weight=get(hObject,'String');
    guidata(hObject, handles);
catch errorObj
    errordlg(getReport(errorObj,'extended','hyperlinks','off'),'Error');
end

% --- Executes during object creation, after setting all properties.
function edit11_CreateFcn(hObject, eventdata, handles)
if ispc && isequal(get(hObject,'BackgroundColor'),
get(0,'defaultUicontrolBackgroundColor'))
    set(hObject,'BackgroundColor','white');
```

```
end

function edit10_Callback(hObject, eventdata, handles)
% "Age" text
try
    handles.age=get(hObject,'String');
    guidata(hObject, handles);
catch errorObj
    errordlg(getReport(errorObj,'extended','hyperlinks','off'),'Error');
end

% --- Executes during object creation, after setting all properties.
function edit10_CreateFcn(hObject, eventdata, handles)
if ispc && isequal(get(hObject,'BackgroundColor'),
get(0,'defaultUicontrolBackgroundColor'))
    set(hObject,'BackgroundColor','white');
end

function edit8_Callback(hObject, eventdata, handles)
% "Gender" text
try
    handles.gender=get(hObject,'String');
    guidata(hObject, handles);
catch errorObj
    errordlg(getReport(errorObj,'extended','hyperlinks','off'),'Error');
end

% --- Executes during object creation, after setting all properties.
function edit8_CreateFcn(hObject, eventdata, handles)
if ispc && isequal(get(hObject,'BackgroundColor'),
get(0,'defaultUicontrolBackgroundColor'))
    set(hObject,'BackgroundColor','white');
end

function edit6_Callback(hObject, eventdata, handles)
% "Species/Strain" text
try
    handles.species=get(hObject,'String');
    guidata(hObject, handles);
catch errorObj
    errordlg(getReport(errorObj,'extended','hyperlinks','off'),'Error');
end

% --- Executes during object creation, after setting all properties.
function edit6_CreateFcn(hObject, eventdata, handles)
if ispc && isequal(get(hObject,'BackgroundColor'),
get(0,'defaultUicontrolBackgroundColor'))
    set(hObject,'BackgroundColor','white');
end



function edit4_Callback(hObject, eventdata, handles)
% "Temperature" text
try
```

```
    handles.temp=get(hObject,'String');
    guidata(hObject, handles);
catch errorObj
    errordlg(getReport(errorObj,'extended','hyperlinks','off'),'Error');
end

% --- Executes during object creation, after setting all properties.
function edit4_CreateFcn(hObject, eventdata, handles)
if ispc && isequal(get(hObject,'BackgroundColor'),
get(0,'defaultUicontrolBackgroundColor'))
    set(hObject,'BackgroundColor','white');
end

function edit3_Callback(hObject, eventdata, handles)
% "monolayer HTC" text
try
    handles.mHTC=get(hObject,'String');
    guidata(hObject, handles);
catch errorObj
    errordlg(getReport(errorObj,'extended','hyperlinks','off'),'Error');
end

% --- Executes during object creation, after setting all properties.
function edit3_CreateFcn(hObject, eventdata, handles)
if ispc && isequal(get(hObject,'BackgroundColor'),
get(0,'defaultUicontrolBackgroundColor'))
    set(hObject,'BackgroundColor','white');
end

function edit2_Callback(hObject, eventdata, handles)
% "Date Cells Collected" text
try
    handles.date_cells_collected=get(hObject,'String');
    guidata(hObject, handles);
catch errorObj
    errordlg(getReport(errorObj,'extended','hyperlinks','off'),'Error');
end

% --- Executes during object creation, after setting all properties.
function edit2_CreateFcn(hObject, eventdata, handles)
if ispc && isequal(get(hObject,'BackgroundColor'),
get(0,'defaultUicontrolBackgroundColor'))
    set(hObject,'BackgroundColor','white');
end

function edit1_Callback(hObject, eventdata, handles)
% "Experiment Date" text
try
    handles.expt_date=get(hObject,'String');
    guidata(hObject, handles);
catch errorObj
    errordlg(getReport(errorObj,'extended','hyperlinks','off'),'Error');
end

% --- Executes during object creation, after setting all properties.
```

```
function edit1_CreateFcn(hObject, eventdata, handles)
if ispc && isequal(get(hObject,'BackgroundColor'),
get(0,'defaultUicontrolBackgroundColor'))
    set(hObject,'BackgroundColor','white');
end

% --- Executes on slider movement.
function slider1_Callback(hObject, eventdata, handles)
% "Intensity Threshold" Slider
try
    handles.int_thresh = round(get(handles.slider1,'Value'));
    set(handles.text3,'String',num2str(round(handles.int_thresh)))
    guidata(hObject, handles);
catch errorObj
    errordlg(getReport(errorObj,'extended','hyperlinks','off'),'Error');
end

% --- Executes during object creation, after setting all properties.
function slider1_CreateFcn(hObject, eventdata, handles)
if isequal(get(hObject,'BackgroundColor'),
get(0,'defaultUicontrolBackgroundColor'))
    set(hObject,'BackgroundColor',[.9 .9 .9]);
end

% --- Executes during object creation, after setting all properties.
function axes4_CreateFcn(hObject, eventdata, handles)

% --- Executes on button press in checkbox1.
function checkbox1_Callback(hObject, eventdata, handles)
% "Apply Top Hat Algorithm" checkbox
try
    handles.tophat=get(hObject,'Value');
    guidata(hObject, handles);
catch errorObj
    errordlg(getReport(errorObj,'extended','hyperlinks','off'),'Error');
end

function edit14_Callback(hObject, eventdata, handles)
% "Animal Treatment" text
try
    handles.treatment=get(hObject,'String');
    guidata(hObject, handles);
catch errorObj
    errordlg(getReport(errorObj,'extended','hyperlinks','off'),'Error');
end

% --- Executes during object creation, after setting all properties.
function edit14_CreateFcn(hObject, eventdata, handles)
if ispc && isequal(get(hObject,'BackgroundColor'),
get(0,'defaultUicontrolBackgroundColor'))
    set(hObject,'BackgroundColor','white');
end

function edit13_Callback(hObject, eventdata, handles)
% "Group" text
```

```
try
    handles.group=get(hObject,'String');
    guidata(hObject, handles);
catch errorObj
    errordlg(getReport(errorObj,'extended','hyperlinks','off'),'Error');
end

% --- Executes during object creation, after setting all properties.
function edit13_CreateFcn(hObject, eventdata, handles)
if ispc && isequal(get(hObject,'BackgroundColor'),
get(0,'defaultUicontrolBackgroundColor'))
    set(hObject,'BackgroundColor','white');
end

function edit17_Callback(hObject, eventdata, handles)
% "Reviewer Initials" text
try
    handles.inits=get(hObject,'String');
    guidata(hObject, handles);
catch errorObj
    errordlg(getReport(errorObj,'extended','hyperlinks','off'),'Error');
end

% --- Executes during object creation, after setting all properties.
function edit17_CreateFcn(hObject, eventdata, handles)
if ispc && isequal(get(hObject,'BackgroundColor'),
get(0,'defaultUicontrolBackgroundColor'))
    set(hObject,'BackgroundColor','white');
end

function edit16_Callback(hObject, eventdata, handles)
% "Date Reviewed" text
try
    handles.date_review=get(hObject,'String');
    guidata(hObject, handles);
catch errorObj
    errordlg(getReport(errorObj,'extended','hyperlinks','off'),'Error');
end

% --- Executes during object creation, after setting all properties.
function edit16_CreateFcn(hObject, eventdata, handles)
if ispc && isequal(get(hObject,'BackgroundColor'),
get(0,'defaultUicontrolBackgroundColor'))
    set(hObject,'BackgroundColor','white');
end

function edit15_Callback(hObject, eventdata, handles)
% "Animal ID" text
try
    handles.ID=get(hObject,'String');
    guidata(hObject, handles);
catch errorObj
    errordlg(getReport(errorObj,'extended','hyperlinks','off'),'Error');
end
```

Appendix B: Python-based Image Analysis Script (for Onset of Stasis Models)

```
"""
Fahraeus-Lyndquist Analysis script -

Organize databases, plot, and analyze intensity distribution of time-
series in vitro blood rheology imaging data.
Data fitted to second order polynomial

2015-2016 Harrison Seidner and Geoffrey Gunter

This script is written for analysis of RoomGas data, and for analysis
of data where oxygen partial pressure is controlled
"""

import os
import matplotlib.pyplot as plt
#import seaborn as sns
from FL_Image import *
from FL_DataFrameGas1 import *
from FL_plots1 import *
from FL_DataGas import *

## source data and output directories
indir = 'C:\\FL_Analyze\\experiments'
outdir = 'C:\\FL_Analyze\\data'

intplotsdir = outdir+'\\'+'intplots'
imgsdir = outdir+'\\'+'imgs'
binimgsdir = outdir+'\\'+'binimgs'
cfaplotsdir = outdir+'\\'+'cfaplots'
deltaSigmaplotsdir = outdir+'\\'+'deltaSigmaplots'
dwplotsdir = outdir+'\\'+'dwplots'
barplotsdir = outdir+'\\'+'barplots'
legendsdir = outdir+'\\'+'legends'

for d in [outdir, intplotsdir, imgsdir, binimgsdir, cfaplotsdir,\
 deltaSigmaplotsdir, dwplotsdir, barplotsdir, legendsdir]:
  if os.path.isdir(d) == False:
    os.mkdir(d)

## Donor demographic info
donors = [{'SubjID':'H02','Gender':'M','Age':58,'CollectionDate':'2015-06-08'},\
          {'SubjID':'H03','Gender':'M','Age':41,'CollectionDate':'2015-06-16'},\
          {'SubjID':'H04','Gender':'M','Age':45,'CollectionDate':'2015-06-16'},\
          {'SubjID':'H05','Gender':'M','Age':33,'CollectionDate':'2015-06-23'},\
          {'SubjID':'H06','Gender':'M','Age':56,'CollectionDate':'2015-06-23'},\
          {'SubjID':'H07','Gender':'M','Age':48,'CollectionDate':'2015-08-10'},\
          {'SubjID':'H08','Gender':'M','Age':27,'CollectionDate':'2015-09-21'},\
          {'SubjID':'H09','Gender':'M','Age':54,'CollectionDate':'2015-10-06'},\
          {'SubjID':'H10','Gender':'M','Age':50,'CollectionDate':'2015-10-13'},\
          {'SubjID':'H11','Gender':'M','Age':53,'CollectionDate':'2015-12-15'},\
          {'SubjID':'H12','Gender':'F','Age':52,'CollectionDate':'2016-01-05'},\
          {'SubjID':'H13','Gender':'M','Age':56,'CollectionDate':'2016-01-05'},\
          {'SubjID':'H14','Gender':'M','Age':37,'CollectionDate':'2016-01-12'},\
          {'SubjID':'H15','Gender':'M','Age':32,'CollectionDate':'2016-01-12'},\
```

```
        {'SubjID':'H16','Gender':'M','Age':57,'CollectionDate':'2016-01-12'},\
        {'SubjID':'H17','Gender':'M','Age':52,'CollectionDate':'2016-01-19'},\
        {'SubjID':'H18','Gender':'M','Age':51,'CollectionDate':'2016-01-19'},\
        {'SubjID':'H19','Gender':'M','Age':27,'CollectionDate':'2016-01-19'},]


## create & save Donor dataframe
print '\nwrite Donor dataframe'
D = None
for donor in donors:
  D = insDonor(donor, D)
D.to_excel(outdir+'\\'+'Donors.xlsx')


## create & save Trial Data dataframes
# WARNING: this will take up a few gigs of RAM for a few minutes, I haven't
# gotten around to implementing the SQL database yet so it has to iterate
# through all the data files
print '\nwrite Trial dataframe'
T = None
time = np.hstack((np.arange(0,180,20),180)).astype(float)
#for dirname in os.listdir(indir):
#  if os.path.isdir(indir+'\\'+dirname):
#    print dirname
#    trial = insTrial(indir+'\\'+dirname)
#    ind = 0
#    s, a, t, d = trial.iloc[0].Solvent, trial.iloc[0].Ab, trial.iloc[0].Temp, \
#                 trial.iloc[0].Date
#    intPlotpdf = intplotsdir+'\\'+s+'_'+a+'_'+np.str(t)+'C_'+d+'.pdf'
#    plotPDF(intPlot, trial, ind, time, intPlotpdf)
#    imgPlotpdf = imgsdir+'\\'+s+'_'+a+'_'+np.str(t)+'C_'+d+'.pdf'
#    plotPDF(imgPlot, trial, ind, time, imgPlotpdf)
#    binImgPlotpdf = binimgsdir+'\\'+s+'_'+a+'_'+np.str(t)+'C_'+d+'.pdf'
#    plotPDF(binImgPlot, trial, ind, time, binImgPlotpdf)
#    T = insTrialData(trial, T)
#T.to_excel(outdir+'\\'+'Data.xlsx')


for dirname in os.listdir(indir):
  if os.path.isdir(indir+'\\'+dirname):
    print dirname
    trial = insTrial(indir+'\\'+dirname)
    ind = 0
    s, a, t, d, o, n = trial.iloc[0].Solvent, trial.iloc[0].Ab,\
    trial.iloc[0].Temp, \
                trial.iloc[0].Date, trial.iloc[0].Oxy, trial.iloc[0].Nitro
    intPlotpdf = intplotsdir+'\\'+s+'_'+a+'_'+np.str(t)+'C_'+d+'.pdf'
    plotPDF(intPlot, trial, ind, time, intPlotpdf)
    imgPlotpdf = imgsdir+'\\'+s+'_'+a+'_'+np.str(t)+'C_'+d+'.pdf'
    plotPDF(imgPlot, trial, ind, time, imgPlotpdf)
    binImgPlotpdf = binimgsdir+'\\'+s+'_'+a+'_'+np.str(t)+'C_'+d+'.pdf'
    plotPDF(binImgPlot, trial, ind, time, binImgPlotpdf)
    T = insTrialData(trial, T)
```

```
T.to_excel(outdir+'\\'+'Data.xlsx')
####################################
## Get aggregation @ 3 min and t_1/2
print '\nwrite Time-Series Stats dataframe'
#T = pd.read_excel(outdir+'\\'+'Data_RoomGas.xlsx')
T = pd.read_excel(outdir+'\\'+'Data_Gas.xlsx')
""" NOTE: Change the filename above to do Max/t_1/2 analysis on a new
Excel file"""
""" Also note that ALL DATA must be on "Sheet 1" and must have a UNIQUE
index number"""

#TS = None
#for d in np.unique(T.Date):
#  for s in np.unique(T[T.Date == d].Solvent):
#    for a in np.unique(T[(T.Date ==d) & (T.Solvent == s)].Ab):
#      for t in np.unique(T[(T.Date ==d) & (T.Solvent == s) &\
# (T.Ab == a)].Temp):
#        ind = filterDF(T,{'Date':d,'Solvent':s,'Ab':a, 'Temp':t}).index
#        TS = insTimeSeriesStats(T.loc[ind], TS)
#TS.to_excel(outdir+'\\'+'Stats.xlsx')

#############################################################################
TS = None
for d in np.unique(T.Date):
  for s in np.unique(T[T.Date == d].Solvent):
    for a in np.unique(T[(T.Date ==d) & (T.Solvent == s)].Ab):
      for o in np.unique(T[(T.Date ==d) & (T.Solvent == s) & (T.Ab == a)].Oxy):
        for n in np.unique(T[(T.Date ==d) & (T.Solvent == s) & (T.Ab == a) &\
        (T.Oxy == o)].Nitro):
          for t in np.unique(T[(T.Date ==d) & (T.Solvent == s) & (T.Ab == a) &\
          (T.Oxy == o) & (T.Nitro == n)].Temp):
            ind = filterDF(T,{'Date':d,'Solvent':s,'Ab':a, "Oxy":o, "Nitro":n,\
            'Temp':t}).index
            TS = insTimeSeriesStats(T.loc[ind], TS)
TS.to_excel(outdir+'\\'+'Stats.xlsx')
#############################################################################
# Generate plots
##C = ('dodgerblue', 'red', 'indigo')
#C = ('dodgerblue', 'red', 'yellow')
#for t in [37, 41, 45, 49]:
#  PBS = T[(T.Temp == t) & (T.Ab == 'noAnt') & (T.Solvent == 'PBS')].index
#  Plasma = T[(T.Temp == t) & (T.Ab == 'noAnt') &\
# (T.Solvent == 'Plasma')].index
#  Dex = T[(T.Temp == t) & (T.Ab == 'noAnt') & (T.Solvent == 'Dex500')].index
#  cfaPDF = cfaplotsdir+'\\'+np.str(t)+'C_'+'noAb'+'.pdf'
#  plotPDF(cfaPlot, T, (PBS, Plasma, Dex), C, cfaPDF)
#  dwPDF = dwplotsdir+'\\'+np.str(t)+'C_'+'noAb'+'.pdf'
#  plotPDF(dwPlot, T, (PBS, Plasma, Dex), C, dwPDF)
#  deltaSigmaPDF = deltaSigmaplotsdir+'\\'+np.str(t)+'C_'+'noAb'+'.pdf'
#  plotPDF(deltaSigmaPlot, T, (PBS, Plasma, Dex), C, deltaSigmaPDF)
#############################################################################################
C = ('red', 'forestgreen', 'lime', 'indigo', 'blueviolet')
for o in [00, 05, 10, 100]:
    for t in [37, 41, 45, 49]:
      Plasma = T[(T.Temp == t) & (T.Ab == 'noAnt') & (T.Oxy == o) &\
```

```
      (T.Solvent == 'Plasma')].index
      ALB50 = T[(T.Temp == t) & (T.Ab == 'noAnt') & (T.Oxy == o) &\
      (T.Solvent == 'ALB50')].index
      ALB20 = T[(T.Temp == t) & (T.Ab == 'noAnt') & (T.Oxy == o) &\
      (T.Solvent == 'ALB20')].index
      FIB08 = T[(T.Temp == t) & (T.Ab == 'noAnt') & (T.Oxy == o) &\
      (T.Solvent == 'FIB08')].index
      FIB02 = T[(T.Temp == t) & (T.Ab == 'noAnt') & (T.Oxy == o) &\
      (T.Solvent == 'FIB02')].index
      deltaSigmaPDF =\ deltaSigmaplotsdir+'\\'+'Solvents'+'_'+np.str(t)+\
      'C_' +'_'+'Oxy%' +np.str(o)+'_'+'noAb'+'.pdf'
      plotPDF(deltaSigmaPlot, T, (Plasma, ALB50, ALB20, FIB08, FIB02),\
      C, deltaSigmaPDF)

C = ('red', 'forestgreen', 'lime', 'indigo', 'blueviolet')
for o in [00, 05, 10, 100]:
    for t in [37, 41, 45, 49]:
      Plasma = T[(T.Temp == t) & (T.Ab == 'DIDS') & (T.Oxy == o) &\
      (T.Solvent == 'Plasma')].index
      ALB50 = T[(T.Temp == t) & (T.Ab == 'DIDS') & (T.Oxy == o) &\
      (T.Solvent == 'ALB50')].index
      ALB20 = T[(T.Temp == t) & (T.Ab == 'DIDS') & (T.Oxy == o) &\
      (T.Solvent == 'ALB20')].index
      FIB08 = T[(T.Temp == t) & (T.Ab == 'DIDS') & (T.Oxy == o) &\
      (T.Solvent == 'FIB08')].index
      FIB02 = T[(T.Temp == t) & (T.Ab == 'DIDS') & (T.Oxy == o) &\
      (T.Solvent == 'FIB02')].index
      deltaSigmaPDF = deltaSigmaplotsdir+'\\'+'Solvents'+'_'+np.str(t)+\
      'C_' +'_'+'Oxy%' +np.str(o)+'_'+'DIDS'+'.pdf'
      plotPDF(deltaSigmaPlot, T, (Plasma, ALB50, ALB20, FIB08, FIB02),\
      C, deltaSigmaPDF)
##############################################################################################
##C = ('yellow', 'orange', 'red', 'darkred')
#C = ('dodgerblue', 'darkorchid', 'red', 'darkred')
#for s in ['PBS', 'Plasma', 'Dex500']:
#  T37 = T[(T.Temp == 37) & (T.Ab == 'noAnt') & (T.Solvent == s)].index
#  T41 = T[(T.Temp == 41) & (T.Ab == 'noAnt') & (T.Solvent == s)].index
#  T45 = T[(T.Temp == 45) & (T.Ab == 'noAnt') & (T.Solvent == s)].index
#  T49 = T[(T.Temp == 49) & (T.Ab == 'noAnt') & (T.Solvent == s)].index
#  cfaPDF = cfaplotsdir+'\\'+s+'_'+'noAb'+'.pdf'
#  plotPDF(cfaPlot, T, (T37, T41, T45, T49), C, cfaPDF)
#  dwPDF = dwplotsdir+'\\'+s+'_'+'noAb'+'.pdf'
#  plotPDF(dwPlot, T, (T37, T41, T45, T49), C, dwPDF)
#  deltaSigmaPDF = deltaSigmaplotsdir+'\\'+s+'_'+'noAb'+'.pdf'
#  plotPDF(deltaSigmaPlot, T, (T37, T41, T45, T49), C, deltaSigmaPDF)
##############################################################################################
C = ('dodgerblue', 'darkorchid', 'red', 'darkred')
for o in [00, 05, 10, 100]:
    for s in ['Plasma', 'ALB50', 'ALB20', 'FIB08', 'FIB02']:
      T37 = T[(T.Temp == 37) & (T.Ab == 'noAnt') & (T.Solvent == s) &\
      (T.Oxy == o)].index
      T41 = T[(T.Temp == 41) & (T.Ab == 'noAnt') & (T.Solvent == s) &\
      (T.Oxy == o)].index
      T45 = T[(T.Temp == 45) & (T.Ab == 'noAnt') & (T.Solvent == s) &\
      (T.Oxy == o)].index
```

```
      T49 = T[(T.Temp == 49) & (T.Ab == 'noAnt') & (T.Solvent == s) &\
      (T.Oxy == o)].index
      deltaSigmaPDF = deltaSigmaplotsdir+'\\'+'Temps'+'_'+s+'_'+\
      '%Oxy'+np.str(o)+'_'+'noAb'+'.pdf'
      plotPDF(deltaSigmaPlot, T, (T37, T41, T45, T49), C, deltaSigmaPDF)

C = ('dodgerblue', 'darkorchid', 'red', 'darkred')
for o in [00, 05, 10, 100]:
    for s in ['Plasma', 'ALB50', 'ALB20', 'FIB08', 'FIB02']:
      T37 = T[(T.Temp == 37) & (T.Ab == 'DIDS') & (T.Solvent == s) &\
      (T.Oxy == o)].index
      T41 = T[(T.Temp == 41) & (T.Ab == 'DIDS') & (T.Solvent == s) &\
      (T.Oxy == o)].index
      T45 = T[(T.Temp == 45) & (T.Ab == 'DIDS') & (T.Solvent == s) &\
      (T.Oxy == o)].index
      T49 = T[(T.Temp == 49) & (T.Ab == 'DIDS') & (T.Solvent == s) &\
      (T.Oxy == o)].index
      deltaSigmaPDF = deltaSigmaplotsdir+'\\'+'Temps'+'_'+s+'_'+\
      '%Oxy'+np.str(o)+'_'+'DIDS'+'.pdf'
      plotPDF(deltaSigmaPlot, T, (T37, T41, T45, T49), C, deltaSigmaPDF)
##############################################################################################
 #C = ('navy', 'dodgerblue', 'forestgreen', 'greenyellow','fuchsia', 'salmon')
#for s in ['PBS', 'Plasma']:
#  for t in [37, 41, 45, 49]:
#    noAb = T[(T.Temp == t) & (T.Ab == 'noAnt') & (T.Solvent == s)].index
#    Band3 = T[(T.Temp == t) & (T.Ab == 'Band3') & (T.Solvent == s)].index
#    GYPC = T[(T.Temp == t) & (T.Ab == 'GYPC') & (T.Solvent == s)].index
#    aVb3 = T[(T.Temp == t) & (T.Ab == 'aVb3') & (T.Solvent == s)].index
#    DIDS = T[(T.Temp == t) & (T.Ab == 'DIDS') & (T.Solvent == s)].index##############
#    Glut = T[(T.Temp == t) & (T.Ab == 'Glut') & (T.Solvent == s)].index#############
#    cfaPDF = cfaplotsdir+'\\'+s+'_'+np.str(t)+'C'+'.pdf'
#    plotPDF(cfaPlot, T, (noAb, Band3, GYPC, aVb3, DIDS, Glut), C, cfaPDF)#############
#    dwPDF = dwplotsdir+'\\'+s+'_'+np.str(t)+'C'+'.pdf'
#    plotPDF(dwPlot, T, (noAb, Band3, GYPC, aVb3, DIDS, Glut), C, dwPDF)#############
#    deltaSigmaPDF = deltaSigmaplotsdir+'\\'+s+'_'+np.str(t)+'C'+'.pdf'
#    plotPDF(deltaSigmaPlot, T, (noAb, Band3, GYPC, aVb3, DIDS, Glut),/
      #C, deltaSigmaPDF)

## Generate bar plots
print '\nGenerate bar plots'
TS = pd.read_excel(outdir+'\\'+'Stats.xlsx')

#C = ('dodgerblue', 'darkorchid', 'red', 'darkred')
#PBS, Plasma, Dex = {}, {}, {}
#for t in [37, 41, 45, 49]:
#  PBS[t] = TS[(TS.Temp == t) & (TS.Ab == 'noAnt') &\
# (TS.Solvent == 'PBS')].index
#  Plasma[t] = TS[(TS.Temp == t) & (TS.Ab == 'noAnt') &\
# (TS.Solvent == 'Plasma')].index
#  Dex[t] = TS[(TS.Temp == t) & (TS.Ab == 'noAnt') &\
# (TS.Solvent == 'Dex500')].index
#ind = ((PBS[37], PBS[41], PBS[45], PBS[49]), \
#       (Plasma[37], Plasma[41], Plasma[45], Plasma[49]), \
#       (Dex[37], Dex[41], Dex[45], Dex[49]))
#sigmamaxbarPDF = barplotsdir+'\\sigmabarmax'+'_'+'noAb'+'_'+'Temp'+'.pdf'
```

```
#plotPDF(sigmamaxBarPlot, TS, ind, C, sigmamaxbarPDF)
#CFAmaxbarPDF = barplotsdir+'\\CFAbarmax'+'_'+'noAb'+'_'+'Temp'+'.pdf'
#plotPDF(CFAmaxBarPlot, TS, ind, C, CFAmaxbarPDF)
#DWmaxbarPDF = barplotsdir+'\\DWbarmax'+'_'+'noAb'+'_'+'Temp'+'.pdf'
#plotPDF(DWmaxBarPlot, TS, ind, C, DWmaxbarPDF)
#sigmat_halfbarPDF = barplotsdir+'\\sigmabarthalf'+'_'+'noAb'+'_'+'Temp'+'.pdf'
#plotPDF(sigmat_halfBarPlot, TS, ind, C, sigmat_halfbarPDF)
#CFAthalfbarPDF = barplotsdir+'\\CFAbarthalf'+'_'+'noAb'+'_'+'Temp'+'.pdf'
#plotPDF(CFAthalfBarPlot, TS, ind, C, CFAthalfbarPDF)
#DWthalfbarPDF = barplotsdir+'\\DWbarthalf'+'_'+'noAb'+'_'+'Temp'+'.pdf'
#plotPDF(DWthalfBarPlot, TS, ind, C, DWthalfbarPDF)
#################################################################################################
#C = ('dodgerblue', 'red', 'yellow')
#T_37, T_41, T_45, T_49 = {}, {}, {}, {}
#for s in ['PBS', 'Plasma', 'Dex500']:
#  T_37[s] = TS[(TS.Temp == 37) & (TS.Ab == 'noAnt') & (TS.Solvent == s)].index
#  T_41[s] = TS[(TS.Temp == 41) & (TS.Ab == 'noAnt') & (TS.Solvent == s)].index
#  T_45[s] = TS[(TS.Temp == 45) & (TS.Ab == 'noAnt') & (TS.Solvent == s)].index
#  T_49[s] = TS[(TS.Temp == 49) & (TS.Ab == 'noAnt') & (TS.Solvent == s)].index
#ind = ((T_37['PBS'], T_37['Plasma'], T_37['Dex500']), \
#       (T_41['PBS'], T_41['Plasma'], T_41['Dex500']), \
#       (T_45['PBS'], T_45['Plasma'], T_45['Dex500']), \
#       (T_49['PBS'], T_49['Plasma'], T_49['Dex500']))
#sigmamaxbarPDF = barplotsdir+'\\sigmabarmax'+'_'+'noAb'+'_'+'Solvents.pdf'
#plotPDF(sigmamaxBarPlot, TS, ind, C, sigmamaxbarPDF)
#CFAmaxbarPDF = barplotsdir+'\\CFAbarmax'+'_'+'noAb'+'_'+'Solvents.pdf'
#plotPDF(CFAmaxBarPlot, TS, ind, C, CFAmaxbarPDF)
#DWmaxbarPDF = barplotsdir+'\\DWbarmax'+'_'+'noAb'+'_'+'Solvents.pdf'
#plotPDF(DWmaxBarPlot, TS, ind, C, DWmaxbarPDF)
#sigmat_halfbarPDF = barplotsdir+'\\sigmabarthalf'+'_'+\
#'noAb'+'_'+'Solvents.pdf'
#plotPDF(sigmat_halfBarPlot, TS, ind, C, sigmat_halfbarPDF)
#CFAthalfbarPDF = barplotsdir+'\\CFAbarthalf'+'_'+'noAb'+'_'+'Solvents.pdf'
#plotPDF(CFAthalfBarPlot, TS, ind, C, CFAthalfbarPDF)
#DWthalfbarPDF = barplotsdir+'\\DWbarthalf'+'_'+'noAb'+'_'+'Solvents.pdf'
#plotPDF(DWthalfBarPlot, TS, ind, C, DWthalfbarPDF)
#################################################################################################
C = ('red', 'forestgreen', 'lime', 'indigo', 'blueviolet')
Plasma, ALB50, ALB20, FIB08, FIB02 = {}, {}, {}, {}, {}
for t in [37, 41, 45, 49]:
    for o in [00, 05, 10, 100]:
      Plasma[o] = TS[(TS.Oxy == o) & (TS.Ab == 'noAnt') &\
      (TS.Solvent == 'Plasma') & (TS.Temp == t)].index
      ALB50[o] = TS[(TS.Oxy == o) & (TS.Ab == 'noAnt') &\
      (TS.Solvent == 'ALB50') & (TS.Temp == t)].index
      ALB20[o] = TS[(TS.Oxy == o) & (TS.Ab == 'noAnt') &\
      (TS.Solvent == 'ALB20') & (TS.Temp == t)].index
      FIB08[o] = TS[(TS.Oxy == o) & (TS.Ab == 'noAnt') &\
      (TS.Solvent == 'FIB08') & (TS.Temp == t)].index
      FIB02[o] = TS[(TS.Oxy == o) & (TS.Ab == 'noAnt') &\
      (TS.Solvent == 'FIB02') & (TS.Temp == t)].index
    ind = ((Plasma[00], ALB50[00], ALB20[00], FIB08[00], FIB02[00]), \
         (Plasma[05], ALB50[05], ALB20[05], FIB08[05], FIB02[05]), \
         (Plasma[10], ALB50[10], ALB20[10], FIB08[10], FIB02[10]), \
         (Plasma[100], ALB50[100], ALB20[100], FIB08[100], FIB02[100]))
```

```
    sigmamaxbarPDF = barplotsdir+'\\sigmabarmax'+'_'+'noAb'+'_'+\
    'Solvents'+'_'+'Oxys'+'_'+np.str(t)+'C'+'.pdf'
    plotPDF(sigmamaxBarPlot, TS, ind, C, sigmamaxbarPDF)
    sigmat_halfbarPDF = barplotsdir+'\\sigmabarthalf'+'_'+'noAb'+\
    '_'+'Solvents'+'_'+'Oxys'+'_'+np.str(t)+'C'+'.pdf'
    plotPDF(sigmat_halfBarPlot, TS, ind, C, sigmat_halfbarPDF)

C = ('red', 'forestgreen', 'lime', 'indigo', 'blueviolet')
Plasma, ALB50, ALB20, FIB08, FIB02 = {}, {}, {}, {}, {}
for t in [37, 41, 45, 49]:
    for o in [00, 05, 10, 100]:
      Plasma[o] = TS[(TS.Oxy == o) & (TS.Ab == 'DIDS') &\
      (TS.Solvent == 'Plasma') & (TS.Temp == t)].index
      ALB50[o] = TS[(TS.Oxy == o) & (TS.Ab == 'DIDS') &\
      (TS.Solvent == 'ALB50') & (TS.Temp == t)].index
      ALB20[o] = TS[(TS.Oxy == o) & (TS.Ab == 'DIDS') &\
      (TS.Solvent == 'ALB20') & (TS.Temp == t)].index
      FIB08[o] = TS[(TS.Oxy == o) & (TS.Ab == 'DIDS') &\
      (TS.Solvent == 'FIB08') & (TS.Temp == t)].index
      FIB02[o] = TS[(TS.Oxy == o) & (TS.Ab == 'DIDS') &\
      (TS.Solvent == 'FIB02') & (TS.Temp == t)].index
    ind = ((Plasma[00], ALB50[00], ALB20[00], FIB08[00], FIB02[00]), \
         (Plasma[05], ALB50[05], ALB20[05], FIB08[05], FIB02[05]), \
         (Plasma[10], ALB50[10], ALB20[10], FIB08[10], FIB02[10]), \
         (Plasma[100], ALB50[100], ALB20[100], FIB08[100], FIB02[100]))
    sigmamaxbarPDF = barplotsdir+'\\sigmabarmax'+'_'+'DIDS'+'_'+'Solvents'+\
    '_'+'Oxys'+'_'+np.str(t)+'C'+'.pdf'
    plotPDF(sigmamaxBarPlot, TS, ind, C, sigmamaxbarPDF)
    sigmat_halfbarPDF = barplotsdir+'\\sigmabarthalf'+'_'+'DIDS'+'_'+\
    'Solvents'+'_'+'Oxys'+'_'+np.str(t)+'C'+'.pdf'
    plotPDF(sigmat_halfBarPlot, TS, ind, C, sigmat_halfbarPDF)
##############################################################################################
C = ('dodgerblue', 'darkorchid', 'red', 'darkred')
Plasma, PlasmaDIDS= {}, {}
for o in [00, 05, 10, 100]:
    for t in [37, 41, 45, 49]:
      Plasma[t] = TS[(TS.Oxy == o) & (TS.Ab == 'noAnt') &\
      (TS.Solvent == 'Plasma') & (TS.Temp == t)].index
      PlasmaDIDS[t] = TS[(TS.Oxy == o) & (TS.Ab == 'DIDS') &\
      (TS.Solvent == 'Plasma') & (TS.Temp == t)].index
    ind = ((Plasma[37], Plasma[41], Plasma[45], Plasma[49]), \
         (PlasmaDIDS[37], PlasmaDIDS[41], PlasmaDIDS[45], PlasmaDIDS[49]))#, \
    sigmamaxbarPDF = barplotsdir+'\\sigmabarmax'+'_'+'noAb_v_DIDS'+\
    '_'+'Plasma'+'_'+'Temp'+'_'+'%0xy'+np.str(o)+'.pdf'
    plotPDF(sigmamaxBarPlot, TS, ind, C, sigmamaxbarPDF)
    sigmat_halfbarPDF = barplotsdir+'\\sigmabarthalf'+'_'+'noAb_v_DIDS'+\
    '_'+'Plasma'+'_'+'Temp'+'_'+'%0xy'+np.str(o)+'.pdf'
    plotPDF(sigmat_halfBarPlot, TS, ind, C, sigmat_halfbarPDF)

C = ('dodgerblue', 'darkorchid', 'red', 'darkred')
ALB50, ALB50DIDS= {}, {}
for o in [00, 05, 10, 100]:
    for t in [37, 41, 45, 49]:
      ALB50[t] = TS[(TS.Oxy == o) & (TS.Ab == 'noAnt') &\
      (TS.Solvent == 'ALB50') & (TS.Temp == t)].index
```

```
      ALB50DIDS[t] = TS[(TS.Oxy == o) & (TS.Ab == 'DIDS') &\
      (TS.Solvent == 'ALB50') & (TS.Temp == t)].index
    ind = ((ALB50[37], ALB50[41], ALB50[45], ALB50[49]), \
         (ALB50DIDS[37], ALB50DIDS[41], ALB50DIDS[45], ALB50DIDS[49]))#, \
    sigmamaxbarPDF = barplotsdir+'\\sigmabarmax'+'_'+'noAb_v_DIDS'+'_'+\
    'ALB50'+'_'+'Temp'+'_'+'%0xy'+np.str(o)+'.pdf'
    plotPDF(sigmamaxBarPlot, TS, ind, C, sigmamaxbarPDF)
    sigmat_halfbarPDF = barplotsdir+'\\sigmabarthalf'+'_'+'noAb_v_DIDS'+'_'+\
    'ALB50'+'_'+'Temp'+'_'+'%0xy'+np.str(o)+'.pdf'
    plotPDF(sigmat_halfBarPlot, TS, ind, C, sigmat_halfbarPDF)

C = ('dodgerblue', 'darkorchid', 'red', 'darkred')
ALB20, ALB20DIDS= {}, {}
for o in [00, 05, 10, 100]:
    for t in [37, 41, 45, 49]:
      ALB20[t] = TS[(TS.Oxy == o) & (TS.Ab == 'noAnt') &\
      (TS.Solvent == 'ALB20') & (TS.Temp == t)].index
      ALB20DIDS[t] = TS[(TS.Oxy == o) & (TS.Ab == 'DIDS') &\
      (TS.Solvent == 'ALB20') & (TS.Temp == t)].index
    ind = ((ALB20[37], ALB20[41], ALB20[45], ALB20[49]), \
         (ALB20DIDS[37], ALB20DIDS[41], ALB20DIDS[45], ALB20DIDS[49]))#, \
    sigmamaxbarPDF = barplotsdir+'\\sigmabarmax'+'_'+'noAb_v_DIDS'+'_'+\
    'ALB20'+'_'+'Temp'+'_'+'%0xy'+np.str(o)+'.pdf'
    plotPDF(sigmamaxBarPlot, TS, ind, C, sigmamaxbarPDF)
    sigmat_halfbarPDF = barplotsdir+'\\sigmabarthalf'+'_'+'noAb_v_DIDS'+\
    '_'+'ALB20'+'_'+'Temp'+'_'+'%0xy'+np.str(o)+'.pdf'
    plotPDF(sigmat_halfBarPlot, TS, ind, C, sigmat_halfbarPDF)

C = ('dodgerblue', 'darkorchid', 'red', 'darkred')
FIB08, FIB08DIDS= {}, {}
for o in [00, 05, 10, 100]:
    for t in [37, 41, 45, 49]:
      FIB08[t] = TS[(TS.Oxy == o) & (TS.Ab == 'noAnt') &\
      (TS.Solvent == 'FIB08') & (TS.Temp == t)].index
      FIB08DIDS[t] = TS[(TS.Oxy == o) & (TS.Ab == 'DIDS') &\
      (TS.Solvent == 'FIB08') & (TS.Temp == t)].index
    ind = ((FIB08[37], FIB08[41], FIB08[45], FIB08[49]), \
         (FIB08DIDS[37], FIB08DIDS[41], FIB08DIDS[45], FIB08DIDS[49]))#, \
    sigmamaxbarPDF = barplotsdir+'\\sigmabarmax'+'_'+'noAb_v_DIDS'+\
    '_'+'FIB08'+'_'+'Temp'+'_'+'%0xy'+np.str(o)+'.pdf'
    plotPDF(sigmamaxBarPlot, TS, ind, C, sigmamaxbarPDF)
    sigmat_halfbarPDF = barplotsdir+'\\sigmabarthalf'+'_'+'noAb_v_DIDS'+\
    '_'+'FIB08'+'_'+'Temp'+'_'+'%0xy'+np.str(o)+'.pdf'
    plotPDF(sigmat_halfBarPlot, TS, ind, C, sigmat_halfbarPDF)

C = ('dodgerblue', 'darkorchid', 'red', 'darkred')
FIB02, FIB02DIDS= {}, {}
for o in [00, 05, 10, 100]:
    for t in [37, 41, 45, 49]:
      FIB02[t] = TS[(TS.Oxy == o) & (TS.Ab == 'noAnt') &\
      (TS.Solvent == 'FIB02') & (TS.Temp == t)].index
      FIB02DIDS[t] = TS[(TS.Oxy == o) & (TS.Ab == 'DIDS') &\
      (TS.Solvent == 'FIB02') & (TS.Temp == t)].index
    ind = ((FIB02[37], FIB02[41], FIB02[45], FIB02[49]), \
         (FIB02DIDS[37], FIB02DIDS[41], FIB02DIDS[45], FIB02DIDS[49]))#, \
```

```
    sigmamaxbarPDF = barplotsdir+'\\sigmabarmax'+'_'+'noAb_v_DIDS'+\
    '_'+'FIB02'+'_'+'Temp'+'_'+'%0xy'+np.str(o)+'.pdf'
    plotPDF(sigmamaxBarPlot, TS, ind, C, sigmamaxbarPDF)
    sigmat_halfbarPDF = barplotsdir+'\\sigmabarthalf'+'_'+'noAb_v_DIDS'+\
    '_'+'FIB02'+'_'+'Temp'+'_'+'%0xy'+np.str(o)+'.pdf'
    plotPDF(sigmat_halfBarPlot, TS, ind, C, sigmat_halfbarPDF)
##########################################################################################
C = ('red', 'forestgreen', 'lime', 'indigo', 'blueviolet')
Plasma, ALB50, ALB20, FIB08, FIB02 = {}, {}, {}, {}, {}
for o in [00, 05, 10, 100]:
    for t in [37, 41, 45, 49]:
      Plasma[t] = TS[(TS.Oxy == o) & (TS.Ab == 'noAnt') &\
      (TS.Solvent == 'Plasma') & (TS.Temp == t)].index
      ALB50[t] = TS[(TS.Oxy == o) & (TS.Ab == 'noAnt') &\
      (TS.Solvent == 'ALB50') & (TS.Temp == t)].index
      ALB20[t] = TS[(TS.Oxy == o) & (TS.Ab == 'noAnt') &\
      (TS.Solvent == 'ALB20') & (TS.Temp == t)].index
      FIB08[t] = TS[(TS.Oxy == o) & (TS.Ab == 'noAnt') &\
      (TS.Solvent == 'FIB08') & (TS.Temp == t)].index
      FIB02[t] = TS[(TS.Oxy == o) & (TS.Ab == 'noAnt') &\
      (TS.Solvent == 'FIB02') & (TS.Temp == t)].index
    ind = ((Plasma[37], ALB50[37], ALB20[37], FIB08[37], FIB02[37]), \
         (Plasma[41], ALB50[41], ALB20[41], FIB08[41], FIB02[41]), \
         (Plasma[45], ALB50[45], ALB20[45], FIB08[45], FIB02[45]), \
         (Plasma[49], ALB50[49], ALB20[49], FIB08[49], FIB02[49]))
    sigmamaxbarPDF = barplotsdir+'\\sigmabarmax'+'_'+'Solvents'+'_'+\
    'Temps'+'_'+'noAb'+'_''%Oxy'+np.str(o)+'.pdf'
    plotPDF(sigmamaxBarPlot, TS, ind, C, sigmamaxbarPDF)
    sigmat_halfbarPDF = barplotsdir+'\\sigmabarthalf'+'_'+'Solvents'+\
    '_'+'Temps'+'_'+'noAb'+'_''%Oxy'+np.str(o)+'.pdf'
    plotPDF(sigmat_halfBarPlot, TS, ind, C, sigmat_halfbarPDF)

C = ('red', 'forestgreen', 'lime', 'indigo', 'blueviolet')
Plasma, ALB50, ALB20, FIB08, FIB02 = {}, {}, {}, {}, {}
for o in [00, 05, 10, 100]:
    for t in [37, 41, 45, 49]:
      Plasma[t] = TS[(TS.Oxy == o) & (TS.Ab == 'DIDS') &\
      (TS.Solvent == 'Plasma') & (TS.Temp == t)].index
      ALB50[t] = TS[(TS.Oxy == o) & (TS.Ab == 'DIDS') &\
      (TS.Solvent == 'ALB50') & (TS.Temp == t)].index
      ALB20[t] = TS[(TS.Oxy == o) & (TS.Ab == 'DIDS') &\
      (TS.Solvent == 'ALB20') & (TS.Temp == t)].index
      FIB08[t] = TS[(TS.Oxy == o) & (TS.Ab == 'DIDS') &\
      (TS.Solvent == 'FIB08') & (TS.Temp == t)].index
      FIB02[t] = TS[(TS.Oxy == o) & (TS.Ab == 'DIDS') &\
      (TS.Solvent == 'FIB02') & (TS.Temp == t)].index
    ind = ((Plasma[37], ALB50[37], ALB20[37], FIB08[37], FIB02[37]), \
         (Plasma[41], ALB50[41], ALB20[41], FIB08[41], FIB02[41]), \
         (Plasma[45], ALB50[45], ALB20[45], FIB08[45], FIB02[45]), \
         (Plasma[49], ALB50[49], ALB20[49], FIB08[49], FIB02[49]))
#   ind = ((Plasma[37], ALB50[00], ALB20[00], FIB08[00], FIB02[00]), \
#         (Plasma[37], ALB50[05], ALB20[05], FIB08[05], FIB02[05]), \
#         (Plasma[37], ALB50[10], ALB20[10], FIB08[10], FIB02[10]), \
#         (Plasma[37], ALB50[100], ALB20[100], FIB08[100], FIB02[100]))
    sigmamaxbarPDF = barplotsdir+'\\sigmabarmax'+'_'+'Solvents'+'_'+\
```

```
    'Temps'+'_'+'DIDS'+'_''%Oxy'+np.str(o)+'.pdf'
    plotPDF(sigmamaxBarPlot, TS, ind, C, sigmamaxbarPDF)
    sigmat_halfbarPDF = barplotsdir+'\\sigmabarthalf'+'_'+'Solvents'+\
    '_'+'Temps'+'_'+'DIDS'+'_''%Oxy'+np.str(o)+'.pdf'
    plotPDF(sigmat_halfBarPlot, TS, ind, C, sigmat_halfbarPDF)

##############################################################################################
#C = ('navy', 'dodgerblue', 'forestgreen', 'greenyellow','fuchsia', 'salmon')##########
#noAb, Band3, GYPC, aVb3, DIDS, Glut = {}, {}, {}, {}, {}, {} ########################
#for s in ['PBS', 'Plasma']:
#  for t in [37, 41, 45, 49]:
#    noAb[t] = TS[(TS.Temp == t) & (TS.Ab == 'noAnt') &\
# (TS.Solvent == s)].index
#    Band3[t] = TS[(TS.Temp == t) & (TS.Ab == 'Band3') &\
# (TS.Solvent == s)].index
#    GYPC[t] = TS[(TS.Temp == t) & (TS.Ab == 'GYPC') &\
# (TS.Solvent == s)].index
#    aVb3[t] = TS[(TS.Temp == t) & (TS.Ab == 'aVb3') &\
# (TS.Solvent == s)].index
#    DIDS[t] = TS[(TS.Temp == t) & (TS.Ab == 'DIDS') &\
# (TS.Solvent == s)].index############
#    Glut[t] = TS[(TS.Temp == t) & (TS.Ab == 'Glut') &\
# (TS.Solvent == s)].index############
#  ind = ((noAb[37], Band3[37], GYPC[37], aVb3[37], DIDS[37], Glut[37]),
#         (noAb[41], Band3[41], GYPC[41], aVb3[41], DIDS[41], Glut[41]),
#         (noAb[45], Band3[45], GYPC[45], aVb3[45], DIDS[45], Glut[45]),
#         (noAb[49], Band3[49], GYPC[49], aVb3[49], DIDS[49], Glut[49]))
#  sigmamaxbarPDF = barplotsdir+'\\sigmabarmax'+'_'+s+'.pdf'
#  plotPDF(sigmamaxBarPlot, TS, ind, C, sigmamaxbarPDF)
#  CFAmaxbarPDF = barplotsdir+'\\CFAbarmax'+'_'+s+'.pdf'
#  plotPDF(CFAmaxBarPlot, TS, ind, C, CFAmaxbarPDF)
#  DWmaxbarPDF = barplotsdir+'\\DWbarmax'+'_'+s+'.pdf'
#  plotPDF(DWmaxBarPlot, TS, ind, C, DWmaxbarPDF)
#  sigmat_halfbarPDF = barplotsdir+'\\sigmabarthalf'+'_'+s+'.pdf'
#  plotPDF(sigmat_halfBarPlot, TS, ind, C, sigmat_halfbarPDF)
#  CFAthalfbarPDF = barplotsdir+'\\CFAbarthalf'+'_'+s+'.pdf'
#  plotPDF(CFAthalfBarPlot, TS, ind, C, CFAthalfbarPDF)
#  DWthalfbarPDF = barplotsdir+'\\DWbarthalf'+'_'+s+'.pdf'
#  plotPDF(DWthalfBarPlot, TS, ind, C, DWthalfbarPDF)


## Legends
C = ('red', 'forestgreen', 'lime', 'indigo', 'blueviolet')
legPDF = legendsdir+'\\'+'solvent'+'.pdf'
plotPDF(Leg, None, ('Plasma', 'Albumin 50 mg/mL', 'Albumin 20 mg/mL',\
 'Fibrinogen 8 mg/mL', 'Fibrinogen 2 mg/mL'), C, legPDF)

C = ('dodgerblue', 'darkorchid', 'red', 'darkred')
legPDF = legendsdir+'\\'+'temperature'+'.pdf'
plotPDF(Leg, None, ('37 C', '41 C', '45 C', '49 C'), C, legPDF)

C = ('navy', 'dodgerblue', 'forestgreen', 'greenyellow', 'fuchsia', 'salmon')
legPDF = legendsdir+'\\'+'antibody'+'.pdf'
plotPDF(Leg, None, ('no Ab','anti-band 3', 'anti-GYPC',\
 'anti-aVb3','DIDS','Glut'), C, legPDF)
```

```
# -*- coding: utf-8 -*-
"""
DataFrame classes and functions for FL_AnalyzeGas1.py

"""

import pandas as pd
import numpy as np
import os
from scipy.misc import imread


class trialInfo(object):
  def __init__(self, dirname):
    if os.path.isdir(dirname):
      trialinfo = dirname.split('\\')[-1].split('_')
      #[self.date, self.subjID, self.solvent, self.Ab] = trialinfo[0:4]
      [self.date, self.subjID, self.solvent, self.Ab] = trialinfo[0:4]
      self.HCT = np.int(trialinfo[4][-2:])
      self.Oxy = np.int(trialinfo[5][:-2])
      self.Nitro = np.int(trialinfo[6][:-2])
      self.temp = np.int(trialinfo[7][:2])

    else:
      raise ValueError('Argument must be a valid directory')

def insImg(fname, d={}, tval=2.5):
 # time = tval*np.float(fname.split('\\')[-1].split('.')[0].split('_')[6])
  time = tval*np.float(fname.split('\\')[-1].split('.')[0].split('_')[8])
  d[time] = imread(fname, flatten=True)
  return d

def insTrial(dirname, df=None):
  t = trialInfo(dirname)
  d = {}
  for fname in os.listdir(dirname):
    if '.tif' in fname:
      d = insImg(dirname+'\\'+fname, d)
  #trial = [t.date, t.subjID, t.solvent, t.Ab, t.HCT, t.temp, d]
  #labels = ['Date', 'SubjID', 'Solvent', 'Ab', 'HCT', 'Temp', 'Data']
  trial = [t.date, t.subjID, t.solvent, t.Ab, t.HCT, t.temp, t.Oxy, t.Nitro, d]
  labels = ['Date', 'SubjID', 'Solvent', 'Ab', 'HCT', 'Temp', 'Oxy',\
  'Nitro', 'Data']
  return insertNewRow(newrow(trial, labels), df)

def insDonor(donorInfo, df=None):
  labels = ['SubjID', 'Gender', 'Age', 'CollectionDate']
  donor = [donorInfo[key] for key in labels]
  return insertNewRow(newrow(donor, labels), df)

def insertNewRow(newrow, df=None):
  if df is not None:
    return df.append(newrow, ignore_index=True)
  else:
    return newrow
```

```
def newrow(data, col):
  return pd.DataFrame(data, index=col).T

def filterDF(df, filt):
  return df[np.all([df[key] == filt[key] for key in filt], axis=0)]
```

```
# -*- coding: utf-8 -*-
"""
Image classes and functions for FL_AnalyzeGas1.py
"""

import numpy as np
from scipy.misc import imread

class FL_intDist(object):
  def __init__(self, I, t, pixSize=(1.068,0.922)):
    self.t = t
    self.pixSize = pixSize
    self.mu = np.mean(I, axis=0)
    self.sigma = np.std(I, axis=0)
    self.r = np.multiply(pixSize[1],np.arange(np.float(I.shape[1]))-\
             (I.shape[1]-1.)/2.)

def crop2ROI(I, xbound=(0, None), ybound=(0, None)):
  return I[ybound[0]:ybound[1], xbound[0]:xbound[1]]

def pcCrop2ROI(I, xbound=(0, 100), ybound=(0, 100)):
  y1 = np.rint(ybound[0]/100.*(I.shape[0]-1))
  y2 = None if ybound[1]==100 else np.rint(ybound[1]/100.*(I.shape[0]))
  x1 = np.rint(xbound[0]/100.*(I.shape[1]-1))
  x2 = None if xbound[1]==100 else np.rint(xbound[1]/100.*(I.shape[1]))
  return crop2ROI(I, xbound=(x1, x2), ybound=(y1, y2))
```

```
# -*- coding: utf-8 -*-
"""
data analysis classes and functions for FL_AnalyzeGas1.py

"""

import numpy as np
from scipy import stats
from FL_Image import *
from FL_DataFrameGas1 import *

from scipy.optimize import curve_fit
##############################################################################################
class plotParams(object):
  def __init__(self, df):
    self.time = sorted(df.iloc[0].Data.viewkeys())
    #self.mode = []
    self.mu = []
    self.cfa = []
    self.dw = []
    self.sigma = []

    for t in self.time:
      I = pcCrop2ROI(df.iloc[0].Data[t], xbound=(2,97), ybound=(25, 75))
      #self.mode.append(stats.mode(I, axis=None)[0])
      self.mu.append(np.mean(I))
      self.sigma.append(np.std(I))
      self.cfa.append(cellFreeArea(I, 100))
      FLI = FL_intDist(I, t)
      self.dw.append(distWidth(FLI.mu, FLI.r))
    self.deltaCFA = np.array(self.cfa) - self.cfa[0]
#    self.deltaSigma = np.array(self.sigma) - self.sigma[0]
#    self.normedDW = np.divide(np.array(self.dw), self.dw[0])

##Second Order Polynomial Fitting of Data

    def f(x, a, b, c):

      x = np.asarray(x)
      y = a*x**2 + b*x + c
      return y


    params, _ = curve_fit(f, self.time, self.sigma)

    self.SigmaFit = f(self.time, *params)
        ##########################################################################
    self.deltaSigmaFit = np.array(self.SigmaFit) - self.SigmaFit[0]
    self.normedDW = np.divide(np.array(self.dw), self.dw[0])
#
class timeseriesParams(object):
  def __init__(self, df):
    self.DWmax = df.iloc[-1].normedDW
    self.DWt_half = t_half(df.normedDW.values, 180.)
    self.CFAmax = df.iloc[-1].deltaCFA
```

```
    self.CFAt_half = t_half(df.deltaCFA.values, 180.)
#    self.sigmamax = df.iloc[-1].deltaSigma
#    self.sigmat_half = t_half(df.deltaSigma.values, 180.)

#Find maximum and t_half of fitted curve to delta sigma
    self.sigmamax = df.iloc[-1].deltaSigmaFit
    self.sigmat_half = t_half(df.deltaSigmaFit.values, 180.)

def findHalfMax(x):
  halfMax = np.divide(np.add(np.max(x), np.min(x)), 2)
  return np.abs(x-halfMax).argmin()

def t_half(x, t):
  x50 = np.divide(np.add(x[-1], x[0]), 2)
  if x50 > x[0]:
    t50 = np.where(x > x50)[0][0]
  elif x50 < x[0]:
    t50 = np.where(x < x50)[0][0]
  elif x50 == x[0]:
    t50 = 0
  return np.float(t50)/x.size*t

def distWidth(x, r):
  xl, xr = np.array_split(x, 2)
  xl50 = findHalfMax(xl)
  xr50 = findHalfMax(xr)
  rl, rr = np.array_split(r, 2)
  return np.abs(rl[xl50]-rr[xr50])

def intThreshold(I, threshold_val):
  return np.where(I<=threshold_val, 0, 1)

def cellFreeArea(I, threshold_val):
  I_bin = intThreshold(I, threshold_val)
  return np.float(I_bin.nonzero()[0].size)/np.float(I_bin.size)*100.

def insTrialData(inDF, outDF=None):
  pp = plotParams(inDF)
  inDF = inDF.iloc[0]
  for time, cfa, dw, deltaCFA, normedDW, sigma, SigmaFit,\
  deltaSigmaFit in zip(pp.time, pp.cfa, pp.dw, pp.deltaCFA, pp.normedDW,\
  pp.sigma, pp.SigmaFit, pp.deltaSigmaFit):

#    trial = [inDF.Date, inDF.SubjID, inDF.Solvent, inDF.Ab, inDF.HCT, \
#             inDF.Temp, time, cfa, deltaCFA, dw, normedDW,\
   #sigma, deltaSigma]#, deltaSigmaFit]
#    labels = ['Date', 'SubjID', 'Solvent', 'Ab', 'HCT', 'Temp', 'Time', \
#              'CFA', 'deltaCFA', 'DW', 'normedDW',\
   #'sigma', 'deltaSigma',]# 'deltaSigmaFit']

    trial = [inDF.Date, inDF.SubjID, inDF.Solvent, inDF.Ab, inDF.HCT,\
    inDF.Oxy, inDF.Nitro,
             inDF.Temp, time, cfa, deltaCFA, dw, normedDW, sigma,\
             SigmaFit, deltaSigmaFit]
    labels = ['Date', 'SubjID', 'Solvent', 'Ab', 'HCT', 'Oxy',\
```

```
    'Nitro', 'Temp', 'Time',
              'CFA', 'deltaCFA', 'DW', 'normedDW', 'sigma',\
              'SigmaFit', 'deltaSigmaFit']

    outDF = insertNewRow(newrow(trial, labels), outDF)
  return outDF

def insTimeSeriesStats(inDF, outDF=None):
  tsp = timeseriesParams(inDF)
  inDF = inDF.iloc[0]
#  trial = [inDF.Date, inDF.SubjID, inDF.Solvent, inDF.Ab, inDF.HCT, \
#           inDF.Temp, tsp.CFAmax, tsp.CFAt_half, tsp.DWmax, tsp.DWt_half,\
  #tsp.sigmamax, tsp.sigmat_half]
#  labels = ['Date', 'SubjID', 'Solvent', 'Ab', 'HCT', 'Temp', \
#            'CFA_max', 'CFA_t_half', 'DW_max', 'DW_t_half',\
  #'deltaSigma_max', 'deltaSigma_t_half']

  trial = [inDF.Date, inDF.SubjID, inDF.Solvent, inDF.Ab, inDF.HCT,\
  inDF.Oxy, inDF.Nitro,
           inDF.Temp, tsp.CFAmax, tsp.CFAt_half, tsp.DWmax,\
           tsp.DWt_half, tsp.sigmamax, tsp.sigmat_half]
  labels = ['Date', 'SubjID', 'Solvent', 'Ab', 'HCT', 'Oxy',\
  'Nitro', 'Temp',
            'CFA_max', 'CFA_t_half', 'DW_max', 'DW_t_half',\
            'deltaSigma_max', 'deltaSigma_t_half']


  outDF = insertNewRow(newrow(trial, labels), outDF)
  return outDF
```

```
# -*- coding: utf-8 -*-
"""
plotting functions for FL_AnalyzeGas1.py

"""
import matplotlib as mpl
import matplotlib.pyplot as plt
import matplotlib.cm as cm
import matplotlib.patches as mpatches
import numpy as np
#import seaborn as sns
from matplotlib import colors
from matplotlib.backends.backend_pdf import PdfPages
from FL_Image import *
from FL_DataFrameGas1 import *
from FL_DataGas import *

def plotPDF(func, T, ind, time, outpdf):
  mpl.rc('font', family='Times New Roman', size=20)
  #sns.set(font_scale=2)
  #sns.set(font='Times New Roman')
  with PdfPages(outpdf) as pp:
    func(T, ind, time, pp)
  plt.close('all')

def colorSpec(cmap, xi, x):
  return cmap((xi-np.min(x))/(np.max(x)-np.min(x)))

def intPlot(T, ind, time, pp):
  #sns.set_style('white')
  #sns.set_style('ticks')
  cm=plt.get_cmap('jet')
  plt.figure()
  for t in time:
    FLI = FL_intDist(pcCrop2ROI(T.loc[ind].Data[t], xbound=(2,97),\
    ybound=(25,75)), t)
    x = FLI.r
    y = FLI.mu
    c = colorSpec(cm, t, time)
    leg = 't = {0} s'.format(np.int(t))
    plt.plot(x, y, color=c)
  plt.ylim(0,255)
  plt.xlabel('radial position')
  plt.ylabel('Average Intensity')
  pp.savefig()

def imgPlot(T, ind, time, pp):
  #sns.set_style('white')
  for t in time:
    plt.figure()
    I = pcCrop2ROI(T.loc[ind].Data[t], xbound=(2,97), ybound=(25,75))
    plt.imshow(I, cmap=cm.Greys_r)
    plt.gca().axes.xaxis.set_ticks([])
    plt.gca().axes.yaxis.set_ticks([])
    pp.savefig()
```

```
def binImgPlot(T, ind, time, pp):
  #sns.set_style('white')
  for t in time:
    plt.figure()
    I = intThreshold(pcCrop2ROI(T.loc[ind].Data[t], xbound=(2,97), \
    ybound=(25,75)), 100)
    plt.imshow(I, cmap=cm.Greys_r)
    plt.gca().axes.xaxis.set_ticks([])
    plt.gca().axes.yaxis.set_ticks([])
    pp.savefig()

def tsPlot(X, Y, c=None):
  x = np.unique(X)
  mu = np.array([np.mean(Y[X == xi]) for xi in x])
  stdev = np.array([np.std(Y[X == xi]) for xi in x])
  plt.plot(x, mu, color=c)
  plt.fill_between(x, np.add(mu, stdev/2.), np.add(mu, -1.*stdev/2.),\
  color=c, alpha=0.25)

def cfaPlot(T, ind, c, pp):
  plt.figure()
  if type(ind) == tuple:
    for ii in range(len(ind)):
      X = T.loc[ind[ii]].Time
      Y = T.loc[ind[ii]].CFA
      tsPlot(X, Y, c=c[ii])
  else:
    X = T.loc[ind].Time
    Y = T.loc[ind].CFA
    tsPlot(X, Y)
  plt.ylim(-5, 75)
  plt.xlabel('time')
  plt.ylabel('Cell Free Area as % of total image area')
  pp.savefig()

def deltaSigmaPlot(T, ind, c, pp):
  plt.figure()
  if type(ind) == tuple:
    for ii in range(len(ind)):
      X = T.loc[ind[ii]].Time
      Y = T.loc[ind[ii]].deltaSigmaFit
      tsPlot(X, Y, c=c[ii])
  else:
    X = T.loc[ind].Time
    Y = T.loc[ind].deltaSigma
    tsPlot(X, Y)
  plt.ylim(-5, 35)
  plt.xlabel('time')
  plt.ylabel('Delta Sigma Fitted')
  pp.savefig()
  ##################################################################

def dwPlot(T, ind, c, pp):
  plt.figure()
```

```
  if type(ind) == tuple:
    for ii in range(len(ind)):
      X = T.loc[ind[ii]].Time
      Y = T.loc[ind[ii]].normedDW
      tsPlot(X, Y, c=c[ii])
  else:
    X = T.loc[ind].Time
    Y = T.loc[ind].normedDW
    tsPlot(X, Y)
  plt.ylim(0.75, 1.1)
  plt.xlabel('time')
  plt.ylabel('Distribution Width\
  (width @ half maximum, normalized to initial value)')
  pp.savefig()

def barPlot(X, Y, c=None, h=None, f=True, w=1):
  plt.axhline(0, color='k')
  for ii in range(len(Y)):
    mu = np.mean(Y[ii])
    stdev = np.std(Y[ii])
    plt.bar(X+ii*w, mu, width=w, color=c[ii], ec='white', yerr=stdev/2.,\
    ecolor='k', hatch=h, fill=f)

def barPlotWrapper(T, ind, c, plotType, pp):
  plt.figure()
  h = (None, '/','x','.')
  for ii in range(len(ind)):
    X = np.float(len(ind[0])+1)*np.float(ii)
    Y = tuple([T.loc[jj][plotType] for jj in ind[ii]])
    barPlot(X, Y, c, h[ii])
  plt.gca().axes.xaxis.set_ticks([])

def CFAmaxBarPlot(T, ind, c, pp):
  barPlotWrapper(T, ind, c, 'CFA_max', pp)
  plt.ylim(-10, 60)
  plt.ylabel('Max. Cell Free Area (% total image area')
  pp.savefig()

  ######################################
def sigmamaxBarPlot(T, ind, c, pp):
  barPlotWrapper(T, ind, c, 'deltaSigma_max', pp)
  plt.ylim(-5, 35)
  plt.ylabel('Max. Delta Sigma')
  pp.savefig()
  ###################################

def DWmaxBarPlot(T, ind, c, pp):
  barPlotWrapper(T, ind, c, 'DW_max', pp)
  plt.ylim(0, 1.2)
  plt.ylabel('Distribution Width\
  (width @ half max., normalized to initial value)')
  pp.savefig()

def CFAthalfBarPlot(T, ind, c, pp):
  barPlotWrapper(T, ind, c, 'CFA_t_half', pp)
```

```
  plt.ylim(0, 140)
  plt.ylabel('half time of Max. Cell Free Area')
  pp.savefig()

  ###################################
def sigmat_halfBarPlot(T, ind, c, pp):
  barPlotWrapper(T, ind, c, 'deltaSigma_t_half', pp)
  plt.ylim(0, 180)
  plt.ylabel('half time of Max. Delta Sigma')
  pp.savefig()
  ########################################

def DWthalfBarPlot(T, ind, c, pp):
  barPlotWrapper(T, ind, c, 'DW_t_half', pp)
  plt.ylim(0, 140)
  plt.ylabel('half time of Distribution Width')
  pp.savefig()

def Leg(T, label, color, pp):
  #sns.set_style('white')
  leg = [mpatches.Patch(color=c, label=l) for c, l in zip(color, label)]
  plt.legend(handles=leg)
  pp.savefig()
```

Appendix C: Protein Solution pH and Dissolved Oxygen Statistics

Table 6: Temperature-Dependence of Solution pH and Dissolved Oxygen. [ALB 20, albumin 20 mg/mL], [ALB 50, albumin 50 mg/mL], [FIB 02, fibrinogen 2 mg/mL], [FIB 08, fibrinogen 8 mg/mL]. Entries are p-values form Welch's two sample t-test. * $p<0.05$.

Temperature-Dependence of pH

ALB 20	37 °C	41 °C	45 °C	49 °C
37 °C	-	0.60	0.62	0.67
41 °C	-	-	0.04 *	0.06
45 °C	-	-	-	0.87
49 °C	-	-	-	-

ALB 50	37 °C	41 °C	45 °C	49 °C
37 °C	-	0.60	0.50	0.48
41 °C	-	-	0.11	0.10
45 °C	-	-	-	0.91
49 °C	-	-	-	-

FIB 02	37 °C	41 °C	45 °C	49 °C
37 °C	-	0.82	0.53	0.68
41 °C	-	-	0.22	0.62
45 °C	-	-	-	0.56
49 °C	-	-	-	-

FIB 08	37 °C	41 °C	45 °C	49 °C
37 °C	-	0.90	0.67	0.67
41 °C	-	-	0.47	0.49
45 °C	-	-	-	1.00
49 °C	-	-	-	-

PBS	37 °C	41 °C	45 °C	49 °C
37 °C	-	0.87	0.95	1.00
41 °C	-	-	0.72	0.67
45 °C	-	-	-	0.88
49 °C	-	-	-	-

Temperature-Dependence of Dissolved Oxygen

ALB 20	37 °C	41 °C	45 °C	49 °C
37 °C	N/A	N/A	N/A	N/A
41 °C	N/A	N/A	N/A	N/A
45 °C	N/A	N/A	N/A	N/A
49 °C	N/A	N/A	N/A	N/A

ALB 50	37 °C	41 °C	45 °C	49 °C
37 °C	N/A	N/A	N/A	N/A
41 °C	N/A	N/A	N/A	N/A
45 °C	N/A	N/A	N/A	N/A
49 °C	N/A	N/A	N/A	N/A

FIB 02	37 °C	41 °C	45 °C	49 °C
37 °C	-	0.62	0.09	0.01 *
41 °C	-	-	0.15	0.06
45 °C	-	-	-	0.09
49 °C	-	-	-	-

FIB 08	37 °C	41 °C	45 °C	49 °C
37 °C	-	0.28	0.55	0.001 *
41 °C	-	-	0.85	2.59E-04 *
45 °C	-	-	-	2.04E-04 *
49 °C	-	-	-	-

PBS	37 °C	41 °C	45 °C	49 °C
37 °C	-	0.26	0.046 *	0.01 *
41 °C	-	-	0.11	0.02 *
45 °C	-	-	-	0.36
49 °C	-	-	-	-

Table 7: Solution-Dependence of pH and Dissolved Oxygen. [ALB 20, albumin 20 mg/mL], [ALB 50, albumin 50 mg/mL], [FIB 02, fibrinogen 2 mg/mL], [FIB 08, fibrinogen 8 mg/mL]. Entries are p-values form Welch's two sample t-test. * $p<0.05$.

Solution-Dependence of pH

37 °C	ALB 20	ALB 50	FIB 02	FIB 08	PBS
ALB 20	-	0.01 *	0.003 *	0.09	0.002 *
ALB 50	-	-	6.34E-04 *	3.30E-03 *	4.32E-04 *
FIB 02	-	-	-	0.03 *	0.27
FIB 08	-	-	-	-	0.01 *
PBS	-	-	-	-	-

41 °C	ALB 20	ALB 50	FIB 02	FIB 08	PBS
ALB 20	-	0.004 *	5.89E-05 *	0.01 *	6.01E-05 *
ALB 50	-	-	9.33E-04 *	6.95E-04 *	0.001 *
FIB 02	-	-	-	0.003 *	0.002 *
FIB 08	-	-	-	-	0.002 *
PBS	-	-	-	-	-

45 °C	ALB 20	ALB 50	FIB 02	FIB 08	PBS
ALB 20	-	2.55E-06 *	6.63E-07 *	6.26E-06 *	5.08E-08 *
ALB 50	-	-	1.17E-08 *	4.28E-07 *	5.58E-09 *
FIB 02	-	-	-	1.16E-05 *	2.87E-04 *
FIB 08	-	-	-	-	4.63E-07 *
PBS	-	-	-	-	-

49 °C	ALB 20	ALB 50	FIB 02	FIB 08	PBS
ALB 20	-	1.97E-05 *	2.19E-06 *	3.18E-04 *	5.22E-07 *
ALB 50	-	-	2.90E-07 *	4.44E-06 *	1.55E-07 *
FIB 02	-	-	-	3.29E-05 *	3.70E-03 *
FIB 08	-	-	-	-	3.73E-06 *
PBS	-	-	-	-	-

Solution-Dependence of Dissolved Oxygen

37 °C	ALB 20	ALB 50	FIB 02	FIB 08	PBS
ALB 20	-	N/A	N/A	N/A	N/A
ALB 50	-	-	N/A	N/A	N/A
FIB 02	-	-	-	2.62E-04 *	0.82
FIB 08	-	-	-	-	1.11E-03 *
PBS	-	-	-	-	-

41 °C	ALB 20	ALB 50	FIB 02	FIB 08	PBS
ALB 20	-	N/A	N/A	N/A	N/A
ALB 50	-	-	N/A	N/A	N/A
FIB 02	-	-	-	0.002 *	0.28
FIB 08	-	-	-	-	3.05E-06 *
PBS	-	-	-	-	-

45 °C	ALB 20	ALB 50	FIB 02	FIB 08	PBS
ALB 20	-	N/A	N/A	N/A	N/A
ALB 50	-	-	N/A	N/A	N/A
FIB 02	-	-	-	2.43E-06 *	0.39
FIB 08	-	-	-	-	2.13E-05 *
PBS	-	-	-	-	-

49 °C	ALB 20	ALB 50	FIB 02	FIB 08	PBS
ALB 20	-	N/A	N/A	N/A	N/A
ALB 50	-	-	N/A	N/A	N/A
FIB 02	-	-	-	2.47E-05 *	0.60
FIB 08	-	-	-	-	1.65E-04 *
PBS	-	-	-	-	-

Table 8: Mean and Standard Deviation of Solution pH and Dissolved Oxygen. [ALB 20, albumin 20 mg/mL], [ALB 50, albumin 50 mg/mL], [FIB 02, fibrinogen 2 mg/mL], [FIB 08, fibrinogen 8 mg/mL]. Entries are mean ± standard deviation. (n=4 each).

pH

mean ± SD	ALB 20	ALB 50	FIB 02	FIB 08	PBS
37 °C	7.13 ± 0.06	6.86 ± 0.08	7.45 ± 0.06	7.26 ± 0.08	7.52 ± 0.06
41 °C	7.15 ± 0.02	6.89 ± 0.05	7.44 ± 0.02	7.25 ± 0.03	7.53 ± 0.01
45 °C	7.11 ± 0.01	6.82 ± 0.02	7.43 ± 0.02	7.24 ± 0.01	7.52 ± 0.02
49 °C	7.11 ± 0.03	6.82 ± 0.03	7.44 ± 0.03	7.24 ± 0.02	7.52 ± 0.03

Dissolved Oxygen

mean ± SD	FIB 02	FIB 08	PBS
37 °C	6.10 ± 0.26	1.30 ± 0.10	6.17 ± 0.38
41 °C	6.30 ± 0.56	1.17 ± 0.15	5.83 ± 0.15
45 °C	5.60 ± 0.37	1.20 ± 0.28	5.33 ± 0.46
49 °C	5.15 ± 0.19	2.80 ± 0.28	5.03 ± 0.39

Appendix D: Onset of Stasis Model Statistics (Room Gas)

Table 9: Temperature-Dependence of Delta Sigma Max. and $T_{1/2}$ for Delta Sigma Max. for conditions in PBS and equilibrated with Room Gas. Entries are p-values form Welch's two sample t-test. * $p<0.05$.

Temperature-Dependence of Delta Sigma Max.

noAb	37 °C	41 °C	45 °C	49 °C
37 °C	-	0.66	0.81	0.44
41 °C	-	-	0.97	0.24
45 °C	-	-	-	0.42
49 °C	-	-	-	-

Band 3	37 °C	41 °C	45 °C	49 °C
37 °C	-	0.50	0.44	0.53
41 °C	-	-	0.76	0.83
45 °C	-	-	-	0.59
49 °C	-	-	-	-

GYPC	37 °C	41 °C	45 °C	49 °C
37 °C	-	0.72	0.59	0.87
41 °C	-	-	0.36	0.54
45 °C	-	-	-	0.64
49 °C	-	-	-	-

αvβ3	37 °C	41 °C	45 °C	49 °C
37 °C	-	0.81	0.64	0.48
41 °C	-	-	0.76	0.52
45 °C	-	-	-	0.65
49 °C	-	-	-	-

Temperature-Dependence of $T_{1/2}$ for Delta Sigma Max.

noAb	37 °C	41 °C	45 °C	49 °C
37 °C	-	0.16	0.14	0.07
41 °C	-	-	0.78	0.60
45 °C	-	-	-	0.87
49 °C	-	-	-	-

Band 3	37 °C	41 °C	45 °C	49 °C
37 °C	-	0.40	0.44	0.97
41 °C	-	-	1.00	0.54
45 °C	-	-	-	0.56
49 °C	-	-	-	-

GYPC	37 °C	41 °C	45 °C	49 °C
37 °C	-	0.29	0.18	0.15
41 °C	-	-	0.45	0.50
45 °C	-	-	-	0.85
49 °C	-	-	-	-

αvβ3	37 °C	41 °C	45 °C	49 °C
37 °C	-	0.68	0.43	0.66
41 °C	-	-	0.43	0.25
45 °C	-	-	-	0.13
49 °C	-	-	-	-

Table 10: Temperature-Dependence of Delta Sigma Max. and $T_{1/2}$ for Delta Sigma Max. for conditions in 0.5 g/dL dextran 500 kDa and equilibrated with Room Gas. Entries are p-values form Welch's two sample t-test. * $p<0.05$.

Temperature-Dependence of Delta Sigma Max.

noAb	37 °C	41 °C	45 °C	49 °C
37 °C	-	0.88	0.93	0.71
41 °C	-	-	0.94	0.78
45 °C	-	-	-	0.74
49 °C	-	-	-	-

Temperature-Dependence of $T_{1/2}$ for Delta Sigma Max.

noAb	37 °C	41 °C	45 °C	49 °C
37 °C	-	0.97	0.03 *	0.90
41 °C	-	-	0.24	0.90
45 °C	-	-	-	0.18
49 °C	-	-	-	-

Table 11: Temperature-Dependence of Delta Sigma Max. and $T_{1/2}$ for Delta Sigma Max. for conditions in autologous plasma and equilibrated with Room Gas. Entries are p-values form Welch's two sample t-test. * $p<0.05$.

Temperature-Dependence of Delta Sigma Max.

noAb	37 °C	41 °C	45 °C	49 °C
37 °C	-	0.79	0.83	0.74
41 °C	-	-	0.59	0.45
45 °C	-	-	-	0.91
49 °C	-	-	-	-

Band 3	37 °C	41 °C	45 °C	49 °C
37 °C	-	0.27	0.48	0.48
41 °C	-	-	0.43	0.14
45 °C	-	-	-	0.23
49 °C	-	-	-	-

GYPC	37 °C	41 °C	45 °C	49 °C
37 °C	-	0.56	0.47	0.30
41 °C	-	-	0.92	0.72
45 °C	-	-	-	0.79
49 °C	-	-	-	-

αvβ3	37 °C	41 °C	45 °C	49 °C
37 °C	-	0.58	0.74	0.83
41 °C	-	-	0.45	0.54
45 °C	-	-	-	0.95
49 °C	-	-	-	-

Temperature-Dependence of $T_{1/2}$ for Delta Sigma Max.

noAb	37 °C	41 °C	45 °C	49 °C
37 °C	-	0.83	0.12	0.03 *
41 °C	-	-	0.13	0.04 *
45 °C	-	-	-	0.35
49 °C	-	-	-	-

Band 3	37 °C	41 °C	45 °C	49 °C
37 °C	-	0.29	0.46	0.85
41 °C	-	-	0.84	0.13
45 °C	-	-	-	0.32
49 °C	-	-	-	-

GYPC	37 °C	41 °C	45 °C	49 °C
37 °C	-	0.45	0.30	0.86
41 °C	-	-	0.86	0.65
45 °C	-	-	-	0.53
49 °C	-	-	-	-

αvβ3	37 °C	41 °C	45 °C	49 °C
37 °C	-	0.46	0.81	0.43
41 °C	-	-	0.36	0.21
45 °C	-	-	-	0.57
49 °C	-	-	-	-

Table 12: Antibody-Dependence of Delta Sigma Max. and $T_{1/2}$ for Delta Sigma Max. for conditions in PBS and equilibrated with Room Gas. Entries are p-values form Welch's two sample t-test. * $p<0.05$.

Antibody-Dependence of Delta Sigma Max.

37°C	noAb	Band 3	GYPC	αvβ3
noAb	-	0.43	0.44	0.68
Band 3	-	-	0.30	0.67
GYPC	-	-	-	0.43
aVb3	-	-	-	-

41°C	noAb	Band 3	GYPC	αvβ3
noAb	-	1.00	0.12	1.00
Band 3	-	-	0.15	1.00
GYPC	-	-	-	0.28
aVb3	-	-	-	-

45°C	noAb	Band 3	GYPC	αvβ3
noAb	-	0.84	0.72	0.75
Band 3	-	-	0.84	0.89
GYPC	-	-	-	0.94
aVb3	-	-	-	-

49°C	noAb	Band 3	GYPC	αvβ3
noAb	-	0.19	0.95	0.99
Band 3	-	-	0.14	0.36
GYPC	-	-	-	0.97
aVb3	-	-	-	-

Antibody-Dependence of $T_{1/2}$ for Delta Sigma Max.

37°C	noAb	Band 3	GYPC	αvβ3
noAb	-	0.47	0.07	0.88
Band 3	-	-	0.20	0.83
GYPC	-	-	-	0.41
aVb3	-	-	-	-

41°C	noAb	Band 3	GYPC	αvβ3
noAb	-	0.96	0.62	0.69
Band 3	-	-	0.59	0.67
GYPC	-	-	-	0.90
aVb3	-	-	-	-

45°C	noAb	Band 3	GYPC	αvβ3
noAb	-	0.75	0.25	0.82
Band 3	-	-	0.30	0.59
GYPC	-	-	-	0.21
aVb3	-	-	-	-

49°C	noAb	Band 3	GYPC	αvβ3
noAb	-	0.33	0.17	0.13
Band 3	-	-	0.66	0.37
GYPC	-	-	-	0.60
aVb3	-	-	-	-

Table 13: Antibody-Dependence of Delta Sigma Max. and $T_{1/2}$ for Delta Sigma Max. for conditions in autologous plasma and equilibrated with Room Gas. Entries are p-values form Welch's two sample t-test. * $p<0.05$.

Antibody-Dependence of Delta Sigma Max.

37°C	noAb	Band 3	GYPC	αvβ3
noAb	-	0.66	0.43	0.63
Band 3	-	-	0.61	0.93
GYPC	-	-	-	0.68
aVb3	-	-	-	-

41°C	noAb	Band 3	GYPC	αvβ3
noAb	-	0.048 *	0.61	0.21
Band 3	-	-	0.32	0.86
GYPC	-	-	-	0.48
aVb3	-	-	-	-

45°C	noAb	Band 3	GYPC	αvβ3
noAb	-	0.45	0.93	0.94
Band 3	-	-	0.39	0.47
GYPC	-	-	-	1.00
aVb3	-	-	-	-

49°C	noAb	Band 3	GYPC	αvβ3
noAb	-	0.56	0.57	0.92
Band 3	-	-	0.89	0.73
GYPC	-	-	-	0.79
aVb3	-	-	-	-

Antibody-Dependence of $T_{1/2}$ for Delta Sigma Max.

37°C	noAb	Band 3	GYPC	αvβ3
noAb	-	0.96	0.20	0.90
Band 3	-	-	0.30	0.96
GYPC	-	-	-	0.17
aVb3	-	-	-	-

41°C	noAb	Band 3	GYPC	αvβ3
noAb	-	0.18	0.76	0.65
Band 3	-	-	0.44	0.07
GYPC	-	-	-	0.52
aVb3	-	-	-	-

45°C	noAb	Band 3	GYPC	αvβ3
noAb	-	0.86	0.26	0.18
Band 3	-	-	0.46	0.47
GYPC	-	-	-	0.89
aVb3	-	-	-	-

49°C	noAb	Band 3	GYPC	αvβ3
noAb	-	0.02 *	0.52	0.27
Band 3	-	-	0.41	0.36
GYPC	-	-	-	0.87
aVb3	-	-	-	-

Table 14: Solution-Dependence of Delta Sigma Max. and $T_{1/2}$ for Delta Sigma Max. for conditions in autologous plasma and equilibrated with Room Gas. Entries are p-values form Welch's two sample t-test. * $p<0.05$.

Solution-Dependence of Delta Sigma Max.

37°C	PBS	Plasma	Dextran
PBS	-	0.01 *	0.01 *
Plasma	-	-	0.18
Dextran	-	-	-

41°C	PBS	Plasma	Dextran
PBS	-	0.0004 *	0.01 *
Plasma	-	-	0.02 *
Dextran	-	-	-

45°C	PBS	Plasma	Dextran
PBS	-	0.01 *	0.01 *
Plasma	-	-	0.23
Dextran	-	-	-

49°C	PBS	Plasma	Dextran
PBS	-	0.01 *	0.04 *
Plasma	-	-	0.42
Dextran	-	-	-

Solution-Dependence of $T_{1/2}$ for Delta Sigma Max.

37°C	PBS	Plasma	Dextran
PBS	-	0.96	0.70
Plasma	-	-	0.53
Dextran	-	-	-

41°C	PBS	Plasma	Dextran
PBS	-	0.09	0.14
Plasma	-	-	0.83
Dextran	-	-	-

45°C	PBS	Plasma	Dextran
PBS	-	0.39	0.01 *
Plasma	-	-	0.0009 *
Dextran	-	-	-

49°C	PBS	Plasma	Dextran
PBS	-	0.53	0.08
Plasma	-	-	0.13
Dextran	-	-	-

Table 15: Mean and Standard Deviation of Delta Sigma Max. and $T_{1/2}$ for Delta Sigma Max. for all conditions equilibrated with Room Gas. Entries are mean ± standard deviation. (n=4 each unless otherwise stated).

Delta Sigma Max.

noAb	PBS	Plasma	Dextran 500
37 °C	-1.79 ± 0.62	17.90 ± 14.20	9.27 ± 4.33
41 °C	-1.96 ± 0.35	19.56 ± 7.94	9.76 ± 4.13
45 °C	-1.94 ± 1.00	16.35 ± 12.97	9.53 ± 3.78
49 °C	-1.39 ± 0.74	15.58 ± 10.86	10.97 ± 7.30

Band 3	PBS	Plasma	Dextran 500
37 °C	-2.90 ± 2.42	15.03 ± 6.64	-
41 °C	-1.95 ± 0.65	9.51 ± 6.12	-
45 °C	-1.80 ± 0.71	12.33 ± 1.23	-
49 °C	-2.04 ± 0.44	19.44 ± 9.43	-

GYPC	PBS	Plasma	Dextran 500
37 °C	-1.33 ± 1.02	11.83 ± 9.76	-
41 °C	-1.10 ± 0.79	16.25 ± 10.49	-
45 °C	-1.69 ± 0.87	16.98 ± 9.35	-
49 °C	-1.42 ± 0.67	18.60 ± 6.32	-

αvβ3	PBS	Plasma	Dextran 500
37 °C	-2.22 ± 1.53	14.56 ± 7.76	-
41 °C	-1.95 ± 0.96	10.66 ± 10.74	-
45 °C	-1.73 ± 0.64	16.96 ± 11.16	-
49 °C	-1.40 ± 0.93	16.42 ± 13.96	-

DIDS (n=1)	PBS	Plasma	Dextran
37 °C	-	0.49 ± NA	-
41 °C	-	0.84 ± NA	-
45 °C	-	2.72 ± NA	-
49 °C	-	6.14 ± NA	-

Glut (n=1)	PBS	Plasma	Dextran 500
37 °C	-	19.79 ± NA	-
41 °C	-	13.00 ± NA	-
45 °C	-	8.24 ± NA	-
49 °C	-	31.03 ± NA	-

$T_{1/2}$ Delta Sigma Max.

noAb	PBS	Plasma	Dextran 500
37 °C	77.05 ± 22.18	76.44 ± 18.45	81.99 ± 9.52
41 °C	53.63 ± 18.93	78.90 ± 23.52	82.60 ± 27.79
45 °C	49.32 ± 23.48	61.64 ± 13.65	103.56 ± 11.57
49 °C	46.85 ± 15.33	53.54 ± 17.07	80.14 ± 26.21

Band 3	PBS	Plasma	Dextran 500
37 °C	65.34 ± 21.16	77.05 ± 21.63	-
41 °C	54.25 ± 11.74	61.03 ± 16.89	-
45 °C	54.25 ± 16.72	64.11 ± 24.49	-
49 °C	64.73 ± 29.20	79.52 ± 12.31	-

GYPC	PBS	Plasma	Dextran 500
37 °C	44.38 ± 23.26	61.64 ± 15.72	-
41 °C	61.03 ± 20.67	73.97 ± 25.55	-
45 °C	79.52 ± 39.47	77.05 ± 21.53	-
49 °C	74.47 ± 34.84	64.73 ± 29.41	-

αvβ3	PBS	Plasma	Dextran 500
37 °C	72.33 ± 46.68	77.67 ± 12.81	-
41 °C	59.18 ± 15.40	83.22 ± 4.67	-
45 °C	45.21 ± 22.24	75.21 ± 14.73	-
49 °C	87.95 ± 31.03	67.81 ± 19.47	-

DIDS (n=1)	PBS	Plasma	Dextran 500
37 °C	-	88.77 ± NA	-
41 °C	-	125.75 ± NA	-
45 °C	-	86.30 ± NA	-
49 °C	-	59.18 ± NA	-

Glut (n=1)	PBS	Plasma	Dextran 500
37 °C	-	51.78 ± NA	-
41 °C	-	29.59 ± NA	-
45 °C	-	24.66 ± NA	-
49 °C	-	54.25 ± NA	-

Appendix E: Onset of Stasis Model Statistics (Controlled Gas)

Table 16: Temperature-Dependence of Delta Sigma Max. and $T_{1/2}$ for Delta Sigma Max. for conditions of no antibody in autologous plasma and equilibrated with prescribed oxygen concentrations. Entries are p-values form Welch's two sample t-test. * $p<0.05$.

Temperature-Dependence of Delta Sigma Max.

0% Oxygen	37 °C	41 °C	45 °C	49 °C
37 °C	-	0.08	0.82	0.16
41 °C	-	-	0.58	0.07
45 °C	-	-	-	0.59
49 °C	-	-	-	-

5% Oxygen	37 °C	41 °C	45 °C	49 °C
37 °C	-	0.65	0.36	0.36
41 °C	-	-	0.55	0.55
45 °C	-	-	-	0.92
49 °C	-	-	-	-

10% Oxygen	37 °C	41 °C	45 °C	49 °C
37 °C	-	0.55	0.02 *	0.20
41 °C	-	-	0.23	0.86
45 °C	-	-	-	0.02 *
49 °C	-	-	-	-

100% Oxygen	37 °C	41 °C	45 °C	49 °C
37 °C	-	0.87	0.86	0.27
41 °C	-	-	0.15	0.01 *
45 °C	-	-	-	0.02 *
49 °C	-	-	-	-

Temperature-Dependence of $T_{1/2}$ for Delta Sigma Max.

0% Oxygen	37 °C	41 °C	45 °C	49 °C
37 °C	-	0.43	0.36	0.03 *
41 °C	-	-	0.83	0.15
45 °C	-	-	-	0.25
49 °C	-	-	-	-

5% Oxygen	37 °C	41 °C	45 °C	49 °C
37 °C	-	0.92	0.91	0.37
41 °C	-	-	0.87	0.31
45 °C	-	-	-	0.65
49 °C	-	-	-	-

10% Oxygen	37 °C	41 °C	45 °C	49 °C
37 °C	-	0.36	0.03 *	0.28
41 °C	-	-	0.31	0.95
45 °C	-	-	-	0.29
49 °C	-	-	-	-

100% Oxygen	37 °C	41 °C	45 °C	49 °C
37 °C	-	0.90	0.41	0.38
41 °C	-	-	0.36	0.34
45 °C	-	-	-	0.94
49 °C	-	-	-	-

Table 17: Temperature-Dependence of Delta Sigma Max. and $T_{1/2}$ for Delta Sigma Max. for conditions of no antibody in fibrinogen 8 mg/mL and equilibrated with prescribed oxygen concentrations. Entries are p-values form Welch's two sample t-test. * $p<0.05$.

Temperature-Dependence of Delta Sigma Max.

0% Oxygen	37 °C	41 °C	45 °C	49 °C
37 °C	-	0.27	0.28	0.29
41 °C	-	-	0.86	0.96
45 °C	-	-	-	0.91
49 °C	-	-	-	-

5% Oxygen	37 °C	41 °C	45 °C	49 °C
37 °C	-	0.65	0.29	0.19
41 °C	-	-	0.43	0.28
45 °C	-	-	-	0.78
49 °C	-	-	-	-

10% Oxygen	37 °C	41 °C	45 °C	49 °C
37 °C	-	0.82	1.00	0.79
41 °C	-	-	0.80	0.96
45 °C	-	-	-	0.74
49 °C	-	-	-	-

100% Oxygen	37 °C	41 °C	45 °C	49 °C
37 °C	-	0.16	0.59	0.55
41 °C	-	-	0.28	0.93
45 °C	-	-	-	0.68
49 °C	-	-	-	-

Temperature-Dependence of $T_{1/2}$ for Delta Sigma Max.

0% Oxygen	37 °C	41 °C	45 °C	49 °C
37 °C	-	0.22	0.85	0.90
41 °C	-	-	0.42	0.44
45 °C	-	-	-	0.97
49 °C	-	-	-	-

5% Oxygen	37 °C	41 °C	45 °C	49 °C
37 °C	-	0.23	0.49	0.89
41 °C	-	-	0.85	0.32
45 °C	-	-	-	0.57
49 °C	-	-	-	-

10% Oxygen	37 °C	41 °C	45 °C	49 °C
37 °C	-	0.93	0.44	0.33
41 °C	-	-	0.44	0.33
45 °C	-	-	-	0.71
49 °C	-	-	-	-

100% Oxygen	37 °C	41 °C	45 °C	49 °C
37 °C	-	0.18	0.22	0.002 *
41 °C	-	-	0.55	0.79
45 °C	-	-	-	0.19
49 °C	-	-	-	-

Table 18: Temperature-Dependence of Delta Sigma Max. and $T_{1/2}$ for Delta Sigma Max. for conditions of no antibody in fibrinogen 2 mg/mL and equilibrated with prescribed oxygen concentrations. Entries are p-values form Welch's two sample t-test. * $p<0.05$.

Temperature-Dependence of Delta Sigma Max.

0% Oxygen	37 °C	41 °C	45 °C	49 °C
37 °C	-	0.88	0.18	0.48
41 °C	-	-	0.30	0.54
45 °C	-	-	-	0.10
49 °C	-	-	-	-

5% Oxygen	37 °C	41 °C	45 °C	49 °C
37 °C	-	0.84	0.80	0.70
41 °C	-	-	0.99	0.60
45 °C	-	-	-	0.53
49 °C	-	-	-	-

10% Oxygen	37 °C	41 °C	45 °C	49 °C
37 °C	-	0.16	0.70	0.13
41 °C	-	-	0.80	0.51
45 °C	-	-	-	0.54
49 °C	-	-	-	-

100% Oxygen	37 °C	41 °C	45 °C	49 °C
37 °C	-	0.25	0.09	0.054
41 °C	-	-	0.58	0.51
45 °C	-	-	-	0.94
49 °C	-	-	-	-

Temperature-Dependence of $T_{1/2}$ for Delta Sigma Max.

0% Oxygen	37 °C	41 °C	45 °C	49 °C
37 °C	-	0.28	0.15	0.57
41 °C	-	-	0.48	0.08
45 °C	-	-	-	0.07
49 °C	-	-	-	-

5% Oxygen	37 °C	41 °C	45 °C	49 °C
37 °C	-	0.41	0.46	0.87
41 °C	-	-	0.97	0.26
45 °C	-	-	-	0.32
49 °C	-	-	-	-

10% Oxygen	37 °C	41 °C	45 °C	49 °C
37 °C	-	0.47	0.85	0.40
41 °C	-	-	0.58	0.89
45 °C	-	-	-	0.51
49 °C	-	-	-	-

100% Oxygen	37 °C	41 °C	45 °C	49 °C
37 °C	-	0.63	0.64	0.73
41 °C	-	-	1.00	0.82
45 °C	-	-	-	0.83
49 °C	-	-	-	-

Table 19: Temperature-Dependence of Delta Sigma Max. and $T_{1/2}$ for Delta Sigma Max. for conditions of no antibody in albumin 50 mg/mL and equilibrated with prescribed oxygen concentrations. Entries are p-values form Welch's two sample t-test. * $p<0.05$.

Temperature-Dependence of Delta Sigma Max.

0% Oxygen	37 °C	41 °C	45 °C	49 °C
37 °C	-	0.35	0.52	0.28
41 °C	-	-	0.42	0.55
45 °C	-	-	-	0.41
49 °C	-	-	-	-

5% Oxygen	37 °C	41 °C	45 °C	49 °C
37 °C	-	0.95	0.57	0.18
41 °C	-	-	0.15	0.02 *
45 °C	-	-	-	0.10
49 °C	-	-	-	-

10% Oxygen	37 °C	41 °C	45 °C	49 °C
37 °C	-	0.84	0.04 *	0.82
41 °C	-	-	0.03 *	0.69
45 °C	-	-	-	0.09
49 °C	-	-	-	-

100% Oxygen	37 °C	41 °C	45 °C	49 °C
37 °C	-	0.44	0.14	0.30
41 °C	-	-	0.27	0.48
45 °C	-	-	-	0.93
49 °C	-	-	-	-

Temperature-Dependence of $T_{1/2}$ for Delta Sigma Max.

0% Oxygen	37 °C	41 °C	45 °C	49 °C
37 °C	-	0.52	0.23	0.19
41 °C	-	-	0.54	0.55
45 °C	-	-	-	0.90
49 °C	-	-	-	-

5% Oxygen	37 °C	41 °C	45 °C	49 °C
37 °C	-	0.71	0.53	1.00
41 °C	-	-	0.64	0.66
45 °C	-	-	-	0.51
49 °C	-	-	-	-

10% Oxygen	37 °C	41 °C	45 °C	49 °C
37 °C	-	0.34	0.20	0.80
41 °C	-	-	0.52	0.50
45 °C	-	-	-	0.30
49 °C	-	-	-	-

100% Oxygen	37 °C	41 °C	45 °C	49 °C
37 °C	-	0.01 *	0.20	0.30
41 °C	-	-	0.64	0.42
45 °C	-	-	-	0.78
49 °C	-	-	-	-

Table 20: Temperature-Dependence of Delta Sigma Max. and $T_{1/2}$ for Delta Sigma Max. for conditions of no antibody in albumin 20 mg/mL and equilibrated with prescribed oxygen concentrations. Entries are p-values form Welch's two sample t-test. * $p<0.05$.

Temperature-Dependence of Delta Sigma Max.

0% Oxygen	37 °C	41 °C	45 °C	49 °C
37 °C	-	0.98	0.71	0.98
41 °C	-	-	0.76	0.96
45 °C	-	-	-	0.61
49 °C	-	-	-	-

5% Oxygen	37 °C	41 °C	45 °C	49 °C
37 °C	-	0.19	0.44	0.28
41 °C	-	-	0.28	0.77
45 °C	-	-	-	0.42
49 °C	-	-	-	-

10% Oxygen	37 °C	41 °C	45 °C	49 °C
37 °C	-	0.26	0.34	0.09
41 °C	-	-	0.85	0.18
45 °C	-	-	-	0.64
49 °C	-	-	-	-

100% Oxygen	37 °C	41 °C	45 °C	49 °C
37 °C	-	0.73	0.34	0.29
41 °C	-	-	0.39	0.33
45 °C	-	-	-	0.79
49 °C	-	-	-	-

Temperature-Dependence of $T_{1/2}$ for Delta Sigma Max.

0% Oxygen	37 °C	41 °C	45 °C	49 °C
37 °C	-	0.61	0.42	0.62
41 °C	-	-	0.78	0.90
45 °C	-	-	-	0.92
49 °C	-	-	-	-

5% Oxygen	37 °C	41 °C	45 °C	49 °C
37 °C	-	0.61	0.82	0.73
41 °C	-	-	0.80	0.82
45 °C	-	-	-	0.95
49 °C	-	-	-	-

10% Oxygen	37 °C	41 °C	45 °C	49 °C
37 °C	-	0.08	0.03 *	0.16
41 °C	-	-	0.82	0.41
45 °C	-	-	-	0.43
49 °C	-	-	-	-

100% Oxygen	37 °C	41 °C	45 °C	49 °C
37 °C	-	0.20	0.22	0.94
41 °C	-	-	0.01 *	0.07
45 °C	-	-	-	0.08
49 °C	-	-	-	-

Table 21: Temperature-Dependence of Delta Sigma Max. and $T_{1/2}$ for Delta Sigma Max. for conditions of DIDS in autologous plasma and equilibrated with prescribed oxygen concentrations.

Entries are p-values form Welch's two sample t-test. * $p<0.05$.

Temperature-Dependence of Delta Sigma Max.

0% Oxygen	37 °C	41 °C	45 °C	49 °C
37 °C	-	0.88	0.15	0.16
41 °C	-	-	0.16	0.18
45 °C	-	-	-	0.88
49 °C	-	-	-	-

5% Oxygen	37 °C	41 °C	45 °C	49 °C
37 °C	-	0.40	0.22	0.051
41 °C	-	-	0.45	0.10
45 °C	-	-	-	0.35
49 °C	-	-	-	-

10% Oxygen	37 °C	41 °C	45 °C	49 °C
37 °C	-	0.82	0.38	0.33
41 °C	-	-	0.51	0.43
45 °C	-	-	-	0.73
49 °C	-	-	-	-

100% Oxygen	37 °C	41 °C	45 °C	49 °C
37 °C	-	0.77	0.31	0.35
41 °C	-	-	0.39	0.49
45 °C	-	-	-	0.77
49 °C	-	-	-	-

Temperature-Dependence of $T_{1/2}$ for Delta Sigma Max.

0% Oxygen	37 °C	41 °C	45 °C	49 °C
37 °C	-	0.30	0.22	0.10
41 °C	-	-	0.83	0.32
45 °C	-	-	-	0.27
49 °C	-	-	-	-

5% Oxygen	37 °C	41 °C	45 °C	49 °C
37 °C	-	0.39	0.72	0.03 *
41 °C	-	-	0.62	0.11
45 °C	-	-	-	0.06
49 °C	-	-	-	-

10% Oxygen	37 °C	41 °C	45 °C	49 °C
37 °C	-	0.80	0.34	0.28
41 °C	-	-	0.39	0.32
45 °C	-	-	-	0.68
49 °C	-	-	-	-

100% Oxygen	37 °C	41 °C	45 °C	49 °C
37 °C	-	0.33	0.98	0.76
41 °C	-	-	0.29	0.47
45 °C	-	-	-	0.74
49 °C	-	-	-	-

Table 22: Temperature-Dependence of Delta Sigma Max. and $T_{1/2}$ for Delta Sigma Max. for conditions of DIDS in fibrinogen 8 mg/mL and equilibrated with prescribed oxygen concentrations.

Entries are p-values form Welch's two sample t-test. * $p<0.05$.

Temperature-Dependence of Delta Sigma Max.

0% Oxygen	37 °C	41 °C	45 °C	49 °C
37 °C	-	0.67	0.91	0.84
41 °C	-	-	0.68	0.59
45 °C	-	-	-	0.96
49 °C	-	-	-	-

5% Oxygen	37 °C	41 °C	45 °C	49 °C
37 °C	-	0.67	0.74	0.97
41 °C	-	-	0.91	0.62
45 °C	-	-	-	0.69
49 °C	-	-	-	-

10% Oxygen	37 °C	41 °C	45 °C	49 °C
37 °C	-	0.71	0.80	0.83
41 °C	-	-	0.88	0.59
45 °C	-	-	-	0.65
49 °C	-	-	-	-

100% Oxygen	37 °C	41 °C	45 °C	49 °C
37 °C	-	0.84	0.63	0.68
41 °C	-	-	0.81	0.85
45 °C	-	-	-	0.97
49 °C	-	-	-	-

Temperature-Dependence of $T_{1/2}$ for Delta Sigma Max.

0% Oxygen	37 °C	41 °C	45 °C	49 °C
37 °C	-	0.46	0.97	0.63
41 °C	-	-	0.29	0.64
45 °C	-	-	-	0.40
49 °C	-	-	-	-

5% Oxygen	37 °C	41 °C	45 °C	49 °C
37 °C	-	0.51	0.60	0.82
41 °C	-	-	0.86	0.61
45 °C	-	-	-	0.73
49 °C	-	-	-	-

10% Oxygen	37 °C	41 °C	45 °C	49 °C
37 °C	-	0.45	0.90	0.16
41 °C	-	-	0.30	0.28
45 °C	-	-	-	0.12
49 °C	-	-	-	-

100% Oxygen	37 °C	41 °C	45 °C	49 °C
37 °C	-	0.94	0.40	0.65
41 °C	-	-	0.39	0.57
45 °C	-	-	-	0.28
49 °C	-	-	-	-

Table 23: Temperature-Dependence of Delta Sigma Max. and $T_{1/2}$ for Delta Sigma Max. for conditions of DIDS in fibrinogen 2 mg/mL and equilibrated with prescribed oxygen concentrations.

Entries are p-values form Welch's two sample t-test. * $p<0.05$.

Temperature-Dependence of Delta Sigma Max.

0% Oxygen	37 °C	41 °C	45 °C	49 °C
37 °C	-	0.99	0.45	0.90
41 °C	-	-	0.60	0.94
45 °C	-	-	-	0.50
49 °C	-	-	-	-

5% Oxygen	37 °C	41 °C	45 °C	49 °C
37 °C	-	0.89	0.67	0.76
41 °C	-	-	0.65	0.73
45 °C	-	-	-	0.88
49 °C	-	-	-	-

10% Oxygen	37 °C	41 °C	45 °C	49 °C
37 °C	-	0.51	0.45	0.78
41 °C	-	-	0.55	0.60
45 °C	-	-	-	0.37
49 °C	-	-	-	-

100% Oxygen	37 °C	41 °C	45 °C	49 °C
37 °C	-	0.93	0.76	0.34
41 °C	-	-	0.80	0.34
45 °C	-	-	-	0.78
49 °C	-	-	-	-

Temperature-Dependence of $T_{1/2}$ for Delta Sigma Max.

0% Oxygen	37 °C	41 °C	45 °C	49 °C
37 °C	-	0.68	0.84	0.92
41 °C	-	-	0.26	0.79
45 °C	-	-	-	0.76
49 °C	-	-	-	-

5% Oxygen	37 °C	41 °C	45 °C	49 °C
37 °C	-	0.46	0.07	0.51
41 °C	-	-	0.03 *	0.24
45 °C	-	-	-	0.27
49 °C	-	-	-	-

10% Oxygen	37 °C	41 °C	45 °C	49 °C
37 °C	-	0.74	0.57	0.62
41 °C	-	-	0.88	0.94
45 °C	-	-	-	0.92
49 °C	-	-	-	-

100% Oxygen	37 °C	41 °C	45 °C	49 °C
37 °C	-	0.47	0.71	0.47
41 °C	-	-	0.63	0.90
45 °C	-	-	-	0.62
49 °C	-	-	-	-

Table 24: Temperature-Dependence of Delta Sigma Max. and $T_{1/2}$ for Delta Sigma Max. for conditions of DIDS in albumin 50 mg/mL and equilibrated with prescribed oxygen concentrations.

Entries are p-values form Welch's two sample t-test. * $p<0.05$.

Temperature-Dependence of Delta Sigma Max.

0% Oxygen	37 °C	41 °C	45 °C	49 °C
37 °C	-	0.70	0.24	0.41
41 °C	-	-	0.48	0.73
45 °C	-	-	-	0.61
49 °C	-	-	-	-

5% Oxygen	37 °C	41 °C	45 °C	49 °C
37 °C	-	0.89	0.85	0.046 *
41 °C	-	-	0.99	0.15
45 °C	-	-	-	0.08
49 °C	-	-	-	-

10% Oxygen	37 °C	41 °C	45 °C	49 °C
37 °C	-	0.69	0.42	0.46
41 °C	-	-	0.46	0.35
45 °C	-	-	-	0.35
49 °C	-	-	-	-

100% Oxygen	37 °C	41 °C	45 °C	49 °C
37 °C	-	0.72	0.78	0.47
41 °C	-	-	0.92	0.24
45 °C	-	-	-	0.27
49 °C	-	-	-	-

Temperature-Dependence of $T_{1/2}$ for Delta Sigma Max.

0% Oxygen	37 °C	41 °C	45 °C	49 °C
37 °C	-	0.07	0.45	0.39
41 °C	-	-	0.40	0.80
45 °C	-	-	-	0.73
49 °C	-	-	-	-

5% Oxygen	37 °C	41 °C	45 °C	49 °C
37 °C	-	0.87	0.85	0.03 *
41 °C	-	-	0.68	0.01 *
45 °C	-	-	-	0.02 *
49 °C	-	-	-	-

10% Oxygen	37 °C	41 °C	45 °C	49 °C
37 °C	-	0.44	0.78	0.33
41 °C	-	-	0.44	0.81
45 °C	-	-	-	0.35
49 °C	-	-	-	-

100% Oxygen	37 °C	41 °C	45 °C	49 °C
37 °C	-	0.66	0.15	0.27
41 °C	-	-	0.30	0.50
45 °C	-	-	-	0.68
49 °C	-	-	-	-

Table 25: Temperature-Dependence of Delta Sigma Max. and $T_{1/2}$ for Delta Sigma Max. for conditions of DIDS in albumin 20 mg/mL and equilibrated with prescribed oxygen concentrations.

Entries are p-values form Welch's two sample t-test. * $p<0.05$.

Temperature-Dependence of Delta Sigma Max.

0% Oxygen	37 °C	41 °C	45 °C	49 °C
37 °C	-	0.54	0.19	0.07
41 °C	-	-	0.53	0.25
45 °C	-	-	-	0.53
49 °C	-	-	-	-

5% Oxygen	37 °C	41 °C	45 °C	49 °C
37 °C	-	0.31	0.62	0.23
41 °C	-	-	0.26	0.72
45 °C	-	-	-	0.06
49 °C	-	-	-	-

10% Oxygen	37 °C	41 °C	45 °C	49 °C
37 °C	-	0.73	1.00	0.45
41 °C	-	-	0.73	0.54
45 °C	-	-	-	0.44
49 °C	-	-	-	-

100% Oxygen	37 °C	41 °C	45 °C	49 °C
37 °C	-	0.58	0.83	0.58
41 °C	-	-	0.72	0.95
45 °C	-	-	-	0.71
49 °C	-	-	-	-

Temperature-Dependence of $T_{1/2}$ for Delta Sigma Max.

0% Oxygen	37 °C	41 °C	45 °C	49 °C
37 °C	-	0.89	0.94	0.75
41 °C	-	-	0.95	0.82
45 °C	-	-	-	0.77
49 °C	-	-	-	-

5% Oxygen	37 °C	41 °C	45 °C	49 °C
37 °C	-	0.47	0.33	0.93
41 °C	-	-	0.11	0.49
45 °C	-	-	-	0.23
49 °C	-	-	-	-

10% Oxygen	37 °C	41 °C	45 °C	49 °C
37 °C	-	0.63	0.76	0.01 *
41 °C	-	-	0.86	0.12
45 °C	-	-	-	0.08
49 °C	-	-	-	-

100% Oxygen	37 °C	41 °C	45 °C	49 °C
37 °C	-	0.55	0.53	0.68
41 °C	-	-	0.08	0.27
45 °C	-	-	-	0.87
49 °C	-	-	-	-

Table 26: Oxygen-Dependence of Delta Sigma Max. and $T_{1/2}$ for Delta Sigma Max. for conditions of no antibody in autologous plasma and equilibrated with prescribed oxygen concentrations. Entries are p-values form Welch's two sample t-test. * $p<0.05$.

Oxygen-Dependence of Delta Sigma Max.

37 °C	0% Oxy	5% Oxy	10% Oxy	100% Oxy
0% Oxy	-	0.64	0.20	0.47
5% Oxy	-	-	0.78	0.38
10% Oxy	-	-	-	0.18
100% Oxy	-	-	-	-

41 °C	0% Oxy	5% Oxy	10% Oxy	100% Oxy
0% Oxy	-	0.48	0.72	0.002 *
5% Oxy	-	-	0.86	0.34
10% Oxy	-	-	-	0.36
100% Oxy	-	-	-	-

45 °C	0% Oxy	5% Oxy	10% Oxy	100% Oxy
0% Oxy	-	0.82	0.54	0.87
5% Oxy	-	-	0.46	0.86
10% Oxy	-	-	-	0.02 *
100% Oxy	-	-	-	-

49 °C	0% Oxy	5% Oxy	10% Oxy	100% Oxy
0% Oxy	-	0.48	0.18	0.08
5% Oxy	-	-	0.34	0.09
10% Oxy	-	-	-	0.24
100% Oxy	-	-	-	-

Oxygen-Dependence of $T_{1/2}$ for Delta Sigma Max.

37 °C	0% Oxy	5% Oxy	10% Oxy	100% Oxy
0% Oxy	-	0.31	0.72	0.20
5% Oxy	-	-	0.23	0.73
10% Oxy	-	-	-	0.15
100% Oxy	-	-	-	-

41 °C	0% Oxy	5% Oxy	10% Oxy	100% Oxy
0% Oxy	-	0.84	0.88	0.46
5% Oxy	-	-	1.00	0.57
10% Oxy	-	-	-	0.65
100% Oxy	-	-	-	-

45 °C	0% Oxy	5% Oxy	10% Oxy	100% Oxy
0% Oxy	-	0.88	0.23	0.64
5% Oxy	-	-	0.55	0.66
10% Oxy	-	-	-	0.13
100% Oxy	-	-	-	-

49 °C	0% Oxy	5% Oxy	10% Oxy	100% Oxy
0% Oxy	-	0.88	0.32	0.13
5% Oxy	-	-	0.42	0.19
10% Oxy	-	-	-	0.58
100% Oxy	-	-	-	-

Table 27: Oxygen-Dependence of Delta Sigma Max. and $T_{1/2}$ for Delta Sigma Max. for conditions of no antibody in fibrinogen 8 mg/mL and equilibrated with prescribed oxygen concentrations. Entries are p-values form Welch's two sample t-test. * $p<0.05$.

Oxygen-Dependence of Delta Sigma Max.

37 °C	0% Oxy	5% Oxy	10% Oxy	100% Oxy
0% Oxy	-	0.23	0.17	0.04 *
5% Oxy	-	-	0.63	0.86
10% Oxy	-	-	-	0.67
100% Oxy	-	-	-	-

41 °C	0% Oxy	5% Oxy	10% Oxy	100% Oxy
0% Oxy	-	0.73	0.89	0.33
5% Oxy	-	-	0.89	0.40
10% Oxy	-	-	-	0.51
100% Oxy	-	-	-	-

45 °C	0% Oxy	5% Oxy	10% Oxy	100% Oxy
0% Oxy	-	0.48	0.82	0.92
5% Oxy	-	-	0.55	0.39
10% Oxy	-	-	-	0.83
100% Oxy	-	-	-	-

49 °C	0% Oxy	5% Oxy	10% Oxy	100% Oxy
0% Oxy	-	0.27	0.86	0.60
5% Oxy	-	-	0.22	0.65
10% Oxy	-	-	-	0.63
100% Oxy	-	-	-	-

Oxygen-Dependence of $T_{1/2}$ for Delta Sigma Max.

37 °C	0% Oxy	5% Oxy	10% Oxy	100% Oxy
0% Oxy	-	0.16	0.69	0.62
5% Oxy	-	-	0.13	0.08
10% Oxy	-	-	-	0.93
100% Oxy	-	-	-	-

41 °C	0% Oxy	5% Oxy	10% Oxy	100% Oxy
0% Oxy	-	0.30	0.18	0.53
5% Oxy	-	-	0.47	0.58
10% Oxy	-	-	-	0.32
100% Oxy	-	-	-	-

45 °C	0% Oxy	5% Oxy	10% Oxy	100% Oxy
0% Oxy	-	0.85	0.87	0.98
5% Oxy	-	-	0.95	0.82
10% Oxy	-	-	-	0.83
100% Oxy	-	-	-	-

49 °C	0% Oxy	5% Oxy	10% Oxy	100% Oxy
0% Oxy	-	0.49	0.65	0.59
5% Oxy	-	-	0.80	0.69
10% Oxy	-	-	-	1.00
100% Oxy	-	-	-	-

Table 28: Oxygen-Dependence of Delta Sigma Max. and $T_{1/2}$ for Delta Sigma Max. for conditions of no antibody in fibrinogen 2 mg/mL and equilibrated with prescribed oxygen concentrations. Entries are p-values form Welch's two sample t-test. * $p<0.05$.

Oxygen-Dependence of Delta Sigma Max.

37 °C	0% Oxy	5% Oxy	10% Oxy	100% Oxy
0% Oxy	-	0.71	0.07	0.38
5% Oxy	-	-	0.17	0.32
10% Oxy	-	-	-	0.04 *
100% Oxy	-	-	-	-

41 °C	0% Oxy	5% Oxy	10% Oxy	100% Oxy
0% Oxy	-	0.70	0.83	0.63
5% Oxy	-	-	0.84	0.96
10% Oxy	-	-	-	0.77
100% Oxy	-	-	-	-

45 °C	0% Oxy	5% Oxy	10% Oxy	100% Oxy
0% Oxy	-	0.64	0.95	0.83
5% Oxy	-	-	0.89	0.54
10% Oxy	-	-	-	0.88
100% Oxy	-	-	-	-

49 °C	0% Oxy	5% Oxy	10% Oxy	100% Oxy
0% Oxy	-	0.68	0.80	0.050
5% Oxy	-	-	0.66	0.13
10% Oxy	-	-	-	0.20
100% Oxy	-	-	-	-

Oxygen-Dependence of $T_{1/2}$ for Delta Sigma Max.

37 °C	0% Oxy	5% Oxy	10% Oxy	100% Oxy
0% Oxy	-	0.31	0.14	0.23
5% Oxy	-	-	0.81	0.86
10% Oxy	-	-	-	0.97
100% Oxy	-	-	-	-

41 °C	0% Oxy	5% Oxy	10% Oxy	100% Oxy
0% Oxy	-	0.40	0.95	0.97
5% Oxy	-	-	0.45	0.53
10% Oxy	-	-	-	0.99
100% Oxy	-	-	-	-

45 °C	0% Oxy	5% Oxy	10% Oxy	100% Oxy
0% Oxy	-	0.26	0.82	0.54
5% Oxy	-	-	0.31	0.61
10% Oxy	-	-	-	0.66
100% Oxy	-	-	-	-

49 °C	0% Oxy	5% Oxy	10% Oxy	100% Oxy
0% Oxy	-	0.10	0.13	0.06
5% Oxy	-	-	0.50	0.73
10% Oxy	-	-	-	0.66
100% Oxy	-	-	-	-

Table 29: Oxygen-Dependence of Delta Sigma Max. and $T_{1/2}$ for Delta Sigma Max. for conditions of no antibody in albumin 50 mg/mL and equilibrated with prescribed oxygen concentrations. Entries are p-values form Welch's two sample t-test. * $p<0.05$.

Oxygen-Dependence of Delta Sigma Max.

37 °C	0% Oxy	5% Oxy	10% Oxy	100% Oxy
0% Oxy	-	0.64	0.99	0.56
5% Oxy	-	-	0.58	0.96
10% Oxy	-	-	-	0.31
100% Oxy	-	-	-	-

41 °C	0% Oxy	5% Oxy	10% Oxy	100% Oxy
0% Oxy	-	0.26	0.35	0.33
5% Oxy	-	-	0.06	0.17
10% Oxy	-	-	-	0.60
100% Oxy	-	-	-	-

45 °C	0% Oxy	5% Oxy	10% Oxy	100% Oxy
0% Oxy	-	0.21	0.002 *	0.86
5% Oxy	-	-	0.17	0.43
10% Oxy	-	-	-	0.08
100% Oxy	-	-	-	-

49 °C	0% Oxy	5% Oxy	10% Oxy	100% Oxy
0% Oxy	-	0.87	0.16	0.57
5% Oxy	-	-	0.07	0.61
10% Oxy	-	-	-	0.51
100% Oxy	-	-	-	-

Oxygen-Dependence of $T_{1/2}$ for Delta Sigma Max.

37 °C	0% Oxy	5% Oxy	10% Oxy	100% Oxy
0% Oxy	-	0.97	0.43	0.56
5% Oxy	-	-	0.41	0.58
10% Oxy	-	-	-	0.15
100% Oxy	-	-	-	-

41 °C	0% Oxy	5% Oxy	10% Oxy	100% Oxy
0% Oxy	-	0.60	0.46	0.75
5% Oxy	-	-	0.58	0.09
10% Oxy	-	-	-	0.08
100% Oxy	-	-	-	-

45 °C	0% Oxy	5% Oxy	10% Oxy	100% Oxy
0% Oxy	-	0.54	0.13	0.47
5% Oxy	-	-	0.34	0.96
10% Oxy	-	-	-	0.27
100% Oxy	-	-	-	-

49 °C	0% Oxy	5% Oxy	10% Oxy	100% Oxy
0% Oxy	-	0.14	0.41	0.31
5% Oxy	-	-	0.52	0.65
10% Oxy	-	-	-	0.85
100% Oxy	-	-	-	-

Table 30: Oxygen-Dependence of Delta Sigma Max. and $T_{1/2}$ for Delta Sigma Max. for conditions of no antibody in albumin 20 mg/mL and equilibrated with prescribed oxygen concentrations. Entries are p-values form Welch's two sample t-test. * $p<0.05$.

Oxygen-Dependence of Delta Sigma Max.

37 °C	0% Oxy	5% Oxy	10% Oxy	100% Oxy
0% Oxy	-	0.23	0.52	0.36
5% Oxy	-	-	0.49	0.14
10% Oxy	-	-	-	0.21
100% Oxy	-	-	-	-

41 °C	0% Oxy	5% Oxy	10% Oxy	100% Oxy
0% Oxy	-	0.71	0.83	0.45
5% Oxy	-	-	0.80	0.70
10% Oxy	-	-	-	0.45
100% Oxy	-	-	-	-

45 °C	0% Oxy	5% Oxy	10% Oxy	100% Oxy
0% Oxy	-	0.63	0.49	0.71
5% Oxy	-	-	0.24	0.34
10% Oxy	-	-	-	0.71
100% Oxy	-	-	-	-

49 °C	0% Oxy	5% Oxy	10% Oxy	100% Oxy
0% Oxy	-	0.96	0.10	0.73
5% Oxy	-	-	0.49	0.76
10% Oxy	-	-	-	0.30
100% Oxy	-	-	-	-

Oxygen-Dependence of $T_{1/2}$ for Delta Sigma Max.

37 °C	0% Oxy	5% Oxy	10% Oxy	100% Oxy
0% Oxy	-	0.51	0.01 *	0.42
5% Oxy	-	-	0.23	0.95
10% Oxy	-	-	-	0.21
100% Oxy	-	-	-	-

41 °C	0% Oxy	5% Oxy	10% Oxy	100% Oxy
0% Oxy	-	0.73	0.79	0.09
5% Oxy	-	-	0.92	0.11
10% Oxy	-	-	-	0.08
100% Oxy	-	-	-	-

45 °C	0% Oxy	5% Oxy	10% Oxy	100% Oxy
0% Oxy	-	0.79	0.69	0.21
5% Oxy	-	-	0.99	0.49
10% Oxy	-	-	-	0.24
100% Oxy	-	-	-	-

49 °C	0% Oxy	5% Oxy	10% Oxy	100% Oxy
0% Oxy	-	0.82	0.75	0.83
5% Oxy	-	-	0.48	0.54
10% Oxy	-	-	-	0.86
100% Oxy	-	-	-	-

Table 31: Oxygen-Dependence of Delta Sigma Max. and $T_{1/2}$ for Delta Sigma Max. for conditions of DIDS in autologous plasma and equilibrated with prescribed oxygen concentrations. Entries are p-values form Welch's two sample t-test. * $p<0.05$.

Oxygen-Dependence of Delta Sigma Max.

37 °C	0% Oxy	5% Oxy	10% Oxy	100% Oxy
0% Oxy	-	0.70	0.45	1.00
5% Oxy	-	-	0.56	0.59
10% Oxy	-	-	-	0.41
100% Oxy	-	-	-	-

41 °C	0% Oxy	5% Oxy	10% Oxy	100% Oxy
0% Oxy	-	0.36	0.32	0.93
5% Oxy	-	-	0.66	0.43
10% Oxy	-	-	-	0.36
100% Oxy	-	-	-	-

45 °C	0% Oxy	5% Oxy	10% Oxy	100% Oxy
0% Oxy	-	0.61	0.85	0.59
5% Oxy	-	-	0.61	0.92
10% Oxy	-	-	-	0.62
100% Oxy	-	-	-	-

49 °C	0% Oxy	5% Oxy	10% Oxy	100% Oxy
0% Oxy	-	0.97	0.95	0.36
5% Oxy	-	-	0.90	0.19
10% Oxy	-	-	-	0.31
100% Oxy	-	-	-	-

Oxygen-Dependence of $T_{1/2}$ for Delta Sigma Max.

37 °C	0% Oxy	5% Oxy	10% Oxy	100% Oxy
0% Oxy	-	0.46	0.54	0.35
5% Oxy	-	-	0.83	0.67
10% Oxy	-	-	-	0.58
100% Oxy	-	-	-	-

41 °C	0% Oxy	5% Oxy	10% Oxy	100% Oxy
0% Oxy	-	0.94	0.55	0.48
5% Oxy	-	-	0.40	0.35
10% Oxy	-	-	-	0.17
100% Oxy	-	-	-	-

45 °C	0% Oxy	5% Oxy	10% Oxy	100% Oxy
0% Oxy	-	0.36	0.80	0.50
5% Oxy	-	-	0.57	0.81
10% Oxy	-	-	-	0.72
100% Oxy	-	-	-	-

49 °C	0% Oxy	5% Oxy	10% Oxy	100% Oxy
0% Oxy	-	0.90	0.57	0.29
5% Oxy	-	-	0.60	0.28
10% Oxy	-	-	-	0.72
100% Oxy	-	-	-	-

Table 32: Oxygen-Dependence of Delta Sigma Max. and $T_{1/2}$ for Delta Sigma Max. for conditions of DIDS in fibrinogen 8 mg/mL and equilibrated with prescribed oxygen concentrations. Entries are p-values form Welch's two sample t-test. * $p<0.05$.

Oxygen-Dependence of Delta Sigma Max.

37 °C	0% Oxy	5% Oxy	10% Oxy	100% Oxy
0% Oxy	-	0.94	0.76	0.99
5% Oxy	-	-	0.74	0.94
10% Oxy	-	-	-	0.77
100% Oxy	-	-	-	-

41 °C	0% Oxy	5% Oxy	10% Oxy	100% Oxy
0% Oxy	-	0.98	0.65	0.64
5% Oxy	-	-	0.64	0.64
10% Oxy	-	-	-	0.96
100% Oxy	-	-	-	-

45 °C	0% Oxy	5% Oxy	10% Oxy	100% Oxy
0% Oxy	-	0.74	0.91	0.76
5% Oxy	-	-	0.80	0.50
10% Oxy	-	-	-	0.65
100% Oxy	-	-	-	-

49 °C	0% Oxy	5% Oxy	10% Oxy	100% Oxy
0% Oxy	-	0.93	0.52	0.81
5% Oxy	-	-	0.53	0.75
10% Oxy	-	-	-	0.46
100% Oxy	-	-	-	-

Oxygen-Dependence of $T_{1/2}$ for Delta Sigma Max.

37 °C	0% Oxy	5% Oxy	10% Oxy	100% Oxy
0% Oxy	-	0.57	0.31	0.38
5% Oxy	-	-	0.10	0.10
10% Oxy	-	-	-	
100% Oxy	-	-	-	-

41 °C	0% Oxy	5% Oxy	10% Oxy	100% Oxy
0% Oxy	-	0.57	0.72	0.86
5% Oxy	-	-	0.70	0.47
10% Oxy	-	-	-	0.44
100% Oxy	-	-	-	-

45 °C	0% Oxy	5% Oxy	10% Oxy	100% Oxy
0% Oxy	-	0.92	0.12	0.86
5% Oxy	-	-	0.21	0.93
10% Oxy	-	-	-	0.28
100% Oxy	-	-	-	-

49 °C	0% Oxy	5% Oxy	10% Oxy	100% Oxy
0% Oxy	-	0.21	0.31	0.35
5% Oxy	-	-	0.78	0.13
10% Oxy	-	-	-	0.14
100% Oxy	-	-	-	-

Table 33: Oxygen-Dependence of Delta Sigma Max. and $T_{1/2}$ for Delta Sigma Max. for conditions of DIDS in fibrinogen 2 mg/mL and equilibrated with prescribed oxygen concentrations. Entries are p-values form Welch's two sample t-test. * $p<0.05$.

Oxygen-Dependence of Delta Sigma Max.

37 °C	0% Oxy	5% Oxy	10% Oxy	100% Oxy
0% Oxy	-	0.59	0.56	0.75
5% Oxy	-	-	0.91	0.87
10% Oxy	-	-	-	0.79
100% Oxy	-	-	-	-

41 °C	0% Oxy	5% Oxy	10% Oxy	100% Oxy
0% Oxy	-	0.87	0.55	0.77
5% Oxy	-	-	0.68	0.93
10% Oxy	-	-	-	0.66
100% Oxy	-	-	-	-

45 °C	0% Oxy	5% Oxy	10% Oxy	100% Oxy
0% Oxy	-	0.85	0.49	0.98
5% Oxy	-	-	0.56	0.90
10% Oxy	-	-	-	0.54
100% Oxy	-	-	-	-

49 °C	0% Oxy	5% Oxy	10% Oxy	100% Oxy
0% Oxy	-	0.47	0.81	0.13
5% Oxy	-	-	0.64	0.67
10% Oxy	-	-	-	0.30
100% Oxy	-	-	-	-

Oxygen-Dependence of $T_{1/2}$ for Delta Sigma Max.

37 °C	0% Oxy	5% Oxy	10% Oxy	100% Oxy
0% Oxy	-	0.94	0.72	0.89
5% Oxy	-	-	0.61	0.76
10% Oxy	-	-	-	0.52
100% Oxy	-	-	-	-

41 °C	0% Oxy	5% Oxy	10% Oxy	100% Oxy
0% Oxy	-	0.13	0.41	0.18
5% Oxy	-	-	0.63	0.98
10% Oxy	-	-	-	0.67
100% Oxy	-	-	-	-

45 °C	0% Oxy	5% Oxy	10% Oxy	100% Oxy
0% Oxy	-	0.06	0.75	0.91
5% Oxy	-	-	0.08	0.08
10% Oxy	-	-	-	0.87
100% Oxy	-	-	-	-

49 °C	0% Oxy	5% Oxy	10% Oxy	100% Oxy
0% Oxy	-	0.87	0.83	0.57
5% Oxy	-	-	0.49	0.33
10% Oxy	-	-	-	0.56
100% Oxy	-	-	-	-

Table 34: Oxygen-Dependence of Delta Sigma Max. and $T_{1/2}$ for Delta Sigma Max. for conditions of DIDS in albumin 50 mg/mL and equilibrated with prescribed oxygen concentrations. Entries are p-values form Welch's two sample t-test. * $p<0.05$.

Oxygen-Dependence of Delta Sigma Max.

37 °C	0% Oxy	5% Oxy	10% Oxy	100% Oxy
0% Oxy	-	0.94	0.47	0.68
5% Oxy	-	-	0.40	0.61
10% Oxy	-	-	-	0.33
100% Oxy	-	-	-	-

41 °C	0% Oxy	5% Oxy	10% Oxy	100% Oxy
0% Oxy	-	0.77	0.61	0.63
5% Oxy	-	-	0.80	0.45
10% Oxy	-	-	-	0.36
100% Oxy	-	-	-	-

45 °C	0% Oxy	5% Oxy	10% Oxy	100% Oxy
0% Oxy	-	0.24	0.57	0.81
5% Oxy	-	-	0.48	0.47
10% Oxy	-	-	-	0.55
100% Oxy	-	-	-	-

49 °C	0% Oxy	5% Oxy	10% Oxy	100% Oxy
0% Oxy	-	0.02 *	0.13	0.16
5% Oxy	-	-	0.80	0.11
10% Oxy	-	-	-	0.32
100% Oxy	-	-	-	-

Oxygen-Dependence of $T_{1/2}$ for Delta Sigma Max.

37 °C	0% Oxy	5% Oxy	10% Oxy	100% Oxy
0% Oxy	-	0.23	0.22	0.50
5% Oxy	-	-	0.89	0.50
10% Oxy	-	-	-	0.55
100% Oxy	-	-	-	-

41 °C	0% Oxy	5% Oxy	10% Oxy	100% Oxy
0% Oxy	-	0.82	0.35	0.67
5% Oxy	-	-	0.44	0.87
10% Oxy	-	-	-	0.51
100% Oxy	-	-	-	-

45 °C	0% Oxy	5% Oxy	10% Oxy	100% Oxy
0% Oxy	-	0.36	0.57	0.16
5% Oxy	-	-	0.94	0.69
10% Oxy	-	-	-	0.90
100% Oxy	-	-	-	-

49 °C	0% Oxy	5% Oxy	10% Oxy	100% Oxy
0% Oxy	-	0.03 *	0.41	0.65
5% Oxy	-	-	0.02 *	0.01 *
10% Oxy	-	-	-	0.22
100% Oxy	-	-	-	-

Table 35: Oxygen-Dependence of Delta Sigma Max. and $T_{1/2}$ for Delta Sigma Max. for conditions of DIDS in albumin 20 mg/mL and equilibrated with prescribed oxygen concentrations. Entries are p-values form Welch's two sample t-test. * $p<0.05$.

Oxygen-Dependence of Delta Sigma Max.

37 °C	0% Oxy	5% Oxy	10% Oxy	100% Oxy
0% Oxy	-	0.38	0.90	0.41
5% Oxy	-	-	0.43	0.73
10% Oxy	-	-	-	0.53
100% Oxy	-	-	-	-

41 °C	0% Oxy	5% Oxy	10% Oxy	100% Oxy
0% Oxy	-	0.43	0.39	0.84
5% Oxy	-	-	0.90	0.50
10% Oxy	-	-	-	0.46
100% Oxy	-	-	-	-

45 °C	0% Oxy	5% Oxy	10% Oxy	100% Oxy
0% Oxy	-	0.75	0.39	0.77
5% Oxy	-	-	0.50	0.92
10% Oxy	-	-	-	0.64
100% Oxy	-	-	-	-

49 °C	0% Oxy	5% Oxy	10% Oxy	100% Oxy
0% Oxy	-	0.02 *	0.02 *	0.23
5% Oxy	-	-	0.98	0.32
10% Oxy	-	-	-	0.33
100% Oxy	-	-	-	-

Oxygen-Dependence of $T_{1/2}$ for Delta Sigma Max.

37 °C	0% Oxy	5% Oxy	10% Oxy	100% Oxy
0% Oxy	-	0.38	0.42	0.76
5% Oxy	-	-	0.77	0.53
10% Oxy	-	-	-	0.62
100% Oxy	-	-	-	-

41 °C	0% Oxy	5% Oxy	10% Oxy	100% Oxy
0% Oxy	-	0.09	0.75	0.18
5% Oxy	-	-	0.22	0.27
10% Oxy	-	-	-	0.58
100% Oxy	-	-	-	-

45 °C	0% Oxy	5% Oxy	10% Oxy	100% Oxy
0% Oxy	-	0.82	0.62	0.86
5% Oxy	-	-	0.70	0.61
10% Oxy	-	-	-	0.52
100% Oxy	-	-	-	-

49 °C	0% Oxy	5% Oxy	10% Oxy	100% Oxy
0% Oxy	-	0.13	0.053	0.80
5% Oxy	-	-	0.02 *	0.24
10% Oxy	-	-	-	0.08
100% Oxy	-	-	-	-

Table 36: DIDS-Dependence of Delta Sigma Max. and $T_{1/2}$ for Delta Sigma Max. for conditions in autologous plasma and equilibrated with prescribed oxygen concentrations. Entries are p-values form Welch's two sample t-test. * p<0.05.

DIDS-Dependence of Delta Sigma Max.

DIDS vs noAb	0% Oxy	5% Oxy	10% Oxy	100% Oxy
37 °C	0.02 *	0.15	0.22	0.03 *
41 °C	0.01 *	0.052	0.21	0.001 *
45 °C	0.41	0.047 *	0.001 *	0.054
49 °C	0.12	0.08	0.25	0.07

DIDS-Dependence of $T_{1/2}$ for Delta Sigma Max.

DIDS vs noAb	0% Oxy	5% Oxy	10% Oxy	100% Oxy
37 °C	0.14	0.01 *	0.09	0.07
41 °C	0.25	0.04 *	0.04 *	0.43
45 °C	0.11	0.12	0.02 *	0.10
49 °C	0.28	0.18	0.41	0.32

Table 37: DIDS-Dependence of Delta Sigma Max. and $T_{1/2}$ for Delta Sigma Max. for conditions in fibrinogen 8 mg/mL and equilibrated with prescribed oxygen concentrations. Entries are p-values form Welch's two sample t-test. * p<0.05.

DIDS-Dependence of Delta Sigma Max.

DIDS vs noAb	0% Oxy	5% Oxy	10% Oxy	100% Oxy
37 °C	0.04 *	0.04 *	0.04 *	0.004 *
41 °C	0.04 *	0.01 *	0.10	0.01 *
45 °C	0.09	0.01 *	0.02 *	0.04 *
49 °C	0.09	0.01 *	3.77E-04 *	0.09

DIDS-Dependence of $T_{1/2}$ for Delta Sigma Max.

DIDS vs noAb	0% Oxy	5% Oxy	10% Oxy	100% Oxy
37 °C	0.81	0.04 *	0.23	0.21
41 °C	0.49	0.72	0.45	0.96
45 °C	0.68	0.52	0.44	0.59
49 °C	0.96	0.07	0.21	0.64

Table 38: DIDS-Dependence of Delta Sigma Max. and $T_{1/2}$ for Delta Sigma Max. for conditions in fibrinogen 2 mg/mL and equilibrated with prescribed oxygen concentrations. Entries are p-values form Welch's two sample t-test. * p<0.05.

DIDS-Dependence of Delta Sigma Max.

DIDS vs noAb	0% Oxy	5% Oxy	10% Oxy	100% Oxy
37 °C	0.42	0.23	0.04 *	0.94
41 °C	0.66	0.41	0.18	0.20
45 °C	0.06	0.13	0.23	0.14
49 °C	0.64	0.24	0.93	0.01 *

DIDS-Dependence of $T_{1/2}$ for Delta Sigma Max.

DIDS vs noAb	0% Oxy	5% Oxy	10% Oxy	100% Oxy
37 °C	0.29	0.92	0.90	0.75
41 °C	0.90	0.06	0.49	0.37
45 °C	0.90	0.85	0.97	0.58
49 °C	0.22	0.61	0.37	0.42

Table 39: DIDS-Dependence of Delta Sigma Max. and $T_{1/2}$ for Delta Sigma Max. for conditions in albumin 50 mg/mL and equilibrated with prescribed oxygen concentrations. Entries are p-values form Welch's two sample t-test. * p<0.05.

DIDS-Dependence of Delta Sigma Max.

DIDS vs noAb	0% Oxy	5% Oxy	10% Oxy	100% Oxy
37 °C	0.23	0.60	0.21	0.25
41 °C	0.19	0.38	0.19	0.0499 *
45 °C	0.004 *	0.048 *	0.41	0.02 *
49 °C	0.02 *	0.06	0.89	0.16

DIDS-Dependence of $T_{1/2}$ for Delta Sigma Max.

DIDS vs noAb	0% Oxy	5% Oxy	10% Oxy	100% Oxy
37 °C	0.72	0.32	0.93	0.02 *
41 °C	0.93	0.19	0.61	0.41
45 °C	0.35	0.85	0.14	0.62
49 °C	0.39	0.03 *	0.63	0.49

Table 40: DIDS-Dependence of Delta Sigma Max. and $T_{1/2}$ for Delta Sigma Max. for conditions in albumin 20 mg/mL and equilibrated with prescribed oxygen concentrations. Entries are p-values form Welch's two sample t-test. * p<0.05.

DIDS-Dependence of Delta Sigma Max.

DIDS vs noAb	0% Oxy	5% Oxy	10% Oxy	100% Oxy
37 °C	0.10	0.07	0.06	0.51
41 °C	0.09	0.50	0.08	0.33
45 °C	0.01 *	0.001 *	0.24	0.07
49 °C	0.003 *	0.41	0.69	0.09

DIDS-Dependence of $T_{1/2}$ for Delta Sigma Max.

DIDS vs noAb	0% Oxy	5% Oxy	10% Oxy	100% Oxy
37 °C	0.56	0.82	0.01 *	0.80
41 °C	0.85	0.23	0.72	0.003 *
45 °C	0.63	0.98	0.71	0.21
49 °C	0.73	0.42	0.06	0.40

Table 41: Solution-Dependence of Delta Sigma Max. and $T_{1/2}$ for Delta Sigma Max. for conditions of no antibody at 37°C and equilibrated with prescribed oxygen concentrations. [ALB 20, albumin 20 mg/mL], [ALB 50, albumin 50 mg/mL], [FIB 02, fibrinogen 2 mg/mL], [FIB 08, fibrinogen 8 mg/mL]. Entries are p-values form Welch's two sample t-test. * $p<0.05$.

Solution-Dependence of Delta Sigma Max.

0% Oxygen	ALB 20	ALB 50	FIB 02	FIB 08	Plasma
ALB 20	-	0.83	0.39	0.001 *	1.52E-04 *
ALB 50	-	-	0.36	0.001 *	1.06E-04 *
FIB 02	-	-	-	0.001 *	2.00E-04 *
FIB 08	-	-	-	-	1.85E-04 *
Plasma	-	-	-	-	-

5% Oxygen	ALB 20	ALB 50	FIB 02	FIB 08	Plasma
ALB 20	-	0.17	0.86	0.052	0.08
ALB 50	-	-	0.20	0.03 *	0.07
FIB 02	-	-	-	0.0497 *	0.08
FIB 08	-	-	-	-	0.13
Plasma	-	-	-	-	-

10% Oxygen	ALB 20	ALB 50	FIB 02	FIB 08	Plasma
ALB 20	-	0.20	0.06	0.051	0.02 *
ALB 50	-	-	0.03 *	0.04 *	0.02 *
FIB 02	-	-	-	0.08	0.02 *
FIB 08	-	-	-	-	0.049 *
Plasma	-	-	-	-	-

100% Oxygen	ALB 20	ALB 50	FIB 02	FIB 08	Plasma
ALB 20	-	0.69	0.47	0.001 *	0.02 *
ALB 50	-	-	0.57	0.003 *	0.02 *
FIB 02	-	-	-	0.002 *	0.02 *
FIB 08	-	-	-	-	0.03 *
Plasma	-	-	-	-	-

Solution-Dependence of $T_{1/2}$ for Delta Sigma Max.

0% Oxygen	ALB 20	ALB 50	FIB 02	FIB 08	Plasma
ALB 20	-	0.19	0.04 *	0.15	0.18
ALB 50	-	-	0.72	0.54	0.48
FIB 02	-	-	-	0.18	0.15
FIB 08	-	-	-	-	0.77
Plasma	-	-	-	-	-

5% Oxygen	ALB 20	ALB 50	FIB 02	FIB 08	Plasma
ALB 20	-	0.58	0.93	0.65	0.75
ALB 50	-	-	0.51	0.23	0.66
FIB 02	-	-	-	0.72	0.66
FIB 08	-	-	-	-	0.07
Plasma	-	-	-	-	-

10% Oxygen	ALB 20	ALB 50	FIB 02	FIB 08	Plasma
ALB 20	-	0.12	0.07	0.03 *	0.002 *
ALB 50	-	-	0.90	0.55	0.84
FIB 02	-	-	-	0.40	0.67
FIB 08	-	-	-	-	0.39
Plasma	-	-	-	-	-

100% Oxygen	ALB 20	ALB 50	FIB 02	FIB 08	Plasma
ALB 20	-	0.26	0.73	0.85	0.68
ALB 50	-	-	0.18	0.01 *	0.046 *
FIB 02	-	-	-	0.55	0.44
FIB 08	-	-	-	-	0.46
Plasma	-	-	-	-	-

Table 42: Solution-Dependence of Delta Sigma Max. and $T_{1/2}$ for Delta Sigma Max. for conditions of no antibody at 41°C and equilibrated with prescribed oxygen concentrations. [ALB 20, albumin 20 mg/mL], [ALB 50, albumin 50 mg/mL], [FIB 02, fibrinogen 2 mg/mL], [FIB 08, fibrinogen 8 mg/mL]. Entries are p-values form Welch's two sample t-test. * $p<0.05$.

Solution-Dependence of Delta Sigma Max.

0% Oxygen	ALB 20	ALB 50	FIB 02	FIB 08	Plasma
ALB 20	-	0.38	0.48	0.06	0.001 *
ALB 50	-	-	0.51	0.13	8.51E-05 *
FIB 02	-	-	-	0.07	0.001 *
FIB 08	-	-	-	-	4.30E-04 *
Plasma	-	-	-	-	-

5% Oxygen	ALB 20	ALB 50	FIB 02	FIB 08	Plasma
ALB 20	-	0.53	0.26	0.01 *	0.02 *
ALB 50	-	-	0.15	0.01 *	0.02 *
FIB 02	-	-	-	0.01 *	0.02 *
FIB 08	-	-	-	-	0.04 *
Plasma	-	-	-	-	-

10% Oxygen	ALB 20	ALB 50	FIB 02	FIB 08	Plasma
ALB 20	-	0.89	0.24	0.08	0.052
ALB 50	-	-	0.22	0.08	0.052
FIB 02	-	-	-	0.10	0.055
FIB 08	-	-	-	-	0.09
Plasma	-	-	-	-	-

100% Oxygen	ALB 20	ALB 50	FIB 02	FIB 08	Plasma
ALB 20	-	0.60	0.13	0.002 *	5.84E-05 *
ALB 50	-	-	0.17	0.004 *	1.18E-04 *
FIB 02	-	-	-	0.002 *	3.17E-05 *
FIB 08	-	-	-	-	7.95E-06 *
Plasma	-	-	-	-	-

Solution-Dependence of $T_{1/2}$ for Delta Sigma Max.

0% Oxygen	ALB 20	ALB 50	FIB 02	FIB 08	Plasma
ALB 20	-	0.93	0.59	0.79	0.52
ALB 50	-	-	0.74	0.76	0.69
FIB 02	-	-	-	0.29	0.93
FIB 08	-	-	-	-	0.14
Plasma	-	-	-	-	-

5% Oxygen	ALB 20	ALB 50	FIB 02	FIB 08	Plasma
ALB 20	-	0.33	0.22	0.52	0.37
ALB 50	-	-	0.46	0.17	0.77
FIB 02	-	-	-	0.17	0.38
FIB 08	-	-	-	-	0.26
Plasma	-	-	-	-	-

10% Oxygen	ALB 20	ALB 50	FIB 02	FIB 08	Plasma
ALB 20	-	0.22	0.42	0.36	0.36
ALB 50	-	-	0.54	0.56	0.51
FIB 02	-	-	-	0.91	0.92
FIB 08	-	-	-	-	0.98
Plasma	-	-	-	-	-

100% Oxygen	ALB 20	ALB 50	FIB 02	FIB 08	Plasma
ALB 20	-	0.01	0.19	0.003	0.03
ALB 50	-	-	0.39	0.51	0.07
FIB 02	-	-	-	0.60	0.74
FIB 08	-	-	-	-	0.10
Plasma	-	-	-	-	-

Table 43: Solution-Dependence of Delta Sigma Max. and $T_{1/2}$ for Delta Sigma Max. for conditions of no antibody at 45°C and equilibrated with prescribed oxygen concentrations. [ALB 20, albumin 20 mg/mL], [ALB 50, albumin 50 mg/mL], [FIB 02, fibrinogen 2 mg/mL], [FIB 08, fibrinogen 8 mg/mL]. Entries are p-values form Welch's two sample t-test. * $p<0.05$.

Solution-Dependence of Delta Sigma Max.

0% Oxygen	ALB 20	ALB 50	FIB 02	FIB 08	Plasma
ALB 20	-	0.95	0.12	0.08	0.12
ALB 50	-	-	0.11	0.08	0.12
FIB 02	-	-	-	0.11	0.12
FIB 08	-	-	-	-	0.16
Plasma	-	-	-	-	-

5% Oxygen	ALB 20	ALB 50	FIB 02	FIB 08	Plasma
ALB 20	-	0.11	0.48	0.03 *	0.03 *
ALB 50	-	-	0.20	0.02 *	0.03 *
FIB 02	-	-	-	0.03 *	0.03 *
FIB 08	-	-	-	-	0.03 *
Plasma	-	-	-	-	-

10% Oxygen	ALB 20	ALB 50	FIB 02	FIB 08	Plasma
ALB 20	-	0.45	0.48	0.02 *	1.16E-04 *
ALB 50	-	-	0.38	0.02 *	1.62E-04 *
FIB 02	-	-	-	0.04 *	3.48E-06 *
FIB 08	-	-	-	-	9.46E-06 *
Plasma	-	-	-	-	

100% Oxygen	ALB 20	ALB 50	FIB 02	FIB 08	Plasma
ALB 20	-	0.73	0.08	0.001 *	3.44E-05 *
ALB 50	-	-	0.11	0.002 *	4.29E-05 *
FIB 02	-	-	-	0.001 *	9.81E-06 *
FIB 08	-	-	-	-	3.17E-06 *
Plasma	-	-	-	-	-

Solution-Dependence of $T_{1/2}$ for Delta Sigma Max.

0% Oxygen	ALB 20	ALB 50	FIB 02	FIB 08	Plasma
ALB 20	-	0.42	0.67	0.99	0.73
ALB 50	-	-	0.63	0.39	0.27
FIB 02	-	-	-	0.62	0.37
FIB 08	-	-	-	-	0.57
Plasma	-	-	-	-	-

5% Oxygen	ALB 20	ALB 50	FIB 02	FIB 08	Plasma
ALB 20	-	0.90	0.42	0.86	0.57
ALB 50	-	-	0.48	0.98	0.65
FIB 02	-	-	-	0.30	0.66
FIB 08	-	-	-	-	0.44
Plasma	-	-	-	-	-

10% Oxygen	ALB 20	ALB 50	FIB 02	FIB 08	Plasma
ALB 20	-	0.06	0.87	0.65	0.11
ALB 50	-	-	0.14	0.02 *	0.35
FIB 02	-	-	-	0.85	0.23
FIB 08	-	-	-	-	0.07
Plasma	-	-	-	-	

100% Oxygen	ALB 20	ALB 50	FIB 02	FIB 08	Plasma
ALB 20	-	0.27	0.16	0.07	0.051
ALB 50	-	-	0.79	0.93	0.80
FIB 02	-	-	-	0.78	0.92
FIB 08	-	-	-	-	0.65
Plasma	-	-	-	-	-

Table 44: Solution-Dependence of Delta Sigma Max. and $T_{1/2}$ for Delta Sigma Max. for conditions of no antibody at 49°C and equilibrated with prescribed oxygen concentrations. [ALB 20, albumin 20 mg/mL], [ALB 50, albumin 50 mg/mL], [FIB 02, fibrinogen 2 mg/mL], [FIB 08, fibrinogen 8 mg/mL]. Entries are p-values form Welch's two sample t-test. * $p<0.05$.

Solution-Dependence of Delta Sigma Max.

0% Oxygen	ALB 20	ALB 50	FIB 02	FIB 08	Plasma
ALB 20	-	0.24	0.51	0.07	0.01 *
ALB 50	-	-	0.38	0.09	0.01 *
FIB 02	-	-	-	0.08	0.01 *
FIB 08	-	-	-	-	0.01 *
Plasma	-	-	-	-	-

5% Oxygen	ALB 20	ALB 50	FIB 02	FIB 08	Plasma
ALB 20	-	0.31	0.53	0.02 *	0.003 *
ALB 50	-	-	0.76	0.02 *	0.004 *
FIB 02	-	-	-	0.02 *	0.003 *
FIB 08	-	-	-	-	0.004 *
Plasma	-	-	-	-	-

10% Oxygen	ALB 20	ALB 50	FIB 02	FIB 08	Plasma
ALB 20	-	0.27	0.78	0.002 *	0.002 *
ALB 50	-	-	0.93	0.002 *	0.002 *
FIB 02	-	-	-	0.001 *	0.001 *
FIB 08	-	-	-	-	0.002 *
Plasma	-	-	-	-	-

100% Oxygen	ALB 20	ALB 50	FIB 02	FIB 08	Plasma
ALB 20	-	0.93	0.08	0.07	0.002 *
ALB 50	-	-	0.12	0.07	0.002 *
FIB 02	-	-	-	0.10	0.002 *
FIB 08	-	-	-	-	0.004 *
Plasma	-	-	-	-	-

Solution-Dependence of $T_{1/2}$ for Delta Sigma Max.

0% Oxygen	ALB 20	ALB 50	FIB 02	FIB 08	Plasma
ALB 20	-	0.55	0.24	0.90	0.50
ALB 50	-	-	0.04 *	0.32	0.10
FIB 02	-	-	-	0.07	0.08
FIB 08	-	-	-	-	0.30
Plasma	-	-	-	-	-

5% Oxygen	ALB 20	ALB 50	FIB 02	FIB 08	Plasma
ALB 20	-	0.29	0.91	0.99	0.24
ALB 50	-	-	0.33	0.18	0.92
FIB 02	-	-	-	0.90	0.29
FIB 08	-	-	-	-	0.03 *
Plasma	-	-	-	-	-

10% Oxygen	ALB 20	ALB 50	FIB 02	FIB 08	Plasma
ALB 20	-	0.79	0.94	0.46	0.95
ALB 50	-	-	0.74	0.75	0.73
FIB 02	-	-	-	0.38	0.98
FIB 08	-	-	-	-	0.26
Plasma	-	-	-	-	-

100% Oxygen	ALB 20	ALB 50	FIB 02	FIB 08	Plasma
ALB 20	-	0.93	0.85	0.43	0.94
ALB 50	-	-	0.82	0.55	0.88
FIB 02	-	-	-	0.60	0.88
FIB 08	-	-	-	-	0.25
Plasma	-	-	-	-	-

Table 45: Solution-Dependence of Delta Sigma Max. and $T_{1/2}$ for Delta Sigma Max. for conditions of DIDS at 37°C and equilibrated with prescribed oxygen concentrations. [ALB 20, albumin 20 mg/mL], [ALB 50, albumin 50 mg/mL], [FIB 02, fibrinogen 2 mg/mL], [FIB 08, fibrinogen 8 mg/mL]. Entries are p-values form Welch's two sample t-test. * $p<0.05$.

Solution-Dependence of Delta Sigma Max.

0% Oxygen	ALB 20	ALB 50	FIB 02	FIB 08	Plasma
ALB 20	-	0.95	0.09	0.39	0.32
ALB 50	-	-	0.10	0.38	0.32
FIB 02	-	-	-	0.86	0.38
FIB 08	-	-	-	-	0.40
Plasma	-	-	-	-	-

5% Oxygen	ALB 20	ALB 50	FIB 02	FIB 08	Plasma
ALB 20	-	0.37	0.21	0.26	0.03 *
ALB 50	-	-	0.37	0.46	0.048 *
FIB 02	-	-	-	0.67	0.054
FIB 08	-	-	-	-	0.06
Plasma	-	-	-	-	-

10% Oxygen	ALB 20	ALB 50	FIB 02	FIB 08	Plasma
ALB 20	-	0.53	0.54	0.60	0.15
ALB 50	-	-	0.83	0.79	0.16
FIB 02	-	-	-	0.90	0.17
FIB 08	-	-	-	-	0.17
Plasma	-	-	-	-	-

100% Oxygen	ALB 20	ALB 50	FIB 02	FIB 08	Plasma
ALB 20	-	0.68	0.17	0.25	0.12
ALB 50	-	-	0.24	0.33	0.13
FIB 02	-	-	-	0.75	0.17
FIB 08	-	-	-	-	0.20
Plasma	-	-	-	-	-

Solution-Dependence of $T_{1/2}$ for Delta Sigma Max.

0% Oxygen	ALB 20	ALB 50	FIB 02	FIB 08	Plasma
ALB 20	-	0.21	0.84	0.36	0.25
ALB 50	-	-	0.61	0.80	0.10
FIB 02	-	-	-	0.71	0.30
FIB 08	-	-	-	-	0.10
Plasma	-	-	-	-	-

5% Oxygen	ALB 20	ALB 50	FIB 02	FIB 08	Plasma
ALB 20	-	0.43	0.43	0.67	0.11
ALB 50	-	-	0.93	0.16	0.30
FIB 02	-	-	-	0.11	0.20
FIB 08	-	-	-	-	0.01 *
Plasma	-	-	-	-	-

10% Oxygen	ALB 20	ALB 50	FIB 02	FIB 08	Plasma
ALB 20	-	0.52	0.27	0.34	0.054
ALB 50	-	-	0.58	0.73	0.18
FIB 02	-	-	-	0.82	0.49
FIB 08	-	-	-	-	0.32
Plasma	-	-	-	-	-

100% Oxygen	ALB 20	ALB 50	FIB 02	FIB 08	Plasma
ALB 20	-	0.63	0.83	0.87	0.47
ALB 50	-	-	0.90	0.46	0.21
FIB 02	-	-	-	0.73	0.45
FIB 08	-	-	-	-	0.52
Plasma	-	-	-	-	-

Table 46: Solution-Dependence of Delta Sigma Max. and $T_{1/2}$ for Delta Sigma Max. for conditions of DIDS at 41°C and equilibrated with prescribed oxygen concentrations. [ALB 20, albumin 20 mg/mL], [ALB 50, albumin 50 mg/mL], [FIB 02, fibrinogen 2 mg/mL], [FIB 08, fibrinogen 8 mg/mL]. Entries are p-values form Welch's two sample t-test. * $p<0.05$.

Solution-Dependence of Delta Sigma Max.

0% Oxygen	ALB 20	ALB 50	FIB 02	FIB 08	Plasma
ALB 20	-	0.90	0.28	0.54	0.15
ALB 50	-	-	0.30	0.58	0.15
FIB 02	-	-	-	0.74	0.20
FIB 08	-	-	-	-	0.17
Plasma	-	-	-	-	-

5% Oxygen	ALB 20	ALB 50	FIB 02	FIB 08	Plasma
ALB 20	-	0.67	0.64	0.88	0.03 *
ALB 50	-	-	0.48	0.74	0.03 *
FIB 02	-	-	-	0.85	0.03 *
FIB 08	-	-	-	-	0.02 *
Plasma	-	-	-	-	-

10% Oxygen	ALB 20	ALB 50	FIB 02	FIB 08	Plasma
ALB 20	-	0.93	0.92	0.51	0.10
ALB 50	-	-	0.89	0.50	0.10
FIB 02	-	-	-	0.55	0.10
FIB 08	-	-	-	-	0.12
Plasma	-	-	-	-	-

100% Oxygen	ALB 20	ALB 50	FIB 02	FIB 08	Plasma
ALB 20	-	0.57	0.23	0.45	0.15
ALB 50	-	-	0.14	0.39	0.14
FIB 02	-	-	-	0.67	0.18
FIB 08	-	-	-	-	0.24
Plasma	-	-	-	-	-

Solution-Dependence of $T_{1/2}$ for Delta Sigma Max.

0% Oxygen	ALB 20	ALB 50	FIB 02	FIB 08	Plasma
ALB 20	-	0.68	0.19	0.54	0.98
ALB 50	-	-	0.25	0.77	0.75
FIB 02	-	-	-	0.37	0.28
FIB 08	-	-	-	-	0.63
Plasma	-	-	-	-	-

5% Oxygen	ALB 20	ALB 50	FIB 02	FIB 08	Plasma
ALB 20	-	0.16	0.07	0.38	0.07
ALB 50	-	-	0.41	0.56	0.45
FIB 02	-	-	-	0.23	0.81
FIB 08	-	-	-	-	0.25
Plasma	-	-	-	-	-

10% Oxygen	ALB 20	ALB 50	FIB 02	FIB 08	Plasma
ALB 20	-	0.50	0.94	0.77	0.39
ALB 50	-	-	0.43	0.54	0.11
FIB 02	-	-	-	0.68	0.41
FIB 08	-	-	-	-	0.04 *
Plasma	-	-	-	-	-

100% Oxygen	ALB 20	ALB 50	FIB 02	FIB 08	Plasma
ALB 20	-	0.53	0.20	0.14	0.88
ALB 50	-	-	0.40	0.74	0.80
FIB 02	-	-	-	0.47	0.35
FIB 08	-	-	-	-	0.61
Plasma	-	-	-	-	-

Table 47: Solution-Dependence of Delta Sigma Max. and $T_{1/2}$ for Delta Sigma Max. for conditions of DIDS at 45°C and equilibrated with prescribed oxygen concentrations. [ALB 20, albumin 20 mg/mL], [ALB 50, albumin 50 mg/mL], [FIB 02, fibrinogen 2 mg/mL], [FIB 08, fibrinogen 8 mg/mL]. Entries are p-values form Welch's two sample t-test. * $p<0.05$.

Solution-Dependence of Delta Sigma Max.

0% Oxygen	ALB 20	ALB 50	FIB 02	FIB 08	Plasma
ALB 20	-	0.94	0.24	0.39	0.07
ALB 50	-	-	0.26	0.39	0.07
FIB 02	-	-	-	0.63	0.07
FIB 08	-	-	-	-	0.08
Plasma	-	-	-	-	-

5% Oxygen	ALB 20	ALB 50	FIB 02	FIB 08	Plasma
ALB 20	-	0.30	0.47	0.45	0.049 *
ALB 50	-	-	0.79	0.61	0.051
FIB 02	-	-	-	0.75	0.052
FIB 08	-	-	-	-	0.054
Plasma	-	-	-	-	-

10% Oxygen	ALB 20	ALB 50	FIB 02	FIB 08	Plasma
ALB 20	-	0.48	0.64	0.49	0.01 *
ALB 50	-	-	0.65	0.33	0.003 *
FIB 02	-	-	-	0.38	0.01 *
FIB 08	-	-	-	-	0.01 *
Plasma	-	-	-	-	-

100% Oxygen	ALB 20	ALB 50	FIB 02	FIB 08	Plasma
ALB 20	-	0.97	0.55	0.28	0.13
ALB 50	-	-	0.53	0.27	0.13
FIB 02	-	-	-	0.42	0.14
FIB 08	-	-	-	-	0.18
Plasma	-	-	-	-	-

Solution-Dependence of $T_{1/2}$ for Delta Sigma Max.

0% Oxygen	ALB 20	ALB 50	FIB 02	FIB 08	Plasma
ALB 20	-	0.32	0.90	0.15	0.86
ALB 50	-	-	0.40	0.67	0.34
FIB 02	-	-	-	0.21	0.97
FIB 08	-	-	-	-	0.11
Plasma	-	-	-	-	-

5% Oxygen	ALB 20	ALB 50	FIB 02	FIB 08	Plasma
ALB 20	-	0.88	0.052	0.25	0.31
ALB 50	-	-	0.053	0.26	0.50
FIB 02	-	-	-	0.29	0.02 *
FIB 08	-	-	-	-	0.10
Plasma	-	-	-	-	-

10% Oxygen	ALB 20	ALB 50	FIB 02	FIB 08	Plasma
ALB 20	-	0.71	0.87	0.58	0.58
ALB 50	-	-	0.78	1.00	1.00
FIB 02	-	-	-	0.59	0.60
FIB 08	-	-	-	-	1.00
Plasma	-	-	-	-	-

100% Oxygen	ALB 20	ALB 50	FIB 02	FIB 08	Plasma
ALB 20	-	0.86	0.69	0.24	0.77
ALB 50	-	-	0.61	0.22	0.90
FIB 02	-	-	-	0.41	0.56
FIB 08	-	-	-	-	0.20
Plasma	-	-	-	-	-

Table 48: Solution-Dependence of Delta Sigma Max. and $T_{1/2}$ for Delta Sigma Max. for conditions of DIDS at 49°C and equilibrated with prescribed oxygen concentrations. [ALB 20, albumin 20 mg/mL], [ALB 50, albumin 50 mg/mL], [FIB 02, fibrinogen 2 mg/mL], [FIB 08, fibrinogen 8 mg/mL]. Entries are p-values form Welch's two sample t-test. * $p<0.05$.

Solution-Dependence of Delta Sigma Max.

0% Oxygen	ALB 20	ALB 50	FIB 02	FIB 08	Plasma
ALB 20	-	0.23	0.01 *	0.23	0.08
ALB 50	-	-	0.04 *	0.31	0.09
FIB 02	-	-	-	0.69	0.09
FIB 08	-	-	-	-	0.10
Plasma	-	-	-	-	-

5% Oxygen	ALB 20	ALB 50	FIB 02	FIB 08	Plasma
ALB 20	-	0.50	0.90	0.52	0.02 *
ALB 50	-	-	0.63	0.62	0.02 *
FIB 02	-	-	-	0.51	0.02 *
FIB 08	-	-	-	-	0.02 *
Plasma	-	-	-	-	-

10% Oxygen	ALB 20	ALB 50	FIB 02	FIB 08	Plasma
ALB 20	-	0.54	0.62	0.95	0.051
ALB 50	-	-	0.90	0.65	0.052
FIB 02	-	-	-	0.71	0.052
FIB 08	-	-	-	-	0.050
Plasma	-	-	-	-	-

100% Oxygen	ALB 20	ALB 50	FIB 02	FIB 08	Plasma
ALB 20	-	0.59	0.78	0.36	0.11
ALB 50	-	-	0.76	0.41	0.12
FIB 02	-	-	-	0.39	0.12
FIB 08	-	-	-	-	0.16
Plasma	-	-	-	-	-

Solution-Dependence of $T_{1/2}$ for Delta Sigma Max.

0% Oxygen	ALB 20	ALB 50	FIB 02	FIB 08	Plasma
ALB 20	-	0.48	0.63	0.13	0.15
ALB 50	-	-	0.91	0.80	0.59
FIB 02	-	-	-	0.99	0.84
FIB 08	-	-	-	-	0.65
Plasma	-	-	-	-	-

5% Oxygen	ALB 20	ALB 50	FIB 02	FIB 08	Plasma
ALB 20	-	0.01 *	0.82	0.83	0.72
ALB 50	-	-	0.02 *	0.001 *	0.001 *
FIB 02	-	-	-	0.65	0.96
FIB 08	-	-	-	-	0.43
Plasma	-	-	-	-	-

10% Oxygen	ALB 20	ALB 50	FIB 02	FIB 08	Plasma
ALB 20	-	0.03 *	0.03 *	0.01 *	0.09
ALB 50	-	-	0.30	0.94	0.39
FIB 02	-	-	-	0.20	0.92
FIB 08	-	-	-	-	0.31
Plasma	-	-	-	-	-

100% Oxygen	ALB 20	ALB 50	FIB 02	FIB 08	Plasma
ALB 20	-	0.98	0.72	0.85	0.98
ALB 50	-	-	0.69	0.81	0.95
FIB 02	-	-	-	0.84	0.73
FIB 08	-	-	-	-	0.87
Plasma	-	-	-	-	-

Table 49: Mean and Standard Deviation of Delta Sigma Max. for conditions of no antibody equilibrated with prescribed oxygen concentrations. [ALB 20, albumin 20 mg/mL], [ALB 50, albumin 50 mg/mL], [FIB 02, fibrinogen 2 mg/mL], [FIB 08, fibrinogen 8 mg/mL]. Entries are mean ± standard deviation. (n=4 each).

Delta Sigma Max.

0% Oxygen	ALB 20	ALB 50	FIB 02	FIB 08	Plasma
37 °C	-0.17 ± 0.36	-0.24 ± 0.47	0.03 ± 0.26	1.69 ± 0.42	17.13 ± 1.68
41 °C	-0.16 ± 0.44	0.73 ± 1.73	0.08 ± 0.45	3.24 ± 2.29	14.21 ± 2.14
45 °C	-0.08 ± 0.33	-0.07 ± 0.08	0.44 ± 0.45	3.57 ± 2.85	18.93 ± 12.26
49 °C	-0.18 ± 0.16	0.14 ± 0.44	-0.09 ± 0.19	3.33 ± 2.58	23.75 ± 7.18

5% Oxygen	ALB 20	ALB 50	FIB 02	FIB 08	Plasma
37 °C	0.10 ± 0.12	-0.43 ± 0.59	0.15 ± 0.53	3.16 ± 1.96	14.28 ± 10.93
41 °C	-0.29 ± 0.45	-0.45 ± 0.15	0.25 ± 0.72	3.75 ± 1.56	17.48 ± 7.99
45 °C	0.02 ± 0.16	-0.23 ± 0.21	0.26 ± 0.59	4.99 ± 2.41	20.91 ± 6.12
49 °C	-0.19 ± 0.43	0.10 ± 0.27	0.01 ± 0.43	5.49 ± 2.45	20.47 ± 4.92

10% Oxygen	ALB 20	ALB 50	FIB 02	FIB 08	Plasma
37 °C	-0.02 ± 0.28	-0.25 ± 0.09	0.73 ± 0.52	3.98 ± 2.55	12.47 ± 5.64
41 °C	-0.22 ± 0.15	-0.23 ± 0.08	0.15 ± 0.50	3.51 ± 2.89	16.29 ± 10.55
45 °C	-0.26 ± 0.37	-0.42 ± 0.10	0.38 ± 1.57	3.99 ± 2.09	24.15 ± 2.08
49 °C	-0.36 ± 0.09	-0.26 ± 0.12	-0.22 ± 0.90	3.59 ± 0.82	17.34 ± 3.22

100% Oxygen	ALB 20	ALB 50	FIB 02	FIB 08	Plasma
37 °C	-0.57 ± 0.68	-0.41 ± 0.27	-0.24 ± 0.49	3.36 ± 0.99	21.15 ± 9.68
41 °C	-0.42 ± 0.44	-0.28 ± 0.16	0.27 ± 0.63	4.66 ± 1.26	22.00 ± 1.74
45 °C	-0.17 ± 0.31	-0.09 ± 0.26	0.52 ± 0.54	3.73 ± 0.86	20.21 ± 1.31
49 °C	-0.09 ± 0.42	-0.06 ± 0.53	0.54 ± 0.42	4.49 ± 3.32	14.53 ± 2.91

Table 50: Mean and Standard Deviation of $T_{1/2}$ for Delta Sigma Max. for conditions of no antibody equilibrated with prescribed oxygen concentrations. [ALB 20, albumin 20 mg/mL], [ALB 50, albumin 50 mg/mL], [FIB 02, fibrinogen 2 mg/mL], [FIB 08, fibrinogen 8 mg/mL]. Entries are mean ± standard deviation. (n=4 each).

$T_{1/2}$ for Delta Sigma Max.

0% Oxygen	ALB 20	ALB 50	FIB 02	FIB 08	Plasma
37 °C	115.27 ± 35.30	57.33 ± 66.63	41.92 ± 44.38	80.75 ± 19.45	84.45 ± 14.15
41 °C	96.78 ± 57.59	92.47 ± 78.71	77.05 ± 39.16	106.03 ± 30.47	75.21 ± 16.78
45 °C	84.45 ± 60.91	130.07 ± 85.16	103.56 ± 58.52	85.07 ± 37.04	72.33 ± 16.04
49 °C	90.00 ± 86.14	123.29 ± 57.97	26.51 ± 22.99	83.84 ± 43.13	56.71 ± 14.52

5% Oxygen	ALB 20	ALB 50	FIB 02	FIB 08	Plasma
37 °C	85.07 ± 76.41	55.48 ± 65.32	90.00 ± 73.41	104.79 ± 23.00	71.51 ± 18.34
41 °C	114.66 ± 78.40	69.04 ± 16.96	52.40 ± 37.74	86.30 ± 13.80	72.74 ± 16.78
45 °C	99.25 ± 89.00	91.23 ± 84.20	53.63 ± 53.62	90.00 ± 32.80	69.04 ± 32.05
49 °C	102.95 ± 60.65	55.48 ± 53.51	98.01 ± 60.85	102.33 ± 24.94	58.56 ± 19.24

10% Oxygen	ALB 20	ALB 50	FIB 02	FIB 08	Plasma
37 °C	28.36 ± 14.31	96.16 ± 63.60	101.71 ± 53.51	73.97 ± 26.33	88.77 ± 18.12
41 °C	109.11 ± 64.44	57.33 ± 35.30	75.21 ± 41.68	72.12 ± 32.55	72.74 ± 26.29
45 °C	99.86 ± 40.09	43.77 ± 16.40	94.32 ± 50.79	88.77 ± 23.82	55.48 ± 15.92
49 °C	73.36 ± 48.12	84.45 ± 64.59	70.89 ± 42.34	96.78 ± 33.53	71.51 ± 22.51

100% Oxygen	ALB 20	ALB 50	FIB 02	FIB 08	Plasma
37 °C	81.99 ± 66.97	35.14 ± 13.71	99.86 ± 73.30	75.21 ± 6.52	66.58 ± 20.03
41 °C	26.51 ± 17.13	107.26 ± 31.99	75.82 ± 58.19	93.70 ± 21.21	64.73 ± 20.76
45 °C	136.23 ± 38.11	88.77 ± 65.89	75.82 ± 63.07	85.68 ± 13.26	79.52 ± 21.63
49 °C	78.90 ± 39.66	75.21 ± 64.06	84.45 ± 41.62	96.78 ± 4.21	80.75 ± 22.63

Table 51: Mean and Standard Deviation of Delta Sigma Max. for conditions of DIDS equilibrated with prescribed oxygen concentrations. [ALB 20, albumin 20 mg/mL], [ALB 50, albumin 50 mg/mL], [FIB 02, fibrinogen 2 mg/mL], [FIB 08, fibrinogen 8 mg/mL]. Entries are mean ± standard deviation. (n=4 each).

Delta Sigma Max.

0% Oxygen	ALB 20	ALB 50	FIB 02	FIB 08	Plasma
37 °C	-0.61 ± 0.25	-0.62 ± 0.29	-0.16 ± 0.36	-0.05 ± 1.09	2.60 ± 4.27
41 °C	-0.74 ± 0.32	-0.70 ± 0.32	-0.15 ± 0.86	-0.38 ± 1.01	3.13 ± 3.97
45 °C	-0.87 ± 0.26	-0.86 ± 0.24	-0.44 ± 0.58	0.08 ± 1.87	11.11 ± 8.57
49 °C	-0.99 ± 0.25	-0.77 ± 0.21	-0.19 ± 0.36	0.14 ± 1.50	12.17 ± 10.23

5% Oxygen	ALB 20	ALB 50	FIB 02	FIB 08	Plasma
37 °C	-1.06 ± 0.85	-0.60 ± 0.14	-0.34 ± 0.50	0.01 ± 1.46	3.77 ± 2.70
41 °C	-0.51 ± 0.43	-0.63 ± 0.33	-0.26 ± 0.89	-0.41 ± 1.19	5.63 ± 3.13
45 °C	-0.82 ± 0.21	-0.63 ± 0.25	-0.53 ± 0.67	-0.30 ± 1.16	8.31 ± 5.69
49 °C	-0.42 ± 0.26	-0.30 ± 0.19	-0.46 ± 0.58	0.05 ± 1.28	12.40 ± 5.81

10% Oxygen	ALB 20	ALB 50	FIB 02	FIB 08	Plasma
37 °C	-0.64 ± 0.45	-0.46 ± 0.27	-0.39 ± 0.63	-0.30 ± 1.09	6.20 ± 7.23
41 °C	-0.54 ± 0.26	-0.56 ± 0.40	-0.50 ± 0.69	0.11 ± 1.76	7.40 ± 6.71
45 °C	-0.64 ± 0.43	-1.72 ± 2.70	-1.00 ± 1.34	-0.06 ± 1.43	10.15 ± 3.69
49 °C	-0.42 ± 0.27	-0.22 ± 0.53	-0.27 ± 0.50	-0.45 ± 0.77	11.75 ± 7.69

100% Oxygen	ALB 20	ALB 50	FIB 02	FIB 08	Plasma
37 °C	-0.87 ± 0.53	-0.73 ± 0.41	-0.27 ± 0.56	-0.06 ± 1.10	2.58 ± 3.19
41 °C	-0.69 ± 0.27	-0.83 ± 0.36	-0.31 ± 0.49	0.18 ± 1.99	3.39 ± 4.29
45 °C	-0.79 ± 0.45	-0.80 ± 0.36	-0.45 ± 0.96	0.52 ± 1.96	7.76 ± 8.21
49 °C	-0.68 ± 0.40	-0.55 ± 0.19	-0.61 ± 0.29	0.47 ± 2.11	6.18 ± 6.21

Table 52: Mean and Standard Deviation of $T_{1/2}$ for Delta Sigma Max. for conditions of DIDS equilibrated with prescribed oxygen concentrations. [ALB 20, albumin 20 mg/mL], [ALB 50, albumin 50 mg/mL], [FIB 02, fibrinogen 2 mg/mL], [FIB 08, fibrinogen 8 mg/mL]. Entries are mean ± standard deviation. (n=4 each).

$T_{1/2}$ for Delta Sigma Max.

0% Oxygen	ALB 20	ALB 50	FIB 02	FIB 08	Plasma
37 °C	99.86 ± 36.04	70.89 ± 15.38	91.23 ± 70.81	75.82 ± 32.86	141.37 ± 43.44
41 °C	102.95 ± 25.58	96.16 ± 17.55	73.97 ± 29.24	91.85 ± 22.63	103.56 ± 39.19
45 °C	101.71 ± 26.20	82.60 ± 24.03	99.25 ± 27.92	76.44 ± 11.57	98.63 ± 19.42
49 °C	106.64 ± 18.71	90.62 ± 37.63	85.68 ± 76.33	85.07 ± 15.13	77.05 ± 29.55

5% Oxygen	ALB 20	ALB 50	FIB 02	FIB 08	Plasma
37 °C	74.59 ± 38.80	96.16 ± 32.77	94.32 ± 25.89	65.34 ± 3.18	118.36 ± 20.43
41 °C	53.01 ± 40.29	92.47 ± 25.66	109.73 ± 28.93	78.90 ± 35.96	105.41 ± 19.14
45 °C	98.01 ± 16.65	100.48 ± 26.66	47.47 ± 34.19	74.59 ± 31.67	112.81 ± 20.86
49 °C	72.12 ± 33.23	155.34 ± 18.67	78.29 ± 37.90	67.81 ± 19.15	79.52 ± 19.87

10% Oxygen	ALB 20	ALB 50	FIB 02	FIB 08	Plasma
37 °C	81.37 ± 20.43	93.08 ± 27.56	106.03 ± 34.23	100.48 ± 29.89	122.05 ± 26.60
41 °C	94.32 ± 44.95	72.12 ± 41.62	96.78 ± 41.33	86.92 ± 12.95	117.74 ± 19.56
45 °C	88.77 ± 41.41	102.95 ± 60.34	93.08 ± 25.26	102.95 ± 24.27	102.95 ± 25.26
49 °C	142.40 ± 22.72	64.11 ± 46.39	94.93 ± 24.20	61.64 ± 37.72	92.47 ± 40.79

100% Oxygen	ALB 20	ALB 50	FIB 02	FIB 08	Plasma
37 °C	91.85 ± 33.47	81.37 ± 24.58	85.07 ± 50.15	95.55 ± 25.81	109.73 ± 32.24
41 °C	80.14 ± 11.12	89.38 ± 24.77	109.11 ± 35.01	94.32 ± 12.31	83.22 ± 37.79
45 °C	104.79 ± 19.15	107.26 ± 18.72	96.78 ± 33.35	72.12 ± 44.03	109.11 ± 21.34
49 °C	101.71 ± 31.28	101.10 ± 21.59	113.42 ± 52.85	106.64 ± 37.69	102.33 ± 32.12

Table 53: Linear Regressions for Oxygen Dependence of Delta Sigma Max. for conditions of noAb and DIDS.

Delta Sigma Max.					
Plasma noAb	Intercept	Intercept Standard Error	Slope	Slope Standard Error	R-Square
37 °C	14.39868	±1.63298	0.06471	±0.03246	0.49793
41 °C	15.6496	±0.89861	0.0643	±0.01786	0.79947
45 °C	21.27562	±1.63504	-0.0079	±0.0325	-0.457
49 °C	20.95686	±1.75232	-0.06729	±0.03483	0.47671
Plasma DIDS	Intercept	Intercept Standard Error	Slope	Slope Standard Error	R-Square
37 °C	4.19255	±1.16552	-0.01416	±0.02317	-0.264
41 °C	5.397	±1.36833	-0.01777	±0.0272	-0.23624
45 °C	9.98444	±0.84873	-0.02259	±0.01687	0.20923
49 °C	12.41719	±0.1669	-0.06223	±0.00332	0.99152